

**Vinexin regulates autophagy through YAP/TAZ:  
implications for health and disease**

**Rebecca Astrid Frake**



**UNIVERSITY OF  
CAMBRIDGE**

**Corpus Christi College**

**September 2017**

**This dissertation is submitted for the degree of Doctor of Philosophy**

## i. Summary

### **Vinexin regulates autophagy through YAP/TAZ: implications for health and disease**

**Rebecca Astrid Frake**

Macroautophagy (hereafter referred to as autophagy) is a highly conserved cellular process that promotes cytoplasmic homeostasis *via* lysosomal degradation of proteins and organelles. Dysfunctional autophagy occurs in numerous human pathologies, including neurodegeneration and cancer. Vinexin (encoded by *SORBS3*) is a physiologically important adaptor protein for two main reasons: 1. *SORBS3* mRNA expression increases in normal human brain ageing, 2. *SORBS3* is a candidate tumour suppressor in hepatocellular carcinoma (HCC).

This dissertation builds on published data from an siRNA screen for autophagy regulations under basal conditions, which indicates vinexin knockdown upregulates autophagy. I replicate this finding in multiple cell lines, before characterising the impact of si*SORBS3* treatment on autophagy; autophagosome biogenesis is increased, while flux through the autophagy pathway remains intact. Having excluded several possible mechanisms suggested by the literature, I focus on the transcriptional coactivators YAP and TAZ. The rationale here is: 1. YAP/TAZ activity is implicated in autophagy, 2. YAP/TAZ and vinexin are both linked to HCC.

My data show that YAP/TAZ transcriptional activity is upregulated upon vinexin depletion. Moreover, increased autophagy following si*SORBS3* treatment requires YAP and TAZ. A key focus of this dissertation is the mechanism by which vinexin knockdown upregulates YAP/TAZ and hence, autophagy. This centres on altered actin cytoskeleton dynamics; an increase in F-actin structures appears to compete with YAP/TAZ for binding to angiomotins, established sequesterers of YAP/TAZ in the cytosol. In this way, si*SORBS3* treatment facilitates YAP/TAZ nuclear localisation and consequent transcriptional activity. Angiomotin overexpression therefore ameliorates the increase in autophagy caused by vinexin depletion.

Published RNA sequencing data is used to confirm that *SORBS3* mRNA expression increases in normal brain ageing, not only in the frontal cortex (as previously published), but also in the hippocampus. This sits alongside decreased expression of core autophagy genes in both tissues. Accordingly, vinexin could contribute to the decline in autophagic potential thought to occur in normal brain ageing.

With regards to *SORBS3* as a candidate tumour suppressor in HCC, I show that stably re-expressing vinexin in a HCC cell line downregulates YAP/TAZ and hence, autophagy. These cells also show reduced clonogenicity. My data therefore support the hypothesis that *SORBS3* is a tumour suppressor in HCC; YAP and TAZ are well-known to increase proliferation and resistance to apoptosis, while autophagy can enable tumour cells to survive stressors such as nutrient starvation.

The conclusions of this dissertation are that vinexin depletion upregulates autophagy in a YAP/TAZ-dependent manner and that this has physiologically important implications, especially with regards to HCC.

## **ii. Preface**

This dissertation is the result of my own work and includes nothing which is the outcome of work done in collaboration except as declared in the Preface and specified in the text.

It is not substantially the same as any that I have submitted, or is being concurrently submitted for a degree or diploma or other qualification at the University of Cambridge or any other University or similar institution except as declared in the Preface and specified in the text. I further state that no substantial part of my dissertation has already been submitted, or, is being concurrently submitted for any such degree, diploma or other qualification at the University of Cambridge or any other University or similar institution except as declared in the Preface and specified in the text

It does not exceed the prescribed word limit for the relevant Degree Committee.

*For Nana Kath & Grandma Marian,*

*in gratitude I do not suffer your poverty of opportunity*

### **iii. Acknowledgements**

Firstly, I would like to express my sincere gratitude to Professor David Rubinsztein for facilitating the rigorous scientific education I have received in his lab. I am grateful for his ongoing support, stimulating discussion (around this thesis and other topics) and the freedom he afforded me in pursuing this project.

I would like to acknowledge the financial support I received from the Sim's Fund and Frank Edward Elmore Fund during the first three years of my PhD. I would also like to express my gratitude to individuals associated with the Cambridge MB/PhD Programme. In particular, Dr Robert Semple for his support as programme director, Lesley Flood for excellent administrative support and my clinical supervisors (Drs Damiano Barone and Harveer Dev) who helped to 'keep my hand in' with regards to clinical medicine.

I am especially grateful to the Rubinsztein lab members that contributed directly to this thesis: Anne Jackson, Dr Carla Bento and Dr Maurizio Renna. Each was exceedingly generous with their time and expertise. Dr Renna was also kind enough to critically review the results chapters of this thesis. I would also like to express my gratitude to Dr Peter Sterk, who performed the bioinformatics included in this thesis. It was a pleasure to collaborate with Dr Sterk, who always listened carefully to my ideas and took the time to explain bioinformatics methodology. In addition, I am grateful to the Cambridge Institute for Medical Research core FACS and microscopy facilities, in particular to Matthew Gratian and Mark Bowen who trained me in confocal microscopy.

I would like to thank all Rubinsztein lab members (too many to name!) for creating a wonderful environment in which to conduct science, one in which I have felt truly at home. I am particularly grateful to: Dr Mariana Pavel for teaching me about YAP/TAZ biology and enabling me to apply her knowledge to my project, Dr Mariella Vicinanza for her support and mentorship (especially during my first years in the lab), our lab managers (Oana Sadiq, Birgitte Bruun and Dr Vicky Barratt) for their invaluable support. I would like to thank my fellow PhD students (if not already mentioned) for helping to make my time in the lab so enjoyable: Cansu Karabiyik, Gautam Runwal and Ye Zhu ('Ruby'). I am also hugely grateful to my 'top women in science' Drs Fiona Menzies, Angie Fleming and Petra Sekyrova for being such inspirations.

Finally, I would like to acknowledge my support network outside the lab. The members of Cambridge University Hare & Hounds, Cambridge and Coleridge Athletics Club and the University of Cambridge Philharmonic Orchestra. Most importantly though, I am grateful to my close friends and family for their unwavering support.

## **iv. Contents (abbreviated)**

<b>1 Introduction</b>	<b>1</b>
1.1 Autophagy	1
1.1.1 Introduction	1
1.1.2 Molecular machinery of autophagosome biogenesis	3
1.1.3 Membrane sources in autophagosome biogenesis	7
1.1.4 Autophagy cargo receptors	8
1.1.5 Late stage autophagy	9
1.1.6 Regulation	12
1.1.7 Normal physiology	19
1.1.7.1 Development	19
1.1.7.2 Ageing	21
1.1.8 Disease	23
1.1.8.1 Cancer	23
1.1.8.2 Neurodegeneration	26
1.1.8.2 Immunity and Inflammation	29
1.1.9 Concluding remarks	32
1.2 Vinexin	33
1.2.1 Introduction	33
1.2.1.1 Isoform expression	33
1.2.1.1 Domain structure	34
1.2.2 Cell biology	34
1.2.2.1 Actin cytoskeleton dynamics	34
1.2.2.2 MAPK signalling	38

1.2.2.3 Oestrogen receptor signalling	39
1.2.2.4 Lipid raft functions	40
1.2.3 Health and disease	40
1.2.3.1 Animal models	41
1.2.3.2 Cancer	42
1.2.3.3 Normal brain ageing	45
1.2.3.4 Neurodegeneration	45
1.2.4 Concluding remarks	46
1.3 YAP and TAZ	47
1.3.1 Introduction	47
1.3.1.1 Conserved domain structure	47
1.3.1.2 Non-conserved domain structure	49
1.3.2 YAP/TAZ transcriptional activity	49
1.3.2.1 TEAD transcription factor-mediated transcriptional activity	49
1.3.2.2 Non-TEAD transcription factor-mediated transcriptional activity	51
1.3.3 Regulation	53
1.3.3.1 Hippo pathway-dependent regulation	54
1.3.3.2 Hippo pathway-independent regulation	55
1.3.4 Normal physiology	58
1.3.5 Disease	62
1.3.5.1 Genetic syndromes	62
1.3.5.2 Polycystic kidney disease	62
1.3.5.3 Cancer	63
1.3.6 Concluding remarks	65

<b>2 Materials &amp; Methods</b>	<b>67</b>
2.1 Cell culture	68
2.2 DNA expression	68
2.3 RNA interference	69
2.4 Pharmacological agents	70
2.5 Western blotting	70
2.6 Immunoprecipitation	71
2.7 Nuclear/cytosolic fractionation	73
2.8 F- to G-actin ratio assay	73
2.9 Microscopy	74
2.10 Luciferase reporter assay	76
2.11 Clonogenic assay	76
2.12 Statistical analysis	76
2.13 Bioinformatics	77
<b>3 Vinexin is a physiologically important autophagy regulator</b>	<b>79</b>
3.1 Introduction	79
3.2 Vinexin beta depletion using siRNA against SORBS3 specifically upregulates autophagy	79
3.3 SORBS3 is transcriptionally upregulated and core autophagy genes transcriptionally downregulation in normal human brain ageing	85
3.4 Vinexin beta depletion using siRNA against SORBS3 promotes functional autophagy	89
3.5 Vinexin regulates autophagy independent of focal adhesion changes	95
3.6 Vinexin beta depletion does not upregulate autophagy via mTOR, ULK1, ERK1/2 or EGFR signalling	98

3.7 Concluding remarks	104
<b>4 Vinexin depletion upregulates autophagy through YAP/TAZ via a filamentous actin-dependent mechanism</b>	<b>106</b>
4.1 Introduction	106
4.2 siSORBS3 treatment increases YAP/TAZ activity upstream of autophagy	106
4.3 Autophagy upregulation upon vinexin beta depletion is YAP/TAZ-dependent	110
4.4 Vinexin beta depletion increases YAP/TAZ activity independent of Hippo signalling	110
4.5 siSORBS3 treatment alters actin cytoskeleton dynamics	114
4.6 Filamentous actin, and to a lesser extent actomyosin tension, contribute to YAP/TAZ nuclear translocation under siSORBS3 treatment	115
4.7 Autophagy upregulation upon vinexin beta depletion requires filamentous actin, but not actomyosin tension	119
4.8 siSORBS3 treatment alters actin cytoskeleton dynamics upstream of YAP/TAZ	123
4.9 Angiomotins counter YAP/TAZ nuclear translocation under siSORBS3 treatment by retaining YAP/TAZ in the cytosol	125
4.10 Altered actin cytoskeleton dynamics upon vinexin beta depletion prevent YAP/TAZ cytosolic sequestration by angiomotins	127
4.11 Autophagy upregulation upon vinexin beta depletion requires YAP/TAZ release from angiomotins	129
4.12 Concluding remarks	132
<b>5 Vinexin decreases hepatocellular carcinoma cell line tumourigenicity by negatively regulating YAP/TAZ activity and autophagy</b>	<b>136</b>
5.1 Introduction	136
5.2 SORBS3 mRNA expression is commonly downregulated in hepatocellular carcinoma	136
5.3 Vinexin-deficient HepG2 cells are unable to upregulate YAP/TAZ activity or	

downstream clonogenicity under siSORBS3 treatment	138
5.4 Vinexin alpha re-expression counters nuclear YAP/TAZ localisation in HepG2 cells	141
5.5 Vinexin deficiency drives autophagy in HepG2 cells	142
5.6 Vinexin negatively regulates clonogenicity in HepG2 cells	144
5.7 Concluding remarks	148
<b>6 Discussion</b>	<b>149</b>
6.1 Results summary	149
6.2 Outstanding questions	149
6.3 Vinexin integrates multiple tumourigenic processes	153
6.4 Concluding remarks	156
<b>7 References</b>	<b>157</b>
<b>8 Appendix</b>	<b>183</b>
8.1 Abbreviations	183

## **v. Contents (detailed)**

<b>1 Introduction</b>	<b>1</b>
1.1 Autophagy	1
1.1.1 Introduction	1
i. Macroautophagy	1
ii. Chaperone-mediated autophagy	3
iii. Microautophagy	3
1.1.2 Molecular machinery of autophagosome biogenesis	3
i. Initiation: the ULK1 complex	3
ii. Membrane nucleation: PI3KC3 complex I	5
iii. Membrane expansion: ubiquitin-like conjugation systems	6
iv. Phagophore closure	7
1.1.3 Membrane sources in autophagosome biogenesis	7
1.1.4 Autophagy cargo receptors	8
1.1.5 Late stage autophagy	9
i. Vesicular trafficking	9
ii. Autophagosome-endosome/lysosome fusion	10
1.1.6 Regulation	12
i. mTOR-dependent regulation	12
ii. mTOR-independent regulation	15
1.1.7 Normal physiology	19
1.1.7.1 Development	19
i. Early embryonic development	19
ii. Developmental pathways	20
iii. Neonatal starvation	20

1.1.7.3 Ageing	21
i. Autophagic decline in ageing	21
ii. Interventions altering lifespan	21
iii. Mechanisms of ageing	22
1.1.8 Disease	23
1.1.8.1 Cancer	23
i. Tumour suppression	24
ii. Tumour progression	24
1.1.8.2 Neurodegeneration	26
i. Pathogenesis	26
ii. Therapeutic potential	28
1.1.8.2 Immunity and Inflammation	29
i. Xenophagy	29
ii. Inflammation	30
iii. Antigen recognition and presentation	31
iv. Immunological memory	31
1.1.9 Concluding remarks	32
1.4 Vinexin	33
1.2.1 Introduction	33
1.2.1.1 Isoform expression	33
1.2.1.1 Domain structure	34
i. SoHo domain	34
ii. SH3 domains	34
1.2.2 Cell biology	34
1.2.2.1 Actin cytoskeleton dynamics	34
i. Cell-extracellular matrix adhesion	34
ii. Cell-cell adhesion	37

iii.	Membrane ruffling	37
iv.	Cytokinesis	37
1.2.2.2	MAPK signalling	38
i.	JNK pathway	38
ii.	ERK pathway	38
iii.	EGFR pathway	39
1.2.2.3	Oestrogen receptor signalling	39
1.2.2.4	Lipid raft functions	40
1.2.3	Health and disease	40
1.2.3.1	Animal models	41
1.2.3.2	Cancer	42
i.	Proliferation	44
ii.	Migration and invasion	44
iii.	SRC-mediated transformation	44
1.2.3.3	Normal brain ageing	45
1.2.3.4	Neurodegeneration	45
1.2.4	Concluding remarks	46
1.5	YAP and TAZ	47
1.3.1	Introduction	47
1.3.1.1	Conserved domain structure	47
i.	TEAD-binding domain	47
ii.	14-3-3-binding domain	48
iii.	WW domain(s)	48
iv.	Transcriptional activation domain	48
v.	Coiled-coil domain	48
vi.	PDZ-binding domain	48
1.3.1.2	Non-conserved domain structure	49

i.	Proline-rich region	49
ii.	SH3-binding domain	49
1.3.2	YAP/TAZ transcriptional activity	49
1.3.2.1	TEAD transcription factor-mediated transcriptional activity	49
1.3.2.2	Non-TEAD transcription factor-mediated transcriptional activity	51
i.	RUNX transcription factors	51
ii.	p53-like transcription factors	51
iii.	T-Box transcription factors	52
iv.	PAX transcription factors	52
v.	NK2 homeobox 1	53
vi.	SMAD transcriptional modulators	53
1.3.3	Regulation	53
1.3.3.1	Hippo pathway-dependent regulation	54
i.	Proteasomal degradation	54
ii.	Cytosolic sequestration by 14-3-3	54
iii.	Cell-cell junction contributions	54
1.3.3.2	Hippo pathway-independent regulation	55
i.	Proteasomal degradation	55
ii.	Angiotensin-mediated regulation	55
iii.	Actomyosin-mediated mechanoregulation	56
iv.	RHO-mediated G protein-coupled receptor signalling	57
1.3.4	Normal physiology	58
i.	Early embryonic development	58
ii.	Organ size control	59
iii.	Cell fate determination	60
iv.	Regenerative responses	61
1.3.5	Disease	62
1.3.5.1	Genetic syndromes	62

1.3.5.2 Polycystic kidney disease	62
1.3.5.4 Cancer	63
i. Hepatocellular carcinoma	63
ii. Non-small cell lung cancer	64
iii. Breast cancer	64
iv. Epithelioid hemangioendothelioma	65
v. Chemotherapy resistance	65
1.3.6 Concluding remarks	65
<b>2 Materials &amp; Methods</b>	<b>67</b>
2.1 Cell culture	68
2.2 DNA expression	68
2.3 RNA interference	69
2.4 Pharmacological agents	70
2.5 Western blotting	70
2.6 Immunoprecipitation	71
2.8 Nuclear/cytosolic fractionation	73
2.8 F- to G-actin ratio assay	73
2.9 Microscopy	74
i. Immunofluorescence	74
ii. Image processing	75
iii. Automated fluorescence microscopy	75
iv. GFP-Htt(Q74) aggregation	75
2.10 Luciferase reporter assay	76
2.11 Clonogenic assay	76
2.12 Statistical analysis	76
2.13 Bioinformatics	77

i.	RNA sequencing data analysis	77
ii.	Microarray data analysis	78
<b>3</b>	<b>Vinexin is a physiologically important autophagy regulator</b>	<b>79</b>
3.1	Introduction	79
3.2	Vinexin beta depletion using siRNA against SORBS3 specifically upregulates autophagy	79
3.3	SORBS3 is transcriptionally upregulated and core autophagy genes transcriptionally downregulation in normal human brain ageing	85
3.4	Vinexin beta depletion using siRNA against SORBS3 promotes functional autophagy	89
3.5	Vinexin regulates autophagy independent of focal adhesion changes	95
3.6	Vinexin beta depletion does not upregulate autophagy via mTOR, ULK1, ERK1/2 or EGFR signalling	98
3.7	Concluding remarks	104
<b>4</b>	<b>Vinexin depletion upregulates autophagy through YAP/TAZ via a filamentous actin-dependent mechanism</b>	<b>106</b>
4.1	Introduction	106
4.2	siSORBS3 treatment increases YAP/TAZ activity upstream of autophagy	106
4.3	Autophagy upregulation upon vinexin beta depletion is YAP/TAZ-dependent	110
4.4	Vinexin beta depletion increases YAP/TAZ activity independent of Hippo signalling	110
4.5	siSORBS3 treatment alters actin cytoskeleton dynamics	114
4.6	Filamentous actin, and to a lesser extent actomyosin tension, contribute to YAP/TAZ nuclear translocation under siSORBS3 treatment	115
4.7	Autophagy upregulation upon vinexin beta depletion requires filamentous actin, but not actomyosin tension	119
4.8	siSORBS3 treatment alters actin cytoskeleton dynamics upstream of YAP/TAZ	123

4.9 Angiomotins counter YAP/TAZ nuclear translocation under siSORBS3 treatment by retaining YAP/TAZ in the cytosol	125
4.10 Altered actin cytoskeleton dynamics upon vinexin beta depletion prevent YAP/TAZ cytosolic sequestration by angiomotins	127
4.11 Autophagy upregulation upon vinexin beta depletion requires YAP/TAZ release from angiomotins	129
4.12 Concluding remarks	132
<b>5 Vinexin decreases hepatocellular carcinoma cell line tumorigenicity by negatively regulating YAP/TAZ activity and autophagy</b>	<b>136</b>
5.1 Introduction	136
5.2 SORBS3 mRNA expression is commonly downregulated in hepatocellular carcinoma	136
5.3 Vinexin-deficient HepG2 cells are unable to upregulate YAP/TAZ activity or downstream clonogenicity under siSORBS3 treatment	138
5.4 Vinexin alpha re-expression counters nuclear YAP/TAZ localisation in HepG2 cells	141
5.5 Vinexin deficiency drives autophagy in HepG2 cells	142
5.6 Vinexin negatively regulates clonogenicity in HepG2 cells	144
5.7 Concluding remarks	148
<b>6 Discussion</b>	<b>149</b>
6.1 Results summary	149
6.2 Outstanding questions	149
i. Does vinexin regulate autophagy through YAP/TAZ/TEAD transcriptional activity?	151
ii. How does siSORBS3 treatment increase F-actin bundles?	151
iii. Is decreased clonogenicity in ‘vinexin reconstituted’ HepG2 cells autophagy-dependent?	151

iv.	Does vinexin suppress cancer cell migration and invasion?	152
6.3	Vinexin integrates multiple tumorigenic processes	153
i.	YAP/TAZ transcriptional activity	153
ii.	Autophagy	153
iii.	Focal adhesion turnover	155
iv.	Other tumorigenic processes	156
6.4	Concluding remarks	156
<b>7</b>	<b>References</b>	<b>157</b>
<b>8</b>	<b>Appendix</b>	<b>183</b>
8.1	Abbreviations	183

# 1 Introduction

In this thesis I investigate the molecular mechanism through which vinexin regulates autophagy, which is relevant to diverse pathophysiological processes.

This introductory chapter comprises three sections: 1.1 introduces the autophagy pathway with regards to molecular machinery, regulatory pathways and pathophysiological associations, 1.2 reviews literature on the candidate autophagy regulator vinexin and 1.3 concerns the transcriptional coactivators YAP and TAZ, through which vinexin is shown in chapters 4 - 5 to regulate autophagy.

## 1.1 Autophagy

### 1.1.1 Introduction

The term 'autophagy' was coined by Christian de Duve in 1963 to describe vacuoles containing cytoplasmic components observed by electron microscopy (De Duve and Wattiaux, 1966). Macroautophagy (commonly referred to as autophagy) has subsequently emerged as an important mechanism for maintaining cellular homeostasis by trafficking cytoplasmic material for enzymatic degradation in the lysosome. Autophagy is both a constitutive process and subject to dynamic regulation by a range of physiological signals, including nutrient starvation (Ravikumar et al., 2010b). The degraded substrates are extremely diverse, ranging from organelles such as mitochondria, through to protein aggregates and invading microorganisms. Consequently, autophagy performs many functions in normal physiology, with dysregulated autophagy implicated in multiple human pathologies (Choi et al., 2013).

#### i. Macroautophagy

This dissertation (in common with most autophagy literature) concerns macroautophagy, as opposed to the other two autophagy types characterised in mammalian cells (chaperone-mediated autophagy and microautophagy). The macroautophagy pathway (summarised in Figure 1.1) entails formation of a cup-shaped, double-membraned phagophore (also referred to as the isolation membrane), which closes around cytoplasmic material to form a spherical, double-membraned autophagosome. The autophagosome outer membrane ultimately fuses with a lysosome to form an autolysosome, resulting in degradation of the inner autophagosome membrane and sequestered cargo (Bento et al., 2016b).

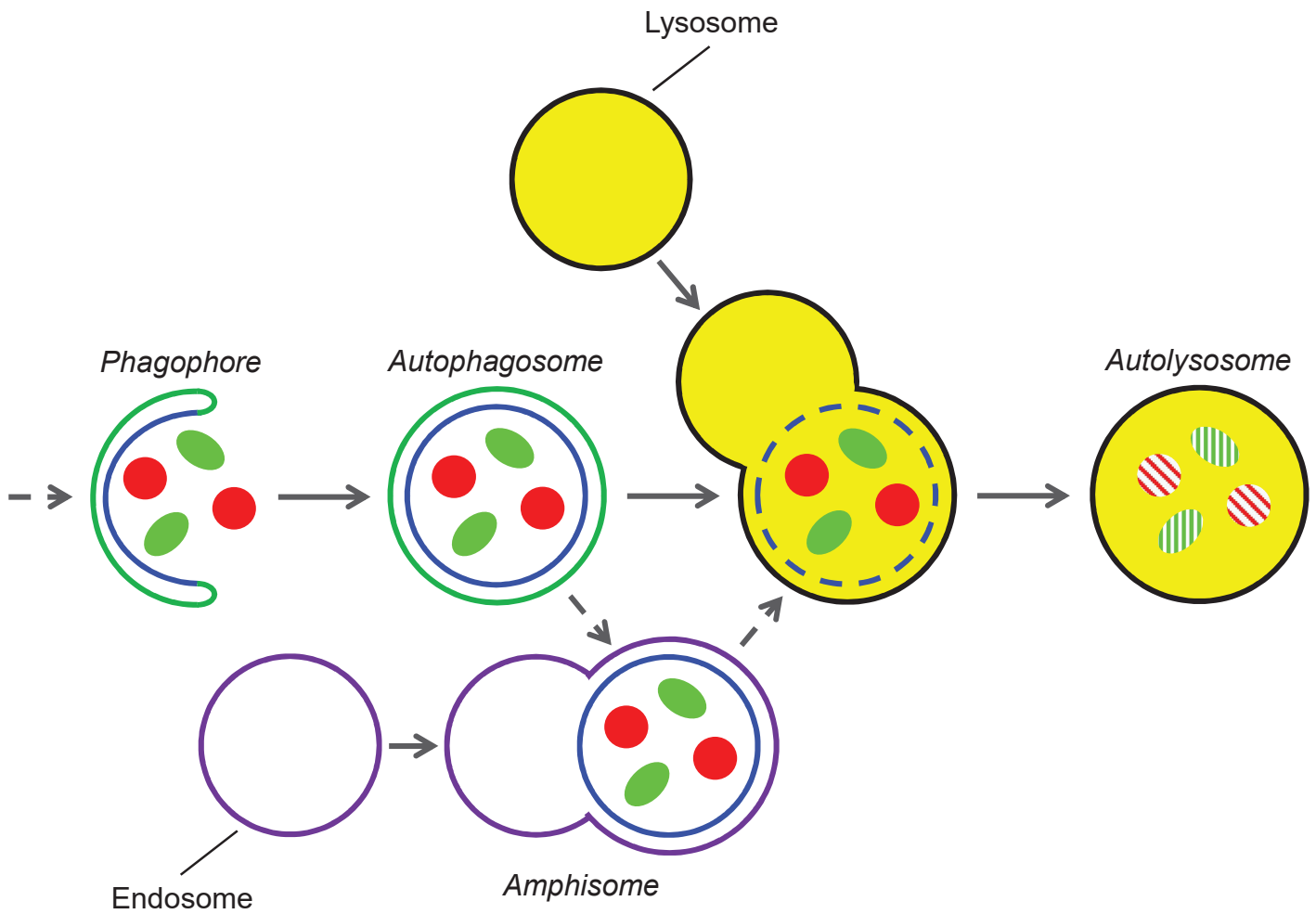


**Figure 1.1: macroautophagy pathway.**

Macroautophagy (commonly referred to as autophagy) involves the formation of double-membraned phagophores (also known as isolation membranes), which close around cytoplasmic cargo (red and green shapes) to form double-membraned autophagosomes. Autophagosome outer membranes (green) fuse with lysosomes to form autolysosomes. This results in the degradation of autophagosome inner membranes (blue) and sequestered cargo. Prior to fusion with lysosomes, autophagosomes may also fuse with endosomal vesicles to form amphisomes.

## **ii. Chaperone-mediated autophagy**

This pathway selectively targets proteins featuring KFERQ or 'KFERQ-like' pentapeptide motifs (Dice et al., 1986) that become accessible to the chaperone Hsc70 (Heat Shock Cognate protein of 70 kDa) due to (amongst other reasons) partial unfolding or dissociation from binding partners (Kaushik and Cuervo, 2012). Upon delivery to the lysosomal surface by Hsc70 (Chiang et al., 1989), substrate proteins bind the single-pass transmembrane protein LAMP2A (Lysosome-Associated Membrane Protein 2A) (Cuervo and Dice, 1996). This triggers substrate protein unfolding and LAMP2A multimerisation, followed by substrate protein translocation into the lysosome for degradation (Bandyopadhyay et al., 2008).

## **iii. Microautophagy**

The first stage in this pathway is lysosomal membrane invagination to form 'autophagic tubes' (Muller et al., 2000). Rapid scission events then produce intralysosomal microautophagic vesicles, which are degraded by lysosomal hydrolases (Kunz et al., 2004). Microautophagy remains poorly understood in mammalian cells; the pathway is thought to be non-selective, plus contribute to lysosomal membrane homeostasis and cell survival under certain starvation conditions (Li et al., 2012).

### ***1.1.2 Molecular machinery of autophagosome biogenesis***

The core autophagy proteins (referred to as ATG proteins in mammals) were identified through genetic screens in yeast, pioneered by the Ohsumi and colleagues (Harding et al., 1995; Klionsky et al., 2003; Thumm et al., 1994; Tsukada and Ohsumi, 1993). This molecular machinery is largely conserved in mammals, although there are important differences between autophagy pathways in yeast and mammalian cells (the latter being the focus of this dissertation) (Bento et al., 2016b). Autophagosome biogenesis (summarised in Figure 1.2) proceeds sequentially from phagophore initiation to closure, facilitated by multiple complexes featuring ATG proteins.

#### **i. Initiation: the ULK1 complex**

In mammalian cells, interaction between ULK1 (Unc-51-Like autophagy activating Kinase 1, equivalent to yeast Atg1p) and the large scaffolding protein FIP200 (FAK family-Interacting Protein of 200 kDa) is mediated by ATG13 (Ganley et al., 2009; Hosokawa et al., 2009a; Jung et al., 2009). This complex is completed by ATG101, which interacts with ULK1 in an ATG13-dependent manner (Hosokawa et al., 2009b; Mercer et al., 2009). Recruitment to

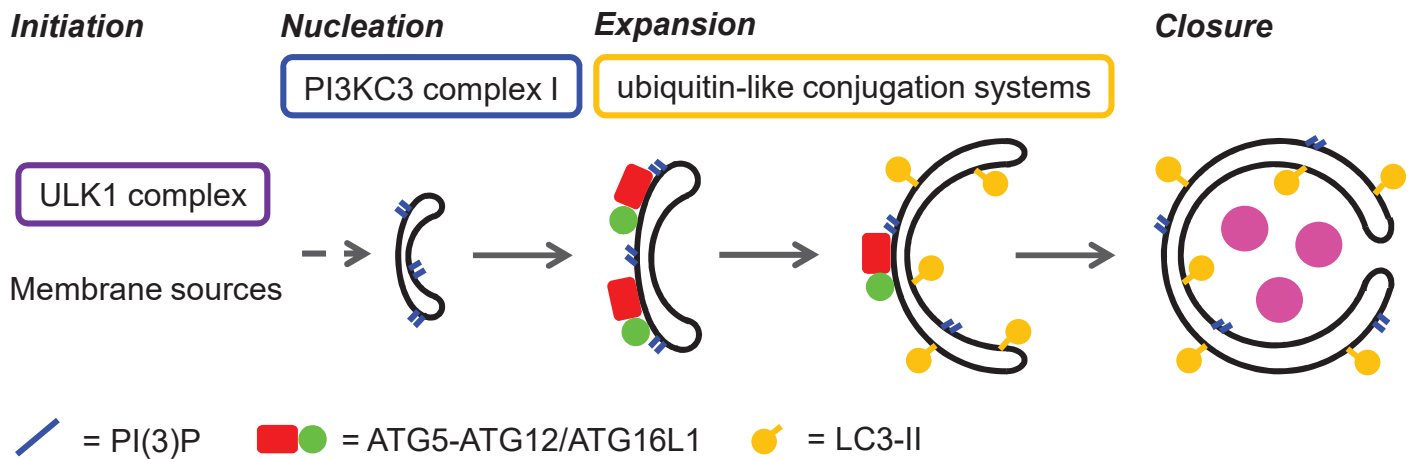


**Figure 1.2: autophagosome biogenesis pathway.**

Autophagosome formation is initiated by the ULK1 complex, which comprises the serine/threonine kinase ULK1, FIP200, ATG13 and ATG101. Initiation is followed by membrane nucleation, which involves PI3KC3 complex I synthesising PI(3)P (phosphatidylinositol 3-phosphate) at phagophore initiation sites. PI3KC3 complex I comprises Beclin 1, ATG14, VPS34 (catalytic subunit) and VPS15. Two ubiquitin-like conjugation reactions then drive membrane expansion: 1. ATG12 is conjugated to ATG5, enabling the ATG5-ATG12 conjugate to form multimeric complexes with ATG16L1, 2. cytosolic LC3-I is conjugated to the membrane phosphoglycerolipid PE (phosphatidylethanolamine) to form membrane-associated LC3-II. Finally the phagophore closes around cargoes (pink circles) to form a completed autophagosome.

phagophore initiation sites requires the ULK1 C-terminal domain (now referred to as the early autophagy targeting/tethering domain) (Chan et al., 2009a). Although less well characterised than Atg1 complex localisation in yeast, ULK1 complex localisation is similarly influenced by multiple protein-protein interactions (Hurley and Young, 2017). For example, C9orf72 interacts with the ULK1 complex (binding ULK1, ATG13 and FIP200) and the small GTPase RAB1A, thereby promoting RAB1A-dependent trafficking of the ULK1 complex to the isolation membrane initiation sites (Webster et al., 2016).

Following ULK1 activation (see section 1.1.6 below), the serine/threonine kinase phosphorylates numerous substrates at consensus motifs characterised by hydrophobic residues surrounding a serine phosphorylation site (Egan et al., 2015). Importantly, ULK1 phosphorylates Beclin 1 (equivalent to yeast Atg6p) at serine 14, together with serine 249 on the class III phosphatidylinositol 3-kinase (PI3KC3) catalytic subunit VPS34, thereby promoting autophagosome biogenesis *via* PI3KC3 complex I activation (Egan et al., 2015; Russell et al., 2013). Comprising around 90% non-enzymatic domains, the ULK1 complex seems likely to perform additional ULK1 kinase activity-independent functions in autophagy (Lin and Hurley, 2016). For instance, ATG13 and FIP200 have been shown to function cooperatively to induce autophagy in ULK1/2 depleted cells (Alers et al., 2011).

## **ii. Membrane nucleation: PI3KC3 complex I**

The tetrameric class III phosphatidylinositol 3-kinase (PI3KC3) complex I comprises the catalytic and regulatory subunits VPS34 and VPS15, together with Beclin 1 and ATG14 (the latter replaced by UVRAG in PI3KC3 complex II) (Itakura et al., 2008). PI3KC3 complex I generates phosphatidylinositol 3-phosphate (PI(3)P) at phagophore initiation sites (Backer, 2016). This function requires ATG14/Beclin 1 binding, which facilitates PI3KC3 complex I localisation and enhances VPS34 kinase activity (Matsunaga et al., 2009; Zhong et al., 2009).

PI(3)P clustering on developing phagophores creates platforms for recruiting downstream autophagic machinery. For example, the PI(3)P-binding protein WIPI2 (WD repeat domain Phosphoinositide-Interacting Protein 2) localises ATG16 to developing phagophores, thereby recruiting the ATG5-ATG12 complex and driving further membrane expansion (Dooley et al., 2014). The biophysical properties of PI(3)P are also thought to contribute to phagophore sculpting (Bento et al., 2016b). Nonetheless, noncanonical autophagy can occur when VPS34 kinase activity is inhibited; PI(5)P (synthesised by the class III phosphatidylinositol 5-kinase

PIKfyve) can perform functions in autophagosome biogenesis previously ascribed solely to PI(3)P (Vicinanza et al., 2015).

Numerous regulatory proteins influence PI3KC3 complex I activity, predominantly by interacting with Beclin 1. These include antiapoptotic BCL2 family proteins (BCL2, BCL2L1, BCL2L2 and MCL1), which bind Beclin 1 and inhibit VPS34 kinase activity (Oberstein et al., 2007; Pattingre et al., 2005). Beclin 1 is also phosphorylated by multiple kinases (see section 1.1.6 below).

### **iii. Membrane expansion: ubiquitin-like conjugation systems**

Yeast Atg12p was found to covalently bind Atg5p, much as ubiquitin tags substrates (Mizushima et al., 1998). This discovery led to the first characterisation of mammalian ATG proteins; human ATG12 and ATG5 were shown to conjugate *via* reactions analogous to those in yeast (Mizushima et al., 1998b). First the carboxyl-terminal glycine of ATG12 is activated by ATG7 (functioning as an E1-like enzyme), then ATG12 is transferred to ATG10 (functioning as an E2-like enzyme) and finally onto an internal lysine of ATG5 (Mizushima et al., 1998b). The ATG5-ATG12 conjugate forms a multimeric complex with ATG16L1, which binds ATG5 and other ATG16L1 monomers (Mizushima et al., 2003). ATG5-ATG12/ATG16L1 remains associated with autophagic membranes until autophagosome maturation and is required for LC3 (microtubule associated protein 1 Light Chain 3, equivalent to yeast Atg8p) localisation to the expanding phagophore (Mizushima et al., 2003; Mizushima et al., 2001).

Mature LC3 exists in two forms; non-lipidated LC3-I in the cytosol and phosphatidylethanolamine (PE)-conjugated LC3-II on autophagic membranes (Kabeya et al., 2000). This second ubiquitin-like reaction was the first example of protein-phosphoglycerolipid conjugation to be discovered and explains how hydrophilic LC3 is able to associate with autophagic membranes (Ichimura et al., 2000). The reaction begins with ATG4B cleaving nascent LC3 to reveal a carboxyl-terminal glycine (Hemelaar et al., 2003). The resultant LC3-I is activated by ATG7 (again functioning as an E1-like enzyme), transferred to ATG3 (functioning as an E2-like enzyme) and finally onto PE to produce LC3-II (Tanida et al., 2002; Tanida et al., 2001). LC3-II specifically associates with the expanding phagophore and remains associated until after lysosomal fusion, hence providing a useful readout for the whole autophagy pathway (Klionsky et al., 2012).

#### **iv. Phagophore closure**

During closure of double-membraned phagophores to form double-membraned autophagosomes, the inner and outer autophagic membranes become separate entities. Knorr and colleagues therefore argue phagophore closure constitutes a membrane scission event (Knorr et al., 2015). The protein complexes involved remain to be characterised, though ATG2A and ATG2B (localised to developing phagophores) are thought to be required (Velikkakath et al., 2012). ATG2A/B double knockdown leads to an accumulation of autophagic membranes, which are suggested by protease protection assay to be unclosed phagophores (Velikkakath et al., 2012).

ATG4B cleaves other ATG8 family proteins in addition to LC3: GABARAP, GABARAPL1 and GABARAPL2, which are also homologous to yeast pAtg8 (Hemelaar et al., 2003). As with LC3, ATG4B-mediated cleavage is a prerequisite for ATG8 protein lipidation and also appears necessary for phagophore closure (Fujita et al., 2008). Overexpressing mutant ATG4B lacking protease activity causes unclosed autophagic structures to accumulate. Hence, Fujita and colleagues suggest that ATG8 family protein lipidation is essential for isolation membrane closure (Fujita et al., 2008).

##### ***1.1.3 Membrane sources in autophagosome biogenesis***

The autophagy literature remains divided on the membrane sources utilised in autophagosome biogenesis. One possibility is that preautophagosomal membrane derives from one pre-existing organelle. Alternatively, membrane from multiple sources might coalesce; either *de novo* or during maturation following initial biogenesis from one pre-existing organelle (Bento et al., 2016b).

A popular hypothesis is that the endoplasmic reticulum (ER) provides a platform for accumulating the protein complexes and PI(3)P required for autophagosome biogenesis (Axe et al., 2008; Hayashi-Nishino et al., 2009). However, whether isolation membranes derive directly from the ER or represent closely apposed (but separate) membrane compartments remains unclear. As does whether all autophagosomes originate in this way, or only a sub-population under certain conditions (Axe et al., 2008; Hayashi-Nishino et al., 2009).

The outer mitochondrial membrane has also been implicated in autophagosome biogenesis. Hailey and colleagues report this membrane is continuous with developing phagophores, meaning autophagosomes can originate directly from mitochondria (Hailey et al., 2010).

Subsequently, the Yoshimori group have suggested autophagosomes derive from mitochondria-associated ER membrane (Hamasaki et al., 2013). Hence, the literature cited above might be reporting the same phenomena observed from different perspectives. Specifically, Hamasaki et al. describe that the PI3KC3 complex I component ATG14 is recruited to ER-mitochondria contact sites by the ER-resident SNARE syntaxin 17, thereby facilitating autophagosome biogenesis (Hamasaki et al., 2013).

Endocytic pathways are also associated with autophagosome biogenesis, contributing preautophagosomal membrane originating from the plasma membrane and recycling endosome. ATG16L1-positive autophagosome precursors are reported to derive from the plasma membrane *via* clathrin-mediated endocytosis, before undergoing homotypic fusion mediated by VAMP7 and partner SNAREs (syntaxin 7, syntaxin 8 and VTI1B) (Moreau et al., 2011; Ravikumar et al., 2010a). mATG9 (the only known mammalian transmembrane ATG protein) is suggested to traffic from distinct clathrin-coated vesicles at the plasma membrane *via* early endosomes, before joining ATG16L1 at recycling endosomes (Puri et al., 2013). Here ATG16L1-positive and mATG9-positive autophagosome precursors undergo heterotypic fusion, this time with the R-SNARE VAMP3 as a critical mediator (Puri et al., 2013).

The endoplasmic reticulum-Golgi intermediate compartment (ERGIC) has also been proffered as a preautophagosomal membrane source (Ge et al., 2013; Ge et al., 2014; Tan et al., 2013). The Schekman group report that ERGIC recruits the PI3KC3 complex I component ATG14, together with the COPII coatomer complex in a VPS34 activity-dependent manner (Ge et al., 2013; Ge et al., 2014). This induces budding of LC3 lipidation-active vesicles from ERGIC, which could contribute to contribute to autophagosome biogenesis (Ge et al., 2014).

#### ***1.1.4 Autophagy cargo receptors***

Autophagy targets certain substrates (including protein aggregates, damaged organelles and invading microorganisms) for degradation through adapter proteins characterised by the ability to: 1. recognise cargo and 2. target the isolation membrane (Zaffagnini and Martens, 2016).

The first cargo receptor investigated was p62 (also known as sequestosome 1), which binds substrates such as polyubiquitinated protein aggregates and intracellular bacteria coated with ubiquitinated proteins using a C-terminal ubiquitin-associated domain (Bjorkoy et al., 2005;

Ciani et al., 2003; Zheng et al., 2009). In common with other cargo receptors, p62 targets the isolation membrane using an LC3-Interacting Region (LIR) motif (Pankiv et al., 2007). Although non-canonical LIR motifs have been identified, LIR motifs typically feature the consensus sequence  $\Theta xx\Gamma$  ( $\Theta$  is an aromatic residue,  $\Gamma$  is hydrophobic and x is any other residue) (Zaffagnini and Martens, 2016). p62 contains just one LIR motif, but is thought to cluster these motifs through oligomerisation to generate high-avidity reactions with LC3 (Wurzer et al., 2015).

Other cargo receptors include NDP52 and optineurin, which facilitate autophagic degradation of both invading bacteria (xenophagy) (Thurston et al., 2009; Wild et al., 2011) and damaged mitochondria (mitophagy) (Lazarou et al., 2015). These receptors have recently been ascribed functions beyond cargo recognition and targeting. NDP52 and optineurin are suggested to recruit autophagy initiating machinery (as in ULK1 and WIPI1) to phosphorylated ubiquitin-tagged mitochondria, thereby driving cargo-induced autophagosome biogenesis (Lazarou et al., 2015).

### ***1.1.5 Late stage autophagy***

In order for autophagy substrates to undergo degradation, autophagosomes must intersect the endolysosomal pathway. Most autophagy literature refers to autolysosome formation through autophagosome-lysosome fusion. However, autophagosome-endosome fusion (producing ‘amphisomes’; see Figure 1.1) has long been recognised (Gordon and Seglen, 1988), with the term amphisome now describing an increasing heterogeneous population of vesicles containing both autophagic and endocytic components. In both cases, endosomal maturation (acidification, together with acquisition of hydrolases and membrane proteins) (Huotari and Helenius, 2011) enables flux through the autophagy pathway by producing competent lysosomes.

The delivery of autophagy cargo to lysosomes is thought to feature the same processes as endocytic trafficking and fusion. Specifically, cytoskeleton-dependent transport mechanisms bring autophagosomes and endosomes/lysosomes together, then fusion occurs driven by RAB GTPases, tethering factors and SNAREs functioning sequentially (Ganley, 2013).

#### **i. Vesicular trafficking**

While most lysosomes localise to the perinuclear region, autophagosomes form randomly throughout the cytoplasm (Jager et al., 2004; Jahreiss et al., 2008). Hence, disrupting

microtubule-dependent movement of autophagosomes towards the nucleus (microtubule minus end) using nocodazole treatment reduces autolysosome formation (Jahreiss et al., 2008). Destabilising the microtubule cytoskeleton with nocodazole also impairs autophagosome-endosome fusion (Kochl et al., 2006). Several motor proteins are linked to autophagosome transport along microtubules. For example, inhibiting dyneins (minus end-directed microtubule motors), either pharmacologically or genetically, impairs autophagosome-lysosome fusion and hence clearance of aggregate-prone proteins (Ravikumar et al., 2005).

Dyneins appear to function in concert with plus end-directed microtubule motors such as KIF5B (kinesin family member 5B) to optimise autophagosome movement (Cardoso et al., 2009). The RAB7 effector FYCO1 (FYVE and coiled-coil domain containing 1) is reported to recruit kinesins to autophagosomes; FYCO1 overexpression redistributes LC3/RAB7 double positive vesicles to the cell periphery in a microtubule-dependent manner, while FYCO1 knockdown has the opposite effect (Pankiv et al., 2010).

In addition to microtubules, autophagosome also move along actin filaments. Tumbarello and colleagues report that myosin VI (minus end-directed actin motor) promotes autophagosome maturation and ultimately autophagosome-lysosome fusion by delivering endosomes to autophagosomes (Tumbarello et al., 2012). This is facilitated by WWY and RRL motifs in the Myosin VI C-terminus, which bind Tom1 on endosomes and autophagy cargo receptors (NDP52, T6BP and optineurin) respectively (Tumbarello et al., 2012).

## **ii. Autophagosome-endosome/lysosome fusion**

As well as functioning in microtubule-dependent trafficking, RAB7 (a small GTPase, also known as RAB7A) localised to outer autophagic membranes participates in autophagosome maturation and autophagosome/lysosomal fusion. This was simultaneously published by two independent research groups; cells overexpressing dominant negative RAB7 (threonine 22 mutated to asparagine) or treated with siRNA against *RAB7A* are reported to accumulate autophagosomes that seem incompetent to fuse with lysosomes (Gutierrez et al., 2004b; Jager et al., 2004). RAB7 regulates autolysosome formation through effector proteins. These include the Beclin 1 interactor Rubicon, which negatively regulates autophagosome maturation by complexing RAB7 with the UVRAG-containing PI3KC3 complex II (Matsunaga et al., 2009; Tabata et al., 2010).

UVRAG (UV radiation Resistance-Associated Gene) can also regulate late stage autophagy in a Beclin 1-independent manner; recruiting both RAB7 and the tethering complex HOPS (homotypic fusion and vacuole protein sorting) to autophagosomes, as well as enhancing RAB7 GTPase activity (Liang et al., 2008a). In this way, UVRAG promotes autophagosome-endosome/lysosome fusion. This concurs with Wartosch and colleagues' more recent finding that all six HOPS complex subunits (VPS11, VPS16, VPS18, VPS39, VPS41 and VPS33A) are essential for autolysosome formation (Wartosch et al., 2015). Another potential tethering factor in autophagosome-lysosome fusion is the lysosomal protein TECPR1, which interacts with conjugated ATG5-ATG12 and PI(3)P on autophagosomes (Chen et al., 2012). As TECPR1 and ATG16L1 form mutually exclusive complexes with ATG5-ATG12, Chen et al. propose TECPR1 initiates autophagosome-lysosome fusion by bringing mature (ATG16L1-negative) autophagosomes into close proximity with lysosomes.

In addition to UVRAG, the HOPS complex is recruited to autophagosomes by PLEKHM1 (McEwan et al., 2015). This RAB7 effector localises to outer autophagic membranes *via* LIR motif-mediated interactions with ATG8 family proteins (McEwan et al., 2015). Accordingly, *Plekhm1* knockout mouse embryonic fibroblasts (MEFs) exhibit impaired flux through the autophagy pathway (McEwan et al., 2015). Another role suggested for ATG8 family proteins (specifically GABARAP and GABARAPL2) in late stage autophagy is recruiting PI4K2A (phosphatidylinositol 4-kinase type 2 alpha) to generate PI(4)P on autophagosomes (Wang et al., 2015). To explain PI4K2A depletion blocking autolysosome formation and acidification, Wang et al. hypothesise that clustered PI(4)P creates platforms on which proteins concerned with autophagosome maturation and autophagosome-endosome/lysosome fusion can operate.

In common with other vesicle fusion events, autophagosome-endosome/lysosome fusion is ultimately mediated by SNARE (soluble *N*-ethylmaleimide-sensitive factor attachment protein receptors) complexes. The Mizushima group have identified the target SNAREs (t-SNAREs) syntaxin 17 and SNAP29 on autophagosomes, which complex with the vesicle SNARE (v-SNARE) VAMP8 on endosomes/lysosomes to drive fusion (Itakura et al., 2012). Subsequently, Diao and colleagues have reported this processes is facilitated by the PI3KC3 complex I component ATG14 (Diao et al., 2015). Oligomeric ATG14 binds syntaxin 17, thereby stabilising the binary t-SNARE complex with SNAP29 and promoting interaction with VAMP8 (Diao et al., 2015). Importantly, syntaxin 17 only localises to the outer membrane of closed autophagosomes (as opposed to unclosed phagophores) (Itakura et al.,

2012). This serves to prevent premature fusion events, though how specificity this is achieved remains unknown.

Other v-SNAREs are also linked to autophagosome-endosome/lysosome fusion. For example, Fader et al. find that VAMP3 and VAMP7 are required for amphisome and autolysosome formation, respectively (Fader et al., 2009). Moreover, depleting cells of the lysosomal SNARE VTI1B impairs autophagosome-lysosome fusion and consequently clearance of group A streptococcus by xenophagy (Furuta et al., 2010). Whether these v-SNAREs work in concert with syntaxin 17/SNAP29 in the same manner as VAMP8 remains to be investigated.

### ***1.1.6 Regulation***

Numerous pathways regulate autophagy through mTOR (mammalian target of rapamycin) signalling (summarised in Figure 1.3), thereby coupling various growth and proliferation pathways to energy balance at the cellular and whole organism level (Zoncu et al., 2011b). Research into mTOR-independent autophagy modulators has been driven by mTOR signalling having many autophagy-independent functions. This in turn has resulted in several mTOR-independent autophagy regulation mechanisms being characterised (summarised in Figure 1.4).

#### **i. mTOR-dependent regulation**

Nutrient starvation is the primordial autophagy activator. Amino acid deprivation has long been known to upregulate autophagy in both cultured cells and animal models (Mitchener et al., 1976; Mortimore and Schworer, 1977). In this way, autophagic degradation contributes cellular energy homeostasis by releasing amino acids for gluconeogenesis and other metabolic pathways.

Using hepatocytes isolated from starved rats, the Meijer group discovered that ribosomal protein S6 phosphorylation correlates with the decrease in autophagy upon amino acid repletion. The immunosuppressive rapamycin, which indirectly inhibits S6 phosphorylation by antagonising mTOR function, was then shown to induce autophagy (Blommaert et al., 1995). This work uncovered the role of mTOR signalling in autophagy regulation and established rapamycin as the first mTOR-dependent autophagy inducer.

mTOR is the catalytic subunit in mTOR complex 1 (mTORC1) and mTOR complex 2 (mTORC2), the former being more commonly studied in autophagy regulation. In addition to

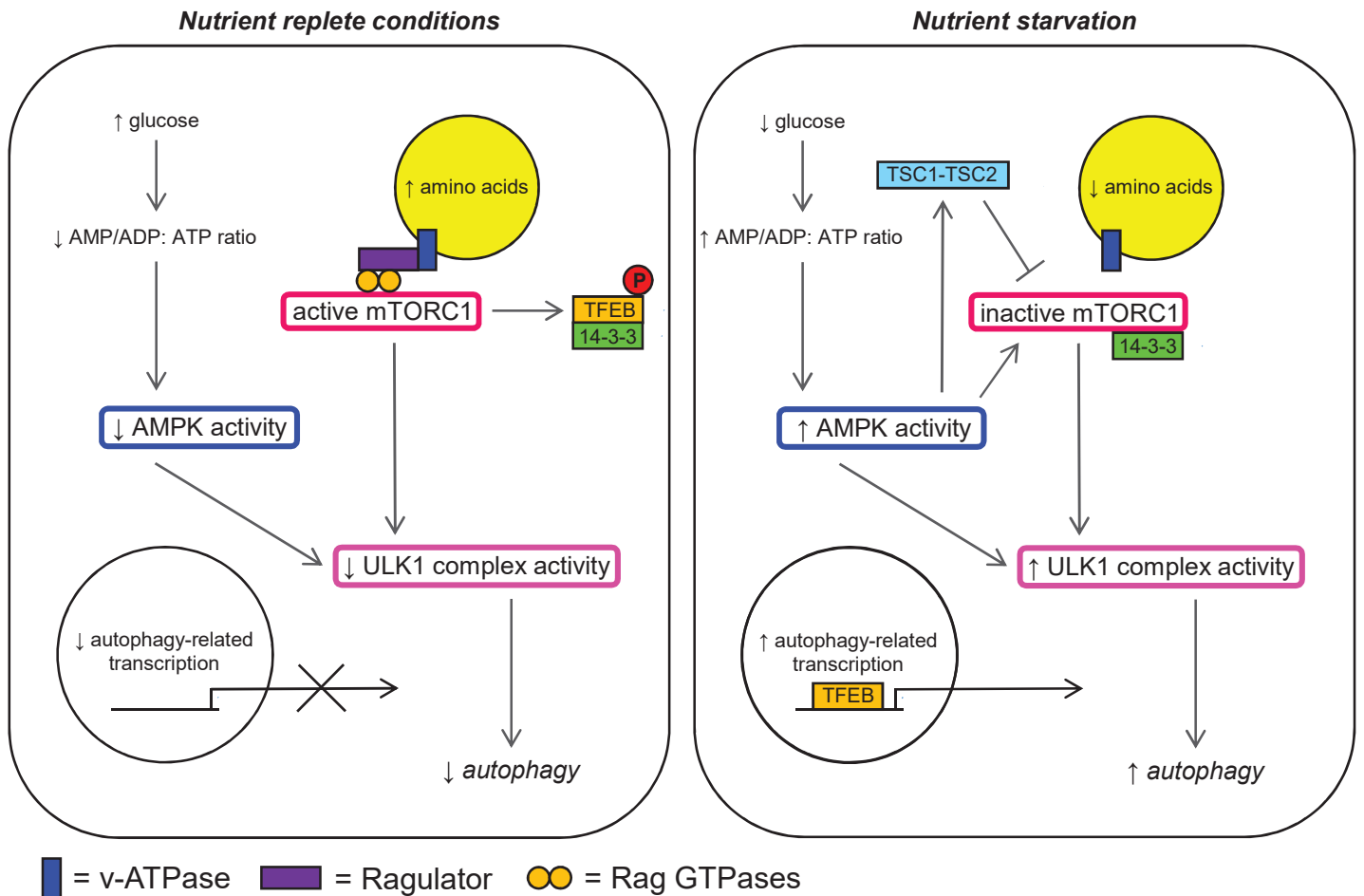


**Figure 1.3: mTOR-dependent autophagy regulation.**

Schematic diagram summarising pathways regulating autophagy through mTORC1 (mTOR complex 1) using example scenarios in which mTORC1 is activated (nutrient replete conditions; left panel) and inactivated (nutrient starvation; right panel). Under nutrient replete conditions amino acids accumulate in the lysosome (yellow circle), causing v-ATPase (vacuolar H<sup>+</sup>-transporting ATPase) to interact with Ragulator. This scaffolding complex localises Rag GTPases to the lysosomal surface, which results in mTORC1 recruitment and activation. mTORC1 inhibits the ULK1 autophagy initiation complex both directly *via* phosphorylation at inhibitory sites and indirectly by inhibiting phosphorylation at activating sites by AMPK (AMP-activated protein kinase). mTORC1 also phosphorylates TFEB (transcription factor EB), which promotes binding to 14-3-3 proteins in the cytoplasm. This prevents TFEB translocation into the nucleus (white circle) and reduces autophagy-associated transcription. Under nutrient starvation, glucose deficiency increases the cellular AMP/ADP:ATP ratio. This activates AMPK, which promotes autophagy initiation through ULK1 complex phosphorylation at activating sites. AMPK also downregulates mTORC1 activity both directly by phosphorylating Raptor (mTORC1 component) to induce mTORC1/14-3-3 cytoplasmic sequestration and indirectly by enhancing TSC1-TSC2 complex-mediated mTORC1 antagonism.

mTOR, mTORC1 comprises Raptor (regulatory-associated protein of mTOR) complexed with the positive regulator mLST8 and negative regulators Deptor and AKT1S1 (also known as PRAS40) (Zoncu et al., 2011b).

How amino acid availability influences mTORC1 activity has been extensively studied by the Sabatini group, amongst others. Under nutrient replete conditions, amino acids accumulate in the lysosome. This causes the vacuolar H<sup>+</sup>-transporting ATPase (v-ATPase), which spans the lysosomal membrane, to interact with the Ragulator scaffolding complex in an ATP hydrolysis-dependent manner (Zoncu et al., 2011a). Ragulator (comprising LAMPTOR1 – 5) localises Rag GTPases to the lysosomal surface and is required for the lysosomal recruitment of mTORC1 under amino acid stimulation (Sancak et al., 2010). Functioning as heterodimers, the Rag GTPases (RagA - D) interact with mTORC1 by binding Raptor, thereby enhancing mTOR activity in response to amino acid availability (Sancak et al., 2008). This function appears to be GTPase activity-dependent as constitutively active (GTP-bound) RagA restores mTORC1 activity in HEK 293 cells under amino acid depletion, as well as promoting cell and organ growth in *Drosophila* (Kim et al., 2008).

One important mechanism through which mTORC1 suppression under amino acid starvation upregulates autophagy is ULK1 complex dephosphorylation at inhibitory phosphorylation sites. This increases ULK1 kinase activity and hence, autophagosome formation (see section 1.1.2). Under nutrient replete conditions, mTORC1 associates with the ULK1 complex and phosphorylates both ULK1 and ATG13 (Ganley et al., 2009; Hosokawa et al., 2009a; Jung et al., 2009). This interaction is reduced upon autophagy induction using amino acid depletion or rapamycin treatment, leading to ULK1 and ATG13 dephosphorylation (Ganley et al., 2009; Hosokawa et al., 2009a; Jung et al., 2009). Murine Ulk1 serine 757 (equivalent to serine 758 in human ULK1) in particular has been identified as an important residue in ULK1 complex inhibition by mTORC1, possibly because serine 757 phosphorylation inhibits Ulk1 phosphorylation at activating sites by AMPK (Kim et al., 2011a). Phosphatases such as PP2A are also implicated in ULK1 regulation, with the phosphatase inhibitor okadaic acid shown to impair autophagosome biogenesis under amino acid starvation (Wong et al., 2015). However, the specific phosphatase for Ulk1 serine 757 remains unidentified.

In addition to amino acid depletion, other metabolic stressors such as glucose starvation can induce autophagy. Such stressors increase the cellular AMP/ADP: ATP ratio, which activates AMPK (Hardie et al., 2012). As already mentioned, AMPK can activate the ULK1 complex

(and hence autophagosome biogenesis) by directly phosphorylating ULK1 (Egan et al., 2011; Kim et al., 2011a). For example, Egan et al. report AMPK phosphorylation of serine 555 in murine Ulk1 (equivalent to serine 556 in human ULK1) is required for mitophagy and cell survival under nutrient starvation (Egan et al., 2011).

Moreover, AMPK can promote autophagy by directly downregulating mTORC1 activity. This is mediated through AMPK phosphorylating Raptor, which is suggested to inhibit mTORC1 activity by inducing Raptor binding to 14-3-3 scaffolding proteins (Gwinn et al., 2008). AMPK also indirectly reduces mTORC1 activity by phosphorylating TSC2 and enhancing mTORC1 antagonism mediated through the TSC1-TSC2 complex (Gao et al., 2002; Inoki et al., 2003).

Transcriptional regulation is an emerging field in autophagy research (Fullgrabe et al., 2016). In this regard, mTORC1 is reported to downregulate TFEB (transcription factor EB)-mediated transcription (Pena-Llopis et al., 2011; Roczniak-Ferguson et al., 2012). TFEB has been described as a lysosomal biogenesis master regulator and also promotes transcription of autophagy genes such as UVRAG and WIPI1 (Sardiello et al., 2009; Settembre et al., 2011). mTORC1 is suggested to interact with TFEB on the lysosomal surface and phosphorylate TFEB serine 211 (Roczniak-Ferguson et al., 2012). Roczniak-Ferguson et al. suggest this prevents TFEB nuclear translocation under nutrient replete conditions by promoting TFEB binding to 14-3-3 proteins in the cytoplasm. However, other kinases may also function as physiologically important TFEB regulators.

## **ii. mTOR-independent regulation**

By screening 253 compounds approved for human use, with aggregate-prone protein (well-characterised autophagy substrate) clearance as the primary readout, our lab identified several mTOR-independent autophagy modulators (Williams et al., 2008). This resulted in the characterisation of two interconnected mTOR-independent autophagy regulation pathways.

L-type  $\text{Ca}^{2+}$  channel antagonists such as verapamil and loperamide were shown to induce autophagy, while the L-type  $\text{Ca}^{2+}$  channel agonist Bay K8644 had the opposite effect (Williams et al., 2008). This requires calpain proteases; decreased cytosolic  $\text{Ca}^{2+}$  concentrations (caused by treatment with L-type  $\text{Ca}^{2+}$  channel antagonists) are well known to inhibit calpain activity (Ono and Sorimachi, 2012), which in turn upregulates autophagy.

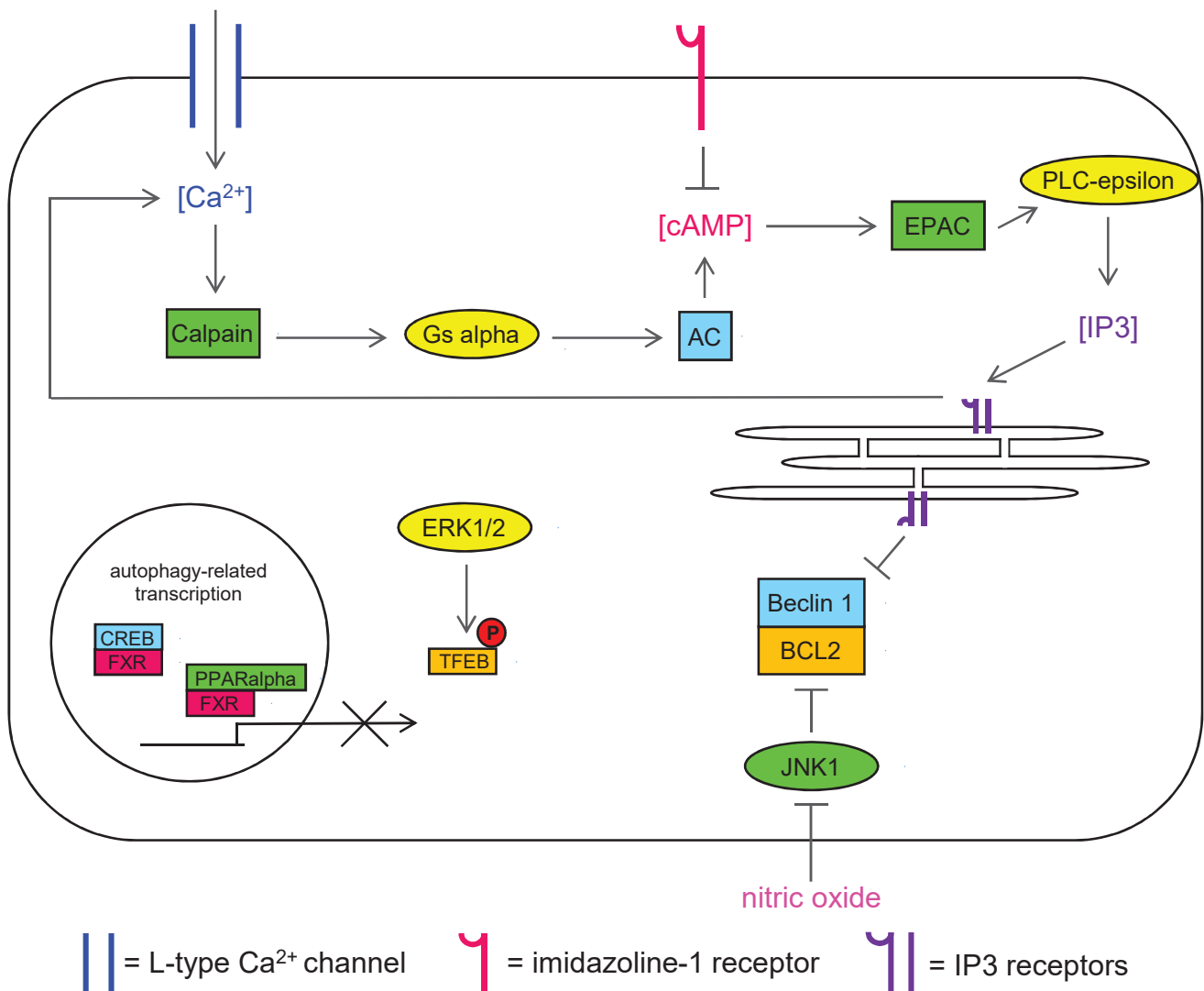


#### Figure 1.4: mTOR-independent autophagy regulation.

Schematic diagram summarising mTOR-independent autophagy regulating pathways. Lower cytosolic Ca<sup>2+</sup> concentrations upregulate autophagy dependent on inhibiting calpain protease activity. In addition to L-type Ca<sup>2+</sup> channel antagonists, cytosolic Ca<sup>2+</sup> concentrations are reduced by I1R (imidazoline-1 receptor) agonists. These decrease cAMP levels, which signals through EPAC guanine nucleotide exchange factors to inhibit PLC-epsilon activity and reduce IP3 (inositol 1,4,5-trisphosphate) synthesis. Lower IP3 levels result in less Ca<sup>2+</sup> release into the cytosol *via* IP3 receptors on the ER. This pathway is cyclical because calpains cleave Gs alpha (stimulator G protein alpha subunit), which stimulates AC (adenylate cyclase) and increases cAMP levels. IP3 receptors can also upregulate autophagy independent to cytosolic Ca<sup>2+</sup> concentrations, possibly by preventing Beclin 1/BCL2 binding that disrupts the autophagy membrane nucleating PI3KC3 complex I. Another mTOR-independent autophagy regulation mechanism involves nitric oxide inhibiting JNK1 (c-Jun N-terminal Kinase) activity through direct S-nitrosylation. In the absence of nitric oxide, JNK1 upregulates autophagy through preventing Beclin 1/BCL2 binding. With regards to transcriptional regulation, in addition to mTORC1, TFEB downregulation can be mediated by ERK1/2 (Extracellular signal-Regulated Kinase 1/2). The nuclear receptor FXR (Farnesoid X Receptor) also downregulates autophagy-related transcription by antagonising CREB (cAMP Response Element Binding) transcriptional factors and/or competing with the nuclear receptor PPARalpha (Peroxisome Proliferator-Activated Receptor alpha).

Cytosolic  $\text{Ca}^{2+}$  concentrations are also reduced by I1R (imidazoline-1 receptor) agonists such as clonidine and rilmenidine. These compounds decrease cAMP levels, thereby signalling through EPAC guanine nucleotide exchange factors to inhibit PLC-epsilon activity (Wang et al., 2017). PLC-epsilon hydrolyses plasma membrane PIP2 (phosphatidylinositol 4,5-bisphosphate) to IP3 (inositol 1,4,5-trisphosphate) and DAG (diacylglycerol), with IP3 acting at receptors on the ER to promote  $\text{Ca}^{2+}$  release into the cytosol (Dusaban and Brown, 2015). In this way, I1R agonists were shown to upregulate autophagy and consequently, aggregate-prone protein clearance by inhibiting calpain activity (Williams et al., 2008). Since calpain proteolysis stimulates adenylate cyclase activity (thereby increasing cAMP levels) through Gs alpha (stimulator G protein alpha subunit) cleavage (Sato-Kusubata et al., 2000), these two interconnected pathways represent an mTOR-independent autophagy regulating cycle (Williams et al., 2008).

In addition to I1R agonists, IP3 levels are also decreased by mood stabilisers such as lithium, sodium valproate and carbamazepine that cause inositol depletion (Williams et al., 2002). Lithium is reported to induce autophagy without affecting mTORC1 activity by inhibiting inositol monophosphatase, which depletes free inositol and decreases IP3 levels (Sarkar et al., 2005). This can now be attributed to calpain inhibition resulting from reduced  $\text{Ca}^{2+}$  release *via* IP3 receptors (IP3R) on the ER.

The IP3R has also been shown to modulate autophagy directly; IP3R knockdown or pharmacological inhibition with xestospongine B induces autophagy independent of alterations in cytosolic  $\text{Ca}^{2+}$  concentration (Criollo et al., 2007). The mechanism has not been fully characterised, but is thought to involve IP3R binding Beclin 1 (see section 1.1.2ii above) (Vicencio et al., 2009). This interaction is suggested to prevent PI3KC3 complex I disruption due to BCL2 anti-apoptotic proteins binding the Beclin 1 BH3-like domain, which constitutes an additional mTOR-independent autophagy regulation mechanism (Maiuri et al., 2007; Pattingre et al., 2005).

PI3KC3 complex I disruption due to Beclin 1/BCL2 binding is also impacted by JNK (c-Jun N-terminal Kinase) signalling, with JNK1 multi-site phosphorylation of BCL2 (murine Bcl2 threonine 69, serine 70 and serine 87) impairing Beclin 1/BCL2 complex formation (Wei et al., 2008). This partially accounts for NO (nitric oxide) downregulating autophagosome biogenesis, as NO inhibits JNK1 activity through direct S-nitrosylation (Sarkar et al., 2011). However, NO also impairs autophagy *via* an mTOR-dependent mechanism; S-nitrosylating

IKK2, which reduces AMPK-mediated TSC2 phosphorylation and disinhibits mTORC1 (Sarkar et al., 2011).

AMPK activity is also influenced by IP3R-mediated  $\text{Ca}^{2+}$  release (Cardenas et al., 2010). As IP3R-released  $\text{Ca}^{2+}$  uptake is required for effective mitochondrial function, IP3R deficient cells are metabolically compromised. Hence, AMPK is activated by the increased AMP/ADP:ATP ratio in these cells (Hardie et al., 2012). This upregulates autophagy, presumably *via* direct ULK1 phosphorylation as mTORC1 complex activity is not altered by IP3R deficiency (Cardenas et al., 2010).

Other small molecules such as the disaccharide trehalose have been identified as mTOR-independent autophagy inducers, which ameliorate neurodegeneration caused by aggregate-prone proteins in both cell culture and animal models (Frake et al., 2015; Sarkar et al., 2007). For many years, the molecular mechanism by which trehalose upregulates autophagy remained elusive. However, DeBosch and colleagues have recently shown that trehalose blocks glucose import through SLC2/GLUT transporters at the plasma membrane (DeBosch et al., 2016). Trehalose is therefore proposed to decouple nutrient intake at the organism level from cellular metabolism, thereby activating AMPK and stimulating ULK1 complex activity (DeBosch et al., 2016).

As mentioned above, autophagy is subject to mTOR-independent transcriptional regulation, together with epigenetic modulation (Fullgrabe et al., 2014). For example, in addition to mTORC1 signalling, TFEB downregulation *via* cytosolic retention is mediated by ERK1/2 (Extracellular signal-Regulated Kinase 1/2) phosphorylation at serine 142 (Settembre et al., 2011).

Another important contributor to the transcriptional regulation of autophagy is the nuclear receptor FXR (Farnesoid X Receptor), which downregulates expression of autophagy genes in mouse liver (Lee et al., 2014; Seok et al., 2014). Seok et al. report FXR functions by antagonising the activation of numerous autophagy genes (including *Atg7* and *Ulk1*) by CREB transcriptional factors, as occurs in the livers of fasted mice. When activated by feeding or GW4064 treatment, FXR functions to dissociate the coactivator CRTC2 from the CREB complex, thereby repressing pro-autophagy transcription (Seok et al., 2014). Since ribosomal protein S6 phosphorylation was unchanged by GW4064 treatment, Seok et al. suggest FXR-mediated autophagy inhibition is mTOR independent. Also studying mouse liver, Lee et al. propose an alternative (though not incompatible) mechanism whereby FXR

competes with the nuclear receptor PPARalpha for binding to shared sites in the promoters of autophagy genes such as *Becn1* and *Atg7*. Activating PPARalpha with GW7647 is shown to reverse autophagy suppression in fed mouse livers, while FXR activation with GW4064 has the opposite effect in starved mouse livers (Lee et al., 2014). Lee et al. do not observe changes in mTORC1 signalling in mouse hepatocytes cultured under these conditions, but do report alterations in Ulk1 phosphorylation at serine 757 (see previous section) that suggest FXR/PPARalpha-mediated autophagy regulation may not be entirely mTOR-independent.

### ***1.1.7 Normal physiology***

Autophagy functions in various normal physiological processes, ranging from wound healing to red blood cell maturation (Ravikumar et al., 2010b). This is illustrated by discussing autophagy in normal development and ageing, the latter being especially relevant to chapter 3.

#### **1.1.7.1 Development**

Autophagy enables developing mammals to survive stressors such as pre-implantation and neonatal nutrient starvation. In addition, autophagy degrades proteins that participate in developmentally important signalling pathways (Wu et al., 2013).

##### **i. Early embryonic development**

Using mice expressing GFP-tagged LC3, Tsukamoto and colleagues observe a spike in autophagosome numbers in early embryogenesis (declining after the four-cell stage) (Tsukamoto et al., 2008). This correlates with increased autophagy-mediated protein recycling, which occurs before implantation in response to fertilisation (not oocyte nutrient starvation) before implantation. Autophagy-deficient embryos generated by fertilising *Atg5*-null oocytes with *Atg5*-null sperm exhibit developmental arrest at the four- to eight-cell stage, suggesting autophagy is required for pre-implantation embryogenesis (Tsukamoto et al., 2008). On the other hand, *Atg5*-null (*Atg5*<sup>-/-</sup>) mice generated by mating *Atg5*<sup>+/-</sup> heterozygotes survive to term (Kuma et al., 2004), presumably because maternal *Atg5* is present in early stage *Atg5*<sup>-/-</sup> embryos.

Autophagy is also implicated in embryonic cavitation, which involves inner ectodermal cells undergoing programmed cell death by apoptosis. Unlike embryoid bodies derived from wild type mouse embryonic stem cells, neither *Atg5*<sup>-/-</sup> nor *Becn1*<sup>-/-</sup> embryoid bodies cavitate (Qu et al., 2007; Yue et al., 2003). This is caused by defective apoptotic corpse engulfment; both

*Atg5<sup>-/-</sup>* and *Becn1<sup>-/-</sup>* dying cells express less surface phosphatidylserine ('eat-me' signal), plus secrete less lysophosphatidylcholine ('come-get-me' signal). As this phenotype can be rescued using the metabolic substrate methylpyruvate, autophagy may facilitate embryonic cavitation by releasing amino acids for gluconeogenesis and other metabolic pathways, thereby enabling ATP-dependent engulfment signalling (Qu et al., 2007).

## ii. Developmental pathways

Autophagy influences development *via* signalling pathways, including SHH (sonic hedgehog) and FGF (fibroblast growth factor) (Wu et al., 2013). For example, Gao et al. report that p62 functions as an autophagy cargo receptor (see section 1.1.4) for ubiquitinated Dvl2 (Dishevelled 2) aggregates (Gao et al., 2010). Dishevelled proteins (Dvl1, Dvl2 and Dvl3) mediate WNT signalling, which orchestrates important developmental processes such as cell fate determination and tissue polarisation (van Amerongen and Nusse, 2009). In this way, autophagy impacts development by negatively regulating WNT signalling (Gao et al., 2010).

In addition, our lab has recently demonstrated that autophagy degrades Notch1 (Wu et al., 2016). An important function of Notch signalling in development is stem cell maintenance (Shi and Stanley, 2006). Accordingly, neurons cultured from *Atg16L1*-deficient mice (*Atg16L1* hypomorphs) with impaired autophagy retain stem cell marker expression, which mirrors delayed stem cell differentiation in *Atg16L1* hypomorph brains (Wu et al., 2016). Similar phenotypes are observed in *Atg16L1* hypomorph gut and bone marrow.

## iii. Neonatal starvation

Despite appearing near-normal at birth, *Atg5<sup>-/-</sup>* mice generated by mating *Atg5<sup>+/-</sup>* heterozygotes die within a day of delivery (Kuma et al., 2004). The same phenotype is observed in *Atg7<sup>-/-</sup>* mice (Komatsu et al., 2005). Autophagy induction is observed in various wild type mouse tissues immediately after birth, while both *Atg5<sup>-/-</sup>* and *Atg7<sup>-/-</sup>* mice exhibit reduced plasma amino acid concentrations compared with littermate controls (Komatsu et al., 2005; Kuma et al., 2004). These findings support the hypothesis that autophagy enables mammals to survive starvation during the transition from placenta- to milk-supplied nutrients. However, autophagy-deficient mice may also have difficulty feeding; no milk was found in the stomachs of *Atg5<sup>-/-</sup>* mice after death (Kuma et al., 2004).

### 1.1.7.2 Ageing

Decreased autophagy has been associated with normal ageing in several species. The hypothesis that autophagic decline contributes to ageing is supported by numerous publications on lifespan extension due to autophagy upregulation (and *vice versa*). Proteostatic stress upon autophagic decline is especially relevant to post-mitotic cells such as neurons and could predispose to age-related neurodegenerative conditions (see section 1.1.8.2 below) (Rubinsztein et al., 2011; Vilchez et al., 2014).

#### i. Autophagic decline in ageing

By analysing previously published microarray data (Loerch et al., 2008), Lipinski and colleagues identified ATG5 and ATG7 mRNA expression as reduced in frontal cortex samples from older ( $\geq 70$ -year-old) human donors, compared with younger samples ( $\leq 40$ -year-old) (Lipinski et al., 2010b). This concurs with decreased BECN1 expression in human prefrontal cortex samples, as measured by qRT-PCR (old =  $83.5 \pm 4.6$  years; young =  $26.8 \pm 3.2$ ) and western blotting (old =  $84.1 \pm 8.8$ ; young =  $27.2 \pm 4.0$ ) (Shibata et al., 2006). Moreover, using immunohistochemistry to compare articular cartilage from 2, 9 and 12 month old mice, Carames et al. demonstrate that Beclin1 and LC3 expression declines with age (Carames et al., 2010). Similar data have been obtained in *Drosophila* neural tissue; Atg2, Atg8a and Atg18 mRNA expression is significantly suppressed from 3 weeks post-hatching onwards (Simonsen et al., 2008).

There are no publications directly addressing whether these gene expression changes are sufficient to cause autophagic decline in ageing. However, reduced autophagic vesicle formation and clearance is reported in liver tissue from older adult mice (20 – 21 months), compared with younger adult mice (5 – 6 months) (Terman, 1995). In addition, autophagic proteolysis in hepatocytes cultured from rats aged 2 – 24 months negatively correlates with age (Donati et al., 2001).

#### ii. Interventions altering lifespan

Several research groups have used genetic or pharmacological interventions to suggest autophagy extends lifespan. Using a microarray-based genetic screen, Matecic and colleagues identified core autophagy genes as ‘aging factors’ in *Saccharomyces cerevisiae* (budding yeast). Yeast with mutations in ATG12, ATG16, ATG18, ATG2, ATG5, ATG7 or ATG8 were short-lived (Matecic et al., 2010). This phenotype was not ameliorated by amino acid

starvation, previously shown to extend yeast lifespan (Alvers et al., 2009), suggesting nutrient deprivation increases lifespan by upregulating autophagy.

This concurs with data obtained by the Levine group using *Caenorhabditis elegans eat-2* mutants (Jia and Levine, 2007). Dietary restriction due to feeding difficulties causes lifespan extension in these mutants, which is ameliorated by treatment with RNAi against the core autophagy genes *bec-1* (equivalent to *BECNI*) and *atg-7* (Jia and Levine, 2007). The Levine group conclude similarly with regards to insulin-like signalling, which negatively regulates *C. elegans* lifespan (Melendez et al., 2003). *Daf-2* (insulin-like tyrosine kinase receptor) mutants exhibit significant lifespan extension; median survival was 48 days, compared with 28 days for wild type *C. elegans* (Melendez et al., 2003). Normal lifespan was restored when *Daf-2* mutants were treated with RNAi against *bec-1*, *atg-7* or *atg-12* (Hars et al., 2007; Melendez et al., 2003).

The median lifespan of mice moderately overexpressing *Atg5* in all tissues is 17% longer than wild type controls (Pyo et al., 2013). These animals also exhibit ‘anti-ageing phenotypes’, such as resistance to age-associated obesity and improved metabolism (lower blood glucose and triglyceride levels, with enhanced insulin sensitivity). Whether these phenotypes are due to increased autophagy is not addressed directly. However, *Atg5* transgenic MEFs are more resistant to  $H_2O_2$ -induced oxidative stress, which is reversed when autophagy is inhibited pharmacologically (Pyo et al., 2013).

A multicentre trial has demonstrated that feeding aged mice (600 days old) the autophagy inducer rapamycin (see section 1.1.6i) increases age at 90% mortality by 14% in females and 9% in males (Harrison et al., 2009). As this study does not include mechanistic experiments, other mTOR signalling functions impacted by rapamycin cannot be excluded. This is not the case for lifespan extension caused by rapamycin treatment in *Drosophila melanogaster*; unlike wild type flies, those with impaired autophagy due to reduced *Atg5* expression fail to show lifespan extension upon rapamycin treatment (Bjedov et al., 2010).

### iii. Mechanisms of ageing

With regards to how autophagy could regulate ageing, one popular theory concerns ageing as ‘proteostasis collapse’ (Taylor and Dillin, 2011). Hence, autophagy upregulation could increase lifespan by degrading misfolded proteins and damaged organelles to maintain cellular homeostasis, while autophagy downregulation in normal ageing would have the opposite effect (Vilchez et al., 2014). These processes are especially relevant to post-mitotic

cells such as neurons, which cannot divide to relieve proteostatic stress (Rubinsztein et al., 2011). For example, neurons in autophagy-deficient *Atg8a* mutant *Drosophila* accumulate insoluble ubiquitinated proteins, together with ROS-modified proteins upon H<sub>2</sub>O<sub>2</sub>-induced oxidative stress (Simonsen et al., 2008). This correlates with reduced lifespan in *Atg8a* mutant flies.

Autophagy is also thought to influence ageing *via* stem cell maintenance in adult organisms. In contrast to findings in other mouse tissues outlined above, Warr and colleagues report increased autophagy in haematopoietic stem cells (HSCs) from older mice ( $\geq 24$  months) compared with younger animals (6 – 12 weeks). However, HSCs from older mice can still upregulate autophagy upon metabolic stress (Warr et al., 2013). This is attributed to increased FOXO3A transcriptional activity, which enhances pro-autophagy gene expression in HSCs from older mice. Increased autophagy protects older HSCs with impaired nutrient uptake from apoptosis that would otherwise occur due to starvation (Warr et al., 2013).

### **1.1.8 Disease**

Dysregulated autophagy is associated with various human pathologies (Ravikumar et al., 2010b). Literature concerning autophagy in cancer, neurodegeneration and immune responses is discussed below, the former being especially relevant to Chapters 4 and 5.

Autophagy modulators have therapeutic potential in numerous diseases, yet it is important to note that diseases sharing common pathology can display contrasting autophagy defects. For example, autophagy induction has therapeutic potential in several neurodegenerative diseases, but could augment neurodegeneration in conditions such as lysosomal storage diseases that show impaired flux through the autophagy pathway (Frake et al., 2015)

#### **1.1.8.1 Cancer**

Autophagy performs multiple, seemingly paradoxical roles in tumorigenesis; suppressing primary malignant transformation by maintaining cellular homeostasis, while also promoting tumour progression (Galluzzi et al., 2015; Mowers et al., 2017).

The context-dependency of these roles is illustrated by Rosenfeldt and colleagues' finding that p53 status can determine whether autophagy is tumour suppressive or required for tumour development (Rosenfeldt et al., 2013). In a mouse model with mutationally activated KRAS, premalignant pancreatic lesions are unable to progress to pancreatic ductal adenocarcinoma (PDAC) in *Atg5*<sup>-/-</sup> or *Atg7*<sup>-/-</sup> mice expressing the tumour suppressor p53. Yet

in the same model on a p53-null background, *Atg5*<sup>-/-</sup> or *Atg7*<sup>-/-</sup> mice shown accelerated PDAC formation compared with age-matched autophagy-competent controls (Rosenfeldt et al., 2013).

### **i. Tumour suppression**

The seminal work linking autophagy to cancer was performed by the Levine group, who identified Beclin 1 as a tumour suppressor in breast cancer; monoallelic *BECN1* deletions and decreased expression are observed in breast cancer patient samples (Liang et al., 1999). Reintroducing Beclin 1 into MCF7 human breast adenocarcinoma cells, which otherwise do not express detectable Beclin 1, results in reduced tumour formation upon subcutaneous injection into immunocompromised mice (Liang et al., 1999).

One mechanism by which autophagy suppresses malignant transformation is genomic stabilisation. Compromised autophagy due to *Becn1* heterozygosity promotes DNA damage (measured by gamma histone 2AX immunofluorescence) in both iMMECs (immortalized mouse mammary epithelial cells) and iBMK (immortalized baby mouse kidney epithelial) cells under metabolic stress (glucose starvation in 1% oxygen) (Karantza-Wadsworth et al., 2007; Mathew et al., 2007). Similar results were obtained using *Atg5*<sup>-/-</sup> iBMK cells (Mathew et al., 2007). Hence, autophagy functions to prevent potentially oncogenic somatic mutations.

Autophagy-dependent proteostasis also contributes to tumour suppression. Both *Becn1*<sup>+/-</sup> and *Atg5*<sup>-/-</sup> iBMK cells accumulate the autophagy substrate (and cargo receptor) p62 under metabolic stress (Mathew et al., 2009). p62 accumulation is sufficient to impair antioxidant defence, which in turn causes ROS-mediated DNA damage. Accordingly, *Atg5*<sup>-/-</sup> iBMK cells expressing p62-GFP show enhanced tumour formation upon subcutaneous injection into immunocompromised mice, compared with autophagy-competent littermate controls (Mathew et al., 2009).

### **ii. Tumour progression**

In recent years our lab has shown that depleting the proto-oncogene product MYC impairs autophagosome formation by reducing JNK1 and BCL2 phosphorylation (see section 1.1.6ii) (Toh et al., 2013), while XIAP and cIAP1 (overexpressed in several human cancers) induce autophagy by upregulating Beclin 1 transcription (Lin et al., 2015).

The oncogenic functions of autophagy include enabling cancer cells to survive stressors such as nutrient starvation. In this regard, Guo and colleagues characterise several cell lines with

activating mutations in KRAS as ‘autophagy addicted’. These include T24 (bladder cancer), H1299 (lung cancer) and HCT-116 (colorectal cancer) cells, which exhibit high basal autophagy alongside decreased proliferation and survival when autophagic flux is blocked with chloroquine (Guo et al., 2011). iBMK cells expressing mutationally activated KRAS accumulate dysfunctional mitochondria, which results in metabolic impairment (reduced oxygen consumption and ATP depletion under starvation). Accordingly, KRAS-transformed *Atg5*<sup>-/-</sup> and *Atg7*<sup>-/-</sup> iBMK cells are unable to survive prolonged nutrient starvation. Tumours formed when these cells were subcutaneously injection into immunocompromised mice exhibited impaired growth and elevated apoptosis, compared with autophagy-competent controls (Guo et al., 2011).

Similar results were obtained using MMTV-PyMT transgenic mice, expressing oncogenic PyMT behind the MMTV promotor, which model metastatic breast cancer (Wei et al., 2011). When crossed with animals lacking the Ulk1 complex component Fip200, tumours in MMTV-PyMT mice show decreased proliferation and increased apoptosis. *Fip200*<sup>-/-</sup> MMTV-PyMT mice therefore survive longer without mammary tumours than autophagy-competent controls, as well as exhibiting fewer lung metastasis (although the latter could be secondary to smaller primary tumours) (Wei et al., 2011).

Recently autophagy has been directly implicated in tumour cell metastasis (Mowers et al., 2017). Following orthotopic injection, autophagy-deficient (*Atg5* or *Atg7* stable knockdown) 4T1 mouse mammary carcinoma cells form similarly sized mammary tumours to autophagy-competent controls (Sharifi et al., 2016). Yet unlike controls, autophagy-deficient cells do not form lung or liver metastasis. Sharifi et al. suggest autophagy is required for initial escape from primary mammary tumours in this model, as autophagy-deficient 4T1 cells can form metastases when injected directly into the circulation (Sharifi et al., 2016).

This concurs with studies implicating autophagy in cell motility. For instance, Tuloup-Minguez et al. report that autophagy modulates cell migration by negatively regulating expression of the transmembrane extracellular matrix (ECM) receptor Integrin Beta 1 at the cell surface (Tuloup-Minguez et al., 2013). Autophagy has since been shown to support cell migration by facilitating the turnover of focal adhesions (Kenific et al., 2016; Sharifi et al., 2016), multi-protein complexes that link intracellular filamentous actin (F-actin) to the ECM (Abercrombie and Dunn, 1975). Kenific et al. implicate the cargo receptor NBR1 in this process; basal autophagy levels are not affected by NBR1 knockdown, while cell motility

(measured by *in vitro* wound healing assay) is reduced due to defective focal adhesion turnover (Kenific et al., 2016). An additional mechanism is proposed by Shafiri et al., who report autophagy degrades the focal adhesion component paxillin in a SRC kinase activity-dependent manner. Autophagy-deficient 4T1 cells therefore exhibit defective focal adhesion disassembly, which accounts for the aforementioned failure to escape primary mammary tumours and metastasise *in vivo* (Sharifi et al., 2016).

Autophagy is also associated with chemotherapy resistance (Galluzzi et al., 2015). Combining the alkylating chemotherapeutic cyclophosphamide with chloroquine (an autophagic flux blocker), enhances tumour regression and delays tumour recurrence in a mouse model of MYC-driven lymphoma when compared with cyclophosphamide alone (Amaravadi et al., 2007). Although chloroquine also inhibits autophagy-independent lysosomal functions, given ATG5 knockdown and chloroquine treatment similarly impair cancer cell survival *in vitro* following pro-apoptotic p53 induction, Amaravadi and colleagues propose autophagy can be utilised as an adaptive mechanism to resist chemotherapy-induced apoptosis.

### **1.1.8.2 Neurodegeneration**

Dysfunctional autophagy predisposes to neurodegeneration, as highlighted by knockout mouse studies showing that autophagy facilitates neuronal survival. Mice lacking *Atg7* in the central nervous system (CNS) suffer massive neuronal death in the cerebral and cerebellar cortices; surviving neurons accumulate intracellular inclusions that increase in size and number with age (Komatsu et al., 2006). Similarly, mice lacking *Atg5* in the CNS develop progressive motor function deficits consistent with neurodegeneration (Hara et al., 2006). Autophagy upregulation therefore has therapeutic potential in several neurodegenerative diseases, which predominantly stems from autophagic clearance of disease-associated aggregate-prone proteins such as alpha-synuclein and tau (Rubinsztein et al., 2015).

#### **i. Pathogenesis**

Several human neurodegenerative conditions are associated with autophagic dysfunction, some directly attributable to mutations in autophagy-associated genes. These include a homozygous missense mutation identified in *ATG5*, which impairs autophagy and causes ataxia with developmental delay in affected patients (Kim et al., 2016). Moreover, mutations in *WIPI4* (related to *WIPI2*, see section 1.1.2ii) cause the rare neurodegenerative disease SENDA (static encephalopathy of childhood with neurodegeneration in adulthood) (Haack et

al., 2012; Saitsu et al., 2013), which is a form of NBIA (neurodegeneration with brain iron accumulation). Lymphoblastoid cell lines derived from these patients display reduced WIPI4 expression and impaired autophagic flux, with accumulation of abnormal LC3-positive vesicles (Saitsu et al., 2013).

With regards to more common neurodegenerative diseases, defective autophagy has been described in Alzheimer's disease (AD), Parkinson's disease (PD) and Huntington's disease (HD), amongst others (Frake et al., 2015). For example, Beclin 1 expression is decreased in post-mortem cortex samples from both AD and amnesic mild cognitive impairment (prodromal AD) patients (Pickford et al., 2008; Rohn et al., 2011). Resultant autophagy defects are implicated in AD pathogenesis, with *Becn1*<sup>+/-</sup> mice expressing mutant human amyloid precursor protein (*APP*<sup>+</sup>*Becn1*<sup>+/-</sup> mice) accumulating the aggregate-prone protein amyloid beta (Abeta) and exhibiting accelerated neurodegeneration compared to *APP*<sup>+</sup>*Becn1*<sup>+/+</sup> littermates (Pickford et al., 2008).

On the other hand, autophagy contributes to Abeta synthesis and secretion. Yu and colleagues observe dystrophic dendrites that accumulate Abeta-containing autophagic vesicles enriched for gamma-secretase complex components (Abeta biosynthetic enzymes) in post-mortem samples from AD patients. Similar accumulation precedes neurodegeneration in *APP/Presenilin 1* mice, which model AD (Yu et al., 2005). This could result from increased autophagosome biogenesis and/or impaired autophagic flux. Focusing on autophagy in Abeta secretion, Nilsson et al. report *APP*<sup>+</sup> mice deficient for *Atg7* in forebrain neurons show reduced extracellular Abeta plaque burden and increased intracellular Abeta accumulation compared with autophagy-competent littermates due in part to impaired secretion (Nilsson et al., 2013). In addition, Abeta amyloidosis *per se* is suggested to inhibit autophagy; autophagy-competent *APP*<sup>+</sup> mice show reduced autophagy compared with wild type controls (Nilsson et al., 2013).

Autophagy degrades both wild type and mutant alpha-synuclein (the major aggregate-prone protein in PD) in a stable, inducible cell lines (Webb et al., 2003). Alpha-synuclein also modulates autophagy in both mammalian cells and transgenic mice; overexpression impairs autophagosome biogenesis by mislocalising mATG9 (Winslow et al., 2010). Further evidence linking defective autophagy to PD pathogenesis is provided by disease-causing mutations. These include the D620N mutation in retromer subunit VPS35, which causes autosomal-dominant late-onset PD (Vilarino-Guell et al., 2011; Zimprich et al., 2011). As

well as mediating endosome-to-Golgi transmembrane protein transport, retromer is involved in recruiting the protein sorting complex WASH that our group has shown to participate in autophagosome biogenesis (Zavodszky et al., 2014). Mutant VPS35 (D620N) impedes WASH recruitment to endosomes, thereby indirectly inhibiting autophagy induction. This is partially explained by defective mATG9 trafficking to autophagosomes (Zavodszky et al., 2014).

In addition, mutations in *PARK2* (encoding the E3 ubiquitin ligase Parkin) and *PINK* (PTEN-induced kinase 1) that cause autosomal recessive juvenile Parkinsonism (Kitada et al., 1998; Valente et al., 2004; Valente et al., 2001) implicate defective mitophagy in PD pathogenesis (Matsuda et al., 2010; Narendra et al., 2008). These findings may also be relevant to spontaneous PD; analysis of post-mortem striatal tissue from patients reveals lower Parkin total protein, together with an accumulation of insoluble and phospho-Parkin compared to age-matched controls, which is predicted to cause defective mitophagy (Lonskaya et al., 2012).

## **ii. Therapeutic potential**

Autophagy was first identified as a potential therapeutic target in neurodegenerative disease when shown to clear polyglutamine-expanded huntingtin (the toxic species in HD), thereby reducing cell death (Ravikumar et al., 2002). This finding has subsequently been translated into animal models, with autophagy induction ameliorating neurodegenerative pathology in mice modelling HD (Rose et al., 2010). While intracellular inclusions decrease under autophagy upregulation, our working model is that autophagy does not clear the large aggregates that characterise various neurodegenerative diseases directly, but rather the soluble aggregate precursors; shifting the equilibrium from aggregate formation towards degradation (Rubinsztein, 2006).

Considering other neurodegenerative conditions, autophagy upregulation promotes clearance of wild-type and mutant tau in *Drosophila* modelling AD (Berger et al., 2006). Likewise, improved behavioural outcomes in a transgenic AD mouse model following treatment with the antihistamine latrepirdine is attributable to autophagy induction (Steele et al., 2013). The tyrosine kinase inhibitor nilotinib similarly protects substantia nigra dopaminergic neurons and improves motor performance in a PD mouse model (injected with human Alpha-synuclein) by enhancing autophagy (Hebron et al., 2013).

Aside from clearing aggregate-prone proteins, the therapeutic potential of autophagy in neurodegeneration may also be due to protecting cells from pro-apoptotic and/or pro-necrotic insults (Ravikumar et al., 2006; Rocchi et al., 2017; Wu et al., 2008). The former is especially important in this context, given increased apoptosis is observed in various neurodegenerative conditions (Ravikumar et al., 2006). Specifically, Ravikumar et al. show autophagy upregulation protects against pro-apoptotic staurosporine treatment in cell culture and paraquat toxicity in *Drosophila* by enhancing mitophagy, thereby reducing downstream caspase activation (Ravikumar et al., 2006).

### **1.1.8.2 Immunity and Inflammation**

Autophagy contributes to innate immunity by targeting intracellular pathogens for lysosomal degradation, known as xenophagy. Several additional functions in both innate and adaptive immunity have since been identified, as well as an association with inflammatory bowel disease (Deretic et al., 2015).

#### **i. Xenophagy**

Xenophagy is possible the most ancient defence against invading microorganisms (Deretic et al., 2015). The first studies on xenophagy were published by the Yoshimori and Deretic groups; reporting that autophagy can eliminate Group A *Streptococcus* and *Mycobacterium tuberculosis*, respectively (Gutierrez et al., 2004a; Nakagawa et al., 2004).

Multiple autophagy cargo receptors (see section 1.1.4) have subsequently been shown to function in xenophagy. In this regard, the Randow lab demonstrate that NDP52 restricts *Salmonella enterica Typhimurium* (hereafter *S. Typhimurium*) growth by recruiting invading bacteria into autophagosomes (Thurston et al., 2009). NDP52 is initially targeted to *Salmonella*-containing vacuoles by the cytosolic lectin galectin-8, which serves as a multipurpose ‘danger receptor’ that signals endolysosomal vesicle damage (Thurston et al., 2012). This is followed by ubiquitin-dependent recruitment, whereby NDP52 simultaneously binds ubiquitinated *S. Typhimurium* and LC3 to facilitate xenophagy (Thurston et al., 2009).

Neither optineurin/NDP52 nor p62/NDP52 double knockdown have additive effects on *S. Typhimurium* proliferation in infected cells, indicating a common receptor-mediated xenophagy pathway (Wild et al., 2011). Wild and colleagues demonstrate that TBK1 (TANK binding kinase 1) associated with ubiquitin-coated cytosolic bacteria phosphorylates optineurin within the extended LIR motif (see section 1.1.4; especially serine 177 in human

optineurin). This increases LC3 binding affinity, thereby enhancing *S. Typhimurium* clearance by autophagy (Wild et al., 2011).

Ubiquitination is also required for xenophagy targeting mycobacteria. The E3 ligase Parkin (encoded by *PARK2*) mediates K63-linked ubiquitination of *M. tuberculosis*, which recruits the autophagy receptors NDP52, p62 and NBR1 (Manzanillo et al., 2013). Accordingly, *Park2*-null (*Park2*<sup>-/-</sup>) mice show enhanced susceptibility to *M. tuberculosis* infection; mycobacterial load was 10-fold greater at 21 days post-infection, with all *Park2*<sup>-/-</sup> mice dying by 85 days post-infection when all wild type animals remain alive (Manzanillo et al., 2013). Dysfunctional xenophagy might therefore explain why *PARK2* regulatory region polymorphisms increase vulnerability to *Mycobacterium leprae* and *Salmonella typhi* (the causative agents in leprosy and typhoid fever, respectively) in humans (Ali et al., 2006; Mira et al., 2004).

On the other hand, certain pathogens have evolved to utilise host autophagy. For example, disrupting autophagy (pharmacologically or genetically) reduces human BK polyomavirus (BKPyV) infection in HeLa cells (Bouley et al., 2014). Given BKPyV is most sensitive to autophagy inhibition during the first 8 hours post-infection, plus viral particles colocalise with GFP-tagged LC3, Bouley et al. propose autophagy functions in polyomavirus entry and trafficking.

## ii. Inflammation

Single-nucleotide polymorphisms in *ATG16L1* are susceptibility loci for the inflammatory bowel condition Crohn's disease (Hampe et al., 2007; Rioux et al., 2007).

This concurs with *ATG16L1* regulating endotoxin-induced inflammatory cytokine production (Saitoh et al., 2008). Saitoh and colleagues demonstrate that *Atg16L1*-deficient mouse macrophages show enhanced IL-1 $\beta$  and IL-18 secretion under lipopolysaccharide stimulation. Accordingly, mice lacking *Atg16L1* in haematopoietic cells exhibit much worse dextran sulphate sodium-induced colitis compared with wild type controls (Saitoh et al., 2008).

Using *Atg16L1* hypomorph mice (introduced in section 1.1.7.1ii), Cadwell et al. propose an alternative (though not incompatible) mechanism linking autophagy to inflammatory bowel disease (Cadwell et al., 2008). In these animals, Paneth cells (ileal epithelial cells implicated in intestinal microbiota control) shown defective antimicrobial enzyme and cytokine secretion. Similar abnormalities are observed in Paneth cells from ileocolic specimens

donated by Crohn's disease patients expressing an *ATG16L1* risk allele (Cadwell et al., 2008).

### iii. Antigen recognition and presentation

Autophagy is required for certain pathogens, as in the single-stranded RNA virus VSV (vesicular stomatitis virus), to be recognised by the innate immune system (Lee et al., 2007). Dendritic cells (DCs) use Toll-like receptors (TLRs) to detect viral intermediates in acidified endolysosomal compartments, thereby avoiding direct infection (Akira and Takeda, 2004). *Atg5*<sup>-/-</sup> mouse DCs (obtained from irradiated wild type mice reconstituted with cells from *Atg5*<sup>-/-</sup> neonates) cannot utilise autophagy to transport VSV replication intermediates into the lysosome, as required for recognition by TLR7 (Lee et al., 2007).

The seminal work on autophagy in antigen presentation was published by Paludan and colleagues (Paludan et al., 2005). When lysosomal acidification in Epstein-Barr virus-transformed lymphoblastoid cells was inhibited with either ammonium chloride or chloroquine, EBNA1 (Epstein-Barr virus nuclear antigen 1) accumulated in autophagosomes (Paludan et al., 2005). Autophagy therefore participates in the EBNA1 delivery to lysosomes where the antigen is processed for presentation at the cell surface on MHC II (major histocompatibility complex class II) molecules. In this way, downregulating autophagy using the PI3KC3 inhibitor 3-MA or ATG12 knockdown decreased MHC II-mediated recognition of EBV-transformed cell lines by CD4-positive T cells (Paludan et al., 2005).

Autophagy has subsequently been shown to function in physiologically-relevant antigen presentation by MHC II on thymic epithelial cells (TECs) and DCs, amongst others (Lee et al., 2010a; Nedjic et al., 2008). The former appears critical for immunological tolerance, with autophagy-deficient (*Atg5*<sup>-/-</sup>) TECs causing autoimmune colitis and multiorgan lymphoid infiltration in mice (Nedjic et al., 2008). Nedjic and colleagues propose autophagy enables TECs to load MHC II with intracellularly-derived peptides, which include otherwise tissue-specific antigens, thereby facilitating self-tolerant T cell selection in the thymus.

### iv. Immunological memory

Multiple branches of long-term adaptive immunity require autophagy. The autophagy pathway is constitutively active in plasma cells ('professional' antibody-secreting B cells) (Pengo et al., 2013). This is reported to facilitate sustainable antibody production; *Atg5*-deficient mouse plasma cells exhibit enhanced immunoglobulin synthesis and secretion,

coupled to impaired energy metabolism and increased cell death by apoptosis. Accordingly, mice lacking *Atg5* in B cells mount defective immune responses to pneumococcal antigens (Pengo et al., 2013).

Again using mice with autophagy-deficient B cells (*Atg7* tissue-specific knockout), Chen and colleagues report immunological memory against influenza requires autophagy (Chen et al., 2014a). After immunisation with influenza A virus, these animals show normal primary antibody responses (assayed at 14 days post-immunisation). However, significantly fewer influenza A antigen-specific memory B cells are observed at eight weeks post-immunisation (Chen et al., 2014a). Unlike wild type controls, mice lacking *Atg7* in the B cells therefore fail to generate protective secondary antibodies upon lethal re-challenge with influenza A virus after the initial sub-lethal dose. This is explained by autophagy promoting memory B cell survival *via* increasing resistance to apoptosis (Chen et al., 2014a).

Autophagy similarly counters apoptosis in CD8-positive T cells (Xu et al., 2014). Using a mouse model in which *Atg7* is conditionally deleted upon CD8-positive T cell activation, Xu et al. demonstrate that autophagy-deficient CD8-positive T cells proliferate and differentiate into effector T cells comparably to controls upon acute LCMV (lymphocytic choriomeningitis virus) infection (Xu et al., 2014). Conversely, the response to chronic LCMV infection is impaired; significantly more autophagy-deficient effector T cells undergo apoptosis, meaning a functional memory T cell pool is not generated (Xu et al., 2014).

### ***1.1.9 Concluding remarks***

The literature concerning autophagy molecular machinery and autophagy regulation is extensive. However, our understanding is far from complete and many unanswered questions remain. Given autophagy performs important functions in normal physiology and defective autophagy is implicated in numerous human diseases, there is a pressing need to characterise novel regulatory mechanisms with pathophysiological relevance.

## 1.2 Vinexin

### 1.2.1 Introduction

Vinexin was identified by Kioka and colleagues *via* yeast two-hybrid screening using the proline-rich hinge region of the focal adhesion protein vinculin as bait (Kioka et al., 1999). Human vinexin is encoded by *SORBS3* (sorbin and SH3 domain containing 3) on chromosome 8p. Homology searches reveal two structurally related proteins; CAP (CBL-Associated Protein) and ARGBP2 (ARG-Binding Protein 2), later termed SORBS1 and SORBS2. All three vinexin family members are multi-domain adaptor proteins lacking intrinsic enzymatic activity (Kioka et al., 2002).

Vinexin was first identified as a potential autophagy regulator by Lipinski and colleagues in a genome-wide, image-based siRNA screen using H4 human neuroblastoma cells stably expressing GFP-tagged LC3; vinexin knockdown increases GFP-positive autophagosomes under basal conditions (Lipinski et al., 2010a). Lipinski and colleagues report this increase is due to enhanced autophagosome biogenesis (rather than impaired flux through the autophagy pathway) and also suggest mTOR signalling is not involved (Lipinski et al., 2010a). Otherwise, the molecular mechanisms by which vinexin regulates autophagy remains to be characterised.

#### 1.2.1.1 Isoform expression

*SORBS3* encodes two commonly studied isoforms (vinexin alpha and vinexin beta) distinguished by the presence or absence of an N-terminal SoHo (sorbin homology) domain. Kioka and colleagues' original study identifies two vinexin mRNAs (Kioka et al., 1999). The longer 3 kb mRNA, corresponding to 82 kDa vinexin alpha, shows restricted tissue expression (absent from most human tissues, though highly expressed in skeletal muscle), while the shorter 2 kb mRNA, corresponding to 37 kDa vinexin beta, is ubiquitously expressed. Subsequent mouse studies report two intermediate-length isoforms, termed vinexin gamma and vinexin delta (Matsuyama et al., 2005; Paz et al., 2007). 76 kDa vinexin gamma, which results from vinexin alpha alternative splicing, is detectable by western blotting in testicular, ovary, heart and lung tissue from E12.5 mouse embryos (Matsuyama et al., 2005). 78 kDa vinexin delta shows even more restricted tissue expression; detectable only in gonad germ cells during embryonic development, together with testicular and ovary tissue

from adult mice (Paz et al., 2007). Vinexin gamma and vinexin delta are thought likely to exist in humans, though *in vivo* evidence is lacking.

### **1.2.1.1 Domain structure**

The domain structure of vinexin is ostensibly simple, featuring only two protein domain families. Additional putative functional domains have been identified, as in a proline-rich ‘linker’ between the second and third SH3 domains (Suwa et al., 2002), but are currently undercharacterised.

#### **i. SoHo domain**

The vinexin alpha N-terminus contains a 115 amino acid SoHo domain (homologous to the porcine gut peptide sorbin) that is both necessary and sufficient for binding the lipid raft-associated protein flotillin (Kimura et al., 2001). Lacking vinexin alpha N-terminal amino acids 1 – 404, vinexin beta does not feature this SoHo domain.

#### **ii. SH3 domains**

The vinexin C-terminus comprises three SH3 domains, which are conserved in vinexin alpha and vinexin beta (Kioka et al., 1999). One or more of these domains is required for binding to most vinexin interactors *via* proline-rich regions. The crystal structure of the first SH3 domain of human vinexin has been solved, including the interface that binds the proline-rich vinculin hinge region (Zhang et al., 2007).

## **1.2.2 Cell biology**

As summarised in Table 1, vinexin has many reported interactors. This complex interactome accounts for the wide ranging cellular functions associated with vinexin. The best characterised of these functions are described below.

### **1.2.2.1 Actin cytoskeleton dynamics**

Vinexin is thought to modulate the actin cytoskeleton through various binding partners. However, the literature is not well-developed; *how* these interactions impact actin cytoskeleton dynamics remains poorly understood.

#### **i. Cell-extracellular matrix adhesion**

Cells form mechanical links between intracellular F-actin and the ECM *via* multi-protein structures known as focal adhesions (Abercrombie and Dunn, 1975). Both exogenous and

Interactor	Function	Isoforms studied	Reference(s)
Vinculin	Cell adhesion-related adaptor protein	Both	(Kioaka et al., 1999; Takahashi et al., 2005)
DLG5	Cell adhesion-related adaptor protein	Both	(Wakabayashi et al., 2003)
p130Cap	Cell adhesion-related adaptor protein	Both	(Ito et al., 2008; Yamauchi et al., 2013)
Beta dystroglycan	Transmembrane adhesion protein	Both	(Thompson et al., 2010)
ERK1/2	Serine/threonine kinase	Vinexin beta	(Ito et al., 2007; Mitsushima et al., 2004; Mitsushima et al., 2007; Mizutani et al., 2007; Suwa et al., 2002)
SOS1	RAS/RAC guanine nucleotide exchange factor	Vinexin beta	(Akamatsu et al., 1999)
SHIP2	Phosphoinositol phosphatase	Vinexin alpha	(Paternotte et al., 2005)
ABL	Tyrosine kinase	Both	(Mitsushima et al., 2006b)
CBL	E3 ubiquitin ligase	Vinexin beta	(Mitsushima et al., 2006c)
SAFB2	Transcriptional corepressor	Both	(Townson et al., 2003)
Oestrogen receptor alpha	Nuclear receptor	Vinexin alpha	(Tujague et al., 2004)
Retinoic acid receptor gamma	Nuclear receptor	Vinexin beta	(Bour et al., 2005)
Rhotekin	Actin cytoskeleton regulator	Vinexin alpha	(Nagata et al., 2009)
WAVE2/WAVE1/N-WASP	Actin cytoskeleton regulator	Vinexin beta	(Mitsushima et al., 2006a)
Flotillin	Lipid raft-related adaptor protein	Vinexin alpha	(Kimura et al., 2001)
SOCS7	Cytokine signalling regulator	Vinexin alpha	(Martens et al., 2004)

**Table 1: Previously characterised vinexin interactors.**

Table summarising vinexin interactors, grouped by function. Cell adhesion-related proteins (blue, upper): vinculin, DLG5, p130Cap, beta dystroglycan; enzymes (yellow): ERK1/2, SOS1, SHIP2, ABL, CBL; proteins with transcriptional activity (direct or indirect; green): SAFB2, oestrogen receptor alpha, retinoic acid receptor gamma; actin cytoskeleton regulators (orange): rhotekin, WAVE2, WAVE1, N-WASP; others (unclassified; blue, lower): flotillin, SOCS7.

endogenous vinexin alpha and vinexin beta localise to focal adhesions in fibroblasts (Kioka et al., 1999; Mizutani et al., 2007a), with Kioka et al. reporting increased vinculin and F-actin staining at focal adhesions upon vinexin alpha overexpression (Kioka et al., 1999). This localisation requires vinexin SH3 domain: vinculin proline-rich region interactions and accordingly, exogenous vinexin is unable to target focal adhesions in vinculin knockout mouse-derived cell lines (Chen et al., 2005; Takahashi et al., 2005).

Cytosolic vinculin exhibits high affinity intramolecular binding, which renders the protein unable to interact with actin or contribute to protein complexes at focal adhesions (Chen et al., 2005). However, most vinculin at focal adhesions is in the so-called 'open' or 'active' conformation that exhibits an estimated threefold-higher binding affinity for vinexin (Takahashi et al., 2005). In this way, vinexin is implicated in sensing ECM stiffness and calibrating actomyosin tension; vinexin binding favours the 'open' or 'active' vinculin conformation, thereby promoting stable association with F-actin at focal adhesions (Yamashita et al., 2014). Cells grown on rigid substrates exhibit high actomyosin-generated intracellular tension (Geiger et al., 2009), with vinexin alpha required to increase focal adhesion-associated vinculin in cells grown on rigid ECM (Yamashita et al., 2014). Despite also binding vinculin, vinexin beta surprisingly does not perform this function (Yamashita et al., 2014).

Another function performed by vinexin at focal adhesions could be scaffolding actin cytoskeleton modulators. Candidates include rhotekin, an effector protein for RHO GTPases that functions in actin cytoskeleton reorganisation (Reid et al., 1996). The third vinexin SH3 domain binds a proline-rich C-terminal motif in rhotekin, independent of RHO GTPase activity (Nagata et al., 2009). This interaction is inhibited by another member of the RHO GTPase subfamily, CDC42; constitutively activated CDC42 reduces vinexin/rhotekin binding (Nagata et al., 2009). Given the third vinexin SH3 domain also interacts with N-WASP (Mitsushima et al., 2006a), an effector protein for CDC42 that promotes actin polymerisation *via* ARP2/3 complex activation (Rohatgi et al., 1999), CDC42-activated N-WASP could compete with rhotekin for binding to vinexin. Nonetheless, the functional implications of vinexin/rhotekin/N-WASP binding for focal adhesion dynamics remain to be elucidated.

In classical focal adhesions, ECM attachment is mediated through transmembrane integrins (Abercrombie and Dunn, 1975). However, beta dystroglycan (the transmembrane product of pro-dystroglycan proteolytic cleavage) is also reported to perform this function (Thompson et

al., 2010). Thompson et al. demonstrate that the third vinexin SH3 domain binds a proline-rich motif on the beta dystroglycan intracellular face. This has functional implications for focal adhesion-mediated cell spreading; re-expressing mutant beta dystroglycan without vinexin binding capacity in dystroglycan knockdown mouse myoblasts fails to rescue the defective spreading of these cells (Thompson et al., 2010). Vinexin is therefore suggested to facilitate crosstalk between the dystroglycan and integrin adhesion systems, possibly by forming beta dystroglycan/vinexin/vinculin ternary complexes (Thompson et al., 2010).

## **ii. Cell-cell adhesion**

Vinexin could also function at adherens junctions, multi-protein complexes that link the actin cytoskeleton to nectin/cadherin-mediated contacts with neighbouring cells (Campbell et al., 2017). The third vinexin SH3 domain binds a proline-rich region in the adherens junction protein DLG5 (Wakabayashi et al., 2003). As DLG5 uses a separate region to bind the canonical adherens junction protein beta-catenin, Wakabayashi et al. speculate vinexin could contribute to adherens junction assembly by forming beta-catenin/DLG5/vinexin complexes, or even beta-catenin/DLG5/vinexin/vinculin heterotetramers (Wakabayashi et al., 2003).

## **iii. Membrane ruffling**

In addition to N-WASP, vinexin binds another WASP family protein; WAVE2 (Mitsushima et al., 2006a). The two proteins colocalise at migratory human breast cancer cell membrane ruffles (Mitsushima et al., 2006a). Moreover, vinexin colocalises with the non-receptor tyrosine kinase ABL at migratory rat astrocyte membranes ruffles (Mitsushima et al., 2006b). Membrane ruffling characterises the leading edge of migratory cells and is caused by protrusive membrane sheets, shaped by underlying F-actin, detaching from the ECM to move backwards (Mitchison and Cramer, 1996). Given WAVE2 is better able to promote actin polymerisation when phosphorylated by ABL (Leng et al., 2005) and vinexin interacts with WAVE2 and ABL using separate regions (first/second SH3 domains and third SH3 domain, respectively) (Mitsushima et al., 2006a; Mitsushima et al., 2006b), these findings suggest vinexin could function as a scaffolding protein in actin-based cell motility.

## **iv. Cytokinesis**

Vinexin/rhotekin binding has recently been described as important for cell division (Chang and Huang, 2017). Vinexin knockdown in HeLa cells delays cell cycle progression, with increased cell abscission time owing to cytoplasmic bridge resolution failure. Since rhotekin

knockdown and overexpression of mutant vinexin without rhotekin binding capacity also produce this phenotype, Chang and Huang propose that vinexin and rhotekin cooperate to promote cell abscission (Chang and Huang, 2017). Although the precise mechanism remains unclear, this stands to reason as cell cycle progression requires extensive and tightly coordinated cytoskeleton remodelling.

#### **1.2.2.2 MAPK signalling**

Possibly the best understood cellular function of vinexin is in ERK (Extracellular signal-Regulated Kinase) signalling. However, vinexin also participates in other MAPK (Mitogen-Activated Protein Kinase) pathways.

##### **i. JNK pathway**

JNK (c-Jun N-terminal Kinase, otherwise known as MAPK8) activity under EGF (epidermal growth factor) stimulation is enhanced by vinexin beta overexpression (Akamatsu et al., 1999). The molecular mechanism remains uncertain, but is thought to involve vinexin binding SOS1. This RAS/RAC guanine nucleotide exchange factor functions between growth factor receptors and JNK activation in MAPK signalling, with EGF stimulation causing SOS1/vinexin dissociation (Akamatsu et al., 1999). Moreover, vinexin beta mutations preventing SOS1 binding are dominant negative and inhibit JNK activity under EGF stimulation (Akamatsu et al., 1999).

##### **ii. ERK pathway**

Vinexin beta overexpression facilitates anchorage-independent ERK1/2 activation (phosphorylation at threonine 202 and tyrosine 204) under EGF stimulation (Suwa et al., 2002). This function requires the proline-rich 'linker' between the second and third vinexin SH3 domains, which directly interacts with ERK1/2 (Mitsushima et al., 2004; Suwa et al., 2002). Mitsushima and colleagues propose vinexin-dependent anchorage-independent ERK1/2 activation is due to delayed ERK1/2 dephosphorylation, rather than enhanced phosphorylation (Mitsushima et al., 2007). This could involve inhibiting MKP3; overexpressing this ERK1/2-specific phosphatase ameliorates anchorage-independent ERK activation caused by vinexin overexpression (Mitsushima et al., 2007). However, various other phosphatases are also implicated in anchorage-dependent ERK1/2 regulation.

ERK/vinexin binding constitutes a 'docking interaction', enabling ERK2 to phosphorylate vinexin beta at serine 189 (equivalent to serine 593 in vinexin alpha) (Mitsushima et al.,

2004). Ito et al. use a phosphospecific antibody against vinexin to show that (unlike unphosphorylated vinexin) phosphorylated vinexin and ERK1/2 colocalise at developing synapses in primary rat neurons (Ito et al., 2007). At synapses in adult rat brain, vinexin interacts with SRCIN1 (Ito et al., 2008). This adaptor protein undergoes rapid tyrosine phosphorylation following EGF stimulation (Di Stefano et al., 2004). Vinexin might therefore collaborate with MAPK signalling in synapse formation and maintenance, which would concur with the notion synapses are specialised cell-cell junctions (see section 1.2.2.1ii).

Phosphorylated vinexin and ERK1/2 also colocalise at membrane ruffles in migrating cells, plus at the cell periphery during early phase spreading (Mizutani et al., 2007a). To further explore these findings, Mizutani and colleagues use four LNCaP (human prostate cancer) cell lines stably expressing 1. Empty vector (GFP-empty), 2. Wild type vinexin beta (GFP-WT; suggested to be partially phosphorylated), 3. Phospho-null mutant vinexin beta (GFP-SA; serine 189 substituted to alanine) and 4. Phosphomimetic mutant vinexin beta (GFP-SD, serine 189 substituted to aspartine) (Mizutani et al., 2007a). The GFP-SD and GFP-WT lines show reduced spreading compared with the GFP-empty and GFP-SA lines. Moreover, the GFP-SD and GFP-WT lines show reduced migration, while the GFP-SA line demonstrates increased migration compared with the GFP-empty line. The biological properties of vinexin are therefore clearly affected by ERK phosphorylation, meaning activated ERK1/2 could function through vinexin as a negative regulator of early phase spreading and migration (Mizutani et al., 2007a).

### **iii. EGFR pathway**

Vinexin also functions upstream in MAPK signalling; prolonging EGF receptor (EGFR) autophosphorylation in response to EGF stimulation (Mitsushima et al., 2006c). Vinexin beta overexpression delays EGFR endocytosis following EGF stimulation, meaning phosphorylated EGFR is retained at the plasma membrane (Mitsushima et al., 2006c). This could be due to vinexin sequestering the E3 ubiquitin ligase CBL (Mitsushima et al., 2006c), which is thought to ubiquitinate activated EGFR and promote internalisation by endocytosis (de Melker et al., 2004).

#### **1.2.2.3 Oestrogen receptor signalling**

Vinexin interacts with the nuclear matrix protein SAFB2, which acts as an oestrogen receptor corepressor in downregulating oestrogen-induced transcriptional activity (Townson et al., 2003). The functional implications of this interaction remain to be explored, though vinexin

is thought to sequester SAFB2 in the cytosol (Townson et al., 2003). Subsequently, Tujague and colleagues have reported that vinexin alpha overexpression enhances exogenous oestrogen receptor alpha transcriptional activity (Tujague et al., 2004). Exogenous vinexin alpha and oestrogen receptor alpha colocalise in the nucleus, with nuclear vinexin alpha suggested to promote transcriptional activation by reducing oestrogen receptor alpha phosphorylation (Tujague et al., 2004). Given vinexin has no intrinsic enzymatic activity, this must require kinase inhibition and/or phosphatase stimulation.

In what could constitute a negative feedback mechanism, vinexin expression can be regulated by oestrogen receptor signalling. Paz et al. report that exposing male mice to 17beta-estradiol (oestrogen receptor ligand) during embryonic and postnatal development depletes vinexin protein, but not mRNA, from testicular tissue (Paz et al., 2007). This suggests an oestrogen receptor signalling-dependent mechanism for vinexin degradation in the developing testes, though this has not been explored in any further detail.

#### **1.2.2.4 Lipid raft functions**

Lipid rafts are subcompartments of the plasma membrane that function in membrane signalling and trafficking (Lingwood and Simons, 2010). As mentioned above, the vinexin alpha SoHo domain interacts with lipid raft-associated flotillin (Kimura et al., 2001). Based on findings concerning the vinexin family member CAP, Kimura and colleagues suggest vinexin alpha could function in targeting various interactors to lipid rafts. This hypothesis is supported by a much more recent publication demonstrating that vinexin alpha recruits vinculin to lipid rafts (Nagasato et al., 2017). Surprisingly, this does not involve vinexin alpha/flotillin binding, but does require actomyosin-generated intracellular tension (Nagasato et al., 2017). Given vinexin alpha functions in sensing ECM stiffness and calibrating actomyosin tension (see section 1.2.2.1i) (Yamashita et al., 2014), the authors suggest vinexin alpha localises vinculin to lipid raft nanodomains within focal adhesions in response to increased ECM stiffness (Nagasato et al., 2017).

#### **1.2.3 Health and disease**

Literature exists linking vinexin to various pathologies and physiological processes. Often these publications use altered vinexin expression in patient samples as a starting point, before moving into mouse models. Perhaps the most convincing publication using patient data characterises *SORBS3* as a tumour suppressor, although the mechanism by which vinexin opposes tumourigenesis is not well understood.

### 1.2.3.1 Animal models

Studies using *Sorbs3* knockout mice, as well as transgenic mice overexpressing human vinexin, implicate this adaptor protein in several human pathologies (Chen et al., 2013; Guan et al., 2017; Kioka et al., 2010; Li et al., 2015; Liu et al., 2015). Mutant ('*ouchless*') zebrafish with impaired dorsal root ganglion development, ostensibly due to reduced vinexin expression, have also been published (Malmquist et al., 2013). However, in recent months the causative mutation has been re-assigned to *adgra2* (Bostaille et al., 2017).

*Sorbs3* knockout mice are born in the predicted Mendelian ratio and exhibit no obvious abnormalities under basal conditions (Kioka et al., 2010). These mice do however show impaired wound healing; full-thickness skin wounds are slower to close due to impaired keratinocyte migration (Kioka et al., 2010). Another phenotype observed in *Sorbs3* knockout mice is exacerbated cardiac hypertrophy in response to chronic pressure overload (modelled with aortic binding) (Chen et al., 2013). In addition, Chen and colleagues generate transgenic mice with cardiac-specific human vinexin beta overexpression. Following aortic binding, these mice exhibit reduced sequelae of pressure overload-induced cardiac hypertrophy. The relevance of these findings to human disease is demonstrated by decreased vinexin beta mRNA and protein levels in samples from dilated cardiomyopathy patients (Chen et al., 2013).

The same research group report that vinexin beta augments myocardial infarction (MI) pathology (Liu et al., 2015). Liu et al. take as a starting point increased vinexin beta protein levels in tissue from ischaemic heart disease patients. This agrees with reduced post-MI mortality in *Sorbs3* knockout mice, which exhibit ameliorated cardiac dysfunction and decreased infarct size upon post-mortem examination. Opposite phenotypes are seen in transgenic mice with cardiac-specific human vinexin beta overexpression. These findings are attributed to vinexin beta increasing cardiocyte apoptosis and inflammation post-MI (Liu et al., 2015).

In a parallel study, Li and colleagues use *Sorbs3* knockout mice to suggest vinexin deficiency protects against cerebral ischaemia-reperfusion injury, as occurs in stroke (Li et al., 2015). Upon transient middle cerebral artery occlusion followed by reperfusion (used to model ischaemia-reperfusion injury), vinexin-deficient mice exhibit smaller brain infarcts and also obtain less pathological scores on a neurological deficit assessment scale. Moreover, fewer apoptotic neurons are observed in *Sorbs3* knockout mouse brain samples following

ischaemia-reperfusion injury, together with lower expression of pro-apoptotic genes and increased expression of anti-apoptotic genes. Patient samples are used to highlight relevance to stroke; vinexin beta expression is significantly increased in brain samples from intracerebral haemorrhage patients (Li et al., 2015).

Most recently, the same research group has crossed *Sorbs3* knockout mice with *ApoE* knockouts (Guan et al., 2017). *ApoE* knockout mice fed a high fat diet rapidly develop atherosclerosis (Imaizumi, 2011), while *Sorbs3/ApoE* double knockout mice fed the same diet exhibit reduced atherosclerosis development and improved atherosclerotic plaque stability (Guan et al., 2017). This is attributed to an altered inflammatory response; aortic sections from *Sorbs3/ApoE* double knockout mice fed a high fat diet exhibit less macrophage proliferation, together with reduced pro-inflammatory and increased anti-inflammatory marker expression (Guan et al., 2017).

Taken together, these studies suggest vinexin is dispensable under normal physiological conditions (possible due to functional redundancy between vinexin family proteins). However, dysregulated vinexin expression clearly impacts several processes important for human health and disease (namely wound healing, cardiac hypertrophy, myocardial infarction and atherosclerosis) in a context-dependent manner (Chen et al., 2013; Guan et al., 2017; Kioka et al., 2010; Li et al., 2015; Liu et al., 2015).

### **1.2.3.2 Cancer**

The first large-scale study linking vinexin to cancer was published in 2012. Roessler and colleagues identify ten genes associated with hepatocellular carcinoma (HCC) progression (Roessler et al., 2012). Among this ten gene signature, deletion of six genes clustered on chromosome 8p (*DLC1*, *CCDC25*, *ELP3*, *PROSC*, *SH2D4A* and *SORBS3*) predicts poor outcomes in a discovery cohort of 76 patients with hepatitis B-related HCC, plus validation cohorts; two HCC cohorts with mixed aetiology (319 patients) and three breast cancer cohorts (637 patients). Interestingly, the 10 gene signature is only predictive of breast cancer survival in cohorts of mixed node-positive (metastatic) and node-negative cases (not in a node-negative only cohort), suggesting predictive capacity links to tumour cell dissemination (see section 1.2.3.2ii below) (Roessler et al., 2012).

Roessler and colleagues' findings concur with reports that chromosome 8p somatic copy number losses are common in HCC (Jou et al., 2004; Nagai et al., 1997; Xue et al., 2012). Examining this phenomenon in more detail, Xue et al. find these deletions typically centre on

*DLCI* (8p22), although most chromosome 8p somatic copy number losses span larger regions (including *SORBS3* at 8p21.3) (Xue et al., 2012). Using the Integrative Genomics Viewer (Thorvaldsdottir et al., 2013) to visualise recently published somatic copy number profiles for 363 HCC cases (The Cancer Genome Atlas Research Network, 2017) similarly reveals frequent chromosome 8p losses resulting in multiple gene deletions.

In analysing public datasets, Xue et al. find no evidence that chromosome 8p genes (aside from *DLCI*) associated with HCC progression (*DLCI*, *CCDC25*, *ELP3*, *PROSC*, *SH2D4A* and *SORBS3*) (Roessler et al., 2012) harbour somatic point mutations predicted to impact individual gene expression (Xue et al., 2012). With regards to *SORBS3*, this remains the case to the present day; NCI CDC (National Cancer Institute Genomic Data Commons; accessed 09/01/2018) lists no *SORBS3* somatic point mutations in HCC tumours (Grossman et al., 2016), while COSMIC (Catalogue Of Somatic Mutations In Cancer; accessed 12/01/2018) returns nine missense substitutions and two synonymous substitutions in *SORBS3* across HCC tumour samples and cultured cell lines all unlikely to alter vinexin expression (Forbes et al., 2017). Taken together, these data suggest chromosome 8p harbours multiple tumour suppressor genes (including *SORBS3*) whose coattenuation promotes tumourigenesis in HCC, while individual gene deletions are insufficient to drive cancer progression.

Notwithstanding, Roessler and colleagues validate the tumour suppressive properties of vinexin in cultured cells and using a mouse xenograft model. Re-expression of vinexin alpha in HCC cell lines reduced migration and colony formation. Moreover, subcutaneous injection of vinexin alpha-transfected Hep3B cells into immunocompromised mice gives significant fewer and smaller tumours, compared to cells transfected with empty vector (Roessler et al., 2012). One possible mechanism by which *SORBS3* could function as a tumour suppressor in HCC has recently been proposed (Ploeger et al., 2016). Vinexin is suggested to collaborate with *SH2D4A* (another candidate tumour suppressor on chromosome 8p) to inhibit IL-6/STAT3 signalling, which is significant given multiple studies demonstrate the proliferative and anti-apoptotic IL-6/STAT3 pathway can be oncogenic in HCC and other cancers (Yu et al., 2009). Specifically, Ploeger and colleagues propose vinexin alpha indirectly inhibits IL-6/STAT3 signalling through increased oestrogen receptor signalling (Townson et al., 2003; Tujague et al., 2004). This publication supports the hypothesis that *SORBS3* is a tumour suppressor gene, though a complete mechanism (particularly with regards to vinexin beta) remains to be elucidated.

### **i. Proliferation**

Although overexpressing vinexin beta in LNCaP androgen-dependent prostate cancer cells reduces anchorage-independent growth (Mizutani et al., 2007a), most publications do not support the notion vinexin suppresses tumour formation by constraining cancer cell proliferation. For example, vinexin knockdown in PC-3 androgen-independent prostate cancer cells slows cell growth and enhances apoptotic cell death following treatment with the chemotherapeutic agent paclitaxel (Mizutani et al., 2007b). Chang and Huang seek to reconcile their finding that vinexin promotes mitotic cell division (see section 1.2.2.1iv) with vinexin as a putative tumour suppressor; improper segregation of genetic materials upon defective mitosis can result in polyploidy and tumourgenesis (Fujiwara et al., 2005), meaning delayed cell abscission upon vinexin depletion generate cells carrying aberrant genetic material (Chang and Huang, 2017).

### **ii. Migration and invasion**

Migratory capacity is central to the invasive and metastatic properties of cancer cells. As discussed above, vinexin is implicated in cell-extracellular matrix adhesion and membrane ruffling. These functions have implications for cell motility and hence, *SORBS3* as a candidate tumour suppressor. For example, LNCaP cells stably overexpressing vinexin beta show reduced migration by *in vitro* wound healing assay (Mizutani et al., 2007a). However, this effect seems cell type and/or context dependent; vinexin knockdown in A431 epidermoid carcinoma cells reduces migration by the same assay (Kioka et al., 2010).

### **iii. SRC-mediated transformation**

The proto-oncogene *SRC* encodes a non-receptor tyrosine kinase, which is overexpressed in many human cancers. The gene product c-SRC, together with the closely related Rous sarcoma virus protein v-SRC, drive tumourgenesis *via* increased proliferation, invasiveness and motility (Yeatman, 2004). v-SRC transformation reduces vinexin mRNA and protein levels in NIH3T3 mouse fibroblasts, though the effect is much more pronounced for vinexin alpha (Umemoto et al., 2009b). v-SRC also phosphorylates vinexin alpha at tyrosines 127, 170 and 198 (not conserved in vinexin beta). This appears to decrease vinexin/vinculin binding affinity, as non-phosphorylatable mutant vinexin co-immunoprecipitates more efficiently with vinculin (Umemoto et al., 2009b).

With regards to the functional implications of these findings, v-SRC transformed NIH3T3 cells stably re-expressing vinexin alpha migrate even slower than non-transformed cells (Umemoto et al., 2009a). Vinexin alpha re-expression also restores stress fibres in some cells, but does not ameliorate the increase in anchorage-independent growth seen upon v-SRC transformation (Umemoto et al., 2009a). Hence, while vinexin downregulation contributes to SRC-driven oncogenic transformation, unsurprisingly this does account for the whole phenotype.

### **1.2.3.3 Normal brain ageing**

One reason to investigate vinexin before other hits identified in Lipinski and colleagues' screen for autophagy regulators (Lipinski et al., 2010a) relates to a follow-up study published by this research group, which demonstrates vinexin mRNA levels are significantly increased in older human brain samples (Lipinski et al., 2010b). Lipinski and colleagues analyse previously published microarray data (Loerch et al., 2008) and identify a subset of hits (including vinexin) from their initial screen that negatively regulate autophagy and are upregulated in older ( $\geq 70$ -year-old) human cerebral cortex samples, compared with younger ( $\leq 40$ -year-old) samples. Reassuringly, core autophagy genes (*ATG5* and *ATG7*) are also shown to be downregulated in normal brain ageing (Lipinski et al., 2010b). In this way, increased vinexin expression could contribute to the general decline in autophagic potential thought to occur in normal ageing (discussed section 1.1.7.2).

### **1.2.3.4 Neurodegeneration**

Sanchez-Mut et al. report the *Sorbs3* locus is hypermethylated in frontal cortex samples from two well-established AD mouse models (APP/Presenilin 1 and 3xTg-AD) (Sanchez-Mut et al., 2013). This finding replicates in human AD frontal cortex samples and corresponds to decreased vinexin expression on both the mRNA and protein level (Sanchez-Mut et al., 2013). According to Lipinski and colleagues, decreased vinexin expression should upregulate autophagy (Lipinski et al., 2010a), meaning vinexin downregulation in AD disagrees with autophagy protecting against neurodegeneration (discussed in section 1.1.8.2). However, analysis of previously published microarray data (Liang et al., 2008b) reveals that autophagy inhibitors are downregulated in entorhinal cortex from AD patients, with the opposite seen with autophagy inducers (Lipinski et al., 2010b). These data suggest decreased vinexin expression could contribute to a transcriptional upregulation of autophagy in Alzheimer's

disease brains, which Lipinski and colleagues postulate represents a reactive attempt to counter the disease pathology (Lipinski et al., 2010b).

#### ***1.2.4 Concluding remarks***

The complex vinexin interactome (see Table 1) implicates this adaptor protein in multiple cellular processes, with functions at focal adhesions and in ERK signalling the best characterised. Vinexin is also associated with pathophysiological processes ranging from wound healing to normal brain ageing. Notably, *SORBS3* is a candidate tumour suppressor in HCC and other cancers.

Aside from Lipinski and colleagues' screen (Lipinski et al., 2010a), there is no literature linking vinexin to autophagy. However, other focal adhesion adaptor proteins are associated with autophagy. These include paxillin, which reportedly functions in autophagosome formation (Chen et al., 2008). Paxillin does not interact with vinexin directly, but does bind the vinculin 'tail region' (Wood et al., 1994). Hence, vinexin/vinculin/paxillin complexes could conceivably form at focal adhesions, especially given vinexin/vinculin binding favours the vinculin 'open' or 'active' conformation (Yamashita et al., 2014). Focal adhesions dynamics are therefore one possible starting point when exploring how vinexin could regulate autophagy. Another is the cell signalling pathways vinexin influences. For instance, both EGFR and ERK signalling have been linked to autophagy through several different mechanisms (Aoki et al., 2007; Jutten and Rouschop, 2014; Tan et al., 2015; Wong et al., 2010).

## 1.3 YAP and TAZ

### 1.3.1 Introduction

YAP (Yes Associated Protein) and TAZ (Transcriptional Coactivator With PDZ-Binding Motif, also known as WWTR1) are evolutionarily conserved transcriptional coactivators that shuttle between the nucleus and cytosol (Piccolo et al., 2014). YAP was identified *via* a screen for proteins that bind the SH3 domain of the non-receptor tyrosine kinase YES1 (Sudol, 1994). The paralogue TAZ was identified more recently, with human YAP and TAZ sharing 45% amino acid identity in a pattern widely distributed across both sequences (Kanai et al., 2000). In humans, *YAP* maps to chromosome 11q13 and *TAZ* to chromosome 3q24 (Kanai et al., 2000; Sudol et al., 1995). Both YAP and TAZ are near-ubiquitously expressed across human tissues at the mRNA level (Kanai et al., 2000; Sudol et al., 1995). Eight YAP splice variants and two TAZ splice variants have been described to date (Sudol, 2013; Webb et al., 2011), which are distinguished principally by WW domain number (see section 1.3.1.1i). However, only one YAP isoform and one TAZ isoform are commonly studied in humans (Varelas, 2014).

#### 1.3.1.1 Conserved domain structure

Most structural features are conserved between YAP and TAZ.

##### i. TEAD-binding domain

YAP and TAZ bind TEAD (TEA Domain) transcription factors in the nucleus *via* an N-terminal region (Chan et al., 2009b; Mahoney et al., 2005; Vassilev et al., 2001). The crystal structures of the YAP/TEAD1 and YAP/TEAD4 binding interfaces have been solved (Chen et al., 2010; Li et al., 2010). However, which residues are essential for TEAD binding remains controversial. Chen et al. (2010) claim a PxxΦP motif is required (where x is any amino acid and Φ is any hydrophobic residue) for TEAD binding, while Li et al. (2010) report YAP fragments lacking this motif still bind TEADs and highlight that TAZ does not contain a PXXΦP motif. YAP/TEAD4 and TAZ/TEAD4 binding have subsequently been compared and found to utilise identical TEAD C-terminal sites with similar affinities, but require different residues on YAP and TAZ (Hau et al., 2013).

## **ii. 14-3-3-binding domain**

TAZ was identified by screening for novel 14-3-3 interactors; TAZ occupies the 14-3-3 dimer phosphopeptide-binding pocket, but only when phosphorylated at serine 89 (Kanai et al., 2000). Similarly, YAP binds 14-3-3 in the cytosol only when phosphorylated at the equivalent residue (serine 127) (Basu et al., 2003). These interactions impair YAP/TAZ transcriptional activity by sequestering YAP and TAZ in the cytosol (Kanai et al., 2000; Vassilev et al., 2001).

## **iii. WW domain(s)**

Most YAP/TAZ effectors, including non-TEAD transcription factors such as RUNX2 (Yagi et al., 1999), interact with the central WW domain(s) of YAP and TAZ using L/PPxY motifs. These domains contain beta strands grouped around four aromatic residues, typically including two tryptophans (Bork and Sudol, 1994). The human YAP isoform commonly studied contains tandem WW domains, while the TAZ isoform contains only one WW domain (Varelas, 2014).

## **iv. Transcriptional activation domain**

The YAP/TAZ C-terminal region is predominantly unstructured, but rich in serine, threonine and acidic amino acids (Yagi et al., 1999). When tethered to DNA, this domain has strong intrinsic transcription stimulation activity (Kanai et al., 2000; Yagi et al., 1999). Some researchers overlap the coiled-coil and PDZ binding domains (see below) of YAP and TAZ with the transcriptional activation domain (Varelas, 2014).

## **v. Coiled-coil domain**

TAZ binds SMAD transcriptional modulators *via* a C-terminal coiled-coil domain, thereby facilitating TGFbeta signalling by promoting SMAD nuclear accumulation (Varelas et al., 2008). This domain is conserved in YAP, though binding partners remain to be identified.

## **vi. PDZ-binding domain**

The YAP/TAZ extreme C-terminus comprises a small PDZ (Postsynaptic density 95/Disc large/Zonula occludens-1) binding domain, which was first characterised when YAP was found to bind the second PDZ domain of the sodium/hydrogen exchanger regulatory cofactor SLC9A3R1 (Kanai et al., 2000; Mohler et al., 1999). The PDZ domain has since been

identified as important for YAP/TAZ subcellular localisation, especially to the nucleus (Kanai et al., 2000; Oka and Sudol, 2009).

### **1.3.1.2 Non-conserved domain structure**

In addition to the extra WW domain, YAP contains two further domains that are not conserved in TAZ.

#### **i. Proline-rich region**

The YAP extreme N-terminus comprises a proline-rich domain, through which YAP interacts with the RNA- and DNA-binding protein HNRNPU in the nucleus. The authors propose this interaction contributes to an alternative mechanism, auxiliary to transcription factor binding, whereby YAP modulates gene expression (Howell et al., 2004). No further interactors have yet been identified for the YAP proline-rich region.

#### **ii. SH3-binding domain**

YAP was identified *via* a screen for proteins that bind the SH3 (Src homology domain 3) domain of the non-receptor tyrosine kinase YES1. The YAP SH3-binding motif (PKQPPPLAP) also facilitates interactions with other kinases and adaptor proteins such as SRC and NCK1/2, respectively (Sudol, 1994).

### **1.3.2 YAP/TAZ transcriptional activity**

YAP/TAZ transcriptional activity is predominantly mediated through TEAD transcription factors. However, YAP and TAZ interact with several other transcription factors mostly *via* the aforementioned WW domain(s).

#### **1.3.2.1 TEAD transcription factor-mediated transcriptional activity**

Humans express four highly conserved TEAD transcription factors (TEAD1, TEAD2, TEAD3 and TEAD4) (Zhou et al., 2016), which feature the TEA domain DNA-binding motif (Burglin, 1991). YAP and TAZ bind all four TEADs both *in vitro* and *in vivo*, thereby functioning as powerful transcriptional coactivators at TEAD-responsive promoters (Mahoney et al., 2005; Vassilev et al., 2001). By screening a human transcription factor library using an unbiased luciferase reporter assay-based strategy, the Guan laboratory identified TEADs as the major target transcription factors of YAP and TAZ (Zhang et al., 2009; Zhao et al., 2008). Accordingly, interaction with TEADs is necessary and sufficient to induce cell phenotypes associated with YAP/TAZ transcriptional activity. These comprise

increased cell proliferation (including to loss of contact inhibition of proliferation), anchorage-independent growth and resistance to apoptosis, together with oncogenic transformation and epithelial–mesenchymal transition (Chan et al., 2009b; Ota and Sasaki, 2008; Zhang et al., 2009; Zhao et al., 2008). For instance, mutant YAP lacking the TEAD-binding domain fails to promote NIH3T3 mouse fibroblast proliferation (Ota and Sasaki, 2008), while mutant TAZ defective for TEAD binding (serine 89 mutated to alanine) is unable to drive anchorage-independent growth of MCF10A human mammary epithelial cells (Chan et al., 2009b). In both cases, these mutants are presumed to function as dominant negatives by disrupting wild type YAP/TAZ/TEAD interactions.

With regards to YAP/TAZ/TEAD target genes, YAP/TAZ and TEADs have been shown to bind the *CTGF* promoter by chromatin immunoprecipitation (ChIP) (Zhang et al., 2009; Zhao et al., 2008). While CTGF is implicated in cell proliferation and oncogenic transformation (Chu et al., 2008), CTGF depletion only partially ameliorates YAP overexpression-induced anchorage-independent MCF10A cell growth (Zhao et al., 2008). This indicates CTGF works in concert with other target genes to induce YAP/TAZ-associated cell phenotypes. Additional YAP/TAZ/TEAD target genes are suggested by gene expression profiling following overexpression of YAP or constitutively active TEAD2 in NIH3T3 cells (Ota and Sasaki, 2008). Yet while these gene expression profiles largely overlap, only two genes (*Tagln* and *Acta2*) validated in *Tead1;Tead2*- and *Yap1*-null mouse embryos (Ota and Sasaki, 2008).

Addressing the lack of YAP/TAZ/TEAD target genes, the Piccolo group recently conducted ChIP experiments followed by next-generation sequencing (ChIP-seq) for endogenous YAP/TAZ and TEAD4 in MDA-MB-231 human breast adenocarcinoma cells (Zanconato et al., 2015). Taken together, these data indicate TEADs are indeed the main drivers of YAP/TAZ recruitment to chromatin. Notably, over 90% of overlapping YAP/TAZ/TEAD4 ChIP-seq peaks localise to enhancers (more distal to target genes than promoters). The Piccolo group linked YAP/TAZ/TEAD4-bound enhancers and promoters to candidate target genes, which were validated *via* gene expression profiling of YAP/TAZ depleted cells. In agreement with previous literature, the 300+ genes validated describe a cell proliferation-associated transcriptional programme; YAP/TAZ/TEAD target genes are particularly associated with DNA synthesis/repair (as in *CDC6* and *GINS1*) and cell cycle progression (as in *MYC* and *MYBL1*). Lastly, the authors report YAP/TAZ and TEADs form transcription factor complexes with AP-1 transcription factors, many of which are function as oncogenes, thereby jointly regulating transcription (Zanconato et al., 2015).

YAP and TAZ also mediate transcriptional repression through TEADs (Kim et al., 2015). Kim and colleagues report that transcription of around 100 genes in MCF10A cells is suppressed by YAP/TAZ in a TEAD-dependent manner. YAP/TAZ/TEAD co-suppressed genes include the tumour suppressors DDIT4 and TNFSF10, resulting in mTORC1 activation and increased resistance to apoptosis respectively. This is mediated, at least in part, through epigenetic changes caused by YAP/TAZ/TEAD recruiting the NuRD (nucleosome remodelling and histone deacetylase) complex to promoters (Kim et al., 2015).

### **1.3.2.2 Non-TEAD transcription factor-mediated transcriptional activity**

YAP and TAZ co-activate or co-repress multiple non-TEAD transcription factors, with particular implications for developmental and cancer biology. This section also highlights functional disparities between YAP and TAZ, which are not well understood.

#### **i. RUNX transcription factors**

RUNXs (runt-related transcription factors) were the first transcription factors shown to interact with YAP and TAZ; YAP/TAZ WW domain(s) bind RUNX L/PPxY motifs to activate transcription (Kanai et al., 2000; Yagi et al., 1999). More recently, the Piccolo group have confirmed RUNX recognition motifs occur in some YAP/TAZ ChIP-seq peaks (Zanconato et al., 2015). RUNX-mediated transcriptional activity is implicated in bone formation, with TAZ promoting osteoblast-specific transcription through RUNX2 (Cui et al., 2003). TAZ can also bind the nuclear receptor PPAR $\gamma$  to repress adipocyte-specific transcription (Hong et al., 2005). In this way, TAZ regulates mesenchymal stem cell (MSC) differentiation; TAZ depletion drives mouse MSCs towards adipogenesis (away from osteogenesis), as well as reducing skeletal ossification in zebrafish (Hong et al., 2005).

#### **ii. p53-like transcription factors**

YAP binds the full-length isoforms of p53 family members p73 (also known as TP73) and p63 (also known as TP63) to bring about transcriptional co-activation, again through WW domain: L/PPxY motif interactions (Strano et al., 2001). YAP stabilises p73 following DNA damage under cisplatin treatment, thereby supporting concomitant recruitment of p73 and the histone acetyltransferase p300 onto pro-apoptotic target gene regulatory regions (Strano et al., 2005). This function is facilitated by the non-receptor tyrosine kinase ABL, which phosphorylates YAP at tyrosine 357 and drives YAP/p79 recruitment onto the BAX promoter to induce apoptosis (Levy et al., 2008). Hence, in contrast to anti-apoptotic functions

mediated through YAP/TAZ/TEAD transcriptional activity (described above), YAP can also promote apoptosis in response to DNA damage.

### **iii. T-Box transcription factors**

The T-box transcription factor TBX5 binds TAZ, independent of WW domain: L/PPxY motif interactions. TAZ consequently co-activates TBX5, possibly by recruiting histone acetyltransferases (such as p300 and PCAF) onto TBX5-dependent promoters (Murakami et al., 2005). YAP also interacts with TBX5, with beta-catenin/YAP/TBX5 complex formation required for beta-catenin-active colon cancer cell line survival and tumourigenicity. The beta-catenin/YAP/TBX5 complex localises to anti-apoptotic promoters, thereby driving transcription of pro-survival genes such as *BIRC5* and *BCL2L1* (Rosenbluh et al., 2012). Surprisingly, Rosenbluh and colleagues report TAZ is dispensable for beta-catenin-dependent survival and tumourigenicity.

### **iv. PAX transcription factors**

PAX (paired box) transcription factors are implicated in several human cancers, as well as tissue differentiation during normal development (Wachtel and Schafer, 2015). Murakami et al. report that TAZ binds PAX3 in the nucleus, thereby co-activating PAX3-dependent transcription (Murakami et al., 2006). This finding is replicated by Manderfield and colleagues, who identify YAP and TAZ in a luciferase reporter assay-based screen for PAX3 coactivators. YAP/TAZ depletion causes decreased expression of PAX3 target genes such as *Mitf*, which is required for melanogenesis. Moreover, in line with PAX transcription factors performing key roles in development, neural crest-specific *Yap/Taz* deletion is embryonic lethal in mice (Manderfield et al., 2014).

TAZ also binds PAX8, which is required for thyroid gland development (Wachtel and Schafer, 2015). Similar to TAZ/TBX5 binding, TAZ co-activation of PAX8 is independent of WW domain: L/PPxY motif interactions and may involve multiple TAZ/PAX8 domains. TAZ is proposed to drive thyroid development-associated transcriptional programmes through PAX8 (Di Palma et al., 2009). However, TAZ-deficient mice do not exhibit thyroid defects (presumably due to YAP/TAZ functional redundancy) (Hossain et al., 2007; Makita et al., 2008; Tian et al., 2007).

**v. NK2 homeobox 1**

TAZ binds the N-terminal domain of NKX2-1 (NK2 homeobox 1), thereby enhancing NKX2-1 transcriptional activity at the *SFTPC* (surfactant protein C) promoter (Park et al., 2004). This implicates YAP and TAZ in pulmonary development and function. However, defective alveolarisation in TAZ-deficient mice is largely explained by dysregulated CTGF expression; SFTPC expression is not significantly altered in lung tissue from these animals (Mitani et al., 2009). Given NKX2-1 is also known as TTF-1 (thyroid transcription factor 1), TAZ/NKX2-1 binding suggests another mechanism by which YAP and TAZ may influence thyroid development by co-activating NKX2-1 at the *TG* (thyroglobulin) promoter (Di Palma et al., 2009).

**vi. SMAD transcriptional modulators**

SMAD2 and SMAD3 are TGF beta receptor-activated SMADs, which complex with SMAD4 before translocating into the nucleus to partner with transcription factors and drive TGF beta-dependent transcription (Budi et al., 2017). Following TGF beta stimulation, TAZ binds SMAD2/SMAD3/SMAD4 complexes (Varelas et al., 2008). This enhances TGF beta-dependent transcription by retaining SMAD complexes in the nucleus, as well as recruiting additional transcriptional machinery. In this way, TAZ is proposed to regulate stem cell pluripotency; TAZ-depleted human embryonic stem cells lose self-renewal markers and differentiate into neuroectoderm (Varelas et al., 2008). Conversely, YAP is reported to bind SMAD7, promoting association with activated TGF beta receptor 1. These interactions potentiate SMAD7-mediated TGF beta receptor 1 degradation, thereby inhibiting TGF beta-dependent transcription (Ferrigno et al., 2002). Hence, YAP and TAZ may play opposing roles in TGF beta signalling, possibly depending on cell type or physiological context.

**1.3.3 Regulation**

YAP/TAZ regulation centres on subcellular localisation. Nuclear YAP/TAZ is transcriptionally 'active', while cytosolic YAP/TAZ is 'inactive' and ultimately subject to proteasomal degradation. The half-life of YAP is significantly longer than that of TAZ, indicating cytosolic sequestration is the main YAP inhibitory mechanism, while proteasomal degradation applies more to TAZ (Piccolo et al., 2014).

### **1.3.3.1 Hippo pathway-dependent regulation**

The core Hippo pathway comprises a kinase cassette, initially characterised in *Drosophila* (Varelas, 2014). In mammals, MST1/2 (orthologues of *Drosophila* kinase Hippo) activate LATS1/2 by phosphorylating serine 909/872 within the LATS1/2 activation loop, together with threonine 1079/1041 in a hydrophobic motif (Chan et al., 2005). LATS1/2 then phosphorylates YAP and TAZ at HxRxxS/T consensus motifs, the most important residues being serine 127 in YAP/serine 89 in TAZ and serine 381 in YAP/serine 311 in TAZ (Lei et al., 2008; Piccolo et al., 2014). Effective functioning of the Hippo kinase cassette requires regulatory proteins; SAV1 binds and activates MST1/2, while MST1/2-phosphorylated MOB1/2 binds and activates LATS1/2 (Chan et al., 2005; Praskova et al., 2008). The Hippo pathway ultimately inhibits YAP/TAZ transcriptional activity, with LATS1/2-phosphorylated YAP and TAZ subject to cytosolic sequestration and/or proteasomal degradation.

#### **i. Proteasomal degradation**

The Guan laboratory report serine 381 in YAP and serine 311 in TAZ contribute to C-terminal phosphodegron motifs (Liu et al., 2010; Zhao et al., 2010). Serine 381/311 phosphorylation by LATS1/2 prompts further YAP/TAZ phosphorylation by casein kinases (CSNK1D/E) to complete these motifs. This recruits the E3 ubiquitin ligase complex SCF(BTRC), which targets YAP and TAZ for proteasomal degradation *via* ubiquitination.

#### **ii. Cytosolic sequestration by 14-3-3**

YAP and TAZ exhibit phosphorylation-dependent binding to 14-3-3 proteins in the cytosol (Basu et al., 2003; Kanai et al., 2000). In canonical Hippo signalling, YAP/TAZ cytosolic sequestration by 14-3-3 requires phosphorylation at serine 127/serine 89 by LATS1/2. However, other kinases such as AKT can also phosphorylate these residues (Basu et al., 2003).

#### **iii. Cell-cell junction contributions**

YAP/TAZ inhibition is facilitated by the adherens junction protein alpha-E-catenin, which binds phospho-YAP (serine 127) to promote 14-3-3 interaction and inhibit dephosphorylation by the phosphatase PP2A (Schlegelmilch et al., 2011; Silvis et al., 2011). As Schlegelmilch et al. report YAP phosphorylation is unchanged in HaCaT human keratinocytes following MST1/2 or LATS1/2 depletion, this does not necessarily constitute canonical Hippo signalling (Schlegelmilch et al., 2011). Other adherens junction proteins also modulate

upstream Hippo signalling; both E-cadherin and beta-catenin depletion cause decreased YAP phosphorylation at Serine 127 and consequent nuclear accumulation (Kim et al., 2011b).

Moreover, LATS1/2-mediated YAP/TAZ phosphorylation is regulated by the tight junction-associated Crumbs complex (a key regulator of cell shape and polarity) (Bulgakova and Knust, 2009; Varelas et al., 2008). YAP/TAZ binds multiple Crumbs complex components and YAP/TAZ nuclear localisation is negatively correlated with Crumbs complex stability (Varelas et al., 2008). Hence, Varelas and colleagues propose the Crumbs complex promotes efficient assembly of the Hippo kinase cassette, thereby augmenting YAP/TAZ phosphorylation.

### **1.3.3.2 Hippo pathway-independent regulation**

The distinction between Hippo pathway-dependent and -independent YAP/TAZ regulation is becoming increasingly arbitrary. Outlined below are the main mechanisms of YAP/TAZ regulation that could function without Hippo signalling, though these pathways are often ‘reinforced’ by LATS1/2 kinase activity.

#### **i. Proteasomal degradation**

In addition to the C-terminal motif described above, the Guan laboratory report an N-terminal phosphodegron in TAZ. Phosphorylation at serine 58/62 by GSK3 (glycogen synthase kinase 3) recruits SCF(BTRC), which targets TAZ for proteasomal degradation *via* ubiquitination (Huang et al., 2012). This motif is not conserved in YAP (Tian et al., 2007), meaning there are incongruences in YAP and TAZ regulation (as highlighted in section 1.3.2).

The Piccolo group report YAP and TAZ also undergo proteasomal degradation consequent to incorporation into the beta-catenin ‘destruction complex’ (Stamos and Weis, 2013). In the absence of WNT stimulation, YAP/TAZ binds the destruction complex component AXIN1. This facilitates docking of the E3 ubiquitin ligase BTRC to the complex, thereby targeting YAP/TAZ and beta-catenin for proteasomal degradation *via* ubiquitination. Under WNT stimulation, LRP6 (LDL receptor related protein 6)/AXIN1 binding displaces YAP/TAZ from AXIN1 and releases YAP/TAZ from the destruction complex (Azzolin et al., 2014).

#### **ii. Angiotensin-mediated regulation**

In 2011, three groups independently published that angiotensins negatively regulate YAP/TAZ (Chan et al., 2011; Wang et al., 2011; Zhao et al., 2011a). YAP and TAZ bind

full-length angiomin (AMOT p130), AMOTL1 (angiomin-like protein 1) and AMOTL2 (angiomin-like protein 2) through WW domain: L/PPxY motif interactions. This interaction retains YAP/TAZ in the cytosol and occurs independent of Hippo pathway-mediated YAP/TAZ phosphorylation (Chan et al., 2011; Wang et al., 2011). However, considerable cross-talk between angiomin- and Hippo pathway-mediated YAP/TAZ regulation exists (Lv et al., 2017). For example, in addition to YAP and TAZ, angiominins also bind and activate LATS2 (Paramasivam et al., 2011). Paramasivam et al. observe increased YAP phosphorylation at serine 127, together with LATS2/AMOTL2/YAP complexes at Caco-2 epithelial cell tight junctions. More recently, the notion angiominins function exclusively as YAP/TAZ inhibitors has been called into question. In HEK 293 cells AMOT p130 can translocate into the nucleus with YAP to promote transcription of certain YAP/TEAD target genes (Yi et al., 2013). Similarly, AMOTL1 is reported to accumulate in the nucleus with YAP upon release from destabilised tight junctions in primary mouse cardiomyocytes lacking the protocadherin Fat4 (Ragni et al., 2017).

### **iii. Actomyosin-mediated mechanoregulation**

The Piccolo group report YAP/TAZ activity is upregulated in various cell lines due to enhanced cell spreading on stiff ECM (Dupont et al., 2011). Cell spreading increases intracellular tension through RHO GTPase-mediated formation of actin stress fibres and tensile actomyosin structures (Schwartz, 2010). Accordingly, Dupont et al. demonstrate RHO GTPase activity and F-actin, together with myosin II-generated intracellular tension, is required to maintain YAP/TAZ in the nucleus (Dupont et al., 2011).

The absence of actin stress fibres in unspread, densely seeded or detached cells has been shown to upregulate LATS1/2 kinase activity, thereby decreasing YAP/TAZ nuclear localisation and activity (Wada et al., 2011; Zhao et al., 2012). However, the Piccolo group report mechanoregulation occurs independent of Hippo signalling; YAP/TAZ knockdown cells reconstituted with LATS1/2-insensitive TAZ remain responsive to mechanical cues and actin depolymerisation (Dupont et al., 2011). In a subsequent publication, the Piccolo group identify the F-actin capping/severing proteins cofilin, CAPZ and gelsolin as negative regulators of YAP/TAZ activity in unspread, densely seeded cells (as in cells under contact inhibition of proliferation) (Aragona et al., 2013). Mechanoregulation can however, synergise with Hippo signalling; combined CAPZ and LATS1/2 knockdown cooperates to maximise YAP/TAZ nuclear localisation and activity under contact inhibition of proliferation (Aragona

et al., 2013). More recently, the relative contributions made by actin stress fibres and actomyosin tension to YAP/TAZ regulation have been called into question. In this vein, Das and colleagues propose distinct F-actin- and myosin II-dependent YAP/TAZ regulatory pathways, with reduced actomyosin tension affecting YAP/TAZ distribution in sparsely seeded cells to a much lesser extent than actin depolymerisation (Das et al., 2016).

With regards to the mechanism by which actin cytoskeleton dynamics impact YAP/TAZ activity, one possibility is that F-actin sequesters YAP/TAZ inhibitory factors. These include AMOTs, which associate with F-actin *via* an actin binding region closely flanked by YAP/TAZ-binding L/PPxY motifs (Mana-Capelli et al., 2014). Mana-Capelli et al. therefore hypothesise that F-actin and YAP/TAZ compete for AMOT binding. In agreement with this hypothesis, mutant AMOT p130 lacking this actin binding region is more effective than wild type AMOT p130 at retaining YAP in the cytosol (Mana-Capelli et al., 2014). Cross-talk with Hippo signalling is again in evidence; LATS1/2 phosphorylate a site in the AMOT actin binding region, thereby inhibiting F-actin binding and freeing AMOT p130 to sequester YAP in the cytosol (Mana-Capelli et al., 2014).

#### **iv. RHO-mediated G protein-coupled receptor signalling**

G protein-coupled receptor (GPCR) signalling was first implicated in YAP/TAZ regulation when the Guan laboratory published that GPCRs activating  $G_{12/13}$ ,  $G_{q/11}$  or  $G_{i/o}$  increase YAP/TAZ nuclear localisation and activity, while GPCRs activating  $G_s$  have the opposite effect (Yu et al., 2012). In Yu and colleagues' model, ligand binding to  $G_{12/13}$ -coupled receptor leads to decreased LATS1/2 kinase activity, dependent on actin cytoskeleton modulation by  $G_{12/13}$ -activated RHO GTPases (Yu et al., 2012). The  $G_s$ -initiated decrease in YAP/TAZ activity is also suggested to result from increased LATS1/2 activity (Yu et al., 2012). More recently, Hippo pathway involvement in YAP/TAZ regulation by GPCRs has been called into question. In agreement with Yu et al.'s findings, Feng et al. report that activating mutations in *GNAQ* (encodes the Gq alpha subunit) promote YAP nuclear translocation and transcriptional activity (Feng et al., 2014). However, while this does require RHO GTPases activity, the proposed mechanism is F-actin-dependent, LATS1/2-independent (Feng et al., 2014).

Notwithstanding, RHO-mediated YAP/TAZ regulation may be separate from both Hippo signalling and mechanoregulation. The mevalonate pathway (also known as the hydroxymethylglutaryl-CoA reductase pathway) promotes RHO membrane localisation and

consequent GTPase activity by providing geranylgeranyl diphosphate (GGPP) for RHO geranylgeranylation (Liao, 2002). Accordingly, inhibiting the mevalonate pathway with statins upregulates YAP/TAZ activity (Sorrentino et al., 2014; Wang et al., 2014b). While statin treatment does increase YAP/TAZ phosphorylation at LATS1/2 target residues, this is mediated by another (as yet unknown) protein kinase (Sorrentino et al., 2014). Since F-actin depolymerisation inhibits YAP/TAZ in a phosphorylation-independent manner (Das et al., 2016; Dupont et al., 2011), Sorrentino et al. propose RHO-mediated YAP/TAZ regulation is functionally distinct from F-actin mediated regulation. In support of this notion, statin concentrations too low to impact actin cytoskeleton dynamics still reduce RHO GTPase activity and decrease YAP/TAZ nuclear localisation (Sorrentino et al., 2014).

#### ***1.3.4 Normal physiology***

As YAP/TAZ double knockout is embryonically lethal in mammals, understanding YAP and TAZ functions in normal physiology relies heavily on tissue-specific transgenics. In many publications YAP or TAZ are studied in isolation. Hence, the extent to which TAZ can perform functions ascribed to YAP (and *vice versa*) is often assumed, but rarely addressed directly.

##### **i. Early embryonic development**

YAP expression is reported in mouse embryonic day 3.5 (E3.5) blastocysts and all later developmental stages, while TAZ expression is reported from E6.5 onwards (Morin-Kensicki et al., 2006). However, YAP/TAZ double knockout mouse embryos die before the morula stage (16 – 32 cells), suggesting YAP and TAZ are necessary for viability even earlier in embryonic development (Nishioka et al., 2009). By overexpressing dominant negative YAP in pre-implantation mouse embryos, Nishioka et al. demonstrate YAP/TAZ/TEAD4 transcriptional activity is required to convert positional information into cell fate; ensuring outer cells become trophectoderm, while those on the inside become the inner cell mass (Nishioka et al., 2009).

YAP single knockout mouse embryos do not undergo developmental arrest until around E8.5 (Morin-Kensicki et al., 2006), which implies YAP and TAZ are somewhat functionally redundant in early embryonic development. However, YAP appears indispensable for placenta formation and embryonic axis elongation (Morin-Kensicki et al., 2006). In contrast, three groups have published liveborn TAZ single knockout mice (Hossain et al., 2007; Makita et al., 2008; Tian et al., 2007). These publications report around half the expected

Mendelian ratio die before weaning, but the remainder grow into fertile adults. These animals are smaller with reduced lifespan (10 – 12 months), exhibiting polycystic kidneys and pulmonary emphysematous changes (Hossain et al., 2007; Makita et al., 2008; Tian et al., 2007). Hence, YAP appears unable to compensate for TAZ in lung and kidney organogenesis.

## ii. Organ size control

YAP and TAZ were first implicated in organ size control by *Drosophila* studies published in the mid-1990s to early 2000s, showing that mutations in Hippo pathway components result in robust tissue overgrowth (Zhao et al., 2011b). Consensus has since emerged that regulated YAP/TAZ activity contributes to mammalian organ size control, balancing cell proliferation with apoptosis in both organogenesis and adult tissue homeostasis. For instance, liver-specific YAP overactivation in adult transgenic mice causes massive, reversible hepatomegaly (Camargo et al., 2007; Dong et al., 2007). Transgenic hepatocytes are smaller and more densely packed than controls, indicating YAP-induced hepatomegaly is caused by hyperplasia (increased cell number) rather than hypertrophy (increased cell size). Moreover, YAP overactivity upregulates the transcription of anti-apoptotic genes such as *Birc5* and *Birc2* in these cells (Dong et al., 2007).

These finds are mirrored in cardiac development; deleting YAP from mouse cardiomyocytes in early development causes lethal myocardial hypoplasia, while overexpressing constitutively active YAP results in myocardial overgrowth (von Gise et al., 2012). This is partially attributable to increased transcription of genes such as *CcnA2* and *Cdc2*, which promote cell cycle progression (von Gise et al., 2012). However, cross-talk between YAP/TAZ regulation and WNT/beta-catenin signalling (see section 1.3.3.2) is also involved. WNT transcriptional programmes, which have been repeatedly linked to cell proliferation and tissue expansion (Clevers, 2006), are upregulated in cardiomyocytes when YAP/TAZ nuclear translocation is induced (Heallen et al., 2011). This was later explained by the Piccolo group's finding that cytosolic YAP/TAZ binds the beta-catenin destruction complex, thereby targeting beta-catenin (and YAP/TAZ) for proteasomal degradation (Azzolin et al., 2014).

YAP/TAZ transcriptional activity is implicated in development and homeostasis of several further tissues including skin, brain and breast (Cao et al., 2008; Chen et al., 2014b; Schlegelmilch et al., 2011). Yet it is important to recognise that YAP/TAZ organ size control is context-dependent. For example, mammary-specific YAP deletion causes no obvious

defects in mouse breast tissue before pregnancy, while pregnant transgenic mice exhibit hypoplastic mammary glands due to increased mammary alveolar cell apoptosis (Chen et al., 2014b).

### iii. Cell fate determination

YAP and TAZ are involved in balancing stem and progenitor cell self-renewal with differentiation, as occurs in both tissue development and homeostasis. The Guan laboratory observe increased YAP expression in human induced pluripotent stem cells (compared with parental fibroblasts), as well as decreased expression during mouse embryonic stem cell differentiation. These changes in YAP expression actively regulate differentiation and self-renewal, with YAP transcriptional activity increasing expression of pluripotency genes such as *SOX2* (Lian et al., 2010).

YAP/TAZ transcriptional activity is implicated in progenitor cell maintenance in several adult tissues including basal epidermal progenitors in the skin (Schlegelmilch et al., 2011; Zhang et al., 2011) and crypt epithelial progenitors in the small intestine (Camargo et al., 2007). Most recently, Hu and colleagues report YAP and TAZ are required to maintain undifferentiated intermediates (transit-amplifying cells) that arise from dental epithelial stem cells in adult mouse incisors (Hu et al., 2017). Dental epithelium-specific YAP/TAZ double knockout increases expression of genes associated with transit-amplifying cell differentiation into ameloblasts, as in genes encoding amelogenin and ameloblastin, as well as reducing transit-amplifying cell proliferation and increasing apoptosis (Hu et al., 2017).

By maintaining stem and progenitor cell pools, YAP and TAZ mediate functions conventionally associated with the Notch signalling pathway (Sancho et al., 2015). Accordingly, intestine-specific YAP overactivation in adult mice increases the undifferentiated crypt progenitor cell population that express the Notch target gene *Hes1*. This induces intestinal dysplasia, which is partially ameliorated when Notch signalling is suppressed using gamma-secretase inhibitors (Camargo et al., 2007). Yimlamai et al. have since reported that YAP/TAZ/TEAD transcriptional activity directly regulates *Notch2* and other notch pathway genes in mouse hepatocytes (Yimlamai et al., 2014). However, the phenotype observed upon liver-specific YAP overactivation is somewhat different to other tissues; progenitor/ductal-like cells are increased due to hepatocyte de-differentiation, as opposed to expansion of the existing progenitor cell population (Yimlamai et al., 2014).

With regards to vertebrate development, most studies suggest YAP and TAZ function in expanding progenitor cell populations, while inhibiting premature differentiation. For example, electroporating dominant negative YAP or TEAD1 into chick neural tube promotes cell cycle exit and neuronal differentiation (Cao et al., 2008). Moreover, pancreas-specific YAP overactivation during ‘secondary transition’ development (mouse E13.5 – 17.5) expands the progenitor/ductal-like cell population at the expense of exocrine and endocrine differentiation (Gao et al., 2013). However, non-TEAD transcription factor-mediated YAP/TAZ transcriptional activity can also drive stem cells towards one or other differentiated lineage (see section 1.3.2.2i). In this case, TAZ co-activates the RUNX2 transcription factor to promote mouse mesenchymal stem cell differentiation into osteoblasts, while repressing PPARgamma-mediated transcription to inhibit differentiation into adipocytes (Hong et al., 2005). This function is not conserved between YAP and TAZ, presumably because TAZ does not bind PPARgamma (Hong et al., 2005).

#### **iv. Regenerative responses**

YAP and TAZ contribute to repair following injury in several mammalian adult tissues. The YAP/TAZ regenerative response was first studied using dextran sodium sulfate (DSS)-induced colitis in mice (Cai et al., 2010). Following DSS treatment, regenerating colonic crypts exhibit increased YAP protein expression. This is causally implicated in crypt regeneration, as intestine-specific YAP single knockout mice show increased mortality following DSS treatment, together with fewer proliferating cells and more apoptotic cells by colon histology (Cai et al., 2010).

In the heart, YAP/TAZ transcriptional activity is thought to promote regeneration after MI (Del Re et al., 2013; Heallen et al., 2013; Xin et al., 2013). Having induced MI in mice using coronary artery ligation, Del Re and colleagues report cardiomyocytes in the infarct border zone exhibit prominently nuclear YAP staining (as opposed to predominantly cytosolic YAP staining in sham-operated hearts). Moreover, heterozygous YAP deletion is sufficient to blunt the cardiomyocyte regenerative response to MI (Beltrami et al., 2001); apoptosis is increased and proliferation is decreased, resulting in reduced functional recovery (Del Re et al., 2013). On the other hand, YAP/TAZ transcriptional activity may be pathogenic in hypertrophic cardiomyopathy (HCM) (Wang et al., 2014a). YAP protein and mRNA levels are upregulated in human HCM patient samples, together with *CTGF* (canonical YAP target gene) expression. These findings replicate when HCM is modelled in mice using transverse aortic

constriction, plus YAP is implicated in the transcription of foetal genes associated with HCM pathogenesis (*Myh7* and *Tnnt2*) (Wang et al., 2014a).

YAP activity also appears upregulated in human liver tissue from patients with chronic cholestasis (Bai et al., 2012). When this is modelled using bile duct ligation (BDL) in liver-specific YAP single knockout mice, these animals show increased mortality due to compromised regeneration. Specifically, hepatocyte and biliary epithelial cell proliferation is reduced and hepatocyte necrosis is increased (Bai et al., 2012). Hence, YAP/TAZ activation in response to injury is typically adaptive, but can be pathogenic under certain circumstances.

### **1.3.5 Disease**

Aberrant YAP/TAZ expression and/or transcriptional activity is predominantly associated with cancer. However, the Hippo pathway (of which YAP and TAZ are effectors) is implicated in multiple human pathologies, mostly not covered here (see Plouffe et al., 2015 for review).

#### **1.3.5.1 Genetic syndromes**

Mutations in transcription factors that prevent coactivation by YAP and TAZ cause two rare genetic syndromes, namely Sveinsson chorioretinal atrophy and Holt-Oram syndrome (Fossdal et al., 2004; Kitagawa, 2007; Murakami et al., 2005). Sveinsson chorioretinal atrophy is a degenerative eye disease resulting from a heterozygous missense mutation in *TEAD1* (tyrosine 421 mutated to histidine) (Fossdal et al., 2004). The equivalent mutation in mouse *Tead1* was subsequently shown to impair TEAD1 binding to YAP/TAZ, thereby abolishing YAP/TAZ/TEAD1 transcriptional activity (Kitagawa, 2007). Holt-Oram syndrome is characterised by upper limb skeletal abnormalities, coupled with congenital heart defects (Hirst et al., 1999). Murakami and colleagues demonstrate that certain disease-associated truncation mutations in *TBX5* (see section 1.3.2.2iii) are pathogenic, even though DNA-binding capacity is retained, as *TBX5* is rendered unable to co-operate with YAP/TAZ to activate transcription (Murakami et al., 2005).

#### **1.3.5.2 Polycystic kidney disease**

As mentioned above (see section 1.3.4i), TAZ single knockout mice have reduced lifespan in part due to impaired renal function (Hossain et al., 2007; Makita et al., 2008; Tian et al., 2007). These animals have polycystic kidneys (typically from birth) that resemble human polycystic kidney disease (PKD), with multiple round cysts of various sizes distributed

throughout the renal cortex (Hossain et al., 2007; Makita et al., 2008; Tian et al., 2007). Moderate transcriptional downregulation of genes associated with PKD, as in *Ofd1* and *Kif3a* (Feather et al., 1997; Lin et al., 2003), is reported in TAZ knockout mice (Hossain et al., 2007). However, the main pathogenic mechanism is post-translational; TAZ binds the *PKD2* gene product (polycystin 2), thereby targeting polycystin 2 for proteasomal degradation by recruiting the E3 ubiquitin ligase complex SCF(BTRC) (Tian et al., 2007). Polycystin 2, which accounts for 15% of human autosomal dominant PKD, therefore accumulates in TAZ knockout kidneys. Interestingly, YAP does not regulate polycystin 2 turnover (Tian et al., 2007).

In this way, TAZ knockout mice provide useful insights into PKD pathogenesis. However, dysregulated TAZ expression has not been identified in human PKD. Conversely, increased YAP nuclear localisation is reported in cystic tissue from autosomal dominant and autosomal recessive PKD patients, compared with healthy controls (Happe et al., 2011). Compatible with this finding, but in contrast to TAZ knockout mice, nephron-specific YAP knockout mice exhibit dysplastic kidneys with minimal nephrogenesis (Reginensi et al., 2013). Using whole-genome transcript profiling, Reginensi et al. report YAP drives differentiation and morphogenesis transcription programmes in kidney development. Hence, YAP and TAZ likely contribute to PKD pathogenesis through different mechanisms.

### **1.3.5.3 Cancer**

YAP and TAZ are dysregulated in many human cancers, ranging from multiple myeloma to glioblastoma (Plouffe et al., 2015). Unsurprisingly, given aforementioned functions in cell proliferation and resistance to apoptosis, together with stem and progenitor cell self-renewal, most studies find YAP/TAZ activity to be oncogenic (Moroishi et al., 2015). However, there are some exceptions to this rule.

#### **i. Hepatocellular carcinoma**

Having analysed 155 human hepatocellular carcinoma (HCC) samples, Zhao et al. report over half show strong YAP staining (predominantly in the nucleus) by immunohistochemistry, as opposed to weak staining in adjacent non-cancerous tissue (Zhao et al., 2007). YAP overexpression in HCC is associated with poorly differentiated tumours, leading to worse clinical outcomes; shorter disease-free and overall survival times (Xu et al., 2009a). In some cases, YAP overexpression is due to amplification at chromosome 11q22 (Zender et al., 2006). The equivalent amplification (chromosome 9qA1) is reported in tumourigenic mouse

hepatoblasts, which produce tumours that resemble human HCC in recipient mice. Accordingly, depleting YAP from hepatoblasts harbouring the 9qA1 amplicon slows tumour progression in these mice (Zender et al., 2006).

## **ii. Non-small cell lung cancer**

In non-small cell lung cancer (NSCLC), YAP expression on immunohistochemistry is predominantly seen in tumours with worse pathological grading, thereby correlating with lymph node metastasis and shorter overall survival (Wang et al., 2010). Similarly, higher YAP/TAZ ‘gene signature’ expression predicts metastasis and shorter overall survival in a large cohort of lung adenocarcinoma patients (Lau et al., 2014). These findings replicate in mouse and cell culture models; TAZ knockdown in human NSCLC cell lines (A549 and H1299) suppresses proliferation and anchorage-independent growth, as well as tumour formation in immunocompromised mice (Zhou et al., 2011). Similarly, YAP or TAZ knockdown reduces mouse lung tumour cell migration *in vitro*, together with lung metastases after tail vein injection into immunocompromised mice (Lau et al., 2014).

## **iii. Breast cancer**

Chan et al. analyse 126 human breast cancer samples by immunohistochemistry and find TAZ is overexpressed in approximately 20% (Chan et al., 2008). Additionally, gene expression analysis suggests increased YAP/TAZ transcriptional activity in poorly differentiated breast tumours, which correlates with shorter metastasis-free survival time (Cordenonsi et al., 2011). In this context, TAZ expression is linked to oncogenic epithelial–mesenchymal transition (EMT); overexpressing EMT-inducing transcription factors in MCF10A human breast epithelial cells increases TAZ protein levels by reducing proteasomal degradation (Cordenonsi et al., 2011). Moreover, TAZ knockdown reduces the tumorigenicity of human breast cancer cell lines in immunocompromised mice (Chan et al., 2008; Cordenonsi et al., 2011).

The literature on YAP in breast cancer is more conflicted. *YAP* was initially identified as a tumour suppressor, with loss of heterozygosity at the gene locus occurring frequently in luminal breast cancer (Yuan et al., 2008). Follow-up experiments using human breast cancer cell lines demonstrate that YAP depletion enhances cell migration, invasion and anchorage-independent growth *in vitro*, as well as promoting tumour formation in nude mice (Yuan et al., 2008). On the other hand, Wang et al and colleagues report YAP is both underexpressed (24%) and overexpressed (29%) in 69 human breast cancer samples examined by

immunohistochemistry (Wang et al., 2012). In addition, YAP overexpression in MCF7 human breast cancer cells increases proliferation and tumourigenicity in nude mice (Wang et al., 2012).

#### **iv. Epithelioid hemangioendothelioma**

Epithelioid hemangioendotheliomas are rare malignant vascular tumours, which express TAZ-CAMTA1 or YAP1-TFE3 fusion proteins arising from acquired chromosomal translocations (Flucke et al., 2014; Patel et al., 2015). YAP1-TFE3 fusion only occurs in a small subset of tumours with distinct morphology, while over 90% express the TAZ-CAMTA1 fusion protein (Antonescu et al., 2013; Flucke et al., 2014). How TAZ-CAMTA1 or YAP1-TFE3 contribute to tumourigenicity remains unknown, though given CAMTA1 and TFE3 are transcription factors, these fusion protein could conceivably drive aberrant gene expression programmes.

#### **v. Chemotherapy resistance**

An emergent topic in YAP and TAZ research is YAP/TAZ involvement in resistance to various chemotherapy drugs (Zhao and Yang, 2015). For example, the Piccolo group report overexpressing TAZ in human breast cancer cells increases resistance to the chemotherapy drugs doxorubicin and paclitaxel (Cordenonsi et al., 2011). Similarly, combining low doses of the chemotherapeutic cisplatin with a YAP inhibitor ('Peptide 17') is equally as effective at reducing neuroblastoma tumour volume in a mouse xenograft model as high-dose cisplatin alone and gives less hepatotoxicity (Yang et al., 2017).

#### ***1.3.6 Concluding remarks***

YAP and TAZ are physiologically important transcriptional coactivators, which are subject to complex regulatory mechanisms and perform multiple functions relevant to human health and disease. Only one publication has directly linked YAP/TAZ to autophagy; Song and colleagues report YAP promotes MCF7 breast cancer cell survival under nutrient starvation by increasing autophagy flux in a TEAD-dependent manner (Song et al., 2015). However, as explored in chapter 4, our group has recently demonstrated that decreased YAP/TAZ activity reduces autophagosome biogenesis in the context of contact inhibition at high cell densities (Pavel et al., manuscript in preparation).

There is no literature directly linking vinexin to YAP and TAZ. Indeed, Zhao et al. report focal adhesions are not required for cell attachment-induced YAP activation (see section

1.3.3.2iii) (Zhao et al., 2012). The most obvious connection between vinexin and YAP/TAZ, which is explored in chapters 4 and 5, relates to hepatocellular carcinoma; *SORBS3* is a candidate tumour suppressor, while YAP is considered an oncoprotein (Roessler et al., 2012; Zhao et al., 2007)

## 2 Materials & Methods

### 2.1 Cell culture

HeLa (human cervical adenocarcinoma) cells (validated by STR profiling; American Type Culture Collection), RPE (human retinal pigment epithelium) cells and HEK (human embryonic kidney) 293 cells (purchased from European Collection of Authenticated Cell Cultures) were maintained in high glucose (4500 mg/L) DMEM (Dulbecco's Modified Eagle Medium; Sigma-Aldrich D6546) completed with 10% foetal bovine serum (Sigma-Aldrich F7524), 100 units/mL penicillin-streptomycin (Sigma-Aldrich P0781) and 2 mM L-glutamine (Sigma-Aldrich G7513) at 37 °C, 5% carbon dioxide.

HeLa cells stably expressing GFP-LC3 and GFP-mRFP-LC3 (described by Kimura et al., 2007) were cultured in high glucose, complete DMEM (as described above) supplemented with 500 µg/mL G418 (Gibco 1181-031). Autophagy-deficient *ATG16L1* CRISPR HeLa cells, together with autophagy-competent controls (Cas9 Cntrl HeLa), were generated by Dr Maria Jimenez-Sanchez following Ran and colleagues' protocols (Ran et al., 2013a; Ran et al., 2013b). These cells were maintained in high glucose, complete DMEM (as described above).

HepG2 (purchased from European Collection of Authenticated Cell Cultures) and Li7 (purchased from RIKEN Cell Bank) human hepatocellular carcinoma (HCC) cells were maintained in RPMI-1640 (Sigma-Aldrich R0883) completed with 10% foetal bovine serum, 100 units/mL penicillin-streptomycin and 2 mM L-glutamine at 37 °C, 5% carbon dioxide. HuH6 (clone 5) and HLE human HCC cells (purchased from JCRB cell bank), as well as HuH7 (validated by STR profiling; American Type Culture Collection), were maintained in low glucose (1000 mg/L) DMEM (Sigma-Aldrich D5921) completed with 10% foetal bovine serum, 100 units/mL penicillin-streptomycin and 2 mM L-glutamine at 37 °C, 5% carbon dioxide.

I prepared polyclonal mEmerald-vinexin alpha HepG2 stable cell lines, together with mEmerald-empty HepG2 controls, in collaboration with PhD student Anne Jackson. HepG2 cells were transfected with mEmerald-empty and mEmerald-vinexin alpha (see section 2.2 below). Cells stably expressing these constructs were selected using G418 (500 µg/mL) and expanded. FACS was used to select cells expressing mEmerald at an intermediate level.

These cells were maintained in complete RPMI-1640 (as described above), supplemented with 500 µg/mL G418.

Unless otherwise stated, nutrient starvation equates to culturing cells in EBSS (Earle's Balanced Salt Solution; Sigma-Aldrich E2888) for four hours (without pre-washing). All cells lines were regularly tested for mycoplasma contamination by PCR detection kit (Roche 05184240001) and treated when necessary.

## **2.2 DNA expression**

GFP-Htt(Q74) refers to huntingtin exon 1 fragment containing 74 glutamine repeats tagged with EGFP at the N-terminus in pEGFP-C1 empty vector (Clontech 6084-1). This construct was produced by our group and is described in Rankin et al. (2000). mEmerald-empty (mEmerald-C1; Addgene 53975) and mEmerald-vinexin alpha (mEmerald-Vinexin-C-14; Addgene 54305) were produced by the Davidson laboratory (Rizzo et al., 2009). pcDNA-empty (pcDNA3.1) was purchased from ThermoFisher (V79020). pGL3b-8xGTIIC-luciferase refers to a synthetic TEAD promoter driving firefly luciferase expression (8xGTIIC-luciferase; Addgene 34615), which was produced by the Piccolo laboratory (Dupont et al., 2011). The *Renilla* luciferase control reporter (pRL-CMV) was purchased from Promega (E2261). pcDNA-HA-AMOT(p130) (HA-AMOT p130; Addgene 32821) was produced by the Guan laboratory (Zhao et al., 2011a). Flag-YAP (p2xFlag CMV2-YAP2; Addgene 19045) was produced by the Sudol laboratory (Oka et al., 2008).

Unless otherwise stated, cells were transfected at 70-80% confluency in 6-well plates with 1 µg DNA for 24 hours before post-transfection assays. 3 µL TransIT 2020 (Mirus MIR5400) was diluted in 200 µL reduced serum OptiMEM (Gibco 11058021) before 1 µg DNA was added, as per the manufacturer's instructions. This mix was added to wells in 2 mL OptiMEM, which was replaced with appropriate complete medium after four hours minimum.

## **2.3 RNA interference**

All siRNA used in chapters 3 – 5 were purchased from Dharmacon (GE Healthcare; see Table 2.1): siCntrl (non-targeting, scrambled siRNA pool), siSORBS3 (depleting vinexin; SMARTpool, Oligos 5 and 7), siPXN (depleting paxillin; SMARTpool), siYAP (depleting YAP; SMARTpool) and siTAZ (depleting TAZ; SMARTpool). siRNA was resuspended in siRNA buffer (Dharmacon B-002000-UB) to a final concentration of 20 µM, as per the

**Table 2.1: siRNA used in chapters 3 – 5.**

<b>Target RNA</b>	<b>Sequence(s)</b>	<b>Supplier</b>	<b>Catalogue number</b>
non-targeting	UGGUUUACAUGUCGACUAA UGGUUUACAUGUUGUGUGA UGGUUUACAUGUUUUCUGA UGGUUUACAUGUUUCCUA	Dharmacon	D-001810-10
<i>SORBS3</i> (SMARTpool)	GAGAGGCUGUGGCCCCAGUA CAUCUUCCCUGCUAAUUUAU CCAAGGAGCUGACUCUGCA CCU AACACCUCUCAGAUAC	Dharmacon	L-015415-00
<i>SORBS3</i> (Oligo 5)	GAGAGGCUGUGGCCCCAGUA	Dharmacon	J-015415-05
<i>SORBS3</i> (Oligo 7)	CCAAGGAGCUGACUCUGCA	Dharmacon	J-015415-07
<i>PXN</i> (SMARTpool)	CAACUGGAAACCACACAUA GGACGUGGCAACCUGAACA CCAAACGGCCUGUGUUCUU UGACGAAAGAGAAGCCUAA	Dharmacon	L-005163-00
<i>YAP</i> (SMARTpool)	GCACCUAUCACUCUCGAGA UGAGAACA AUGACGACCAA GGUCAGAGAUACUUCUUA CCACCAAGCUAGAUAAAGA	Dharmacon	L-012200-00
<i>TAZ</i> (SMARTpool)	CCGCAGGGCUCAUGAGUAU GGACAAACACCCAUGAACA AGGAACAAACGUUGACUUA CCAAAUCUCGUGAUGAAUC	Dharmacon	L-016083-00

manufacturer's instructions.

Unless otherwise stated, cells were transfected twice in 6-well plates: 1. at 40-50% confluency, 2. at 70-80% confluency. 4  $\mu$ L of each siRNA (stock concentration 20  $\mu$ M) was transfected per well, with assays conducted 72 hours after the second transfection. 4  $\mu$ L Lipofectamine 2000 (ThermoFisher 11668019) and 4  $\mu$ L siRNA were diluted in 500  $\mu$ L OptiMEM. 450  $\mu$ L of this mix was added to 2 mL of the appropriate complete media per well.

#### ***2.4 Pharmacological agents***

Bafilomycin A1 (BAF; Sigma-Aldrich 19-148) was resuspended in DMSO to produce a 100  $\mu$ M stock solution, which was diluted 1:250 in the appropriate complete media. In order to block flux through the autophagy pathway, cells were treated with BAF at 400 nM for 4 hours. Latrunculin A (Santa Cruz sc-202691) was resuspended in DMSO to produce a 500  $\mu$ M stock solution. In order to inhibit actin polymerisation, cells were treated with latrunculin A at 0.5  $\mu$ M (diluted in complete media) for 6 hours. Blebbistatin (Sigma Aldrich B0560) was resuspended in DMSO to produce a 5 mM stock solution. In order to inhibit non-muscle myosin, cells were treated with blebbistatin at 0.5  $\mu$ M (diluted in complete media) for 6 hours. In experiments using BAF, latrunculin A and blebbistatin, an equivalent volume of DMSO was used as the vehicle control. For stimulation with human epidermal growth factor (EGF; Sigma Aldrich E9644), cells were serum starved for 18 hours using high glucose, complete DMEM (described in section 2.1) lacking foetal bovine serum, then treated with 10 ng/mL EGF (timings specified in Figure 3.12 legend).

#### ***2.5 Western blotting***

Cells were lysed directly in 1X Laemmli buffer (62.5 mM Tris pH 6.8, 2% w/v SDS, 10% glycerol, 50 mM DTT, 0.01% w/v bromophenol blue), supplemented with protease inhibitor cocktail (Sigma Aldrich 11873580001). Samples were boiled for 10 minutes at 100°C then separated by SDS-PAGE using self-cast polyacrylamide gels (10 or 15%, as dictated by molecular weights of interest) in 0.1% SDS running buffer (25 mM Tris pH 8.6, 192 mM glycine, 0.1% SDS). Proteins were transferred to PVDF membranes (Millipore IPFL00005 or IPVH00005) in 20% methanol transfer buffer (25 mM Tris pH 8.6, 192 mM glycine, 20% methanol).

When using primary antibodies from Cell Signalling Technology (see Table 2.2), membranes were first incubated in BSA blocking buffer (5% BSA in PBS/0.01% Tween). Otherwise membranes were incubated in milk blocking buffer (5% BSA in PBS/0.01% Tween). In both cases, this incubation was 20 minutes minimum at room temperature. Membranes were subsequently incubated with primary antibodies (see Table 2.2) for at least 12 hours at 4 °C or 4 hours at room temperature, then secondary antibodies for at least 40 minutes at room temperature. All antibodies were diluted in the appropriate blocking buffer. Membranes were washed extensively with PBS/0.01% Tween between steps.

Protein levels were typically visualised using fluorescent dye-labelled secondary antibodies purchased from LI-COR, diluted 1:4,000: IRDye800CW goat anti-mouse (925-32210), IRDye800CW goat anti-rabbit (925-32211), IRDye680RD goat anti-mouse (925-68070) and IRDye680RD goat anti-rabbit (925-68071). Images were acquired using an Odyssey Imager (LI-COR), then quantified using Image Studio Lite software (LI-COR). Otherwise horseradish peroxidase (HRP)-linked secondary antibodies purchased from GE Healthcare were used, diluted 1:2,000: HRP-linked sheep anti-mouse (NA931) and HRP-linked donkey anti-rabbit (NA934). These antibodies were used in conjunction with electrochemiluminescent (ECL) detection reagents (GE Healthcare RPN2232) and X-ray film exposure. If necessary, these films were scanned and quantified using Image Studio Lite software.

## ***2.6 Immunoprecipitation***

Cells were cultured in 25 cm<sup>3</sup> dishes and lysed on ice in 1 mL buffer (50 mM Tris pH 7.5, 150 mM NaCl, 1mM EDTA, 0.5% Triton X-100) supplemented with protease and phosphatase (Sigma Aldrich P5726 and P0044) inhibitor cocktails. Lysates were centrifuged at 30,000 g for 15 minutes at 4 °C. The pellet was discarded and protein concentration of the supernatant determined by Bradford protein assay (Bio-Rad 500-0201). Samples containing 1 mg total protein were incubated with primary antibodies (see Table 2.3) for at least 18 hours on a rotator mixer at 4 °C. Samples from each experimental condition were also incubated with normal mouse or rabbit IgG (also diluted 1:200; Santa Cruz sc-2025 or sc-2027) to control for non-specific binding. Precipitated immunocomplexes were separated by incubation with Protein G magnetic beads (Dynabeads Protein G; Thermo Fisher 10004D) for 4 hours on a rotator

**Table 2.2: primary antibodies used in chapters 3 – 5 for western blotting.**

Target protein	Description	Supplier	Catalogue number	Dilution
Actin	rabbit polyclonal	Sigma-Aldrich	A2066	1:2,000
AMOTL1	rabbit monoclonal	Abcam	ab171977	1:1,000
CTGF	goat polyclonal	Santa Cruz	sc-14939	1:200
EGFR	rabbit polyclonal	Santa Cruz	sc-03	1:200
P-EGFR (Y1068)	rabbit monoclonal	Abcam	ab32430	1:10,000
ERK1/2	rabbit polyclonal	Cell Signalling Technology	9102	1:1,000
P-ERK1/2 (T202/185 and Y202/187)	rabbit polyclonal	Cell Signalling Technology	9101	1:1,000
Flag	mouse monoclonal	Sigma-Aldrich	A2220	1:1,000
GAPDH	mouse monoclonal	Abcam	ab8245	1:1,000
GFP	rabbit polyclonal	Clontech	632592	1:10,000
HA	rabbit polyclonal	Sigma-Aldrich	H6908	1:1,000
Lamin B	rabbit polyclonal	Abcam	ab16048	1:1,000
LC3	rabbit polyclonal	Novus Biologicals	NB100-2220	1:1,000
Paxillin	mouse monoclonal	BD Biosciences	610619	1:1,000
P-p70S6K (T389)	rabbit polyclonal	Cell Signalling Technology	9205	1:1,000
p70S6K	rabbit polyclonal	Cell Signalling Technology	9202	1:1,000
Tubulin	mouse monoclonal	Sigma-Aldrich	T9026	1:10,000
ULK1	rabbit polyclonal	Cell Signalling Technology	4773	1:1,000
P-ULK1 (S556)	rabbit polyclonal	Cell Signalling Technology	5869	1:1,000
P-ULK1 (S758)	rabbit polyclonal	Cell Signalling Technology	14202	1:1,000
Vinexin	rabbit polyclonal	Abcam	ab126971	1:500
YAP/TAZ	mouse monoclonal	Santa Cruz	sc-101199	1:200
P-YAP (S127)	rabbit monoclonal	Cell Signalling Technology	13008	1:1,000

**Table 2.3: primary antibodies used in chapters 3 – 5 for immunoprecipitation.**

Target protein	Description	Supplier	Catalogue number	Dilution
YAP/TAZ	mouse monoclonal	Santa Cruz	sc-101199	1:200
Flag	mouse monoclonal	Sigma-Aldrich	A2220	1:200
HA	rabbit polyclonal	Sigma-Aldrich	H6908	1:200

**Table 2.4: primary antibodies used in chapters 3 – 5 for immunofluorescence.**

Target protein	Description	Supplier	Catalogue number	Dilution
ATG16L1	rabbit monoclonal	Cell Signalling Technology	8089	1:100
CD63	mouse monoclonal	Abcam	ab8219	1:100
HA	rabbit polyclonal	Sigma-Aldrich	H6908	1:100
LC3	rabbit polyclonal	Novus Biologicals	NB100-2220	1:100
Paxillin	mouse monoclonal	BD biosciences	610619	1:100
Vinculin	mouse monoclonal	Millipore	MAB3574	1:100
YAP/TAZ	mouse monoclonal	Santa Cruz	sc-101199	1:50

mixer at 4 °C. Input samples were stored at 4 °C during this time. All samples (immunoprecipitated and input) were boiled in 1X Laemmli buffer for 4 minutes at 100°C, then analysed by western blotting (see section 2.5).

### ***2.7 Nuclear/cytosolic fractionation***

Subcellular fractionation was performed by Dr Carla Bento, as previously described (Bento et al., 2016a). In summary, cells were lysed with Buffer A (10 mM HEPES, 10 mM KCl, 0.1 mM EDTA, 0.4% NP-40, 1 mM DTT) supplemented with protease and phosphatase inhibitor cocktails on ice for 30 minutes. Lysates were centrifuged at 30,000 g for 10 minutes at 4 °C. Supernatants containing cytosolic proteins were collected and stored at 4 °C. Nuclear pellets were resuspended in Buffer B (20 mM HEPES, 0.4 M NaCl, 1 mM EDTA, 10% glycerol, 1 mM DTT) supplemented with protease inhibitor cocktail and incubated on ice for 1 hour. After centrifugation at 30,000g for 10 minutes at 4 °C, supernatants containing nuclear proteins were collected. Protein concentrations were determined by Bradford protein assay. Both fractions were analysed by western blotting (see section 2.5) using primary antibodies against YAP/TAZ, Lamin B and GAPDH (see Table 2.2).

### ***2.8 F- to G-actin ratio assay***

F- to G-actin ratios were determined by Dr Carla Bento, using a commercially available kit (Tebu-Bio BK037) in accordance with the manufacturer's instructions ([www.cytoskeleton.com](http://www.cytoskeleton.com)). Pelleted cells were resuspended and homogenized in warm 'LAS2 Buffer' (lysis and F-actin stabilization buffer) containing 1 mM ATP, then lysates were incubated at 37°C for 10 min. In order to pellet cellular debris, lysates were centrifuged at 500 g for 5 minutes at room temperature. Supernatant (100 µL per sample) was then centrifuged at 30,000 g for 1 hour at 37°C. This step pelleted F-actin, leaving G-actin in the supernatant. In order to inhibit F-actin depolymerisation, lysates were incubated with 1X F-actin enhancing solution (phalloidin; Abcam ab143533) before the initial centrifugation step. After denaturing with 5X SDS sample buffer (0.25 M Tris pH 6.8, 10 % SDS, 0.5 M DTT, 50% glycerol), G-actin and F-actin samples were analysed by western blotting against actin (see Table 2.2 and section 2.5). The ratio of F-actin (pellet after second centrifugation step) to G-actin (supernatant after second centrifugation step) was calculated by western blot quantification (see section 2.5).

## 2.8 Microscopy

### i. Immunofluorescence

Prior to fixation, cells were cultured on glass coverslips in 6-well plates. When using primary antibodies against ATG16L1, HA, paxillin and YAP/TAZ (see Table 2.4), cells were fixed with PFA (paraformaldehyde) at 37°C: 2 minutes in 2% PFA (4% PFA in PBS mixed 1:1 with complete media), then 5 minutes in 4% PFA in PBS. For immunofluorescence using primary antibodies against LC3 and CD63 (see Table 2.4), cells were fixed with cold methanol for 5 minutes at -20°C. In both cases, fixation was followed by permeabilisation using 0.1% Triton X-100 in PBS for 5 minutes at room temperature. Coverslips were then incubated in BSA (bovine serum albumin) blocking buffer (0.5% BSA in PBS, 50 mmol ammonium chloride) for at least 30 minutes at room temperature. When using anti-vinculin antibody (see Table 2.4), coverslips were first washed in Buffer C (100 mM PIPES pH 6.9, 0.5 mM MgCl<sub>2</sub>, 0.1 mM EDTA, 0.01M EGTA), then fixed with Buffer D for 15 minutes at room temperature (1.4% PFA, 0.2% Triton X-100, 2M Glycerol in Buffer C). Blocking was performed with 0.5% BSA in Buffer C (supplemented with 50 mmol ammonium chloride) for at least 30 minutes at room temperature.

In all experiments, coverslips were incubated with primary antibody diluted in the appropriate blocking buffer for 4 hours at room temperature or 18 hours at 4°C. Coverslips were then incubated with Alexa Flour-conjugated secondary antibodies (purchased from Thermo Fisher) diluted 1:400 in the appropriate blocking buffer for 1 hour at room temperature protected from light: goat anti-mouse Alexa Flour 488 (A32723), goat anti-rabbit Alexa Flour 568 (A11036) and goat anti-mouse Alexa Flour 647 (A21235). In order to visualise F-actin, Alexa Flour 488 phalloidin (Thermo Fisher A12379) was added at the blocking step (diluted 1:500 in the appropriate blocking buffer).

Coverslips were mounted using ProLong Gold Antifade with DAPI (Thermo Fisher P36935) and slides stored in the dark at 4°C. Imaging was performed using an LSM880 confocal microscope (x63 oil immersion lens; Carl Zeiss) in conjunction with ZEN software (black edition; Carl Zeiss).

## **ii. Image processing**

Scale bars were added using ZEN software, which was also used to make general brightness/contrast adjustments (applied equally to all images in any given experiment). Integrated intensity (gray levels) and colocalisation (Manders' colocalisation coefficients M1 and M2) were measured from confocal images using Volocity software (Perkin Elmer), with automatic thresholding employed (Costes et al., 2004). If not counted manually (see figure legends), puncta were counted using the Analyze Particles tool in ImageJ software (Schindelin et al., 2012) with manual thresholding applied equally to all images in any given experiment. The same approach was used to quantify F-actin structures visualised by phalloidin staining.

YAP/TAZ localisation was predominantly quantified manually from confocal images viewed with ZEN software. Cells were classified as follows: mostly nuclear YAP/TAZ ( $N > C$ ), YAP/TAZ equally distributed between nucleus and cytosol ( $N = C$ ) and mostly cytosolic YAP/TAZ ( $C > N$ ). In other cases (see figure legends), the YAP/TAZ nuclear integrated intensity to YAP/TAZ cytosolic integrated intensity ratio was calculated using CellProfiler software (Carpenter et al., 2006).

## **iii. Automated fluorescence microscopy**

When not used in immunofluorescence experiments, GFP and mRFP puncta in HeLa cells stably expressing GFP-LC3 and GFP-mRFP-LC3 were quantified using a Cellomics ArrayScan VTI HCS Reader (spot detector application; Thermo Fisher). Cells were cultured in clear bottom, black polystyrene 96-well plates (Sigma-Aldrich CLS3603). Plates were washed with hypotonic media (25% complete media in water) for 5 minutes at room temperature to reduce vesicle clumping, then fixed with 4% PFA in PBS for 2 minutes at room temperature before imaging.

## **iv. GFP-Htt(Q74) aggregation**

Cells cultured on glass coverslips in 6-well plates were transfected with 1.5  $\mu$ g GFP-Htt(Q74) (see section 2.2). After 48 hours, coverslips were fixed with 4% PFA in PBS for 10 minutes at room temperature and mounted using ProLong Gold Antifade with DAPI. Slides were labelled so as to conceal coverslip identity. As previously described by Ravikumar et al. (2002), percentage transfected cells containing aggregates was scored using an Eclipse E600 fluorescence microscope (Nikon). At least 200 cells were analysed per coverslip.

## ***2.9 Luciferase reporter assay***

Cells cultured in 6-well plates were transfected with 0.4 µg pGL3b-8xGTIIIC-luciferase and 40 ng pRL-CMV (see section 2.2). I used a commercially available dual-luciferase report assay kit (Promega E1910), which included all buffers mentioned below. 24 hours post-transfection, cells were lysed in 300 µL ‘Passive Lysis Buffer’ per well for 20 minutes at room temperature. Lysates were centrifuged at 15,000 rpm for 5 minutes at 4 °C. The pellets were discarded and 10 µL of each supernatant combined with 50 µl ‘Luciferase Assay Buffer II’ (prepared following the manufacturer’s instructions) in duplicate in white 96-well plates (Greiner 655074). Firefly luminescence was measured using a GloMax 96 Microplate Luminometer (Promega). 50 µl ‘Stop & Glo Buffer’ (again prepared following the manufacturer’s instructions) was subsequently added to all wells. After 5 minutes, *Renilla* luminescence was measured using the GloMax 96 Microplate Luminometer. Firefly luciferase activity relative to *Renilla* luciferase activity was calculated in Excel (Microsoft) for each well.

## ***2.10 Clonogenic assay***

Clonogenicity was assessed as previously described by Roessler et al. (2012). Following automated counting (Countess Automated Cell Counter; Invitrogen), cells were seeded in triplicate in 6-well plates at 1,000 cells per well. Over the next 10 days, media was exchanged every 2 days. When using HepG2 cells stably expressing mEmerald-empty or mEmerald-vinexin alpha (see section 2.1), complete RPMI-1640 supplemented with 500 µg/mL G418 continued to be used. After 10 days, cells were fixed and stained with crystal violet solution (0.05% crystal violet, 1% PFA, 1% methanol in PBS) for 20 minutes at room temperature. After washing the plates in running water, colonies were counted manually.

## ***2.11 Statistical analysis***

Initial calculations were performed in Excel (Microsoft), before statistical testing and graph construction using PRISM software (version 5.01, GraphPad). As appropriate (see figure legends), PRISM was used to perform: paired t-tests (equivalent to one-sample t-tests for normalised wester blotting data; see below), student's t-tests, one-way ANOVAs followed by Tukey's multiple comparison test and odds ratios followed by 2-tailed Fisher's exact test. Error bars indicate the standard deviation (SD), standard error of the mean (SEM) or 95% confidence interval, as appropriate to the data presented (see figure legends). Unless otherwise stated, # = ns (p value), \* =  $p < 0.05$ , \*\* =  $p < 0.01$ , \*\*\* =  $p < 0.001$ .

Western blotting data was typically generated from at least 3 independent experiments in technical triplicate. In order to normalise these data, protein levels ('protein X') in the experimental condition(s) were expressed relative to loading control protein levels and mean protein X/loading control in the experimental condition(s) normalised to mean protein X/loading control in the control condition. Accordingly, while there is within-condition variability (represented by the SD) between technical replicates, within-condition variability between control values generated from independent experiments is abolished (all mean values are 1). Within-condition variability (represented by the SEM) remains between protein X/loading control values in the experimental condition(s). Paired t-tests performed on these normalised data sets are therefore equivalent one sample t-tests.

## ***2.12 Bioinformatics***

All bioinformatic analysis was performed by Dr Peter Sterk.

### **i. RNA sequencing data analysis**

RNA sequencing data from 'neuropathological normal' human frontal cerebral cortex and hippocampal tissue was obtained from the Genotype-Tissue Expression (GTEx) Consortium (2013). Donors labelled as follows in the subject metadata file were excluded: amyotrophic lateral sclerosis, Alzheimer's disease OR dementia, Alzheimer's disease, dementia with unknown cause, major depression (unipolar depression, major depressive disorder), active encephalitis, Creutzfeldt Jakob relatives, active meningitis, multiple sclerosis, Parkinson's disease, Reyes syndrome, schizophrenia, syphilis infection, unexplained weakness. Donors were also excluded when cause of death was annotated with the following ICD10 codes: C70 to C72 (malignant neoplasms of brain and other parts of central nervous system), F00 to F99 (mental and behavioural disorders), G00 to G99 (diseases of the nervous system) and I60 to I69 (cerebrovascular disease).

Rpkm (Reads Per Kilobase of transcript per Million) values for the genes of interest in both tissues were provided by the GTEx Consortium (2013). Data frames for rpkm values and sample metadata were generated in R ([www.R-project.org/](http://www.R-project.org/); R Core Team, 2014) for both tissues. Scatter plots with linear regression lines were then generated in R for a selection of genes. Overall significance of the regression analysis was established by F-test performed in R, with the adjusted coefficient of determination (adjusted  $R^2$ ) also calculated.

## **ii. Microarray data analysis**

Raw Agilent microarray data (originally published by Thurnherr et al., 2016) was downloaded from NCBI ([www.ncbi.nlm.nih.gov/geo/query/acc.cgi?acc=GSE62043](http://www.ncbi.nlm.nih.gov/geo/query/acc.cgi?acc=GSE62043)). These two-colour data were analysed in Chipster 3.11.2 (Kallio et al., 2011), which uses the R/Bioconductor software package limma (Ritchie et al., 2015). Normalisation and background correction were performed as previously published (Ritchie et al., 2007; Smyth and Speed, 2003), using the following parameters: background treatment = normexp, background offset = 50, array normalisation = loess, gene normalisation = none, control probe removal = no, chiptype = Agilent human whole genome (4112a). In order to identify genes that were statistically significantly differentially expressed in human HCC samples compared with adjacent non-malignant tissue, one sample t-testing was performed in Chipster 3.11.2 using the following parameters: scale to same mean = yes, p-value adjustment method = Benjamini-Hochberg, p-value threshold = 0.05, assumed mean = 0.0.

## 3 Vinexin is a physiologically important autophagy regulator

### 3.1 Introduction

In this chapter I set out to evaluate Lipinski and colleagues' conclusion that vinexin negatively regulates autophagy (Lipinski et al., 2010a) by replicating this observation in multiple cell lines and examining the possibility this finding is due to siRNA off-target effects. I sought to characterise in detail how vinexin beta depletion affects components and function of the autophagy pathway, together with autophagy flux. Using RNA sequencing data generated by the Genotype-Tissue Expression (GTEx) project (GTEx Consortium, 2013) and in collaboration with bioinformatician Dr Peter Sterk, I also aimed to establish the physiological importance of vinexin as an autophagy regulator by examining whether *SORBS3* transcription upregulation could contribute to a general transcriptional decline in autophagy in normal human brain ageing. Finally, I set out to exclude several potential mechanisms by which vinexin might negatively regulate autophagy, including changes in focal adhesion dynamics and kinase signalling pathways with established links to either autophagy or vinexin (mTOR, ULK1, ERK1/2 and EGFR).

### 3.2 *Vinexin beta depletion using siRNA against SORBS3 specifically upregulates autophagy*

Using a genome-wide, image-based siRNA screen, Lipinski and colleagues identified vinexin as a negative regulator of autophagy in H4 human neuroblastoma cells (Lipinski et al., 2010a). I was able to replicate this finding using siRNA against *SORBS3* in HeLa cervical cancer cells, retinal pigment epithelium (RPE) cells and HEK 293 embryonic kidney cells. Autophagy was assessed by measuring lipidated LC3 (LC3-II) levels by western blotting in the presence and absence of the macrolide antibiotic bafilomycin A1 (BAF), which prevents autophagosome-lysosome fusion (Yamamoto et al., 1998). In this way, while changes in LC3-II under basal conditions (DMSO solvent control) could reflect alterations in either autophagosome biogenesis or autophagic flux, changes in the presence of BAF at a saturating concentration must reflect alterations in autophagosome formation (Klionsky et al., 2016; Figure 3.1a). Treating cells with siRNA against *SORBS3* (si*SORBS3*) brought about a robust reduction in vinexin beta protein levels by western blot, which corresponded to an increase in LC3-II (lower band of LC3 doublet) both under basal conditions (DMSO) and in the presence of BAF (Figure 3.1b). When quantified relative to tubulin loading control, LC3-II levels were around 3-fold higher in si*SORBS3* treated cells, compared with nontargeting control siRNA

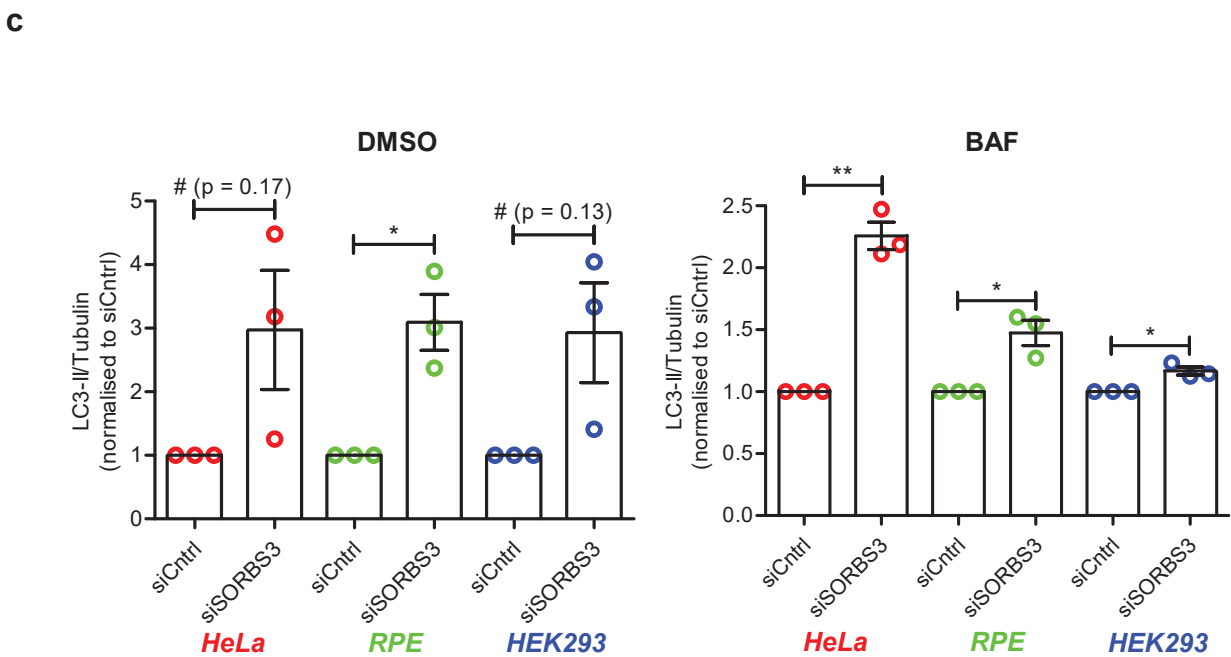
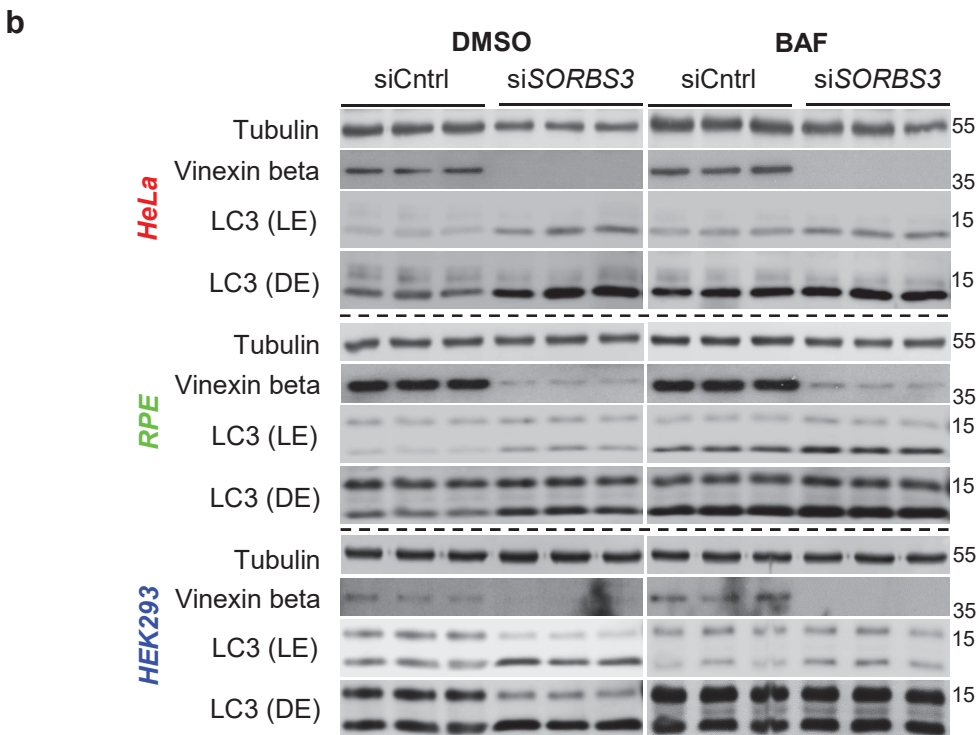
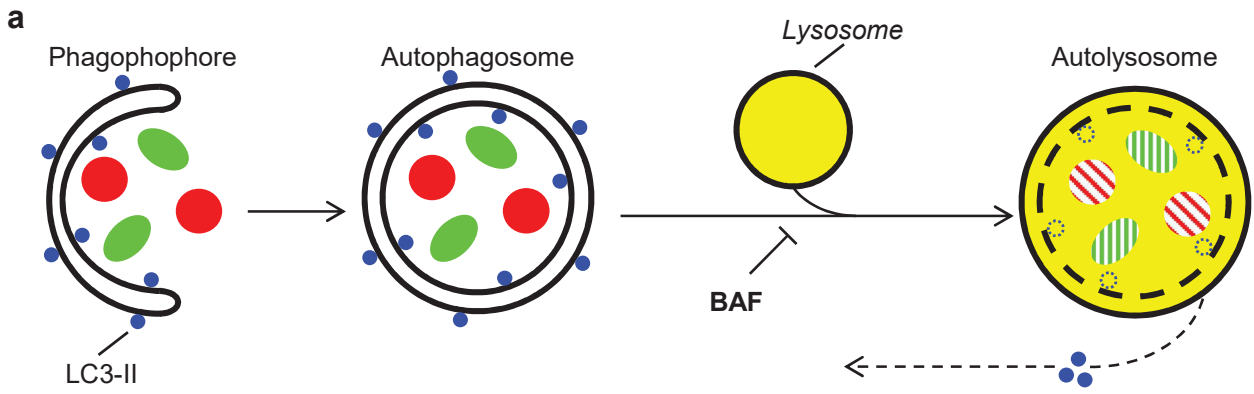


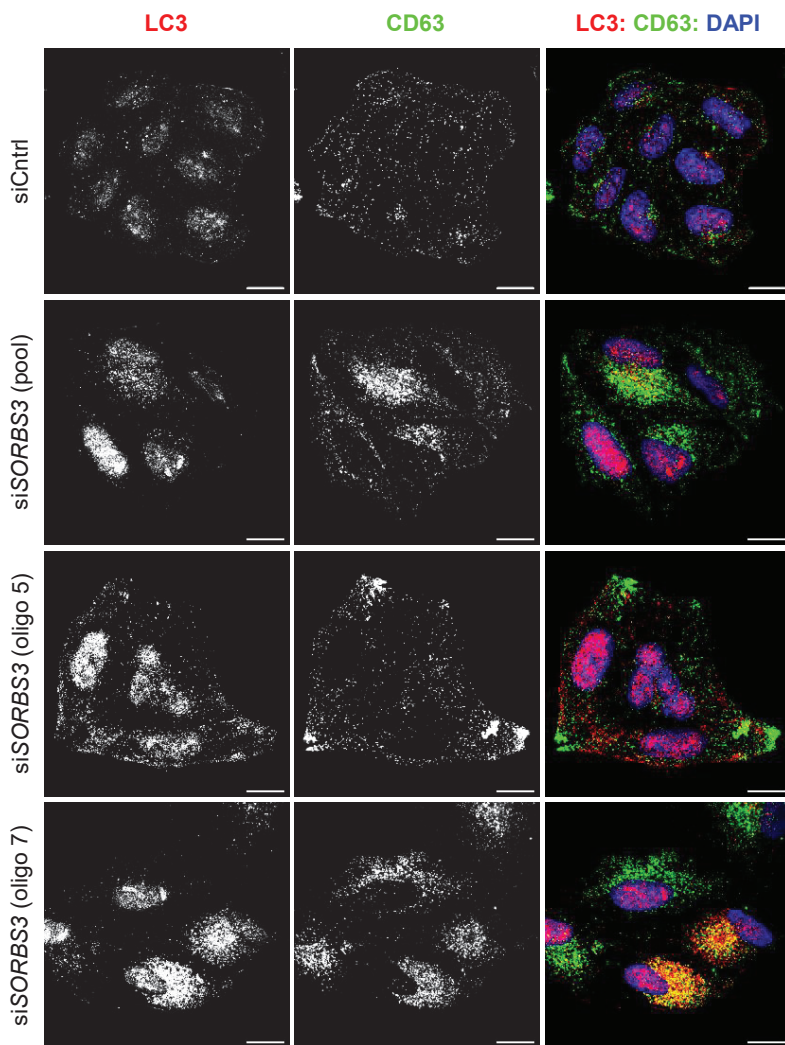
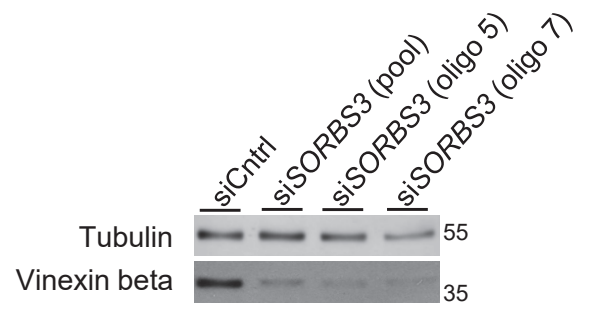
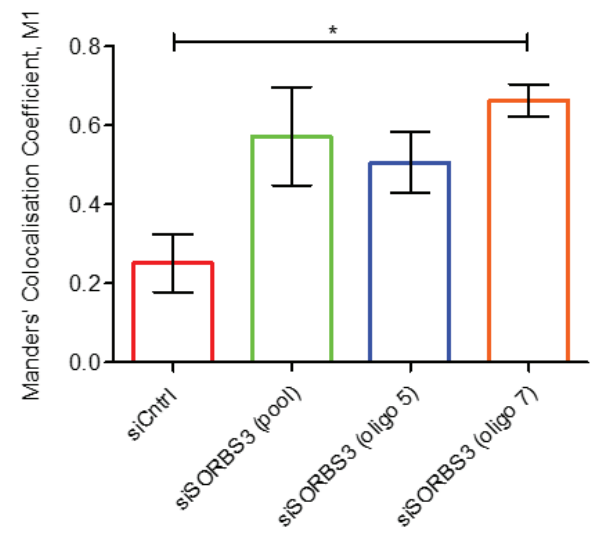
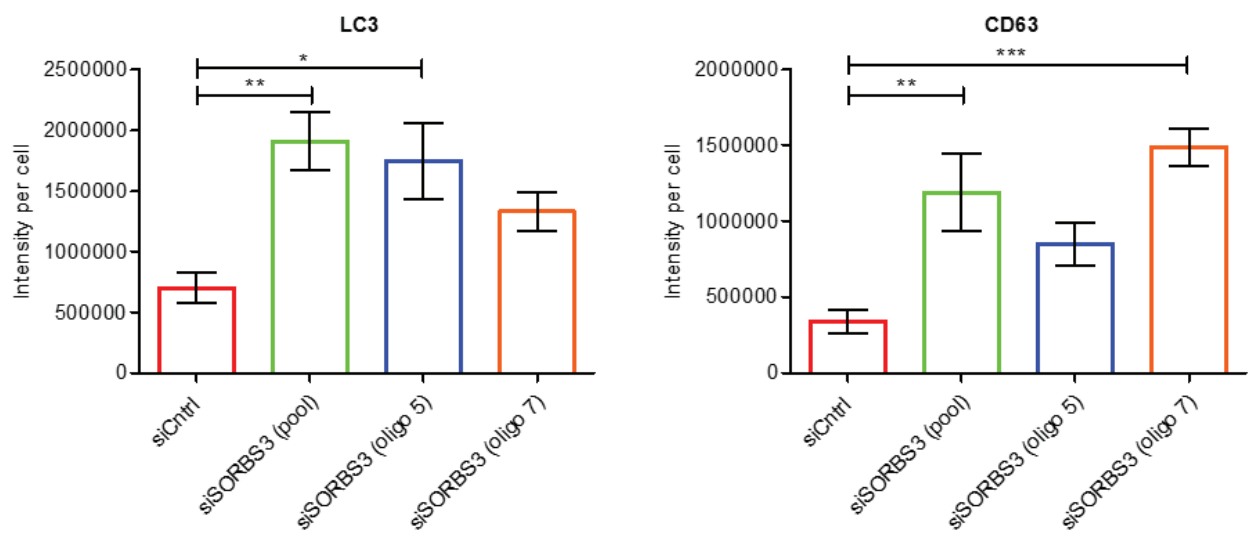
**Figure 3.1: vinexin beta depletion using siRNA against *SORBS3* upregulates autophagy in multiple cell lines.**

- a. Schematic diagram of the autophagic cascade. LC3-II associates with developing and mature autophagosomes, as well as fused autolysosomes, under basal conditions. Bafilomycin A1 (BAF) treatment blocks autophagosome-lysosome fusion, enabling autophagosome biogenesis to be assessed in the absence of autophagosome degradation.
- b. HeLa, RPE and HEK293 cells were depleted of vinexin beta using an individual siRNA oligonucleotide against *SORBS3* (si*SORBS3*; oligo 7). Cells were treated with bafilomycin A1 (BAF; 400 nM) or DMSO vehicle control for 4 hours. Endogenous tubulin, LC3 and vinexin beta protein levels were examined by western blotting. Representative blots from 3 independent experiments per cell line are shown. LE = lighter exposure; DE = darker exposure; molecular weights shown in kDa.
- c. Quantification of 3 independent experiments per cell line. LC3-II (lower band of LC3 doublet) levels are expressed relative to tubulin loading control and normalised to LC3-II/tubulin in control siRNA (siCntrl) treated cells. # = ns (p value); \* =  $p < 0.05$ ; \*\* =  $p < 0.01$  by 2-tailed one-sample t-test. Error bars indicate SEM.

(siCntrl) treated cells under basal conditions (Figure 3.1c). As Lipinski et al. find using the lysosomal protease inhibitor E64d in place of BAF (Lipinski et al., 2010a), the increase in LC3-II levels was smaller when autophagic flux was blocked. Nonetheless, this statistically significant increase in LC3-II levels in the presence of BAF (Figure 3.1c) supports the hypothesis that si*SORBS3* treatment upregulates autophagy. In all three cell lines, vinexin beta seemed the only vinexin isoform expressed at the protein level, as only one of the bands revealed by western blotting (~37 kD; Figure 3.1b) showed reduced density upon si*SORBS3* treatment. For HeLa cells, this agrees with published findings (Kioka et al., 1999), while vinexin expression in RPE and HEK293 cells has not been examined in the literature.

Endogenous LC3 puncta observed by immunofluorescence were increased in HeLa cells treated with two independent siRNA oligonucleotides against *SORBS3* (oligo 5 and oligo 7), together with a pool of four siRNA oligonucleotides against *SORBS3* (pool; Figure 3.2a). There was also an increase in puncta positive for the lysosomal marker CD63 in all three vinexin beta depleted conditions (Figure 3.2a). All three si*SORBS3* treatments brought about a robust reduction in vinexin beta protein levels by western blot (Figure 3.2b). When LC3/CD63 colocalisation was examined, the proportion of LC3-positive pixels colocalising with CD63-positive pixels (Manders' colocalisation coefficient, M1) was found to be comparably increased across the three si*SORBS3* conditions (0.25 to 0.51 - 0.66), though this was only statistically significant for oligo 7 (Figure 3.2c). Similar results were obtained when the intensity of LC3-positive and CD63-positive pixels per cell was calculated; LC3 and CD63 intensity was increased in all si*SORBS3* conditions, with pool and oligo 5 reaching statistical significance for LC3 and pool and oligo 7 for CD63 (Figure 3.2d). Pixel intensity was used as a proxy for puncta number as vesicle clumping made individual puncta difficult to discern in this experiment. Given that LC3 puncta represent both autophagosomes and fused autolysosomes, with LC3/CD63 double positive puncta corresponding to autolysosomes, an increase in LC3/CD63 colocalisation (Figure 3.2c) coupled to a general increase in LC3 and CD63 puncta (Figure 3.2a and d) supports the hypothesis that si*SORBS3* treatment upregulates autophagy with autophagic flux intact. Importantly, obtaining the same results using two independent siRNA oligonucleotides targeting different regions of *SORBS3* goes partway to excluding siRNA off-target effects.

The next step in excluding siRNA off-target effects was to show that si*SORBS3* effects can be rescued by re-expressing vinexin. As vinexin alpha comprises vinexin beta plus an additional N-terminal domain (Kioka et al., 1999), this was achieved by depleting vinexin

**a****b****c****d**

**Figure 3.2: vinexin beta depletion using independent siRNA oligonucleotides targeting *SORBS3* increases endogenous LC3 and CD63 puncta, as well as LC3/CD63 colocalisation.**

- a. HeLa cells were depleted of vinexin beta using a pool of 4 siRNA oligonucleotides against *SORBS3* [si*SORBS3* (pool)] and two individual siRNA oligonucleotides against *SORBS3* [si*SORBS3* (oligo 5) and si*SORBS3* (oligo 7)]. Endogenous LC3 and CD63 were examined by immunofluorescence and confocal microscopy. Representative images from 2 independent experiments are shown. Red = LC3 (Alexa Fluor 568); green = CD63 (Alexa Fluor 488); blue = DAPI. Scale bars indicate 20  $\mu$ m.
- b. In parallel to the imaging described in a., endogenous tubulin and vinexin beta protein levels were examined by western blotting. A representative blot from the 2 independent experiments is shown. Molecular weights shown in kDa.
- c. The proportion of LC3-positive pixels colocalising with CD63-positive pixels (Manders' colocalisation coefficient, M1) was determined from confocal images using Volocity software. Quantification of the representative experiment shown in a. \* =  $p < 0.05$  by one-way ANOVA followed by Tukey's multiple comparison test.  $n = 47$  (siCntrl), 27 [si*SORBS3* (pool)], 25 [si*SORBS3* (oligo 5)], 29 [si*SORBS3* (oligo 7)]. Error bars indicate SD.
- d. Intensity of LC3-positive and CD63-positive pixels (gray levels) were determined from confocal images using Volocity software. Quantification of the representative experiment shown in a. \* =  $p < 0.05$ , \*\* =  $p < 0.01$ , \*\*\* =  $p < 0.001$  by one-way ANOVA followed by Tukey's multiple comparison test.  $n = 47$  (siCntrl), 27 [si*SORBS3* (pool)], 25 [si*SORBS3* (oligo 5)], 29 [si*SORBS3* (oligo 7)]. Error bars indicate SD.

beta from HeLa cells using siRNA against *SORBS3*, then restoring vinexin expression by overexpressing mEmerald-tagged vinexin alpha. In agreement with Figure 3.2, si*SORBS3* treatment in HeLa cells overexpressing empty vector control (mEmerald-empty) gave a statistically significant increase in endogenous LC3 puncta by immunofluorescence (Figure 3.3a and b). However, the increase in LC3 puncta was ameliorated in HeLa cells expressing mEmerald-tagged vinexin alpha at an appropriate level (outlined in white; Figure 3.3a and b). In this way, I began to generate data supporting Lipinski and colleagues' report that vinexin negatively regulates autophagy, as well as establishing that my findings using siRNA against *SORBS3* did not represent off-target effects.

### ***3.3 Vinexin beta depletion using siRNA against SORBS3 promotes functional autophagy***

I went on to characterise in detail how vinexin beta depletion impacts autophagy. HeLa cells stably expressing GFP-LC3 are a useful tool for studying autophagosomes in isolation (Figure 3.64a). Treating GFP-LC3 HeLa with si*SORBS3* caused a statistically significant increase in GFP-LC3 puncta per cell under basal conditions (DMSO) and in the presence of BAF (Figure 3.4b and c). Taken together, these results suggest vinexin beta depletion increases autophagosome numbers, predominantly by upregulating autophagosome formation.

I used HeLa cells stably expressing GFP-mRFP-LC3 to examine the effect of si*SORBS3* on autophagic flux. As GFP fluorescence is quenched at more alkali pH than mRFP fluorescence, this construct can be used to track autophagosome maturation (Kimura et al., 2007); GFP-positive vesicles are autophagosomes, while RFP-positive vesicles can be either autophagosomes or autolysosomes (Figure 3.4d). Treating GFP-mRFP-LC3 HeLa with si*SORBS3* increased both GFP/mRFP-double positive autophagosomes and mRFP-single positive autolysosomes per cell in the presence and absence of BAF (Figure 3.4e and f). This finding supports the hypothesis that flux through the autophagy pathway remains intact when autophagosome formation is upregulated by vinexin beta depletion.

I next sought to establish whether pre-autophagosomal structures were increased by vinexin beta depletion. This was achieved by immunostaining for ATG16L1, which localises to the outer surface of developing autophagosomes and dissociates from mature autophagosomes (Mizushima et al., 2003). Endogenous Atg16L1 has an obvious punctate staining pattern only upon autophagy induction, as in under starvation (Ravikumar et al., 2010a). Accordingly, while ATG16L1 puncta were barely visible under basal conditions (data not shown),

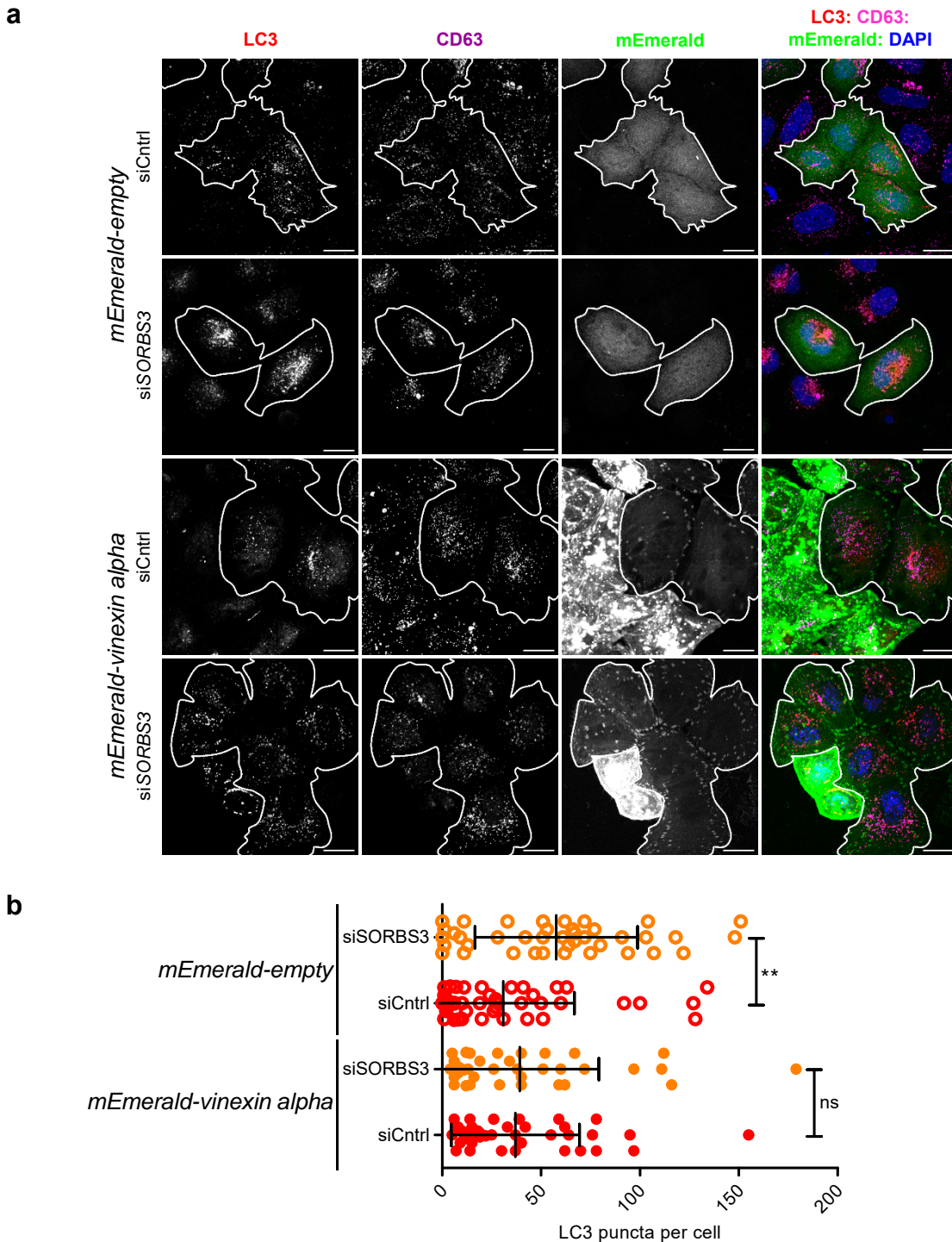


**Figure 3.3: vinexin alpha overexpression ameliorates the increase in endogenous LC3 puncta caused by vinexin beta depletion.**

a. HeLa cells were depleted of vinexin beta using an individual siRNA oligonucleotide against SORBS3 (siSORBS3; oligo 7). siCntrl and siSORBS3 treated cells were transfected with mEmerald-vinexin alpha or empty vector control (mEmerald-empty) for 48 hours. Endogenous LC3 and CD63, as well as mEmerald, were examined by immunofluorescence and confocal microscopy. Representative images from 3 independent experiments are shown. Red = LC3 (Alexa Fluor 568); purple = CD63 (Alexa Fluor 647); green = mEmerald; blue = DAPI. Scale bars indicate 20  $\mu$ m.

b. LC3 puncta were counted from confocal images acquired as described in a. using ImageJ software. Quantification of the representative experiment shown in a. ns =  $p > 0.05$ ; \*\* =  $p < 0.01$  by one-way ANOVA followed by Tukey's multiple comparison test. n = 45 (mEmerald-empty, siCntrl), 40 (mEmerald-empty, siSORBS3), 41 (mEmerald-empty, siSORBS3), 38 (mEmerald-vinexin alpha, siSORBS3). Error bars indicate SD.

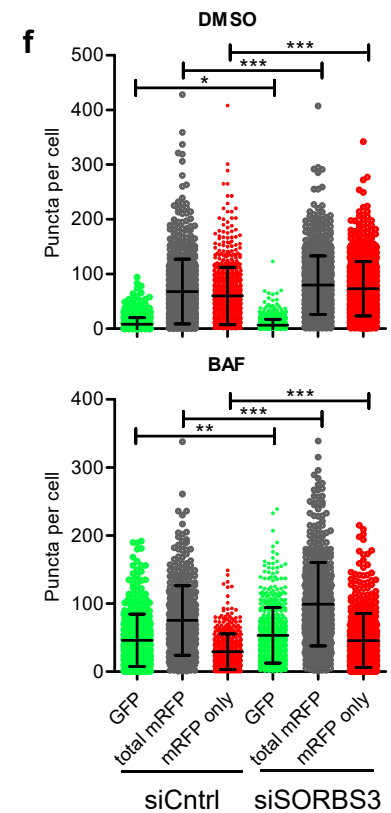
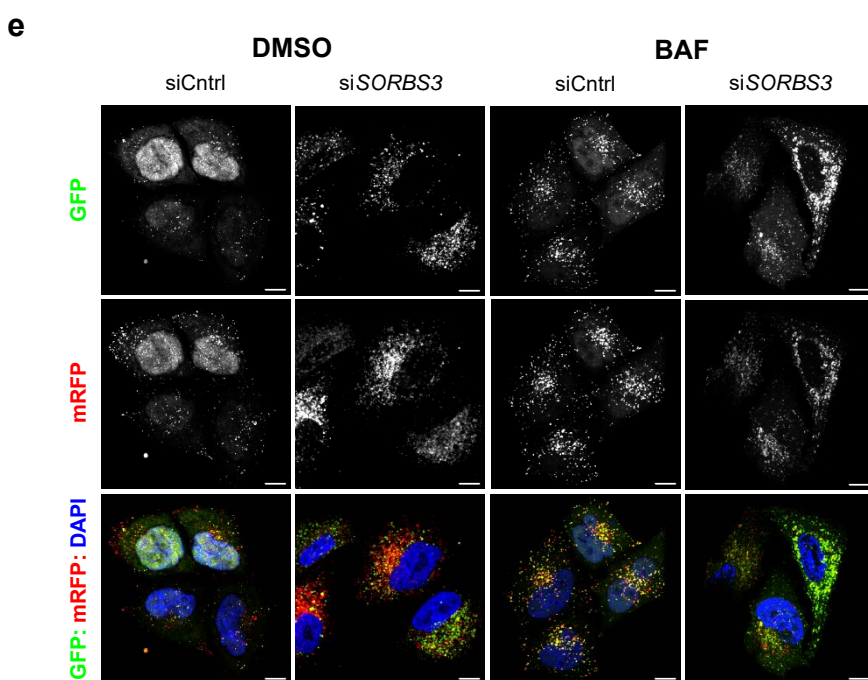
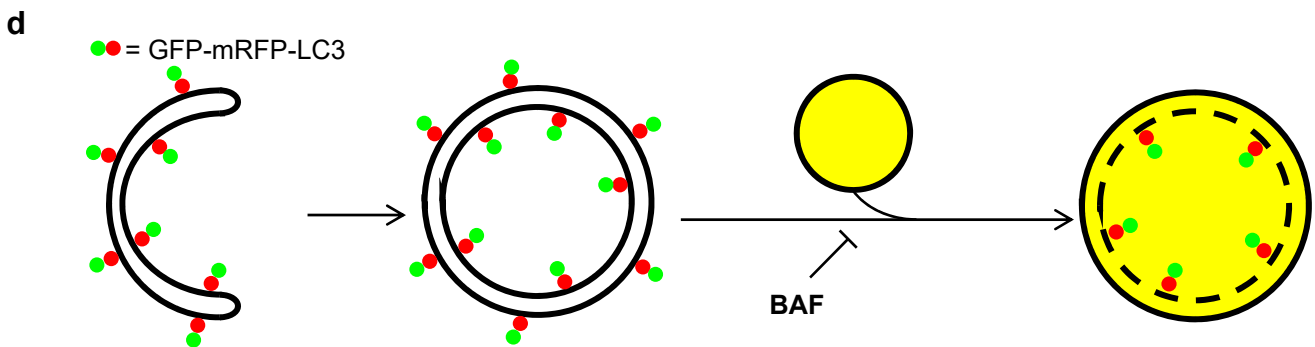
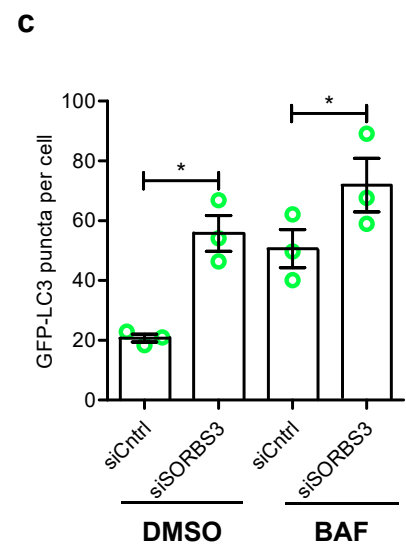
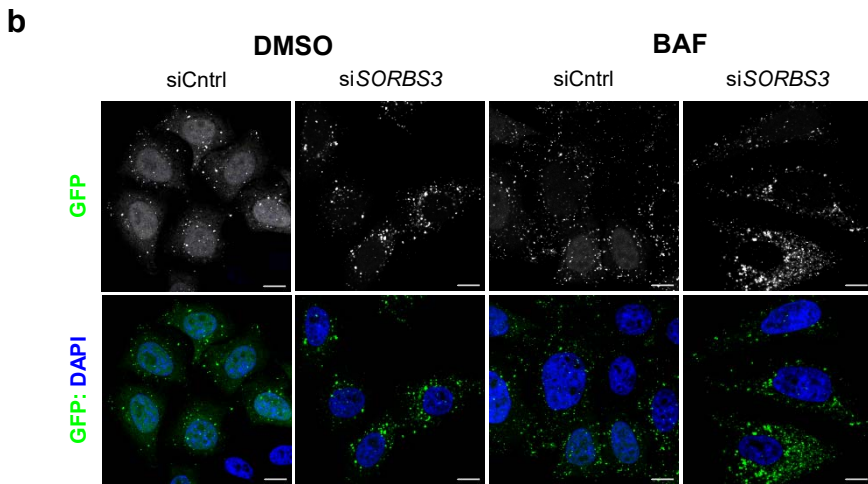
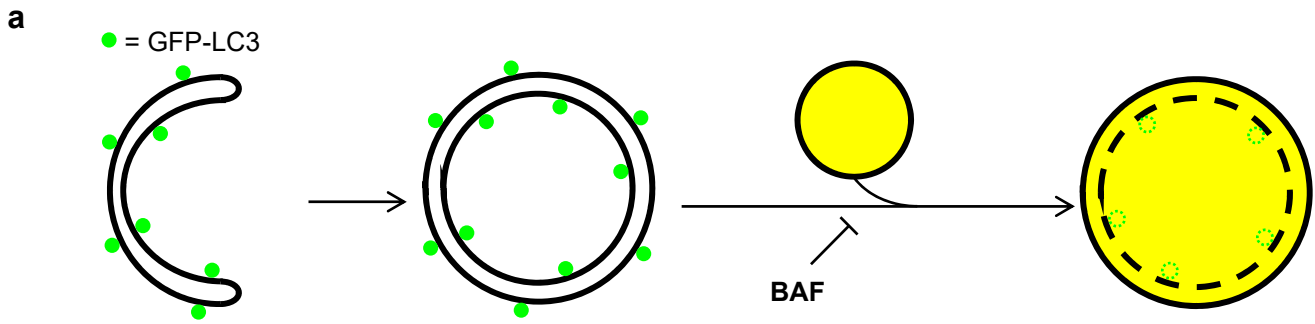


**Figure 3.4: vinexin beta depletion using siRNA against *SORBS3* increases autophagosome and autolysosome numbers.**

- a. Schematic diagram of the autophagic cascade showing that GFP-LC3 marks developing and mature autophagosomes. The green fluorescence exhibited by GFP is quenched in autolysosomes due to the lower pH. Bafilomycin A1 (BAF) treatment prevents this effect by blocking autophagosome-lysosome fusion, causing GFP-positive autophagosomes to accumulate.
- b. HeLa cells stably expressing GFP-LC3 were depleted of vinexin beta using an individual siRNA oligonucleotide against *SORBS3* (si*SORBS3*; oligo 7). Cells were treated with BAF (400 nM) or DMSO vehicle control for 4 hours. GFP-LC3 was examined by confocal microscopy. Representative images from 3 independent experiments are shown. Green = GFP; blue = DAPI. Scale bars indicate 10  $\mu$ m.
- c. GFP-LC3 puncta from the experiments described in a. were counted by Cellomics automated fluorescence microscopy. Quantification of 3 independent experiments is shown. \* =  $p < 0.05$  by 2-tailed paired t-test. Error bars indicate SEM.
- d. Schematic diagram of the autophagic cascade showing that GFP-mRFP-LC3 marks developing and mature autophagosomes, as well as fused autolysosomes. Since GFP green fluorescence is quenched in autolysosomes due to the lower pH, only autophagosomes are GFP-positive, while both autophagosomes and autolysosomes are mRFP-positive. BAF treatment causes GFP/mRFP-double positive autophagosomes to accumulate.
- e. HeLa cells stably expressing GFP-mRFP-LC3 were depleted of vinexin beta using an individual siRNA oligonucleotide against *SORBS3* (si*SORBS3*; oligo 7). Cells were treated with BAF (400 nM) or DMSO vehicle control for 4 hours. GFP-mRFP-LC3 was examined by confocal microscopy. Representative images from 3 independent experiments are shown. Green = GFP; red = mRFP, blue = DAPI. Scale bars indicate 10  $\mu$ m.
- f. GFP-mRFP-LC3 puncta from the experiments described in e. were counted by Cellomics automated fluorescence microscopy. GFP = autophagosomes, total mRFP = autophagosomes and autolysosomes, mRFP only = autolysosomes. Quantification of the representative experiment shown in e. \* =  $p < 0.05$ , \*\* =  $p < 0.01$ , \*\*\* =  $p < 0.001$  by 2-tailed Student's t-test. n = 709 (siCntrl, DMSO), 828 (si*SORBS3*, DMSO), 437 (siCntrl, BAF), 544 (si*SORBS3*, BAF). Error bars indicate SD.

si*SORBS3* clearly increased ATG16L1 puncta per cell upon starvation in Earle's Balanced Salt Solution (EBSS; Figure 3.5b-c). These data suggests si*SORBS3* does increase in ATG16L-positive pre-autophagosomal structures, which contributes to autophagy upregulation upon vinexin beta depletion.

In order to assess whether vinexin beta depletion promotes functional autophagy, I used the aggregate-prone model autophagy substrate GFP-Htt(Q74) (GFP-tagged huntingtin exon 1 fragment containing 74 glutamine repeats) (Ravikumar et al., 2002). Both autophagy-competent (Cas9 Cntrl) and autophagy-deficient (*ATG16L1* CRISPR) HeLa cells were treated with si*SORBS3* or control non-targeting siRNA (siCntrl) before transfection with GFP-Htt(Q74) (Figure 3.6a and b). si*SORBS3* reduced the percentage of transfected Cas9 Cntrl cells with GFP-Htt(Q74) aggregates, while there was no statically significant change in the percentage of transfected *ATG16L1* CRISPR cells with aggregates (Figure 3.6c). These findings indicate vinexin beta depletion reduces aggregate load, with the fact only autophagy-competent cells showed a statically significant reduction suggesting this is predominantly due to an increase in functional autophagy.

### ***3.4 SORBS3 is transcriptionally upregulated and core autophagy genes transcriptionally downregulation in normal human brain ageing***

Following on from their initial siRNA screen, Lipinski and colleagues utilise previously published microarray data (Loerch et al., 2008) to identify a subset of hits, including vinexin, that negatively regulate autophagy and are upregulated in older human cerebral cortex samples (Lipinski et al., 2010b). This is proposed to form part of a general transcription downregulation of autophagy in normal human brain ageing (see chapter 1, section 1.1.7.2), with *BECN1*, *ATG5* and *ATG7* expression reported to decline in normal brain ageing (Lipinski et al., 2010b; Shibata et al., 2006).

In collaboration with Dr Sterk, I sought to replicate these findings using RNA sequencing data generated by the GTEx project (GTExConsortium, 2013). Dr Sterk used RNA sequencing data from donors deemed 'neuropathological normal' (defined in chapter 2) to perform regression analysis examining the relationship between chronological age (independent variable) and mRNA expression (dependent variable) for the genes of interest. For the canonical autophagy genes *BECN1*, *ATG5*, *ATG7* and *PIK3C3*, mRNA expression is negatively correlated with age in samples from both frontal cerebral cortex and hippocampus

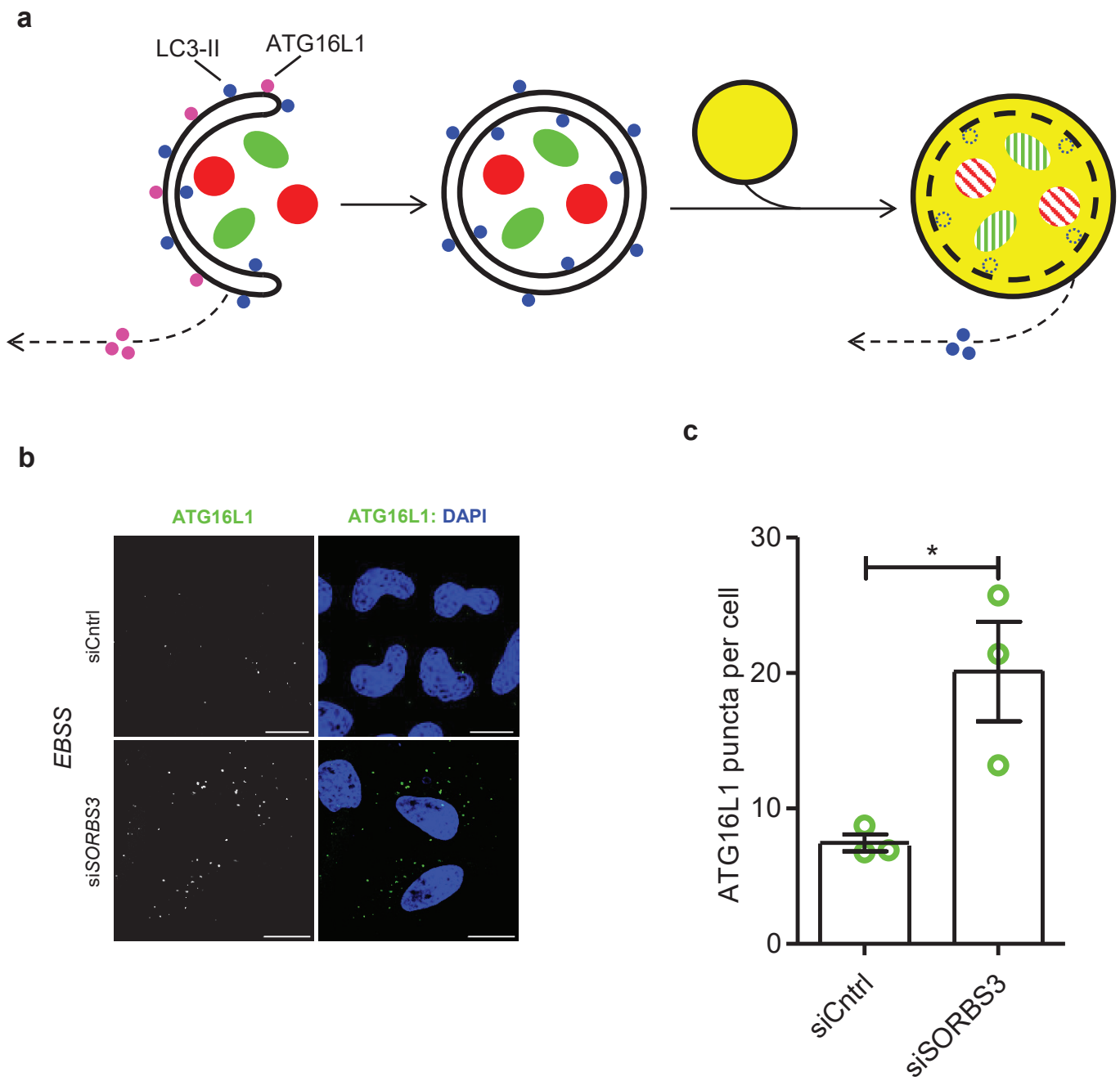


**Figure 3.5: vinexin beta depletion using siRNA against *SORBS3* increases ATG16L1-positive autophagosome precursor numbers.**

- a. Schematic diagram of the autophagic cascade showing that ATG16L1 marks developing autophagosomes, but dissociates from mature autophagosomes.
- b. HeLa cells were depleted of vinexin beta using an individual siRNA oligonucleotide against *SORBS3* (si*SORBS3*; oligo 7). Cells were starved in Earle's Balanced Salt Solution (EBSS) for 4 hours. Endogenous ATG16L1 was examined by confocal microscopy. Representative images from 3 independent experiments are shown. Green = ATG16L1; blue = DAPI. Scale bars indicate 20  $\mu\text{m}$ .
- c. ATG16L1 puncta were counted from confocal images acquired as described in b. using ImageJ software. Quantification of 3 independent experiments is shown. \* =  $p < 0.05$  by 1-tailed paired t-test. Error bars indicate SEM.

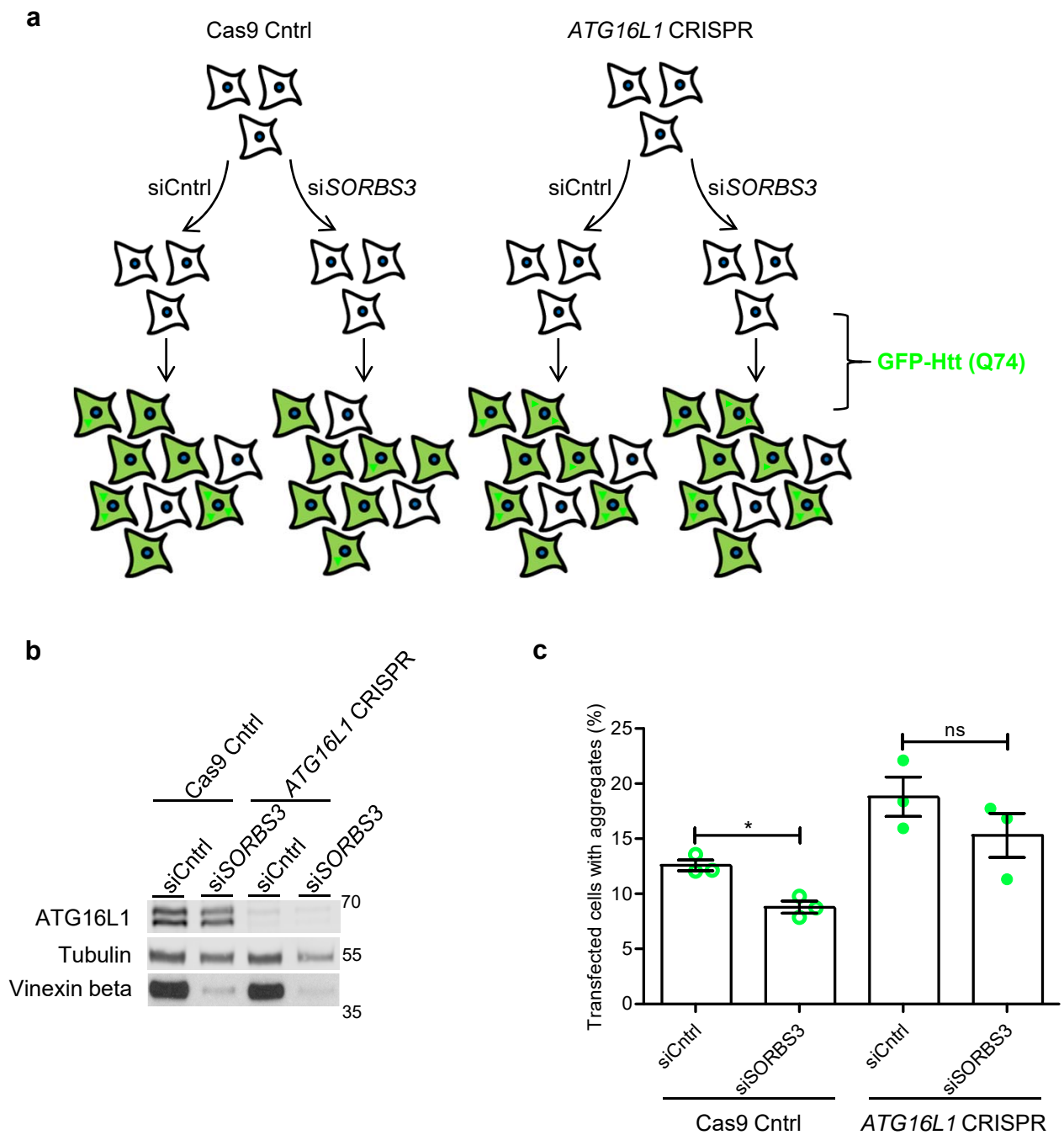


**Figure 3.6: vinexin beta depletion decreases the percentage of GFP-Htt(Q74) transfected cells with aggregates in an autophagy-dependent manner.**

- a. Schematic diagram of the experimental setup. Autophagy-competent (Cas9 Cntrl) and autophagy-deficient (*ATG16L1* CRISPR) HeLa cells were depleted of vinexin beta using an individual siRNA oligonucleotide against *SORBS3* (si*SORBS3*; oligo 7). Cells were transfected with an aggregate-prone GFP-tagged huntingtin exon 1 fragment containing 74 glutamine repeats [GFP-Htt (Q74)] for 48 hours. GFP-positive (total transfected) cells and cells with aggregates were counted manually by fluorescence microscopy.  $n \geq 600$  per condition.
- b. As part of the experiment described in a., endogenous *ATG16L1*, tubulin and vinexin beta protein levels were examined by western blotting. A representative blot from 3 independent experiments is shown. Molecular weights shown in kDa.
- c. Percentage of transfected cells with aggregates was calculated. Quantification of 3 independent experiments is shown. ns =  $p > 0.05$ ; \* =  $p < 0.05$  by 2-tailed paired t-test. Error bars indicate SEM.

(Figures 3.7a-d and 3.8a-d). Concurrently, *SORBS3* mRNA expression is positively correlated with age in frontal cortex and hippocampus samples (Figures 3.7e and 3.8e).

In order to validate this approach, we selected positive control genes from the published literature. Using microarray expression profiling, Loerch et al. identified *CAMK4* as robustly age-downregulated in cortical samples from humans, rhesus macaques and mice (Loerch et al., 2008). This study seemed especially relevant given the human microarray data forms the basis of Lipinski and colleagues' later findings with regards to age-related changes in *ATG5*, *ATG7* and *SORBS3* expression (Lipinski et al., 2010b). As part of the first analysis of the GTEx project RNA sequencing data, *EDA2R* was found to be globally upregulated with age (Mele et al., 2015). Using regression analysis similar to that performed by Dr Sterk, Mele et al. report that *EDA2R* mRNA expression is positively correlated with age in nerve and artery samples. We were therefore reassured to find that, while mRNA expression of the housekeeping gene *TUBA1A* (negative control) did not correlate with age (Figures 3.7f and 3.8f), *CAMK4* expression was negatively correlated and *EDA2R* positively correlated with age in frontal cortex and hippocampus samples (Figures 3.7g-h and 3.8g-h).

For all genes showing age-correlated expression in this analysis, it should be noted that the adjusted  $R^2$  statistic (adjusted coefficient of determination, which ranges from 0 – 1) is small. This could be taken to indicate the regression line is not a good fit for the data. However, the inherently high unexplainable variability in data obtained *via* a large, multi-centre study using samples from individual donors must be taken into consideration. Indeed, Mele et al. report regression coefficients close to zero (-0.015 – 0.023) for all genes identified as significantly differentially expressed with age using the same RNA sequencing data (Mele et al., 2015).

Using a considerably larger sample size than previous studies, we concluded that we had replicated changes in *BECN1*, *ATG5*, *ATG7* and *SORBS3* expression in normal ageing reported in frontal cortex samples (Lipinski et al., 2010b; Shibata et al., 2006). We also expanded the list of brain regions in which autophagy may be transcription downregulated with age to include the hippocampus, which is significant given this structure is particularly vulnerable to damage in the early stages of Alzheimer's disease (Braak et al., 1993). Lastly, we added another core autophagy gene (*PIK3C3*) to those that may be subject to downregulation in normal brain ageing.

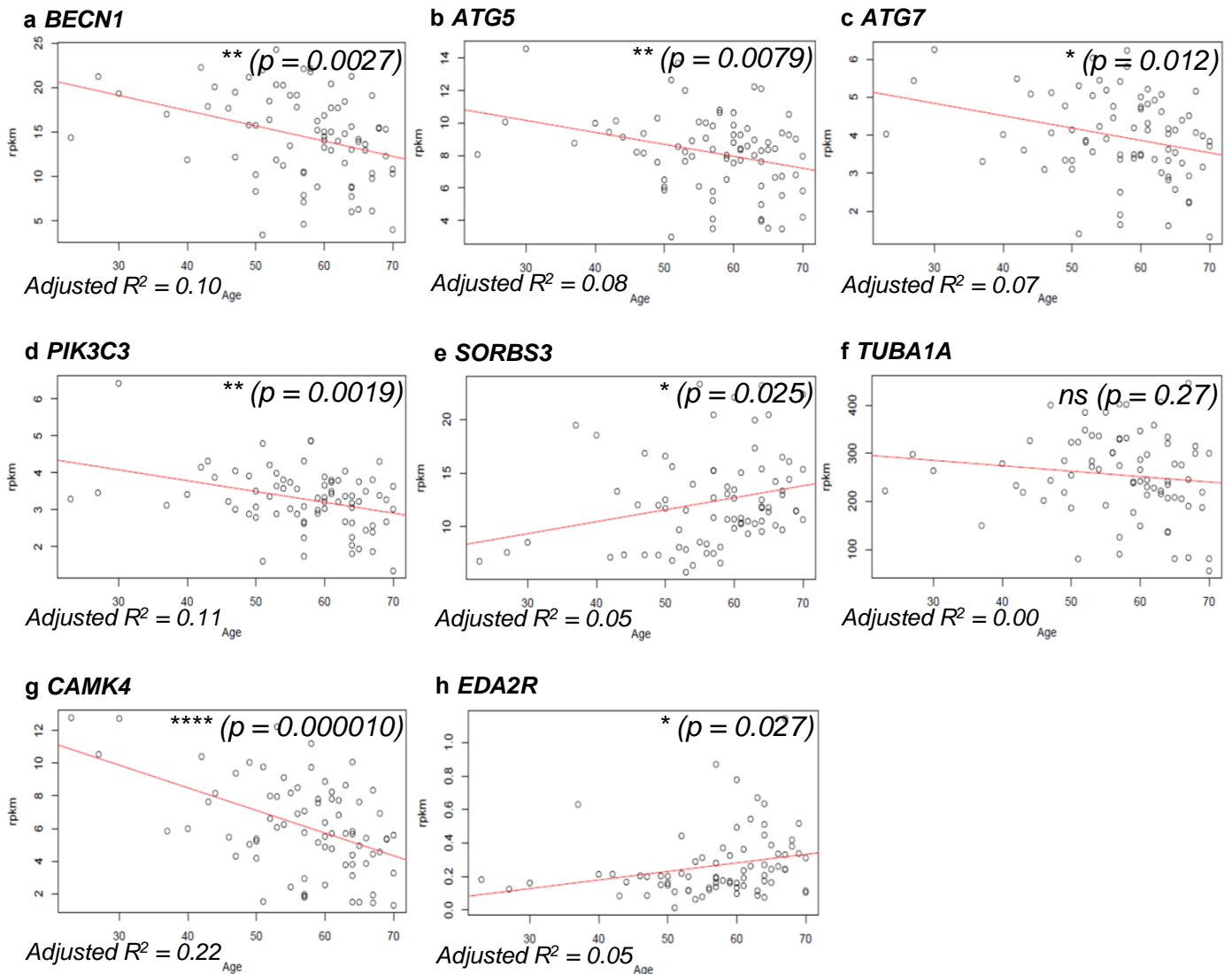


**Figure 3.7: autophagy is transcriptionally downregulated with age in normal human frontal cortex.**

- a. *BECN1* mRNA expression (Reads Per Kilobase of transcript per Million; rpkm) determined by RNA sequencing of samples from 'neuropathological normal' frontal cerebral cortex was plotted against chronological age of donors. A scatterplot and regression line were generated using R. The adjusted coefficient of determination (adjusted  $R^2$ ) was calculated and displayed on the scatter plot (bottom left). Overall significance of the regression analysis was established by F-test and the p value displayed on the scatter plot (top right).  $n = 77$ .
- b. *ATG5* mRNA expression; c. *ATG7* mRNA expression, d. *PIK3* mRNA expression, e. *SORBS3* mRNA expression, f. *TUBA1A* mRNA expression (negative control), g. *CAMK4* mRNA expression (positive control) and h. *EDA2R* mRNA expression (positive control) determined by RNA sequencing of samples from frontal cerebral cortex were subject to the same analysis as described in a.  $n = 77$ .

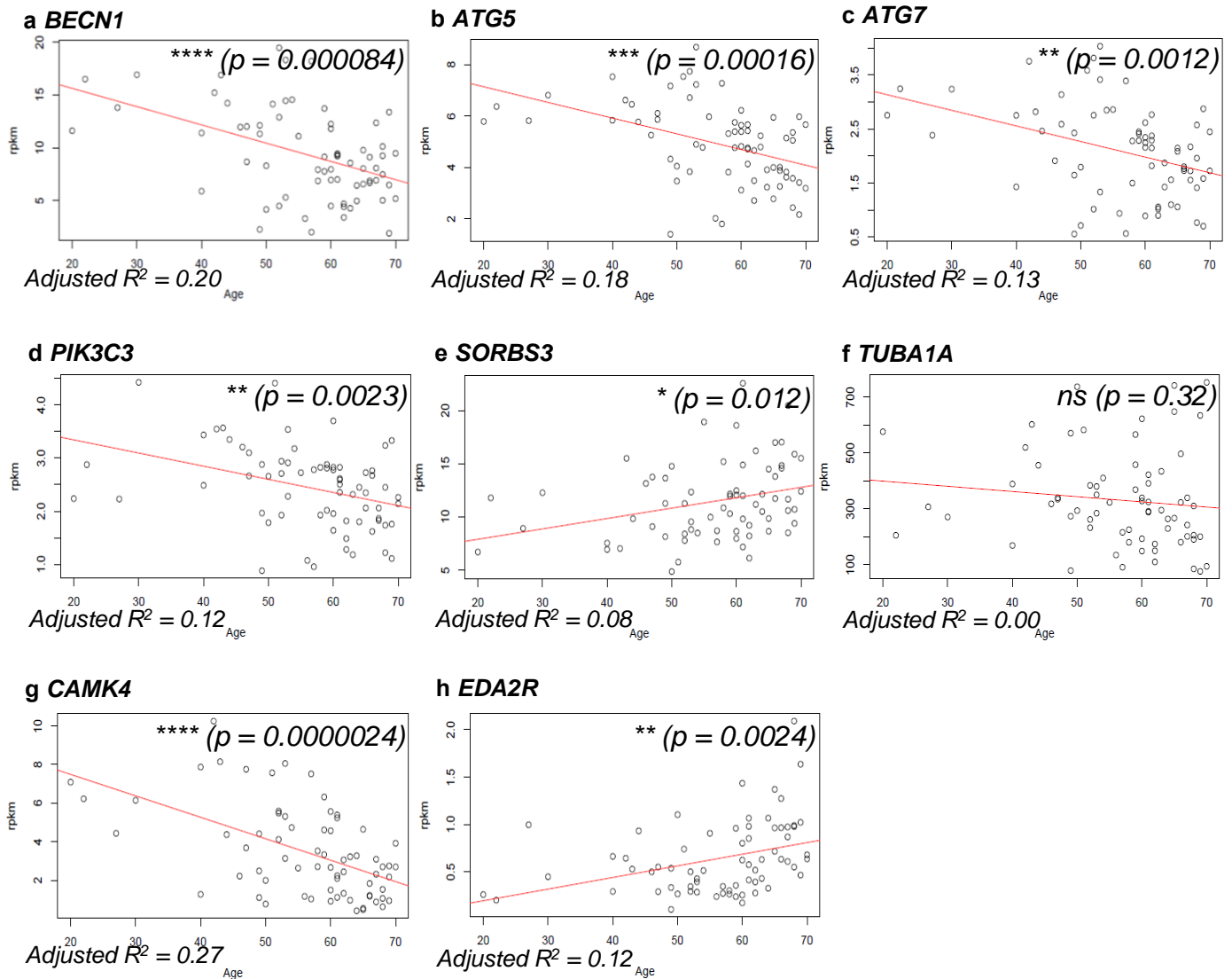


**Figure 3.8: autophagy is transcriptionally downregulated with age in normal human hippocampus.**

- a. *BECN1* mRNA expression (Reads Per Kilobase of transcript per Million; rpkm) determined by RNA sequencing of samples from ‘neuropathological normal’ hippocampus was plotted against chronological age of donors. A scatterplot and regression line were generated using R. The adjusted coefficient of determination (adjusted  $R^2$ ) was calculated and displayed on the scatter plot (bottom left). Overall significance of the regression analysis was established by F-test and the p value displayed on the scatter plot (top right).  $n = 69$ .
- b. *ATG5* mRNA expression; c. *ATG7* mRNA expression, d. *PIK3* mRNA expression, e. *SORBS3* mRNA expression, f. *TUBA1A* mRNA expression (negative control), g. *CAMK4* mRNA expression (positive control) and h. *EDA2R* mRNA expression (positive control) determined by RNA sequencing of samples from hippocampus were subject to the same analysis as described in a.  $n = 69$ .

### ***3.5 Vinexin regulates autophagy independent of focal adhesion changes***

Vinexin is reported to stabilise focal adhesions in NIH 3T3 cells (Kioka et al., 1999), interact with several focal adhesion proteins (Kioka et al., 1999; Nagata et al., 2009; Thompson et al., 2010) and function in focal adhesion-mediated responses to extracellular matrix stiffness in mouse embryonic fibroblasts (Yamashita et al., 2014). Hence, I set out to characterise how vinexin impacts focal adhesions in HeLa cells and whether focal adhesions changes are causally related to the effect of si*SORBS3* on autophagy.

In their publication on modulation of focal adhesion dynamics by the vinexin interactor beta dystroglycan, Thompson and colleagues define three focal adhesion types (Figure 3.9a), which represent a continuum from dynamic to stable cell-matrix adhesion; 1. small focal complexes, 2. larger focal adhesions and 3. large, centrally-located fibrillar adhesions (Kioka et al., 1999; Nagata et al., 2009; Thompson et al., 2010). Applying these definitions to immunostaining for the canonical focal adhesion proteins vinculin (Figure 3.9b) and paxillin (Figure 3.9c) in HeLa cells, vinexin beta depletion appeared to shift focal adhesion dynamics in favour of small focal complexes. Accordingly, HeLa cells overexpressing mEmerald-tagged vinexin alpha showed more and larger focal adhesions by immunostaining for endogenous vinculin (Figure 3.9d). This concurs with Kioka et al., who report that exogenous vinexin alpha increases vinculin immunostaining at focal adhesions in NIH 3T3 cells (Kioka et al., 1999). While mEmerald-vinexin alpha clearly localises to focal adhesions (Figure 3.9d), I was unable to obtain specific immunostaining for vinexin beta (data not shown). However, the expectation from the literature is that endogenous vinexin beta does localise to vinculin-positive focal adhesions (Mizutani et al., 2007a).

Since destabilisation of focal adhesions by si*SORBS3* (Figure 3.9b-c) appeared to correlate with increased autophagy (Figures 3.1-3 and 3.7-9), I examined whether stabilisation of focal adhesions by mEmerald-vinexin alpha overexpression (Figure 3.9d) correlated with decreased autophagy. Using western blotting, I found that mEmerald-vinexin alpha overexpression decreased LC3-II (lower band of LC3 doublet) under basal conditions (Figure 3.9e). When quantified relative to tubulin loading control, LC3-II levels in mEmerald-vinexin alpha transfected cells were reduced to around half those in mEmerald-empty transfected cells (Figure 3.9f).

As these data suggest an inverse correlation between focal adhesion stability and autophagy, I investigated whether this relationship held true when focal adhesion dynamics were

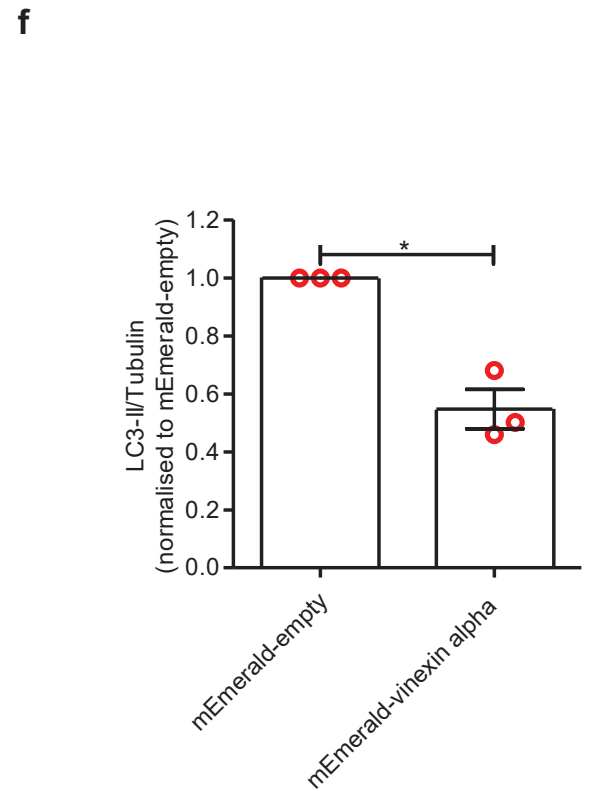
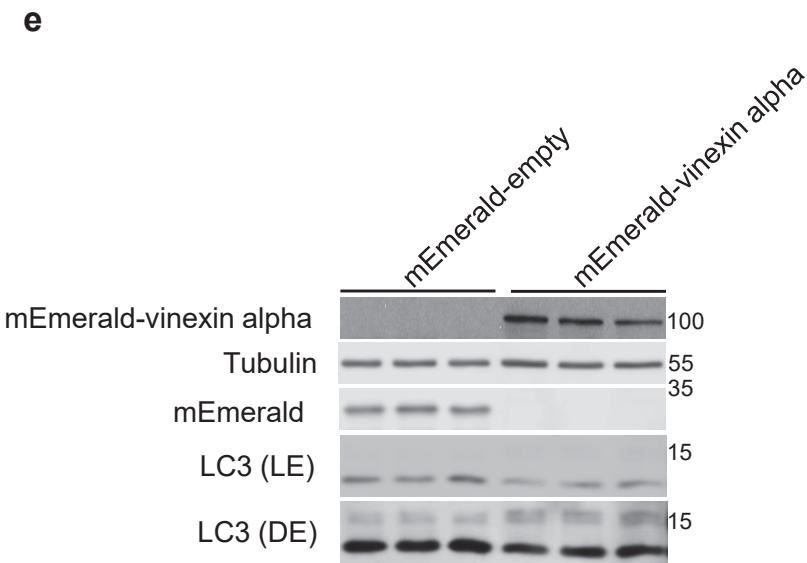
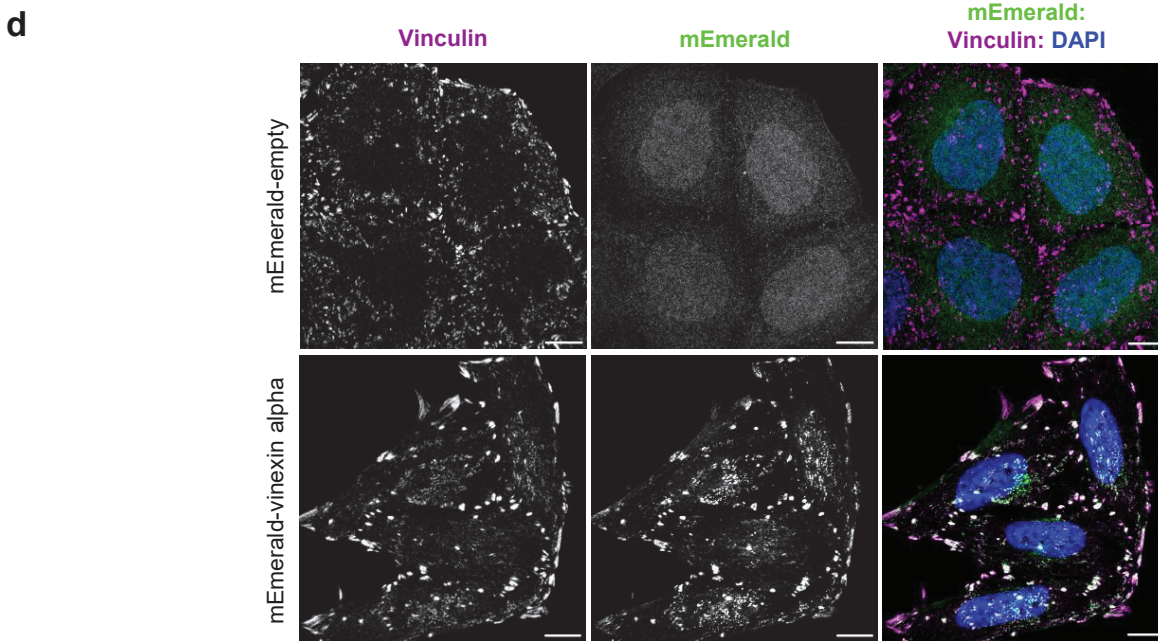
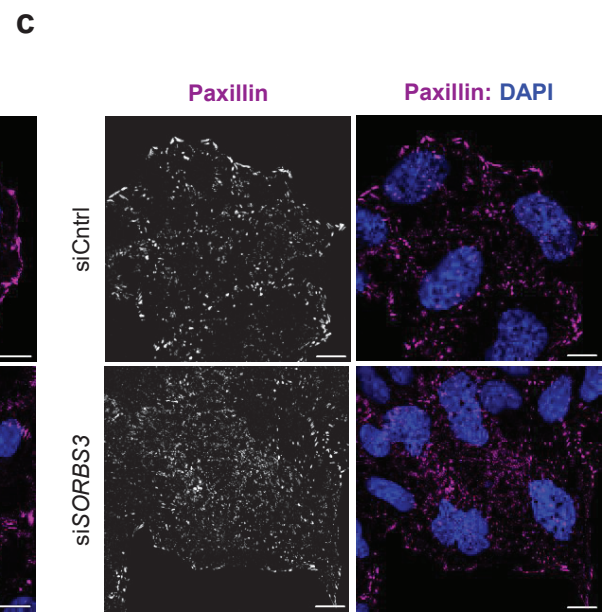
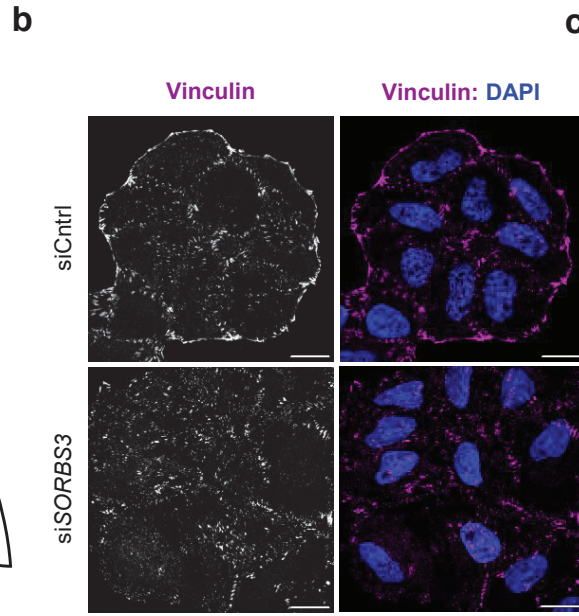
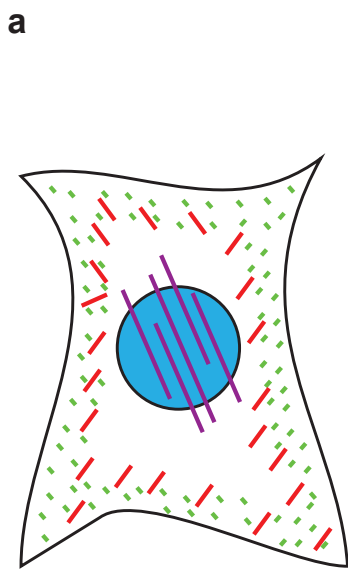


**Figure 3.9: focal adhesion destabilisation and stabilisation due to vinexin beta depletion and vinexin alpha overexpression correlate with autophagy upregulation and downregulation, respectively.**

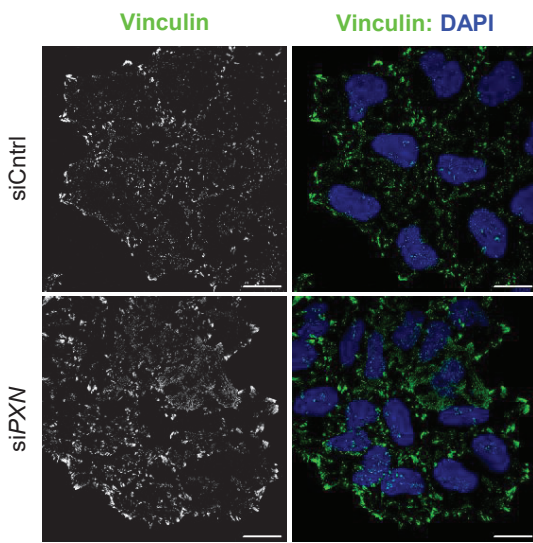
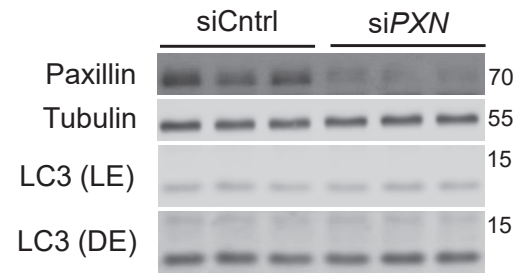
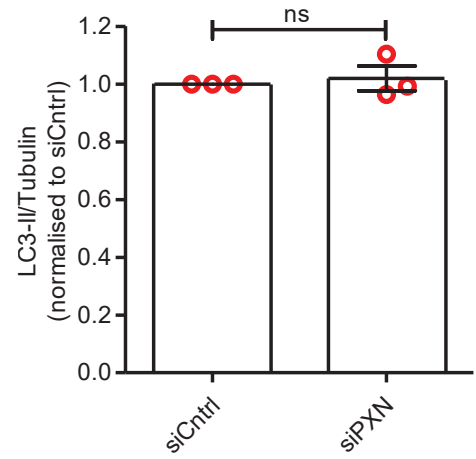
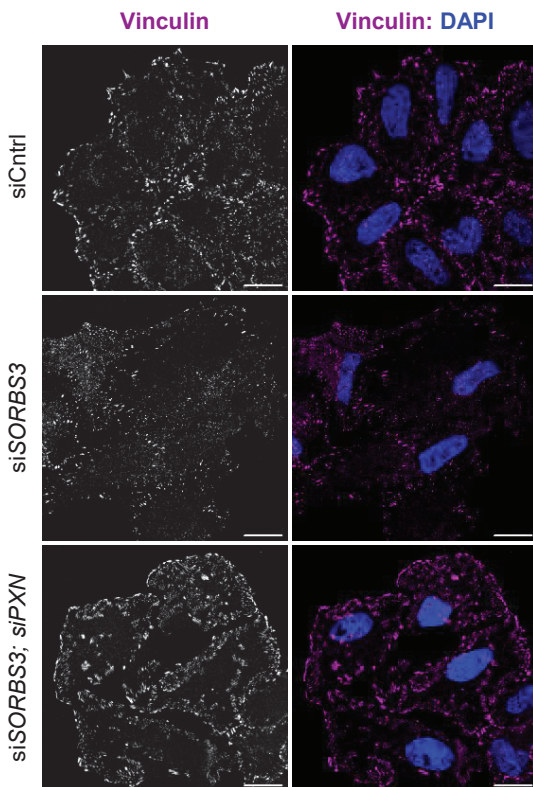
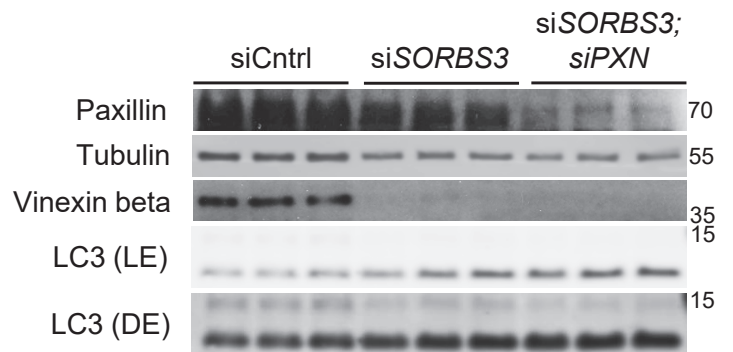
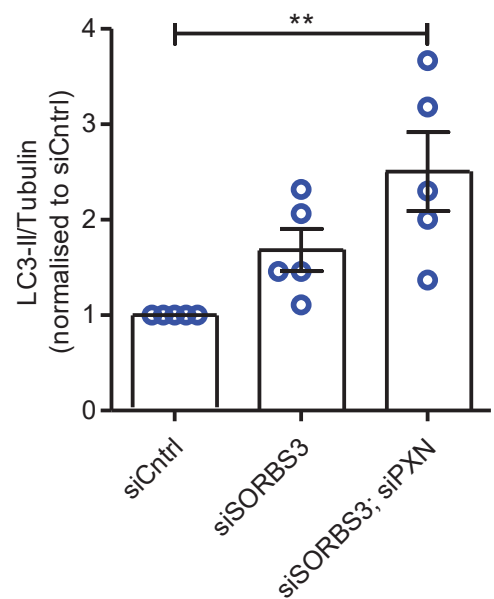
- a. Schematic diagram depicting the three focal adhesion types described by Thompson et al., 2010: 1. small focal complexes (green), 2. larger focal adhesions (red) and 3. large, centrally-located fibrillar adhesions (purple) (Thompson et al., 2010).
- b. HeLa cells were depleted of vinexin beta using an individual siRNA oligonucleotide against *SORBS3* (si*SORBS3*; oligo 7). Endogenous vinculin was examined by confocal microscopy. Representative images from 3 independent experiments are shown. Purple (Alexa Fluor 647) = vinculin; blue = DAPI. Scale bars indicate 20  $\mu$ m.
- c. HeLa cells were depleted of vinexin beta, as in b. Endogenous paxillin was examined by confocal microscopy. Representative images from 3 independent experiments are shown. Purple (Alexa Fluor 647) = paxillin; blue = DAPI. Scale bars indicate 10  $\mu$ m.
- d. HeLa cells were transfected with mEmerald-vinexin alpha or empty vector control (mEmerald-empty) for 48 hours. Endogenous vinculin, as well as mEmerald, were examined by immunofluorescence and confocal microscopy. Representative images from 3 independent experiments are shown. Purple = vinculin (Alexa Fluor 647); green = mEmerald; blue = DAPI. Scale bars indicate 10  $\mu$ m.
- e. HeLa cells were transfected with mEmerald-empty or mEmerald-vinexin alpha, as in d. Levels of the transfected proteins were examined by western blotting, as well as endogenous tubulin and LC3 protein levels. Representative blots from 3 independent experiments are shown. LE = lighter exposure; DE = darker exposure; molecular weights shown in kDa.
- f. Quantification of 3 independent experiments. LC3-II (lower band of LC3 doublet) levels are expressed relative to tubulin loading control and normalised to LC3-II/tubulin in mEmerald-empty transfected cells. \* =  $p < 0.05$  by 2-tailed one-sample t-test. Error bars indicate SEM.

modulated without altering vinexin expression. Here I built on literature suggesting the absence of paxillin stabilises focal adhesions; nutrient starvation redistributes vinculin away from focal adhesions in wild-type mouse embryonic fibroblasts (MEFs), but not in paxillin knockout MEFs (Chen et al., 2008). These experiments also served to test whether the proposed role of paxillin in autophagosome formation (Chen et al., 2008) could be involved in upregulating autophagy following vinexin beta depletion (see chapter 1, section 1.2.4). As expected, immunostaining for endogenous vinculin appeared to shift focal adhesion dynamics in favour of larger, more stable focal adhesions (Figure 3.10a). Yet contrary to Chen and colleagues' findings in paxillin knockout MEFs, although siRNA against *PXN* (*siPXN*) brought about a robust reduction in paxillin protein levels by western blot, LC3-II levels were unchanged under basal conditions (Figure 3.10b). When quantified relative to tubulin loading control, there was no significant change in LC3-II levels compared with siCntrl treated cells (Figure 3.10c). These findings contradict the hypotheses that 1. focal adhesion destabilisation contributes to the mechanism by which si*SORBS3* promotes autophagy and 2. paxillin is involved in upregulating autophagy following vinexin beta depletion.

In order to test these hypotheses more directly, I conducted experiments in which HeLa cells were treated with si*SORBS3* in the presence and absence of si*PXN*. Paxillin depletion ameliorated the effect of vinexin beta depletion on focal adhesion stability; focal adhesions were increased and focal complexes decreased by vinculin immunostaining in si*SORBS3*/si*PXN* (si*SORBS3*; si*PXN*) double knockdown cells, compared with si*SORBS3* single knockdown cells (Figure 3.10d). However, si*PXN* treatment did not ameliorate the increase in LC3-II levels observed by western blot upon si*SORBS3* treatment under basal conditions (Figure 3.10e). In fact, there was a statistically significant increase in LC3-II/tubulin levels in si*SORBS3*; si*PXN* treated cells, compared with siCntrl treated cells (Figure 3.10f). I therefore concluded that, while vinexin does appear to stabilise focal adhesions in HeLa cells, neither this function nor the putative role of paxillin in autophagosome formation contribute to the mechanism by which vinexin negatively regulates autophagy.

### ***3.6 Vinexin beta depletion does not upregulate autophagy via mTOR, ULK1, ERK1/2 nor EGFR signalling***

Given the literature linking vinexin to multiple cell signalling pathways, I examined the effect of si*SORBS3* on canonical autophagy signalling (mTOR and ULK1; see chapter 1), together with the signalling pathways in which vinexin is most heavily implicated (ERK1/2 and

**a****b****c****d****e****f**

**Figure 3.10: focal adhesion destabilisation and stabilisation are not causally related to autophagy upregulation and downregulation in HeLa cells.**

- a. HeLa cells were depleted of paxillin using a pool of 4 siRNA oligonucleotides against *PXN* (*siPXN*). Endogenous vinculin was examined by confocal microscopy. Representative images from 3 independent experiments are shown. Green (Alexa Fluor 488) = vinculin; blue = DAPI. Scale bars indicate 20  $\mu\text{m}$ .
- b. HeLa cells were depleted of paxillin, as in a. Endogenous tubulin, LC3 and paxillin protein levels were examined by western blotting. Representative blots from 3 independent experiments are shown. LE = lighter exposure; DE = darker exposure; molecular weights shown in kDa.
- c. Quantification of 3 independent experiments. LC3-II (lower band of LC3 doublet) levels are expressed relative to tubulin loading control and normalised to LC3-II/tubulin in control siRNA (*siCntrl*) treated cells. ns =  $p > 0.05$  by 2-tailed one-sample t-test. Error bars indicate SEM.
- d. HeLa cells were depleted of vinexin beta using an individual siRNA oligonucleotide against *SORBS3* (*siSORBS3*; oligo 7) and paxillin using a pool of 4 siRNA oligonucleotides against *PXN* (*siPXN*). Endogenous vinculin was examined by confocal microscopy. Representative images from 3 independent experiments are shown. Purple (Alexa Fluor 647) = vinculin; blue = DAPI. Scale bars indicate 20  $\mu\text{m}$ .
- e. HeLa cells were depleted of vinexin beta and paxillin, as in d. Endogenous tubulin, LC3, vinexin beta and paxillin protein levels were examined by western blotting. Representative blots from 5 independent experiments are shown. LE = lighter exposure; DE = darker exposure; molecular weights shown in kDa.
- f. Quantification of 5 independent experiments. LC3-II (lower band of LC3 doublet) levels are expressed relative to tubulin loading control and normalised to LC3-II/tubulin in *siCntrl* treated cells. \*\* =  $p < 0.01$  by one-way ANOVA followed by Tukey's multiple comparison test. Error bars indicate SEM.

EGFR) (Mitsushima et al., 2006c, 2007; Suwa et al., 2002). mTOR-dependent autophagy induction is associated with reduced phosphorylation of the downstream effector ribosomal protein S6 kinase (p70S6K) (Brown et al., 1995). I therefore assayed mTOR signalling by western blotting for p70S6K phosphorylated at threonine 389 (P-p70S6K). This was unchanged by si*SORSB3* treatment under basal conditions (Figure 3.11a) and when I calculated the ratio of P-p70S6K to total p70S6K, there was no significant change compared with siCntrl treated cells (Figure 3.11b).

ULK1 activation *via* phosphorylation at serine 556 by AMPK promotes autophagy upon nutrient starvation (Egan et al., 2011), while phosphorylation at serine 758 by mTOR prevents ULK1 activation upon nutrient sufficiency by disrupting the ULK1/AMPK interaction (Kim et al., 2011a). Western blotting revealed ULK1 phosphorylation at both residues (P-ULK1 (S758); P-ULK1 (S556)) remained unchanged following vinexin beta depletion (Figure 3.11c). When the ratio of P-ULK1 to total ULK1 was calculated for S758 and S556, there were no significant changes compared with siCntrl (Figure 3.11d).

The Kioka group report that vinexin promotes ERK1/2 activation in NIH 3T3 mouse fibroblasts and A549 human lung carcinoma cells by delaying ERK1/2 dephosphorylation (Mitsushima et al., 2007; Suwa et al., 2002). However, ERK1/2 phosphorylation at threonine 202/185 and tyrosine 202/187 (P-ERK1/2) in HeLa cells was unchanged upon si*SORSB3* treatment when assayed by western blotting under basal conditions (Figure 3.12a). This is hardly surprising given the aforementioned publications refer to vinexin prolonging ERK1/2 activation after EGF stimulation, as opposed to under basal conditions. Yet even if I had found si*SORSB3* treatment promoted ERK1/2 inactivation, the literature is divided on whether this could account for increased autophagy following vinexin beta depletion (Aoki et al., 2007; Settembre et al., 2011; Wong et al., 2010).

EGFR tyrosine kinase inhibitors are reported to promote autophagy *via* both mTOR-dependent and mTOR-independent mechanisms (Jutten and Rouschop, 2014; Tan et al., 2015), the latter more relevant here given Figure 3.11a-b. With regards to vinexin, overexpression prolongs EGFR phosphorylation at the plasma membrane in response to EGF stimulation (Mitsushima et al., 2006c). I therefore set out to test the hypothesis that vinexin beta depletion upregulates autophagy by accelerating EGFR inactivation. EGFR phosphorylation at tyrosine 1068 (P-EGFR) was unchanged upon si*SORSB3* treatment when assayed by western blotting under basal conditions (Figure 3.12b). Next I examined the effect

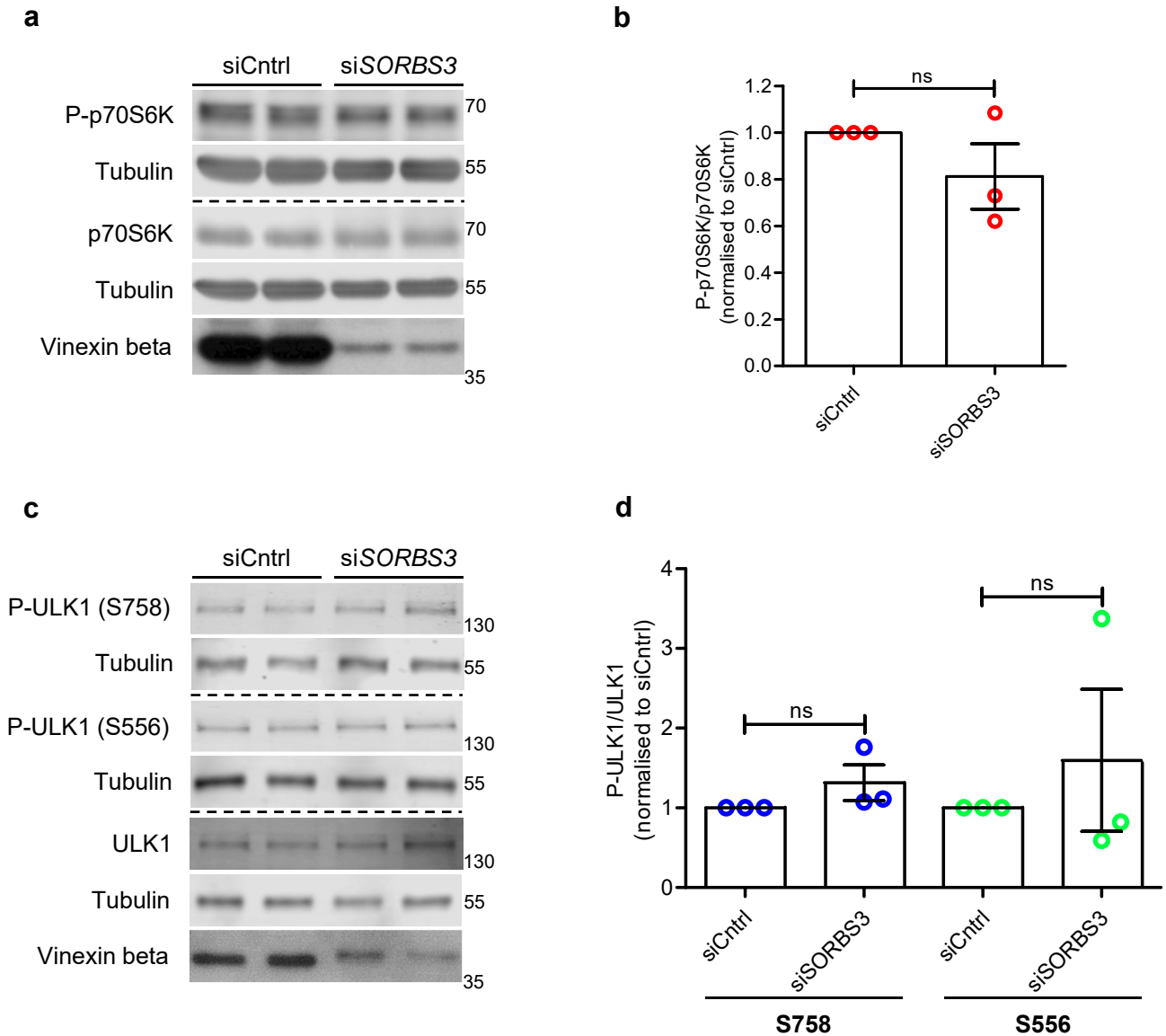


**Figure 3.11: vinexin beta depletion does not affect p70S6K or ULK1 phosphorylation.**

- a. HeLa cells were depleted of vinexin beta using a pool of 4 siRNA oligonucleotides against *SORBS3* (si*SORBS3*). Endogenous total ribosomal protein S6 kinase (p70S6K), p70S6K phosphorylated at threonine 389 (P-p70S6K), tubulin and vinexin beta protein levels were examined by western blotting. Representative blots from 3 independent experiments are shown. Molecular weights in kDa.
- b. Quantification of 3 independent experiments. P-p70S6K and p70S6K are expressed relative to tubulin loading control, the ratio of P-p70S6K/tubulin: p70S6K/tubulin taken and then normalised to P-p70S6K/p70S6K in siCntrl treated cells. ns =  $p > 0.05$  by 2-tailed one-sample t-test. Error bars indicate SEM.
- c. HeLa cells were depleted of vinexin beta using an individual siRNA oligonucleotide against *SORBS3* (si*SORBS3*; oligo 7). Endogenous total ULK1, ULK1 phosphorylated at serine 758 [P-ULK1 (S758)], ULK1 phosphorylated at serine 556 [P-ULK1 (S556)], tubulin and vinexin beta protein levels were examined by western blotting. Representative blot from 3 independent experiments are shown. Molecular weights in kDa.
- d. Quantification of 3 independent experiments. P-ULK1 and ULK1 are expressed relative to tubulin loading control, the ratio of P-ULK1/tubulin: ULK1/tubulin taken and then normalised to P-ULK1/ULK1 in siCntrl treated cells. ns =  $p > 0.05$  by 2-tailed one-sample t-test. Error bars indicate SEM.

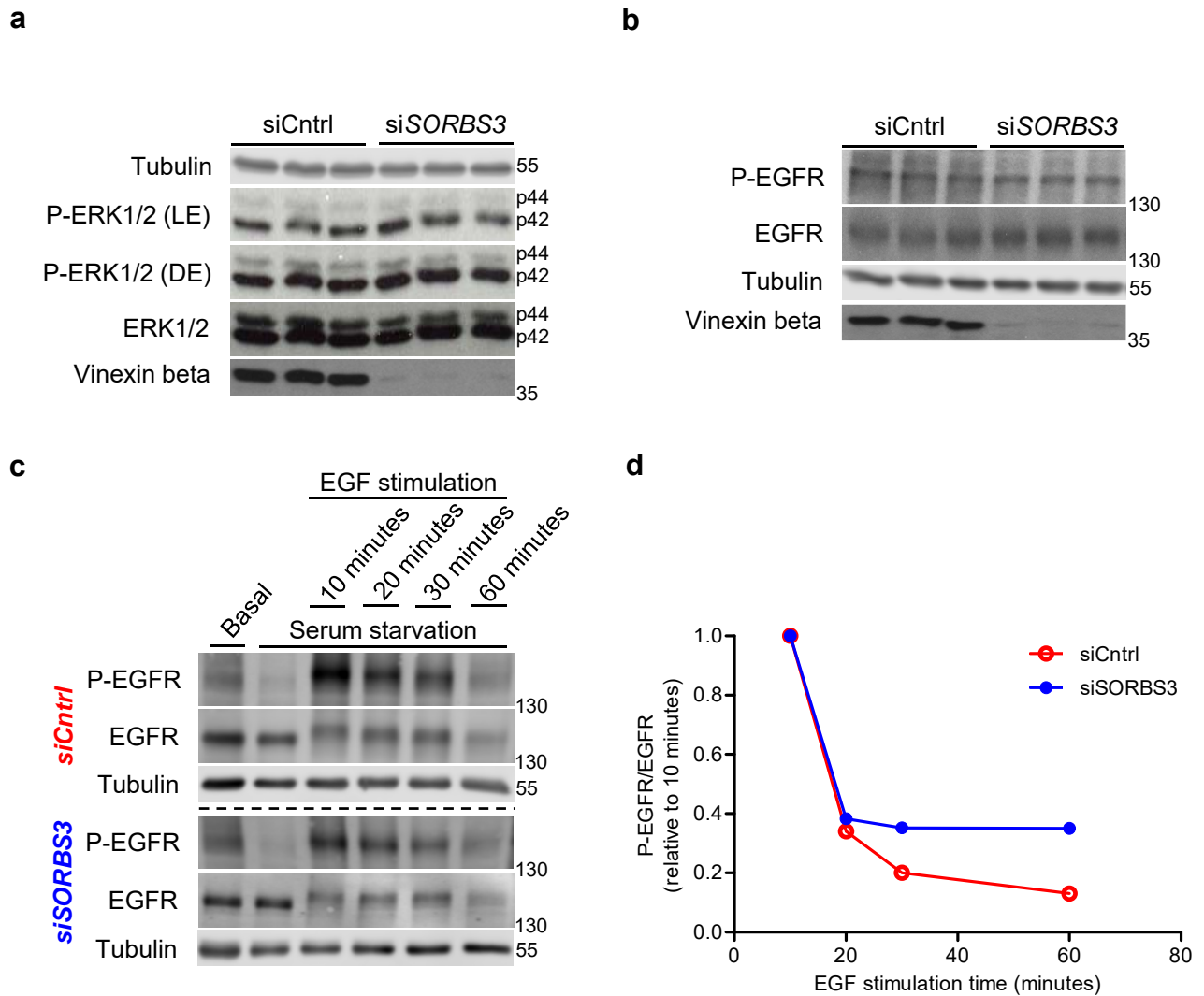


**Figure 3.12: vinexin beta depletion does not affect ERK1/2 or EGFR phosphorylation.**

- HeLa cells were depleted of vinexin beta using a pool of 4 siRNA oligonucleotides against *SORBS3* (siSORBS3). Endogenous total ERK1/2, ERK1/2 phosphorylated at threonine 202/185 and tyrosine 202/187 (P-ERK1/2), tubulin and vinexin beta protein levels were examined by western blotting. Representative blot from 3 independent experiments are shown. LE = lighter exposure; DE = darker exposure; molecular weights in kDa.
- HeLa cells were depleted of vinexin beta, as in a. Endogenous total EGFR, EGFR phosphorylated at tyrosine 1068 (P-EGFR), tubulin and vinexin beta protein levels were examined by western blotting. Representative blot from 3 independent experiments are shown. Molecular weights in kDa.
- HeLa cells were depleted of vinexin beta, as in a. and b. Cells were cultured in serum-free media overnight (serum starvation) or left in complete media (basal). Serum starved cells were stimulated with EGF (10 ng/ml) for the times shown. Endogenous total EGFR, P-EGFR and tubulin protein levels were examined by western blotting. Molecular weights in kDa.
- Quantification of the blots shown in c. P-EGFR and EGFR are expressed relative to tubulin loading control, the ratio of P-EGFR/tubulin: EGFR/tubulin taken and then normalised to maximal P-EGFR/EGFR after 10 minutes EGF stimulation. Red = siCntrl; Blue = siSORBS3.

of vinexin beta depletion on EGFR inactivation following EGF stimulation under serum starvation (Figure 3.12c). When the ratio of P-EGFR to EGFR was calculated and expressed relative to maximal EGFR activation after 10 minutes EGF stimulation, EGFR dephosphorylating was if anything slower in si*SORBS3* treated cells (Figure 3.12d).

These findings indicate vinexin regulates autophagy by an mTOR-independent mechanism, which does not involve altered ULK1 phosphorylation at key residues (serine 758 and serine 556). ERK1/2 and EGFR signalling, which have previously been linked to vinexin, are also unlikely to contribute to the mechanism by which vinexin impacts autophagy. Of course this does not preclude the involvement of other kinase signalling pathways or these pathways under conditions not tested here.

### **3.7 Concluding remarks**

In this chapter I replicated Lipinski and colleagues' finding that vinexin negatively regulates autophagy in HeLa, RPE and HEK293 cells. I showed this is unlikely to constitute a siRNA off-target effect as 1. two independent siRNA oligonucleotides targeting different regions of *SORBS3* similarly upregulated autophagy and 2. mEmerald-vinexin alpha overexpression ameliorated the increase in autophagy in si*SORBS3* treated cells.

Findings presented in this chapter obtained by Dr Sterk using RNA sequencing data from the GTEx project (GTEx Consortium, 2013) replicate changes in *BECN1*, *ATG5*, *ATG7* and *SORBS3* expression in normal ageing previously reported in human frontal cortex samples (Lipinski et al., 2010b; Shibata et al., 2006). These data also expand the list core autophagy genes that may be transcriptionally downregulated with age to include *PIK3C3* (encoding the class III PI3-kinase catalytic subunit VPS34), as well as the list of potentially affected brain regions to include the hippocampus. Taken together, these findings support the physiological importance of vinexin as an autophagy regulator.

With regards to how vinexin beta depletion affects the autophagy pathway, data I acquired by western blotting for endogenous LC3-II and imaging cells stably expressing GFP-LC3 in the presence and absence of BAF support the hypothesis that autophagosome formation is upregulated. Experiments using cells stably expressing GFP-mRFP-LC3 suggest autophagic flux remains intact upon si*SORBS3* treatment. These findings appear to represent functional autophagy upregulation, as fewer vinexin beta knockdown cells transfected with the aggregate-prone model autophagy substrate GFP-Htt(Q74) form aggregates.

The mechanism by which vinexin impacts autophagy seems unlikely to involve changes in focal adhesion dynamics. Focal adhesion destabilisation upon si*SORBS3* treatment and stabilisation due to mEmerald-vinexin alpha overexpression did correlate with autophagy upregulation and downregulation, respectively. However, no causal relationship was observed; 1. autophagy was unchanged upon focal adhesion stabilisation by paxillin depletion using siRNA against *PXN* and 2. si*PXN* treatment restored focal adhesion stability in si*SORBS3* treated cells, but did not ameliorate the increase in autophagy. These findings also oppose the hypothesis that the putative role of paxillin in autophagosome formation (Chen et al., 2008) contributes to the mechanism by which vinexin negatively regulates autophagy.

Finally, data presented in this chapter suggest vinexin depletion upregulates autophagy by an mTOR-independent mechanism, which does not involve altered ULK1 phosphorylation at key residues (serine 758 and serine 556). I also that conclude the published functions of vinexin in promoting ERK1/2 and EGFR activation (Mitsushima et al., 2006c, 2007; Suwa et al., 2002) are unlikely to be relevant to the role of vinexin in regulating autophagy.

## **4 Vinexin depletion upregulates autophagy through YAP/TAZ via a filamentous actin-dependent mechanism**

### ***4.1 Introduction***

YAP and TAZ (also known as WWTR1) are evolutionarily conserved transcriptional coactivators that shuttle between the nucleus and cytosol (Piccolo et al., 2014). Though also subject to Hippo pathway-independent regulation, YAP and TAZ are best known as Hippo pathway effectors (see chapter 1). YAP/TAZ transcription activity was first implicated in cancer by *Drosophila* studies showing that mutations in Hippo pathway components result in robust tissue overgrowth (Zhao et al., 2011b). Focusing on the liver, increased YAP/TAZ activity has been linked to hepatoma development in mouse models (Lee et al., 2010b; Lu et al., 2010; Zhou et al., 2009), with increased YAP protein levels and nuclear localisation reported in human hepatocellular carcinoma (HCC) samples (Zhao et al., 2007). Moreover, YAP overexpression predicts tumour recurrence and shorter survival time in HCC patients (Xu et al., 2009a). *SORBS3* deletion similarly predicts poor prognosis in HCC, meaning vinexin is suggested to have tumour suppressive functions (Roessler et al., 2012).

YAP is reported to promote MCF7 breast cancer cell survival under nutrient starvation by increasing autophagy flux in a TEAD transcription factor-dependent manner (Song et al., 2015). In addition, our group has recently demonstrated that decreased YAP/TAZ activity reduces autophagosome biogenesis in the context of contact inhibition at high cell densities (Pavel et al., manuscript in preparation). In light of these findings, I set out to investigate whether vinexin depletion upregulates autophagy by increasing YAP/TAZ activity. In this chapter I aimed to demonstrate that upregulation of autophagy upon *siSORBS3* treatment is due to increased translocation of YAP/TAZ into the nucleus and consequent upregulation of YAP/TAZ transcriptional activity. I also sought to characterise the mechanism by which vinexin beta depletion promotes YAP/TAZ activity, as well as to order functional components in the pathway.

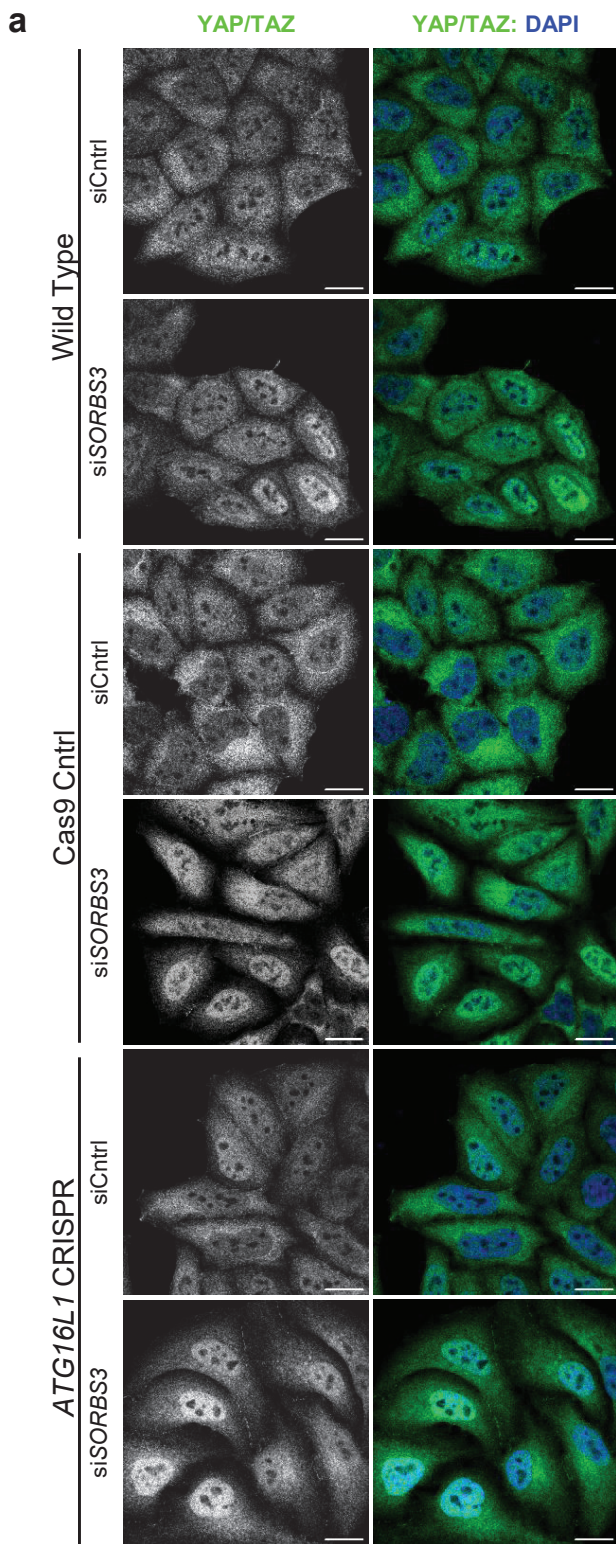
### ***4.2 siSORBS3 treatment increases YAP/TAZ activity upstream of autophagy***

Ploeger and colleagues reported that YAP protein levels and YAP/TAZ-responsive mRNA levels remain unchanged upon overexpression of either vinexin alpha or vinexin beta in HuH1 and HepG2 liver cancer cells (Ploeger et al., 2016). However, there is no literature concerning the impact of vinexin depletion on YAP/TAZ activity. Using an antibody that

recognises both YAP and TAZ, a higher proportion of HeLa cells treated with siRNA against *SORBS3* (si*SORBS3*) showed nuclear YAP/TAZ staining compared with nontargeting control siRNA (siCntrl) treated cells (Wild Type; Figure 4.1a). Since Liang et al. report YAP is an autophagy substrate in mouse embryonic fibroblasts (Liang et al., 2014), I also performed these experiments in autophagy-deficient HeLa cells (*ATG16L1* CRISPR) and autophagy-competent control cells (Cas9 Cntrl). si*SORBS3* treatment again increased nuclear YAP/TAZ staining, to a similar extent in Cas9 Cntrl and *ATG16L1* CRISPR cells (Cas9 Cntrl and *ATG16L1* CRISPR; Figure 4.1a). This result was confirmed by measuring the intensity of nuclear and cytosolic YAP/TAZ-positive pixels, then calculating the odds that nuclear: cytosolic YAP/TAZ intensity is greater than 0.5 given si*SORBS3* treatment (odds ratio); the odds increased at least 2.5-fold for all three cells lines (Figure 4.1b).

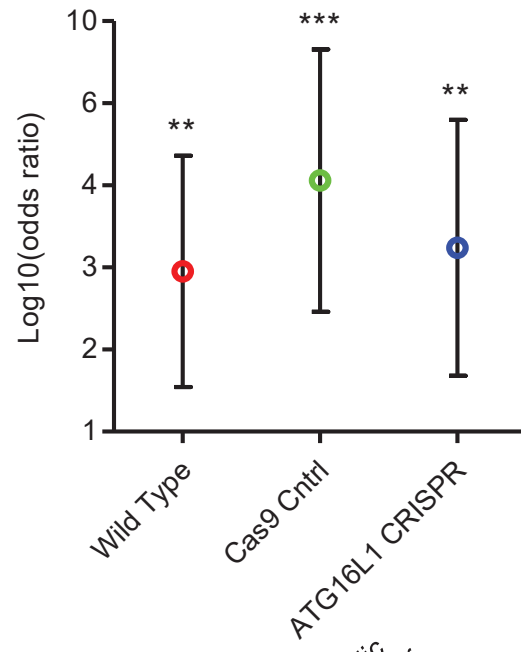
Nuclear/cytosolic fractionation was performed by Dr Carla Bento in order to replicate this finding biochemically. Western blotting nuclear and cytosolic fractions from HeLa cells confirmed the presence of YAP (upper band of YAP/TAZ doublet) and TAZ (lower band of YAP/TAZ doublet) in both factions and validated the fractionation protocol, as the nuclear envelope protein lamin B and cytosolic protein GAPDH were highly enriched in the appropriate fractions (Figure 4.1c). In agreement with Figure 4.1a-b, Vinexin beta depletion decreased cytosolic and increased nuclear YAP/TAZ by western blotting following nuclear/cytosolic fractionation (Figure 4.1d). When quantified relative to GAPDH loading control, YAP and TAZ levels were significantly lower in cytosolic fractions from si*SORBS3* treated cells. Accordingly, TAZ levels relative to lamin B were significantly higher in nuclear fractions from si*SORBS3* treated cells (YAP levels were non-significantly higher; Figure 4.1 e).

Taken together, these immunofluorescence and nuclear/cytosolic fractionation data suggest vinexin beta depletion promotes YAP/TAZ translocation into the nucleus. The expectation from the literature is that this corresponds to increased YAP/TAZ transcriptional activity (Zhao et al., 2007). In order to test this hypothesis, HeLa cells were transfected with a YAP/TAZ-responsive synthetic TEAD promoter driving luciferase expression (8xGTIIC-luciferase). As expected, luminescence measured over 2.5-fold higher by dual-luciferase reporter assay in si*SORBS3* treated cells compared with siCntrl treated cells (Wild Type; Figure 4.2a). To counter the possibility this increase in TEAD promotor activity is due to altered autophagy in si*SORBS3* treated cells, these experiments were also performed in *ATG16L1* CRISPR and Cas9 Cntrl HeLa cells. Concurrent with Figure 4.1a-b, vinexin beta

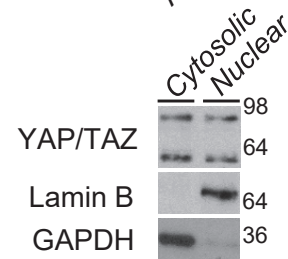


**b**

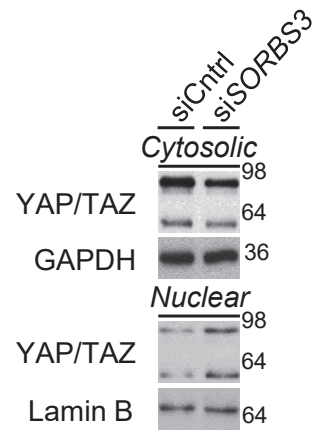
Odds YAP/TAZ nuclear: cytosolic integrated intensity > 0.5



**c**



**d**



**e**

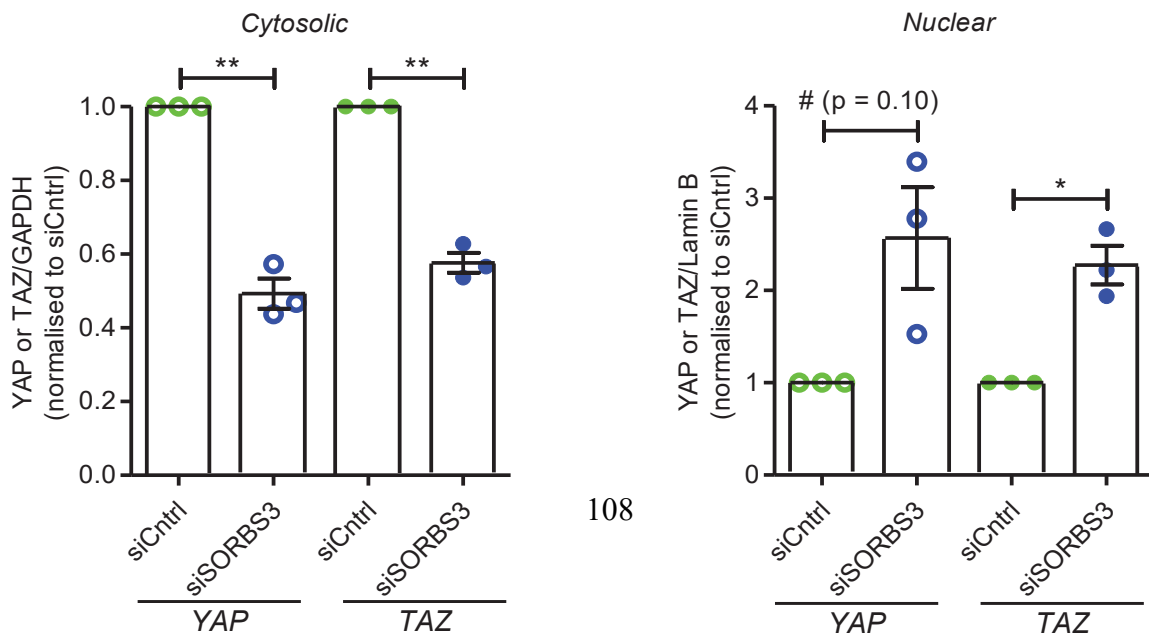


**Figure 4.1: vinexin beta depletion increases YAP/TAZ nuclear localisation.**

- a. Wild type, Cas9 control (Cntrl) and *ATG16L1* CRISPR HeLa cells were depleted of vinexin beta using an individual siRNA oligonucleotide against *SORBS3* (si*SORBS3*; oligo 7). Endogenous YAP/TAZ were examined by immunofluorescence and confocal microscopy. Representative images from 3 independent experiments per cell line are shown. Green = YAP/TAZ (Alexa Fluor 488); blue = DAPI. Scale bars indicate 20  $\mu$ m.
- b. Integrated intensity of YAP/TAZ-positive pixels in nucleus and cytoplasm was determined from confocal images using CellProfiler software. Odds that YAP/TAZ nuclear: cytosolic integrated intensity > 0.5 given si*SORBS3* treatment (odds ratio) was calculated for the representative experiments shown in a. \*\* =  $p < 0.01$ ; \*\*\* =  $p < 0.001$  by 2-tailed Fisher's exact test. n = 78 (wild type, siCntrl); 78 (wild type, si*SORBS3*); 120 (Cas9 Cntrl, siCntrl); 74 (Cas9 Cntrl, si*SORBS3*), 55 (*ATG16L1* CRISPR, siCntrl); 86 (*ATG16L1* CRISPR, si*SORBS3*). Error bars indicate 95% confidence interval.
- c. Wild type HeLa cell lysate was subject to nuclear/cytosolic fractionation. Endogenous YAP/TAZ, lamin B and GAPDH protein levels in the nuclear and cytosolic fractions were examined by western blotting. Representative blot from the 3 independent experiments is shown. Molecular weights shown in kDa.
- d. HeLa cells were depleted of vinexin beta using si*SORBS3* (oligo 7) and lysates subject to nuclear/cytosolic fractionation and western blotting, as described in c. Representative blots from the 3 independent experiments in technical triplicate are shown. Molecular weights shown in kDa.
- e. Quantification of 3 independent nuclear/cytosolic fractionation experiments. YAP (upper band of YAP/TAZ doublet) and TAZ (lower band of YAP/TAZ doublet) are expressed relative to GAPDH (cytosolic fraction) or lamin B (nuclear fraction) loading control. YAP or TAZ/GAPDH or lamin B was normalised to control siRNA (siCntrl) treated cells. # = ns (p value); \* =  $p < 0.05$ ; \*\* =  $p < 0.01$  by 2-tailed one-sample t-test. Error bars indicate SEM.

depletion significantly increased TEAD promoter activity in both autophagy-competent and autophagy-deficient cells (Cas9 Cntrl and *ATG16L1* CRISPR; Figure 4.2a). In addition, Dr Bento examined expression of the YAP/TAZ/TEAD direct target gene *CTGF* (connective tissue growth factor) (Zhao et al., 2008) in HeLa whole cell lysates by western blotting (Figure 4.2b). When quantified relative to GAPDH loading control, *CTGF* levels were higher upon vinexin beta depletion (Figure 4.2c). These findings support the hypothesis that increased YAP/TAZ nuclear localisation in si*SORBS3* treated cells corresponds to upregulated YAP/TAZ transcriptional activity mediated by TEAD transcription factors.

#### ***4.3 Autophagy upregulation upon vinexin beta depletion is YAP/TAZ-dependent***

In order to investigate whether autophagy upregulation upon vinexin beta depletion is YAP/TAZ-dependent, I conducted experiments in which HeLa cells were treated with si*SORBS3* in the presence and absence of siRNA against *YAP* and *TAZ*. These experiments required robust knockdown of both transcriptional coactivators, as *YAP* and *TAZ* predominantly show functional redundancy (see chapter 1) (Moroishi et al., 2015). As introduced in the previous chapter, autophagy was assessed by measuring LC3-II (lower band of LC3 doublet) by western blotting. si*YAP/TAZ* treatment ameliorated the increase in LC3-II levels observed upon si*SORBS3* treatment (siCntrl; si*SORBS3* compared with si*YAP/TAZ*; si*SORBS3* in Figure 4.3a). When quantified relative to tubulin loading control, LC3-II levels were not significantly increased in si*YAP/TAZ*; si*SORBS3* triple knockdown cells compared with either siCntrl or si*YAP/TAZ*; siCntrl double knockdown cells (Figure 4.3b).

I therefore concluded that the mechanism by which vinexin beta depletion promotes autophagy requires *YAP* and *TAZ*. Given si*SORBS3* treatment upregulates YAP/TAZ transcriptional activity (Figure 4.2), it seems reasonable to suggest this mechanism involves *YAP* and *TAZ* functioning as transcriptional coactivators. However, these data do not exclude a non-transcriptional mechanism.

#### ***4.4 Vinexin beta depletion increases YAP/TAZ activity independent of Hippo signalling***

*YAP* and *TAZ* are the principle effectors of the Hippo pathway. In mammalian cells, the final regulatory step comprises *YAP/TAZ* phosphorylation by *LATS1/2*. This inhibits *YAP/TAZ* transcriptional activity by promoting sequestration and proteasomal degradation of *YAP/TAZ* in the cytosol (see chapter 1) (Varelas, 2014). I therefore assayed Hippo signalling by western blotting for *YAP* phosphorylated at the *LATS1/2* target residue serine 127 (P-*YAP*) (Zhao et al., 2007). This was unchanged by si*SORBS3* treatment (Figure 4.4a) and when I calculated

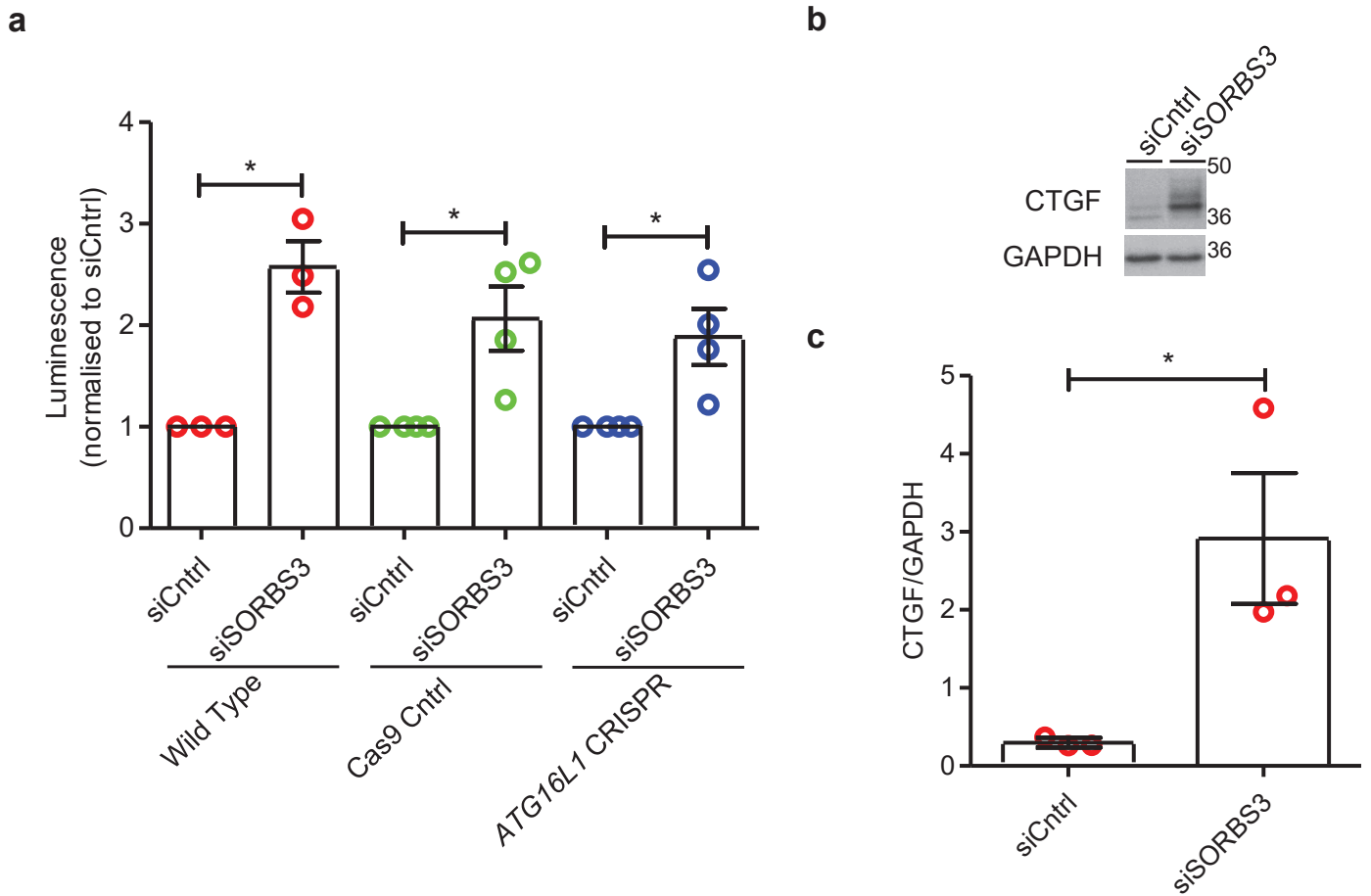


**Figure 4.2: vinexin beta depletion increases YAP/TAZ transcriptional activity.**

- a. Wild type, Cas9 control (Cntrl) and *ATG16L1* CRISPR HeLa cells were depleted of vinexin beta using an individual siRNA oligonucleotide against *SORBS3* (siSORBS3; oligo 7). Cells were co-transfected with synthetic TEAD (YAP/TAZ-responsive) promoter driving luciferase expression (pGL3b-8xGTIIC-luciferase) and *Renilla* luciferase control reporter for 24 hours. Luminescence (firefly luciferase activity relative to *Renilla* luciferase activity) was measured by dual-luciferase reporter assay and normalised to control siRNA (siCntrl) treated cells. Quantification of 3 (wild type) or 4 (Cas9 Cntrl and *ATG16L1* CRISPR) independent experiments is shown. \* =  $p < 0.05$  by 2-tailed one-sample t-test. Error bars indicate SEM.
- b. Wild type HeLa cells were depleted of vinexin beta using siSORBS3 (oligo 7). Levels of CTGF protein (YAP/TAZ/TEAD direct target) and GAPDH (loading control) were examined by western blotting. Representative blot from the 1 experiment in technical triplicate is shown. Molecular weights shown in kDa.
- c. Quantification of the representative experiment shown in b. \* =  $p < 0.05$  by 2-tailed Student's t-test. Error bars indicated SD.

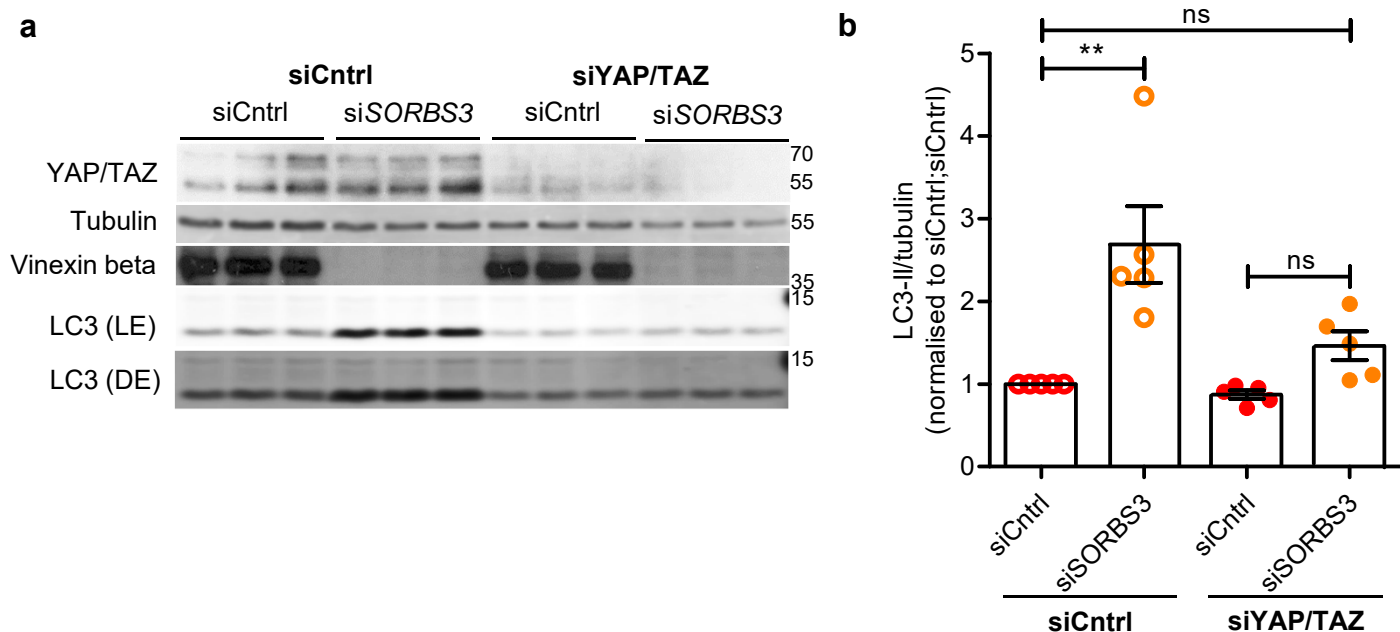


**Figure 4.3: YAP/TAZ depletion ameliorates the increase in LC3-II caused by vinexin beta depletion.**

- a. HeLa cells were depleted of vinexin beta using an individual siRNA oligonucleotide against *SORBS3* (si*SORBS3*; oligo 7) and *YAP/TAZ* using a pools of 4 siRNA oligonucleotides against *YAP* and *TAZ* (si*YAP/TAZ*). Endogenous *YAP/TAZ*, tubulin, vinexin beta and LC3 and protein levels were examined by western blotting. Representative blots from 5 independent experiments are shown. LE = lighter exposure; DE = darker exposure; molecular weights shown in kDa.
- b. Quantification of 5 independent experiments described in a. LC3-II (lower band of LC3 doublet) levels are expressed relative to tubulin loading control and normalised to LC3-II/tubulin in siCntrl treated cells. ns =  $p > 0.05$ ; \*\* =  $p < 0.01$  by one-way ANOVA followed by Tukey's multiple comparison test. Error bars indicate SEM.

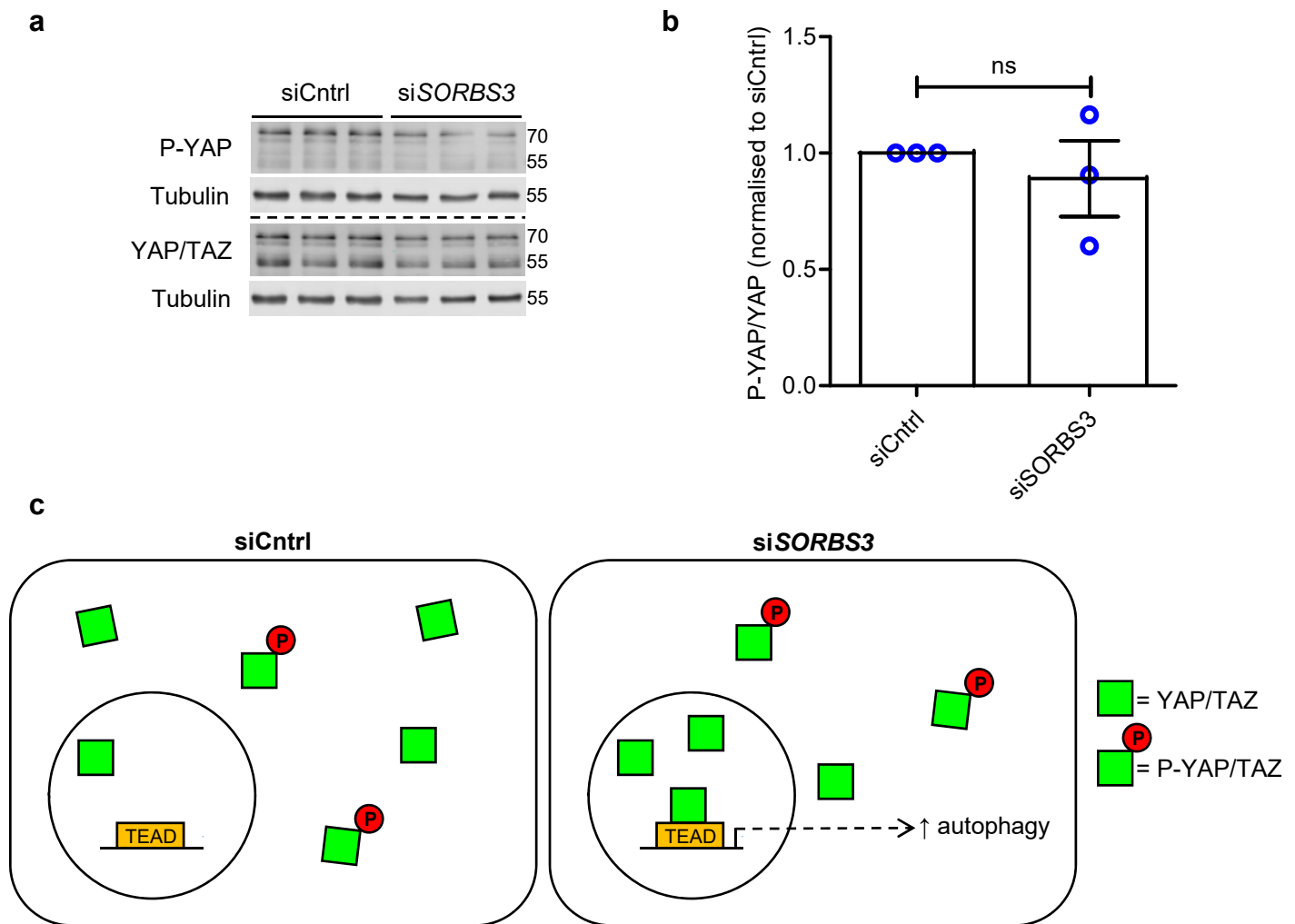


**Figure 4.4: increased YAP/TAZ activity under siSORBS3 treatment is Hippo pathway-independent.**

- HeLa cells were depleted of vinexin beta using an individual siRNA oligonucleotide against *SORBS3* (siSORBS3; oligo 7). Endogenous total YAP/TAZ, YAP phosphorylated at serine 127, tubulin and vinexin beta protein levels were examined by western blotting. Representative blot from 3 independent experiments is shown. Molecular weights in kDa.
- Quantification of 3 independent experiments. P-YAP and YAP (upper band of YAP/TAZ doublet) are expressed relative to tubulin loading control, the ratio of P-YAP/tubulin: YAP/tubulin taken and then normalised to P-YAP/YAP in siCntrl treated cells. ns =  $p > 0.05$  by 2-tailed one-sample t-test. Error bars indicate SEM.
- Schematic diagram of the hypothesised situation in siCntrl and siSORBS3 treated cells. Vinexin beta depletion is theorised to increase nuclear localisation of nonphosphorylated YAP/TAZ; driving transcriptional activity *via* TEAD transcription factors and somehow upregulating autophagy. YAP/TAZ phosphorylation by the Hippo pathway kinases LATS1/2 is suggested to remain unchanged under siSORBS3 treatment.

the ratio of P-YAP to total YAP there was no significant change compared with siCntrl treated cells (Figure 4.4b). I therefore hypothesised that vinexin beta depletion upregulates autophagy by increasing YAP/TAZ nuclear translocation and consequent transcriptional activity, while LATS1/2 phosphorylation-mediated YAP/TAZ regulation remains unaltered (summarised in Figure 4.4c).

The Hippo pathway kinase MST1 is reported to inhibit autophagy independent of YAP/TAZ; MST1 phosphorylates threonine 108 in the Beclin 1 BH3 domain, thereby disrupting PI3KC3 complex I (see section 1.1.2ii) by promoting Beclin 1 binding to BCL2 family proteins (Maejima et al., 2013). As MST1/2 regulates LATS1/2 kinase activity (Chan et al., 2005), the results presented in Figure 4.4a-b also serve to indicate this mechanism does not contribute to autophagy upregulation upon vinexin beta depletion.

#### ***4.5 siSORBS3 treatment alters actin cytoskeleton dynamics***

In the absence of changes in Hippo pathway-mediated YAP/TAZ phosphorylation under siSORBS3 treatment (Figure 4.4), I considered alternative regulatory mechanisms. The Piccolo group reported that YAP/TAZ nuclear localisation and activity are increased in cells cultured on rigid (compared with soft) substrates. This response to extracellular matrix (ECM) stiffness requires actin stress fibres and actomyosin tension, but is independent of Hippo signalling (Dupont et al., 2011). In this way, the filamentous actin (F-actin) capping and severing proteins cofilin, CAPZ and gelsolin negatively regulate YAP/TAZ activity in a manner formally distinct from Hippo signalling (Aragona et al., 2013). I therefore examined the actin cytoskeleton in vinexin beta depleted HeLa cells using fluorophore-labelled phalloidin, which forms tight complexes with F-actin (Wulf et al., 1979). siSORBS3 treated cells appeared to contain more phalloidin-positive F-actin bundles by confocal microscopy, which were smaller in diameter than those seen in siCntrl treated cells (Figure 4.5a). This impression was confirmed when this phalloidin staining was analysed using ImageJ software; vinexin beta depletion increased F-actin structures per cell, but the average size of these structures was smaller (Figure 4.5b).

To investigate whether this finding represented an altered F-actin to monomeric globular actin (G-actin) ratio, Dr Bento performed experiments using an F-: G-actin *in vivo* assay kit. To our surprise, given the increase in F-actin structures per cell by phalloidin staining (Figure 4.5a-b), vinexin beta depletion appeared to decrease the F- to G-actin ratio under basal conditions (Figure 4.5c-d). However, these data are compatible with the hypothesis that

increased F-actin structures contribute to the mechanism by which si*SORBS3* treatment increases YAP/TAZ activity. This result is consistent with the Piccolo group's findings regarding YAP/TAZ regulation by ECM stiffness; the group used various techniques to manipulate the F- to G-actin ratio and established that, while actin stress fibres are required for increased YAP/TAZ activity in cells cultured on rigid substrates, F-actin polymerisation *per se* is not required (Dupont et al., 2011).

Dr Bento also performed F- to G-actin ratio experiments in the presence of phalloidin, which strongly stabilises F-actin (Wulf et al., 1979). Under these conditions, vinexin beta depletion had the opposite effect; increasing the F- to G-actin ratio (Figure 4.5c-d). Taken together, these phalloidin staining and F-: G-actin assay data require complex interpretation. One possible explanation is that si*SORBS3* treatment increases the labile F-actin pool. Distinct F-actin pools were first characterised by Watts and Howard (1992), who describe loss of labile (triton soluble) F-actin from cells lysed with triton prior to formaldehyde fixation ('PostFix') compared with cells fixed prior to lysis ('PreFix') (Watts and Howard, 1992). Given I prepared cells for phalloidin staining using the 'PreFix' method, it is conceivable the F-actin structures shown in Figure 4.5a correspond to both the labile and stable (triton insoluble) F-actin pools, while the labile F-actin pool only becomes apparent by F-: G-actin assay when F-actin is stabilised using phalloidin (Figure 4.5c). Hence, the data presented in Figure 4.5 could indicate vinexin beta depletion shifts the tripartite equilibrium between labile F-actin, stable F-actin and G-actin in favour of the labile F-actin pool. This could also explain the decrease in F- to G-actin ratio with si*SORBS3* treatment under basal conditions, which would correspond to a decrease in the stable F-actin pool. Moreover, an increase in labile F-actin structures fits with the focal adhesions changes discussed in the previous chapter, with vinexin beta depletion appearing to destabilise focal adhesions and promote the formation of dynamic focal complexes (Figure 3.9b-c).

#### ***4.6 Filamentous actin, and to a lesser extent actomyosin tension, contribute to YAP/TAZ nuclear translocation under siSORBS3 treatment***

In order to test the hypothesis that increased F-actin structures following vinexin beta depletion contributes to the mechanism by which YAP/TAZ activity is upregulated, I conducted experiments in which HeLa cells were treated with si*SORBS3* in the presence and absence of latrunculin A. This toxin is thought to inhibit actin polymerisation by sequestering G-actin (Coue et al., 1987) and is used here under conditions the Piccolo group report localise

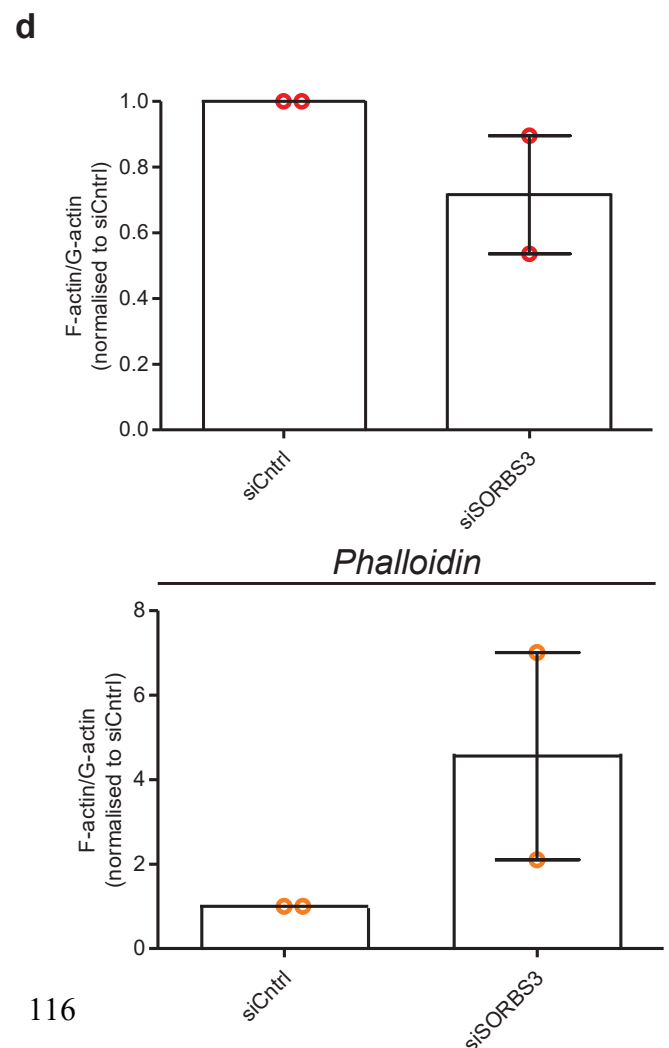
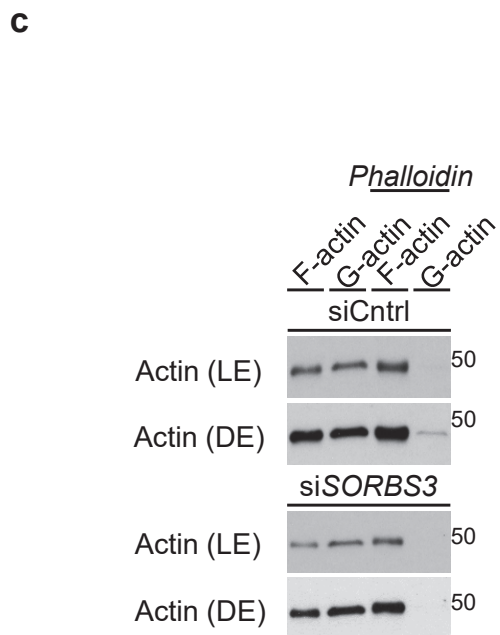
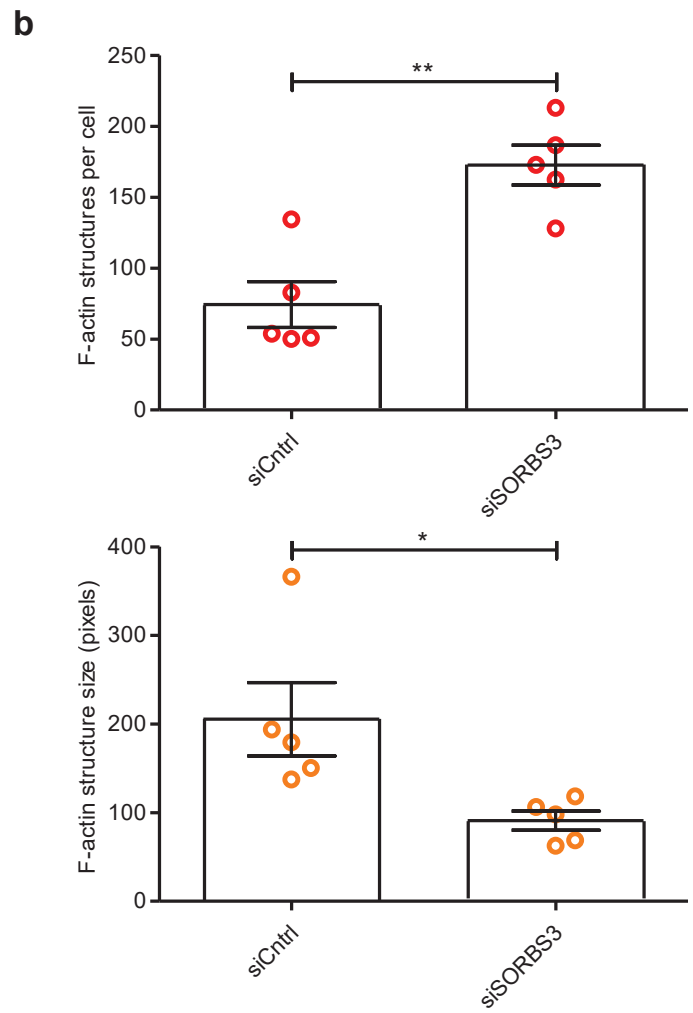
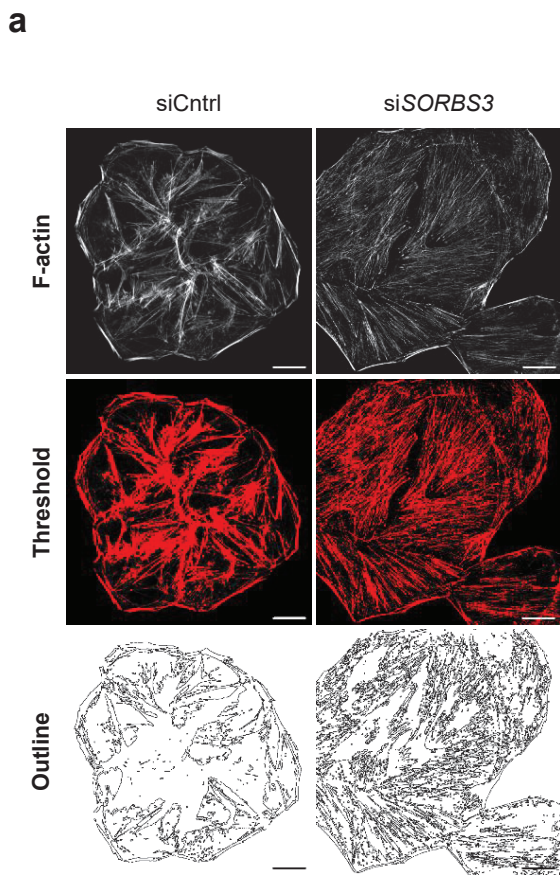


**Figure 4.5: labile F-actin structures are upregulated under siSORBS3 treatment.**

- a. HeLa cells were depleted of vinexin beta using an individual siRNA oligonucleotide against *SORBS3* (si*SORBS3*; oligo 7). Endogenous F-actin was visualised using Alexa Fluor 488-conjugated phalloidin and confocal microscopy (F-actin). Confocal images were analysed using ImageJ software; F-actin structures were first identified by thresholding (threshold), then outlined (outline). Representative images from 5 independent experiments are shown. Scale bars indicate 20  $\mu\text{m}$ .
- b. Quantification of F-actin structures per cell and F-actin structure size (pixels) from 5 independent experiments, measured as described in a. \* =  $p < 0.05$ ; \*\* =  $p < 0.01$  by 2-tailed paired t-test. Error bars indicate SEM.
- c. HeLa cells were depleted of vinexin beta, as in a. Endogenous F- and G-actin levels were examined by western blotting following sample processing using an F-: G-actin *in vivo* assay kit. Experiments were performed in the presence and absence of F-actin enhancing solution (phalloidin). Representative blots from 2 independent experiments in technical duplicate are shown. LE = lighter exposure; DE = darker exposure; molecular weights shown in kDa.
- d. Quantification of 2 independent experiments, described in c. F-: G-actin ratio was calculated and normalised to control siRNA (siCntrl) treated cells. Graphs display data generated in the presence and absence of F-actin enhancing solution (phalloidin). Error bars indicate SEM.

YAP/TAZ to the cytosol in several cell lines (0.5  $\mu$ M for 6 hours) (Dupont et al., 2011). As expected, latrunculin A treatment destroyed cytoskeletal F-actin by phalloidin staining in both siCntrl and siSORBS3 treated cells. This corresponded to reduced YAP/TAZ nuclear staining, even in siSORBS3 treated cells (Figure 4.6a). While the percentage of cells showing predominantly nuclear YAP/TAZ staining ( $N > C$ ) significantly increased and the percentage showing predominantly cytosolic staining ( $N < C$ ) significantly decreased upon vinexin beta depletion in the absence of latrunculin A (DMSO), most siCntrl and siSORBS3 treated cells showed  $C > N$  staining upon F-actin inhibition with latrunculin A (Figure 4.6b).

As these data support the hypothesis that increased F-actin structures under siSORBS3 treatment promote YAP/TAZ activity, I considered the other factor Dupont et al. (2011) report is necessary for YAP/TAZ nuclear localisation; actomyosin tension. This was achieved by treating cells with the non-muscle myosin inhibitor blebbistatin, which maintains myosin II in the actin-detached state and thereby prevents generation of tension by actomyosin crosslinking (Kovacs et al., 2004). Again this inhibitor was used under conditions the Piccolo group report localises YAP/TAZ to the cytosol (50  $\mu$ M for 6 hours) (Dupont et al., 2011). Blebbistatin treatment did reduce YAP/TAZ nuclear staining in both siCntrl and siSORBS3 treated cells, but not to the same extent as latrunculin A (Figure 4.6a). Unlike in the presence of DMSO vehicle control, the percentage of cells showing  $N > C$  and  $N < C$  staining was not significantly altered by siSORBS3 treatment in the presence of blebbistatin (Figure 4.6b). However, quantified changes in YAP/TAZ localisation under blebbistatin treatment were much less dramatic than those seen with latrunculin A treatment; YAP/TAZ distribution in blebbistatin; siSORBS3 cells was comparable to that in DMSO; siCntrl cells, which was not true of latrunculin A; siSORBS3 cells (Figure 4.6b).

The lesser effect of blebbistatin on YAP/TAZ distribution compared with latrunculin A correlates with the observation that blebbistatin did disrupt cytoskeletal F-actin, but to a much lesser extent than latrunculin A (Figure 4.6a). Accordingly, I speculated that blebbistatin treatment might localise YAP/TAZ to the cytosol predominantly *via* actin stress fibres destabilisation, secondary to prolonged loss of actomyosin tension due to 6 hours myosin II inhibition. This contradicts the Piccolo group's assertion that both actin stress fibres and actomyosin tension are together required for YAP/TAZ nuclear localisation, but is in agreement with a recent publication by Das et al. who propose distinct F-actin- and myosin II-dependent YAP/TAZ regulatory pathways (Das et al., 2016). Akin to my findings, Das and colleagues report loss of actomyosin tension due to blebbistatin treatment or pharmacological

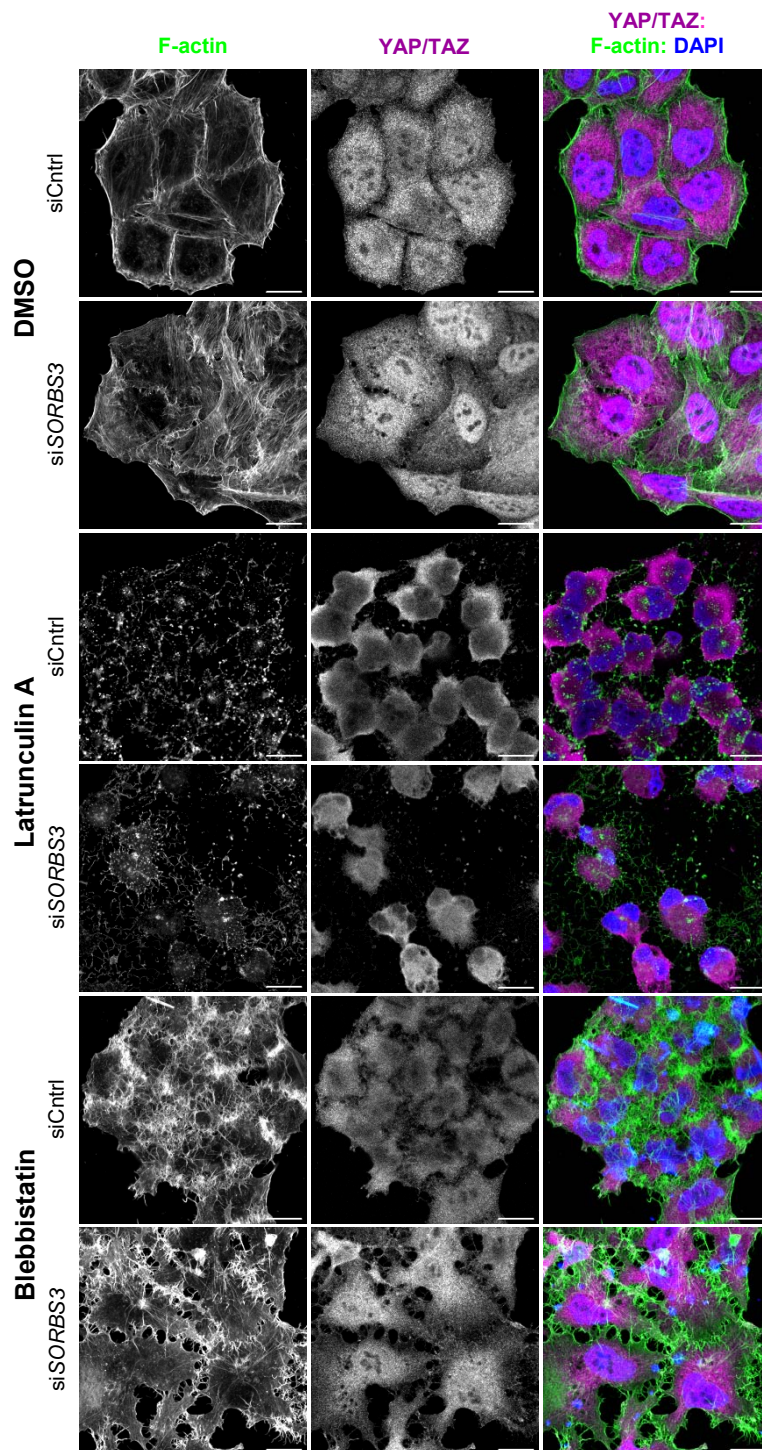
inhibition of ROCK (RHO-associated kinase) had a much lesser effect on YAP/TAZ distribution in sparsely seeded MEFs and MCF10A cells than inhibiting actin polymerisation with latrunculin A (Das et al., 2016). Regardless of the relative contributions of F-actin and actomyosin tension, the data presented in Figure 4.6 supports the hypothesis that actin cytoskeletal changes are involved in increasing YAP/TAZ activity upon vinexin beta depletion.

#### ***4.7 Autophagy upregulation upon vinexin beta depletion requires filamentous actin, but not actomyosin tension***

Considering data presented in Figures 4.1-3 supports the hypothesis vinexin beta depletion increases autophagy by upregulating YAP/TAZ activity, I investigated whether amelioration of YAP/TAZ nuclear localisation under si*SORBS3* treatment by actomyosin cytoskeleton manipulations (as shown in Figure 4.6) was sufficient to prevent this increase in autophagy. Inhibiting actin polymerisation with latrunculin A treatment (0.5  $\mu$ M for 6 hours) ameliorated the increase in LC3-II levels observed by western blotting upon si*SORBS3* treatment (DMSO; si*SORBS3* compared with Latrunculin A; si*SORBS3* in Figure 4.7a). When quantified relative to tubulin, although LC3-II levels were significantly increased in Latrunculin A; si*SORBS3* cells compared with Latrunculin A; siCntrl cells, this increase was much smaller than that seen under basal conditions (DMSO) and LC3-II levels were not significantly increased in Latrunculin A; si*SORBS3* cells compared with DMSO; siCntrl cells (Figure 4.7b). As described above, treatment with 0.5  $\mu$ M latrunculin A for 6 hours appears sufficient to destroy cytoskeletal F-actin and localise YAP/TAZ to the cytosol in both siCntrl and si*SORBS3* treated cells (Figure 4.6). Accordingly, these data support the hypotheses that increased F-actin structures upon vinexin beta depletion contribute to the mechanism by which autophagy is upregulated and also that autophagy upregulation could result from an F-actin-dependent increase in YAP/TAZ nuclear localisation under si*SORBS3* treatment.

I next examined whether the lesser effect of blebbistatin (compared with latrunculin A) on cytoskeletal F-actin and YAP/TAZ distribution (Figure 4.6) was sufficient to prevent increased autophagy upon vinexin beta depletion. Loss of actomyosin tension due to blebbistatin treatment (50  $\mu$ M for 6 hours) did not ameliorate the increase in LC3-II levels observed upon si*SORBS3* treatment (DMSO; si*SORBS3* compared with blebbistatin; si*SORBS3* in Figure 4.7c). When quantified relative to tubulin, LC3-II levels were significantly increased upon vinexin beta depletion in both the presence and absence of

**a**



**b**

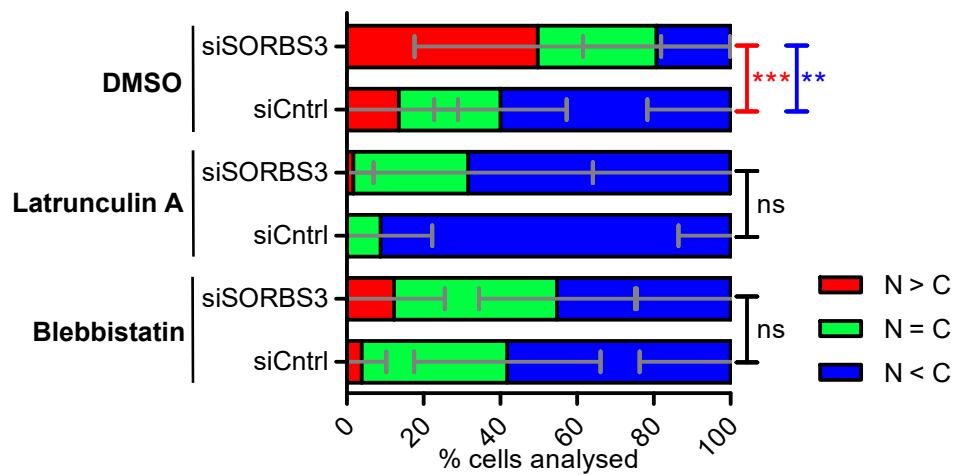


**Figure 4.6: latrunculin A treatment ameliorates YAP/TAZ nuclear translocation due to vinexin beta depletion more effectively than blebbistatin treatment.**

- a. HeLa cells were depleted of vinexin beta using an individual siRNA oligonucleotide against SORBS3 (siSORBS3; oligo 7). Cells were treated with latrunculin A (0.5  $\mu$ M), blebbistatin (50  $\mu$ M) or DMSO vehicle control for 6 hours. Endogenous F-actin was visualised using Alexa Fluor 488-conjugated phalloidin and YAP/TAZ was examined by immunofluorescence. Representative confocal images from 3 independent experiments are shown. Green = F-actin (Alexa Fluor 488); purple = YAP/TAZ (Alexa Fluor 647); blue = DAPI. Scale bars indicate 20  $\mu$ m.
- b. Cells with predominantly nuclear YAP/TAZ (N > C), YAP/TAZ equally distributed between nucleus and cytosol (N = C) and predominantly cytosolic YAP/TAZ (C > N) were manually quantified. Quantification of the representative experiment shown in a. ns =  $p > 0.05$ ; \*\* =  $p < 0.01$ ; \*\*\* =  $p < 0.001$  by 2-tailed Student's t-test. Red asterisks represent p value for N > C; blue asterisks represent N < C p vale. n = 122 (siCntrl; DMSO); 75 (siSORBS3; DMSO); 165 (siCntrl; latrunculin A); 96 (siSORBS3; latrunculin A); 111 (siCntrl; blebbistatin); 73 (siSORBS3; blebbistatin). Error bars indicate SD.

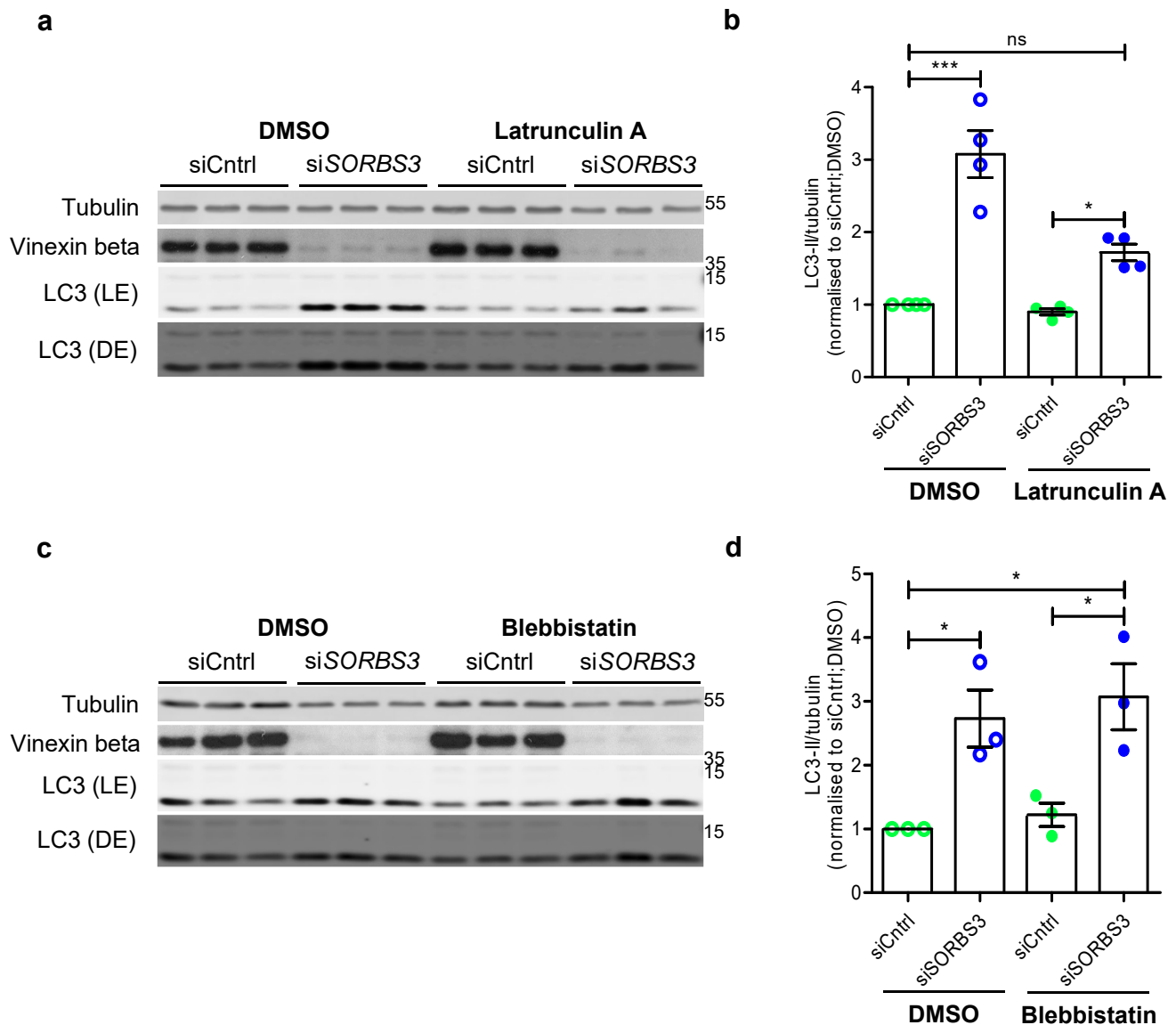


**Figure 4.7: latrunculin A treatment, but not blebbistatin treatment, ameliorates the increase in LC3-II caused by vinexin beta depletion.**

- a. HeLa cells were depleted of vinexin beta using an individual siRNA oligonucleotide against *SORBS3* (siSORBS3; oligo 7). Cells were treated with latrunculin A (0.5  $\mu$ M) or DMSO vehicle control for 6 hours. Endogenous tubulin, LC3 and vinexin beta protein levels were examined by western blotting. Representative blots from 4 independent experiments are shown. LE = lighter exposure; DE = darker exposure; molecular weights shown in kDa.
- b. Quantification of 4 independent experiments. LC3-II (lower band of LC3 doublet) levels are expressed relative to tubulin loading control and normalised to LC3-II/tubulin in DMSO treated siCntrl cells. ns =  $p > 0.05$ ; \* =  $p < 0.05$ ; \*\*\* =  $p < 0.001$  by one-way ANOVA followed by Tukey's multiple comparison test. Error bars indicate SEM.
- c. HeLa cells were depleted of vinexin beta, as in a. Cells were treated with blebbistatin (50  $\mu$ M) or DMSO vehicle control for 6 hours. Endogenous tubulin, LC3 and vinexin beta protein levels were examined by western blotting. Representative blots from 3 independent experiments are shown. LE = lighter exposure; DE = darker exposure; molecular weights shown in kDa.
- d. Quantification of 3 independent experiments. LC3-II levels are expressed relative to tubulin loading control and normalised to LC3-II/tubulin in DMSO treated siCntrl cells. \* =  $p < 0.05$  by one-way ANOVA followed by Tukey's multiple comparison test. Error bars indicate SEM.

blebbistatin. Moreover, LC3-II levels remained significantly higher in Blebbistatin; si*SORBS3* cells compared with DMSO; siCntrl cells (Figure 4.7b). Taken together, data presented thus far in this chapter indicate si*SORBS3* treatment might upregulate autophagy *via* altered actin cytoskeleton dynamics. This could result from upregulated YAP/TAZ activity owing to increased F-actin structures, with lesser changes in YAP/TAZ distribution due to decreased actomyosin tension being insufficient to ameliorate the increase in autophagy caused by vinexin beta depletion.

#### ***4.8 siSORBS3 treatment alters actin cytoskeleton dynamics upstream of YAP/TAZ***

The results presented so far indicate vinexin beta depletion upregulates autophagy (see chapter 3) and this increase in autophagy is downstream of YAP/TAZ (Figure 4.3) and F-actin polymerisation (Figure 4.7a-b). However, several alternative chronologies linking autophagy upregulation under si*SORBS3* treatment to increased F-actin structures and YAP/TAZ activity remain formally possible (Figure 4.8a).

In support of Scenarios A and B (Figure 4.8a), actin cytoskeleton dynamics are implicated in both autophagosome biogenesis and flux through the autophagy pathway (reviewed in Kast and Dominguez, 2017). Particularly relevant are recent publications from our lab in which actin depolymerisation with latrunculin A or the ARP2/3 inhibitor CK-666 is shown to impair autophagosome formation owing to defective ATG9A sorting from endosomes (Moreau et al., 2015), while actin depolymerisation with latrunculin A or cytochalasin D can also impair autophagosome clearance by inducing lysosomal dysfunction (Pavel et al., 2016). Notably, these publications use latrunculin A under different conditions (1 $\mu$ M for 1 hour in Moreau et al. and 1 $\mu$ M for 3 hours in Pavel et al.), which could explain why LC3-II levels in siCntrl treated cells are unchanged by latrunculin A (0.5 $\mu$ M for 6 hours) in my hands (Figure 4.7a).

In further support of Scenario B, the Piccolo group have identified several actomyosin modulators such as the actin polymerising formin DIAPH3 (Goode and Eck, 2007) as YAP/TAZ/TEAD direct target genes (Zanconato et al., 2015). Additionally, our group has recently demonstrated Hippo pathway-dependent inhibition of actin stress fibre formation in the context of contact inhibition at high cell densities (Pavel et al., manuscript in preparation).

With this literature in mind, I conducted experiments in which HeLa cells were treated with si*SORBS3* in the presence and absence of siRNA against YAP and TAZ. si*YAP/TAZ* double knockdown cells (outlined in white) did exhibit fewer stress fibres by phalloidin staining (si*YAP/TAZ*; siCntrl in Figure 4.8b). However, si*YAP/TAZ* treatment was not sufficient to



ameliorate the increase in F-actin structures observed upon siSORBS3 treatment (siCntrl; siSORBS3 compared with siYAP/TAZ; siSORBS3 in Figure 4.8b). When quantified, these experiments replicated data presented in Figure 4.5a-b; vinexin beta depletion increased F-actin structures per cell, although the average size of these structures was smaller, in both the presence and absence of siYAP/TAZ (Figure 4.8c). I interpreted these findings as support for Scenario C (Figure 4.8a) in which increased F-actin structures under siSORBS3 treatment promote autophagy *via* a downstream, YAP/TAZ-dependent mechanism.

#### ***4.9 Angiotensins counter YAP/TAZ nuclear translocation under siSORBS3 treatment by retaining YAP/TAZ in the cytosol***

I next considered the mechanism by which increased F-actin structures upon vinexin beta depletion might upregulate YAP/TAZ activity. This could involve angiotensins (AMOTs), which are reported to function between actin cytoskeleton dynamics and YAP/TAZ regulation (see chapter 1) (Mana-Capelli et al., 2014). AMOT family proteins interact with YAP/TAZ in the cytosol *via* N-terminal L/PPxY motifs binding the WW domains of YAP/TAZ (Chan et al., 2011; Wang et al., 2011; Zhao et al., 2011a). Accordingly, overexpression of full-length AMOT p130 or AMOTL1 (angiotensin-like protein 1) causes YAP/TAZ retention in the cytosol (Chan et al., 2011), while AMOTL2 (angiotensin-like protein 2) knockdown promotes YAP/TAZ nuclear localisation (Zhao et al., 2011a). As the AMOT F-actin binding region was found to be closely flanked by the aforementioned L/PPxY motifs, Mana-Capelli et al. propose F-actin and YAP/TAZ compete for AMOT binding. Indeed, recombinant YAP displaces pre-bound F-actin from recombinant AMOT p130 by *in vitro* competition assay and overexpressing F-actin binding-deficient AMOT p130 mutants inhibited YAP/TAZ activity to an even greater extent than overexpressing wild type AMOT p130 (Mana-Capelli et al., 2014).

As expected, overexpression of haemagglutinin-tagged AMOT p130 (pcDNA-HA-AMOT(p130)) seemed to sequester YAP/TAZ in the cytosol (pcDNA-empty; siCntrl compared with pcDNA-HA-AMOT(p130); siCntrl in Figure 4.9a). In this way, HA-AMOT(p130) overexpression reduced YAP/TAZ nuclear staining, even in siSORBS3 treated cells (Figure 4.9a). The percentage of cells showing predominantly nuclear YAP/TAZ staining ( $N > C$ ) was not significantly increased, nor the percentage showing predominantly cytosolic staining ( $N < C$ ) significantly decreased, under siSORBS3 treatment when HA-AMOT(p130) was overexpressed (Figure 4.9b). These data suggest increased YAP/TAZ

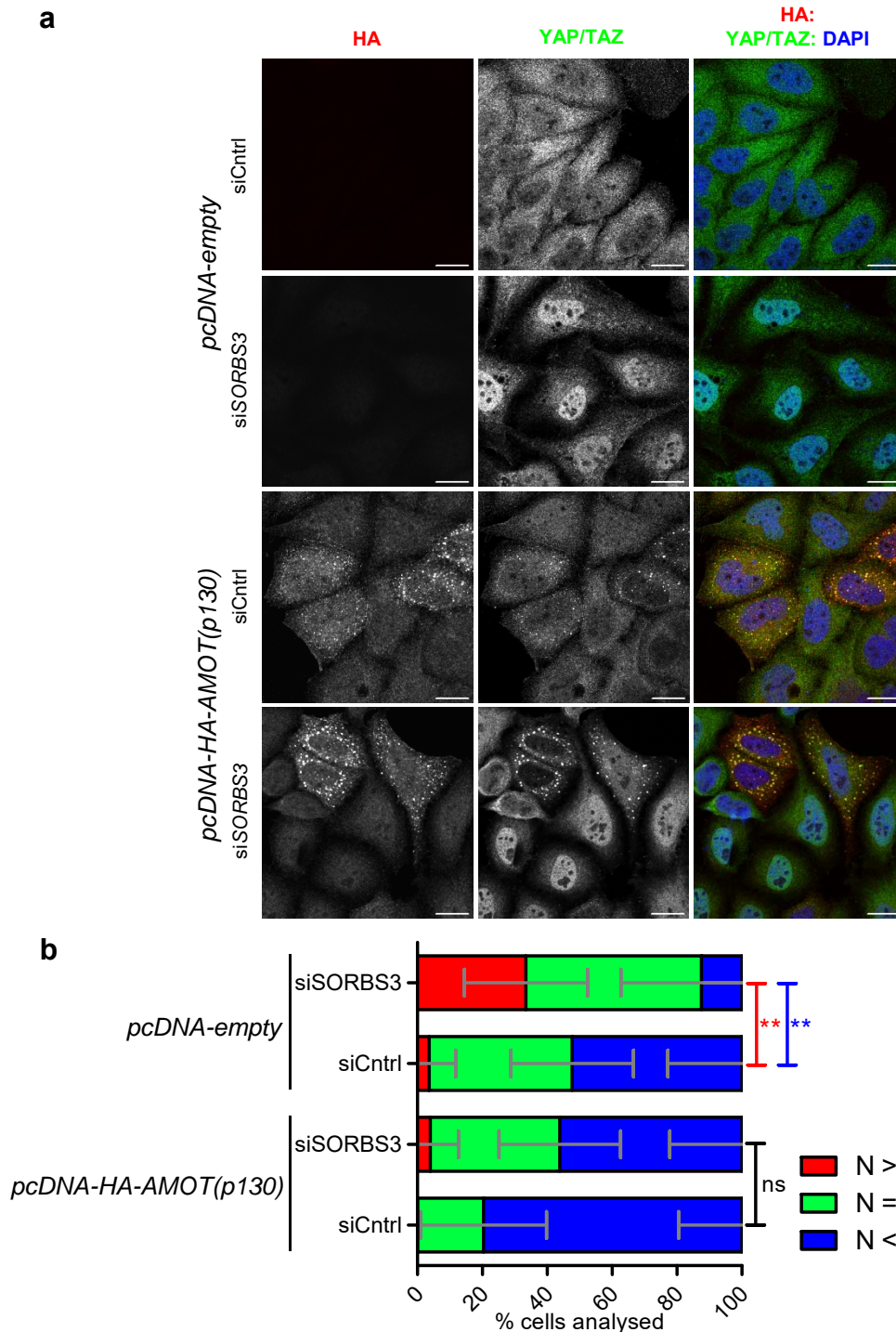


**Figure 4.9: angiotensin p130 overexpression ameliorates YAP/TAZ nuclear translocation caused by vinexin beta depletion.**

- a. HeLa cells were depleted of vinexin beta using an individual siRNA oligonucleotide against *SORBS3* (siSORBS3; oligo 7). siCntrl and siSORBS3 treated cells were transfected with pcDNA-HA-AMOT(p130) or empty vector control (pcDNA-empty) for 24 hours. Haemagglutinin (HA) and endogenous YAP/TAZ were examined by immunofluorescence. Representative confocal images from 3 independent experiments are shown. Red = HA (Alexa Fluor 568); green = YAP/TAZ (Alexa Fluor 488); blue = DAPI. Scale bars indicate 20  $\mu$ m.
- b. Cells with predominantly nuclear YAP/TAZ (N > C), YAP/TAZ equally distributed between nucleus and cytosol (N = C) and predominantly cytosolic YAP/TAZ (C > N) were manually quantified. Quantification of the representative experiment shown in a. ns =  $p > 0.05$ ; \*\* =  $p < 0.01$ ; \*\*\* =  $p < 0.001$  by 2-tailed Student's t-test. Red asterisks represent p value for N > C; blue asterisks represent N < C p value. n = 56 (pcDNA-empty; siCntrl); 68 (pcDNA-empty; siSORBS3); 70 (pcDNA-HA-AMOT; siCntrl); 45 (pcDNA-HA-AMOT; siSORBS3). Error bars indicate SD.

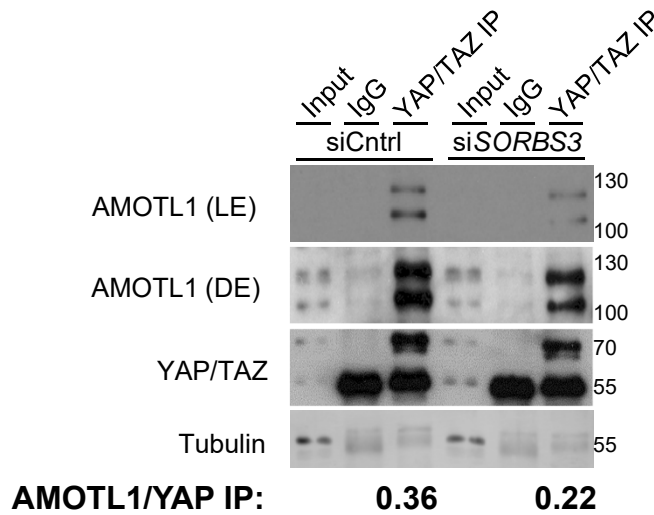
nuclear localisation upon vinexin beta depletion can be ameliorated by saturating AMOT binding sites on F-actin *via* AMOT overexpression, thereby freeing excess AMOT to sequester YAP/TAZ in the cytosol.

#### ***4.10 Altered actin cytoskeleton dynamics upon vinexin beta depletion prevent YAP/TAZ cytosolic sequestration by angiomotins***

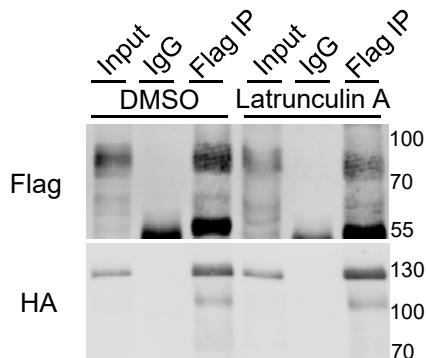
Findings presented in Figure 4.9 are consistent with the hypothesis that increased F-actin structures under si*SORBS3* treatment upregulate YAP/TAZ activity by sequestering YAP/TAZ inhibitors, namely members of the AMOT protein family. I aimed to test this hypothesis by examining the effect of vinexin beta depletion on the interaction between AMOTs and YAP/TAZ. Endogenous YAP and TAZ were immunoprecipitated from HeLa cell lysate using an antibody that recognises both proteins (YAP/TAZ IP; Figure 4.10a). Unfortunately, immunoprecipitated TAZ was obscured on western blotting by IgG heavy chain (as seen with immunoprecipitation using negative control normal IgG). Considering immunoprecipitated YAP; slightly less protein was pulled down from si*SORBS3* treated cells than siCntrl treated cells, which corresponds to slightly lower total protein levels in the input by tubulin loading control. However, upon densitometry quantification (AMOTL1/YAP IP; Figure 4.10a) this did not account for the dramatic reduction in endogenous AMOTL1 pulled down with YAP/TAZ from vinexin beta depleted cells (Figure 4.10a). Unfortunately, I could not find commercially available antibodies able to identify AMOT(p130) or AMOTL2 by western blotting using either whole cell lysate or YAP/TAZ IP samples. It was also not possible to pull down YAP/TAZ or actin by immunoprecipitating any of the AMOTs (data not shown), which would have allowed the effect of vinexin beta depletion on competition between F-actin and YAP/TAZ for AMOT binding to be examined.

This apparent reduction in YAP/AMOTL1 binding in si*SORBS3* treated cells (Figure 4.10a) does lend support to the notion increased F-actin structures upon vinexin beta depletion upregulate YAP/TAZ activity by sequestering AMOTs. However, a more artificial system was required to further test this hypothesis. HeLa cells were co-transfected with Flag-tagged YAP (Flag-YAP) and HA-AMOT(p130), then treated with latrunculin A or DMSO vehicle control. Importantly, latrunculin A treatment was under the same conditions shown previously to ameliorate increased YAP/TAZ nuclear localisation and LC3-II levels upon vinexin beta depletion (0.5  $\mu$ M for 6 hours; Figures 4.6 - 4.7). When exogenous Flag-YAP was immunoprecipitated (Flag IP) under actin depolymerising conditions (latrunculin A),

**a**



**b**



**c**

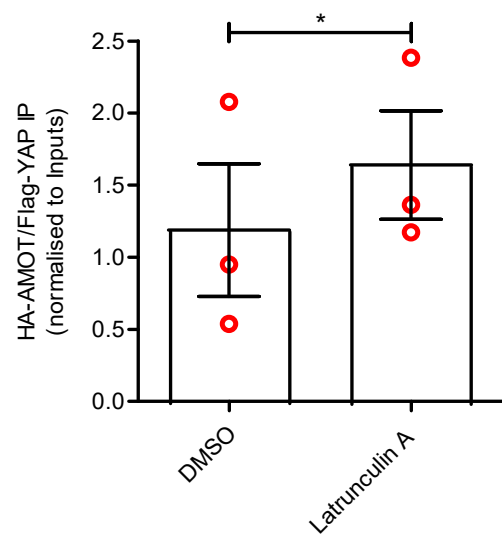


**Figure 4.10: YAP sequestration by angiomotins is influenced by actin cytoskeleton dynamics.**

- HeLa cells were depleted of vinculin using an individual siRNA oligonucleotide against *SORBS3* (si*SORBS3*; oligo 7). Endogenous YAP/TAZ were immunoprecipitated using an antibody raised in mouse (YAP/TAZ IP). Normal mouse IgG was used as a negative control (IgG). Endogenous angiomin-like protein 1 (AMOTL1), YAP/TAZ and tubulin were examined by western blotting. AMOTL1/YAP IP values are densitometry quantification: amount of YAP and AMOTL1 (both bands in doublet) in YAP/TAZ IP are expressed relative to YAP and AMOTL1 in Input and AMOTL1 IP normalised to YAP IP. TAZ is not quantified as obscured by IgG heavy chain in IP. LE = lighter exposure; DE = darker exposure; molecular weights shown in kDa.
- HeLa cells were co-transfected with Flag-YAP and HA-AMOT(p130) for 48 hours. Cells were treated with latrunculin A (0.5  $\mu$ M) or DMSO vehicle control for 6 hours. Exogenous Flag-YAP was immunoprecipitated using a mouse antibody against Flag (Flag IP). Normal mouse IgG was used as a negative control (IgG). Flag-YAP and HA-AMOT(p130) were examined by western blotting. Representative blot from 3 independent experiments is shown. Molecular weights shown in kDa.
- Quantification of 3 independent experiments. Amount of Flag-YAP and HA-AMOT(p130) in Flag IP are expressed relative to Flag-YAP and HA-AMOT(p130) in Input and HA-AMOT(p130) IP normalised to Flag-YAP IP. \* =  $p < 0.05$  by 2-tailed paired t-test. Error bars indicate SEM.

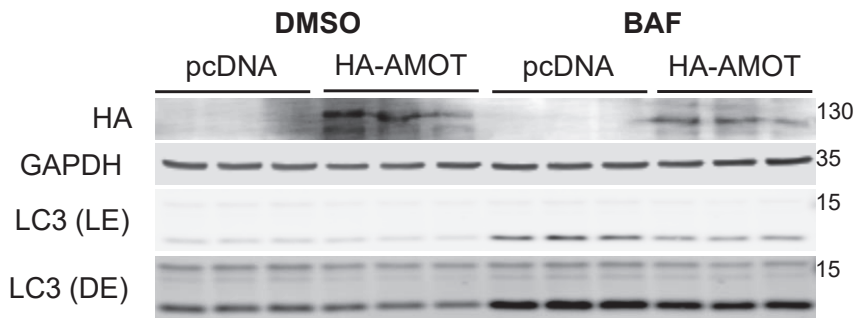
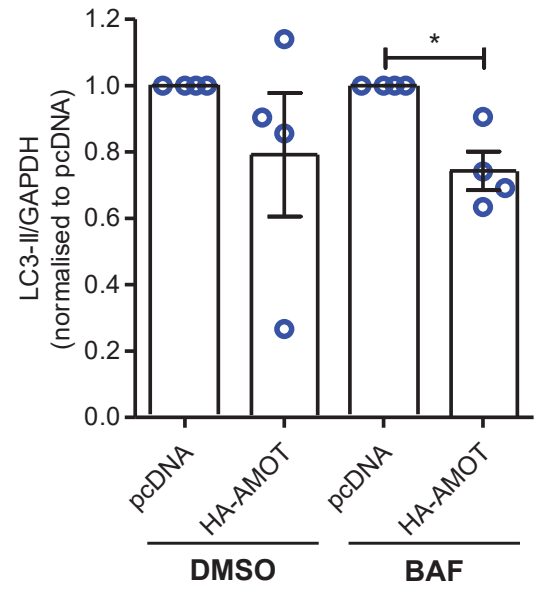
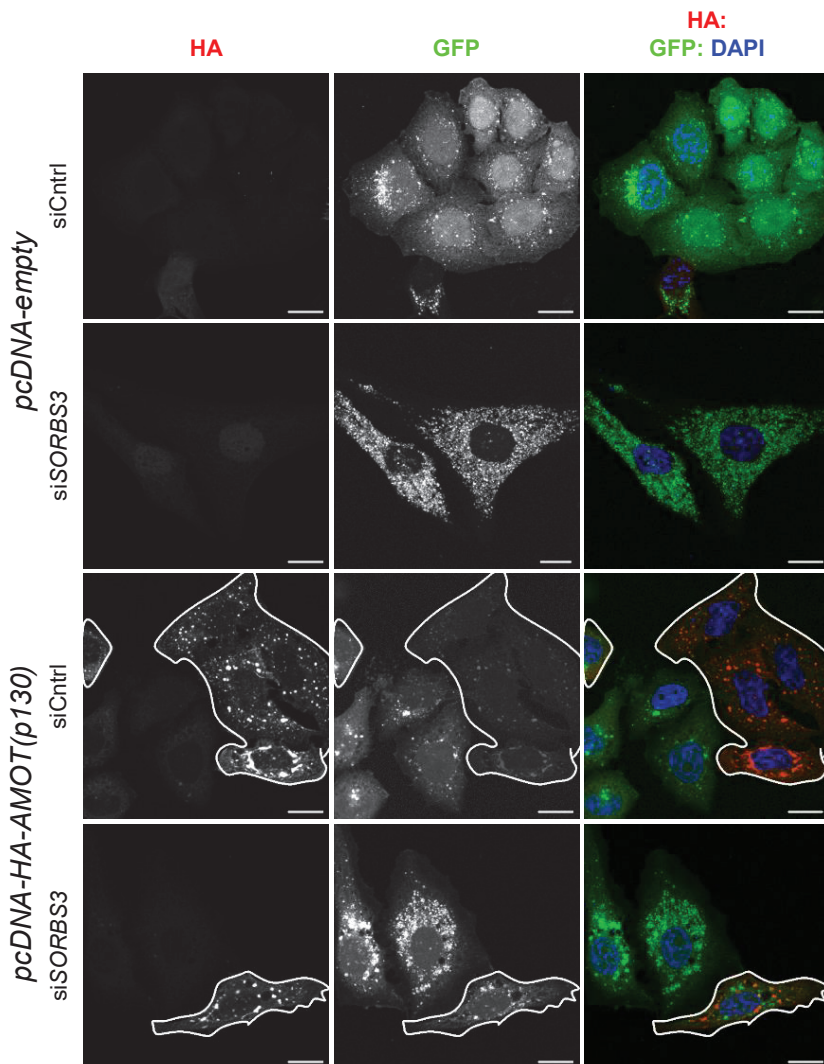
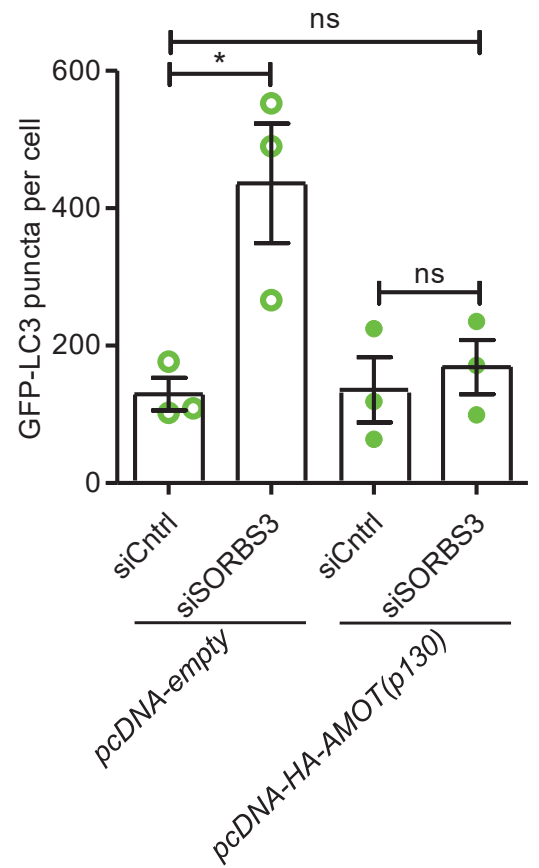
more HA-AMOT(p130) appeared to be pulled down upon western blotting for HA (Figure 4.10b). This result was confirmed by quantification using fluorescent dye-labelled secondary antibodies and infrared fluorescence detection (see Chapter 2); when Flag-YAP and HA-AMOT(p130) levels in Flag IP samples are expressed relative to those in the relevant inputs, levels of HA-AMOT(p130) pulled down by Flag IP were significantly higher in cells treated with latrunculin A compared with DMSO. Unfortunately, it was again not possible to pull down YAP, TAZ or actin by immunoprecipitating exogenous HA-AMOT(p130) (data not shown).

Although this experiment does not directly test the hypothesis that altered actin cytoskeleton dynamics upon vinexin beta depletion oppose YAP/TAZ retention in the cytosol by angiomotins, I interpreted the finding that latrunculin A treatment increases YAP/AMOT(p130) interaction as strong circumstantial evidence. In other words, that the mechanism by which destruction of F-actin structures with latrunculin A ameliorates increased YAP/TAZ nuclear localisation and LC3-II levels under siSORBS3 treatment could involve freeing actin-bound AMOTs to sequester YAP/TAZ in the cytosol.

#### ***4.11 Autophagy upregulation upon vinexin beta depletion requires YAP/TAZ release from angiomotins***

Next I hoped to recapitulate the autophagy phenotype seen under siSORBS3 treatment (see chapter 3) using AMOT depletion, which upregulates YAP/TAZ activity by promoting YAP/TAZ nuclear localisation (Mana-Capelli et al., 2014; Wang et al., 2011; Zhao et al., 2011a). However, using several experimental setups I was unable to achieve the robust triple knockdown of AMOT(p130), AMOTL1 and AMOTL2 that Mana-Capelli and colleagues report is necessary to bring about YAP/TAZ nuclear retention (data not shown) (Mana-Capelli et al., 2014).

I therefore investigated whether changes in YAP/TAZ localisation due to AMOT overexpression (Figure 4.9) were sufficient to impact autophagy. As expected, overexpressing HA-AMOT(p130) decreased LC3-II levels by western blotting, most noticeably when autophagy flux was blocked using bafilomycin A1 (BAF; Figure 4.11a). When quantified relative to GAPDH loading control, LC3-II levels were significantly increased upon HA-AMOT(p130) overexpression in the presence of BAF (Figure 4.11b). This finding is consistent with reduced autophagosome biogenesis owing to YAP/TAZ retention in the cytosol due by excess AMOT.

**a****b****c****d**

**Figure 4.11: angiotensin p130 overexpression decreases LC3-II levels and ameliorates the increase in autophagy under siSORBS3.**

- a. HeLa cells were transfected with pcDNA-HA-AMOT(p130) or empty vector control (pcDNA-empty) for 24 hours. Cells were treated with BAF (400 nM) or DMSO vehicle control for 4 hours. Haemagglutinin (HA), GAPDH and LC3 protein levels were examined by western blotting. Representative blot from 4 independent experiments is shown. LE = lighter exposure; DE = darker exposure; molecular weights shown in kDa.
- b. Quantification of 4 independent experiments described in a. LC3-II (lower band of LC3 doublet) levels are expressed relative to GAPDH loading control and normalised to LC3-II/GAPDH in control siRNA (siCntrl) treated cells. \* =  $p < 0.05$  by 2-tailed one-sample t-test. Error bars indicate SEM.
- c. HeLa cells stably expressing GFP-LC3 were depleted of vinexin beta using an individual siRNA oligonucleotide against *SORBS3* (siSORBS3; oligo 7). siCntrl and siSORBS3 treated cells were transfected with pcDNA-HA-AMOT(p130) or empty vector control (pcDNA-empty) for 24 hours. HA was labelled by immunofluorescence and imaged, together with GFP-LC3, by confocal microscopy. Representative images from 3 independent experiments are shown. Red = HA (Alexa Fluor 568); green = GFP-LC3; blue = DAPI. Scale bars indicate 20  $\mu\text{m}$ .
- d. GFP-LC3 puncta from the experiments described in a. were counted manually. Quantification of 3 independent experiments is shown. ns =  $p > 0.05$ ; \* =  $p < 0.05$  by one-way ANOVA followed by Tukey's multiple comparison test. Error bars indicate SEM.

To examine whether decreased autophagy due to AMOT overexpression was sufficient to counter autophagy upregulation in vinexin beta depleted cells, I conducted experiments in which HeLa cells stably expressing GFP-LC3 were treated with si*SORBS3* in the presence and absence of HA-AMOT(p130) overexpression. Treating GFP-LC3 HeLa with si*SORBS3* caused a statistically significant increase in GFP-LC3 puncta per cell under basal conditions (pcDNA-empty; siCntrl compared with pcDNA-empty; si*SORBS3* in Figure 4.11c and d), which was not seen in cells overexpressing HA-AMOT(p130) (outlined in white in Figure 4.11c; quantified in Figure 4.11d). These data indicate AMOT overexpression is sufficient to ameliorate increased autophagosome numbers upon vinexin beta depletion. This supports the hypothesis that autophagy upregulation under si*SORBS3* treatment is due to sequestration of the AMOT family of YAP/TAZ inhibitors by F-actin.

#### **4.12 Concluding remarks**

In this chapter I demonstrate vinexin beta depletion increases endogenous YAP/TAZ nuclear localisation by immunofluorescence microscopy and nuclear/cytosolic fractionation. Consequently, vinexin beta negatively regulates YAP/TAZ transcriptional activity *via* TEAD transcription factors. This is shown by luciferase reporter assay using a synthetic TEAD promoter and by examining expression of the YAP/TAZ/TEAD target gene *CTGF*. By obtaining similar results in autophagy-deficient (*ATG16L1* CRISPR) cells, I demonstrate increased YAP/TAZ nuclear localisation and activity under si*SORBS3* treatment is upstream of, and not consequent to, autophagy upregulation following vinexin beta depletion. As LATS1/2-mediated YAP/TAZ phosphorylation was unchanged under si*SORBS3* treatment, vinexin beta depletion is proposed to increase YAP/TAZ activity independent of Hippo signalling.

Linking back to findings described in chapter 3, experiments presented in this chapter in which LC3-II levels under si*SORBS3* treatment were examined by western blotting in the presence and absence of si*YAP/TAZ* indicate autophagy upregulation following vinexin beta depletion requires YAP and TAZ. Given vinexin beta depletion upregulates YAP/TAZ activity, it seems reasonable to suggest the mechanism involves YAP and TAZ functioning as transcriptional coactivators. However, these data do not exclude a non-transcriptional mechanism.

This chapter includes the observation that si*SORBS3* treatment increases the number of fluorescent phalloidin-labelled F-actin structures per cell, but that the average size of these

structures is smaller. Taken together with complementary data obtained by Dr Bento using an F-: G-actin *in vivo* assay kit, this observation requires complex interpretation. The explanation outlined above is that vinexin beta depletion shifts the tripartite equilibrium between labile (triton soluble) F-actin, stable (triton insoluble) F-actin and G-actin in favour of the labile F-actin pool.

In agreement with published literature describing Hippo signalling-independent YAP/TAZ regulation by actin cytoskeleton dynamics (Aragona et al., 2013; Das et al., 2016; Dupont et al., 2011), F-actin depolymerisation with latrunculin A is reported to ameliorate the increase in YAP/TAZ nuclear staining upon vinexin beta depletion. Loss of actomyosin tension following myosin II inhibition with blebbistatin is also shown to counter YAP/TAZ nuclear translocation under si*SORBS3* treatment, though to a lesser extent than latrunculin A. However, only latrunculin A treatment ameliorates increased LC3-II levels upon vinexin beta depletion. These data are taken to indicate vinexin beta depletion promotes autophagy by increasing F-actin structures and upregulating YAP/TAZ activity, with lesser changes in YAP/TAZ distribution following blebbistatin treatment being insufficient to ameliorate the increase in autophagy caused by si*SORBS3* treatment.

At this point several alternative chronologies linking autophagy upregulation under si*SORBS3* treatment to increased F-actin structures and YAP/TAZ activity remained formally possible. However, *SORBS3/YAP/TAZ* triple knockdown experiments presented above reveal the same alterations in actin cytoskeleton dynamics upon vinexin beta depletion in both the presence and absence of si*YAP/TAZ*. This favours the hypothesis that increased F-actin structures under si*SORBS3* treatment promote autophagy *via* a downstream, YAP/TAZ-dependent mechanism.

In the last sections of this chapter I describe how overexpression of the F-actin and YAP/TAZ binding protein AMOT p130 counters both increased YAP/TAZ nuclear localisation and autophagy upregulation upon vinexin beta depletion. This is shown using immunofluorescence microscopy and cells stably expressing GFP-LC3, respectively. The explanation suggested above is that AMOT overexpression saturates AMOT binding sites on F-actin, thereby freeing excess AMOT to sequester YAP/TAZ in the cytosol and downregulate autophagy, even when F-actin structures are increased by si*SORBS3* treatment. Moreover, less endogenous AMOTL1 is pulled down by YAP/TAZ immunoprecipitation from cells depleted of vinexin beta. Given F-actin depolymerisation with latrunculin A is

found to increase interaction between exogenously expressed Flag-YA and HA-AMOT(p130) by immunoprecipitation, this finding concurs with F-actin competing with YAP/TAZ for binding to AMOTs.

As summarised in Figure 4.12, the conclusions I draw from data presented in this chapter are that increased F-actin structures following vinexin beta depletion compete with YAP/TAZ for AMOT binding. In this way, YAP/TAZ is released from sequestration in the cytosol by AMOTs to enter the nucleus and increase YAP/TAZ transcriptional activity through TEAD transcription factors, thereby upregulating autophagy.

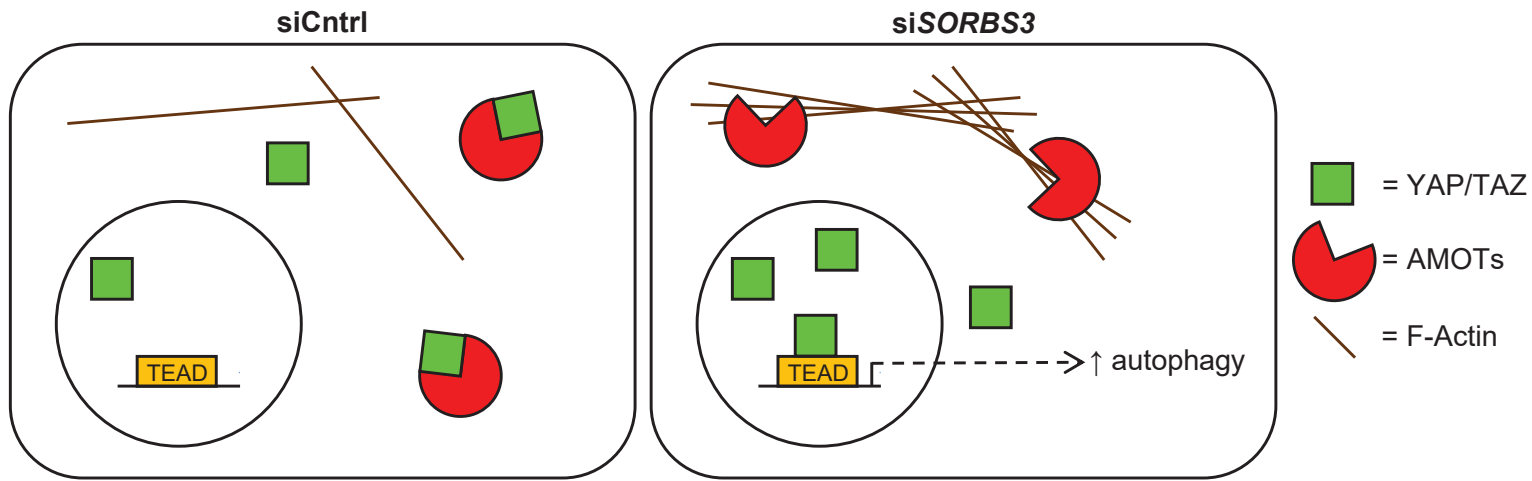


**Figure 4.12: increased F-actin structures in vinexin beta depleted cells sequester angiomotins, thereby releasing YAP/TAZ to enter the nucleus.**

Schematic diagram of the hypothesised situation in siCntrl and siSORBS3 treated cells. siCntrl: angiomotins (AMOTs) bind and retain YAP/TAZ in the cytosol, thereby preventing YAP/TAZ activity from upregulating autophagy. siSORBS3: increased F-actin structures compete with YAP/TAZ for AMOT binding. YAP/TAZ is released to enter the nucleus and upregulate YAP/TAZ transcriptional activity through TEAD transcription factors to upregulate autophagy.

## **5 Vinexin decreases hepatocellular carcinoma cell line tumourigenicity by negatively regulating YAP/TAZ activity and autophagy**

### ***5.1 Introduction***

Roessler and colleagues' reported that deletion of a six gene cluster on chromosome 8p, which includes *SORBS3* predicts poor outcomes in hepatocellular carcinoma (HCC) patients (Roessler et al., 2012). In this publication, the tumour suppressive properties of the *SORBS3* gene product vinexin are validated in both cell culture and mouse xenograft experiments; re-expression of vinexin alpha in HCC cell lines reduced migration and colony formation, with vinexin-transfected Hep3B cells giving fewer and smaller tumours upon subcutaneous injection into immunocompromised mice than cells transfected with empty vector (Roessler et al., 2012). It has subsequently been suggested that vinexin functions as a tumour suppressor by indirectly inhibiting the proliferative and anti-apoptotic IL-6/STAT3 pathway *via* altered oestrogen receptor signalling (Ploeger et al., 2016). However, this does not preclude the existence of other mechanisms by which *SORBS3* deletion could drive cancer progression, as in YAP/TAZ disinhibition and/or increased autophagy.

Using published mRNA microarray data (Thurnherr et al., 2016), again in collaboration with bioinformatician Dr Peter Sterk, I sought to replicate Roessler and colleagues' finding that *SORBS3* is commonly underexpressed in HCC (Roessler et al., 2012). By comparison with vinexin-replete HuH7 HCC cells, I aimed to characterise HepG2 HCC cells as vinexin-deficient and therefore unable to upregulate YAP/TAZ activity or downstream clonogenicity following si*SORBS3* treatment. This characterisation provided a context for the key experiments in this chapter, in which vinexin alpha was stably re-expressed in HepG2 cells with consequences for YAP/TAZ localisation, autophagy and clonogenicity that are relevant to *SORBS3* being a candidate tumour suppressor gene.

### ***5.2 SORBS3 mRNA expression is commonly downregulated in hepatocellular carcinoma***

Dr Sterk analysed published two-colour microarray data from 100 primary human HCC samples and adjacent non-malignant tissue (Thurnherr et al., 2016). This revealed significant lower *SORBS3* mRNA expression in HCC samples, compared with adjacent non-malignant tissue (Figure 5.1). 76 out of the 100 HCC samples analysed show lower *SORBS3* mRNA expression than adjacent non-malignant tissue and the median fold change in *SORBS3* mRNA expression between tumour and non-tumour samples was around 0.7. This replicates Roessler

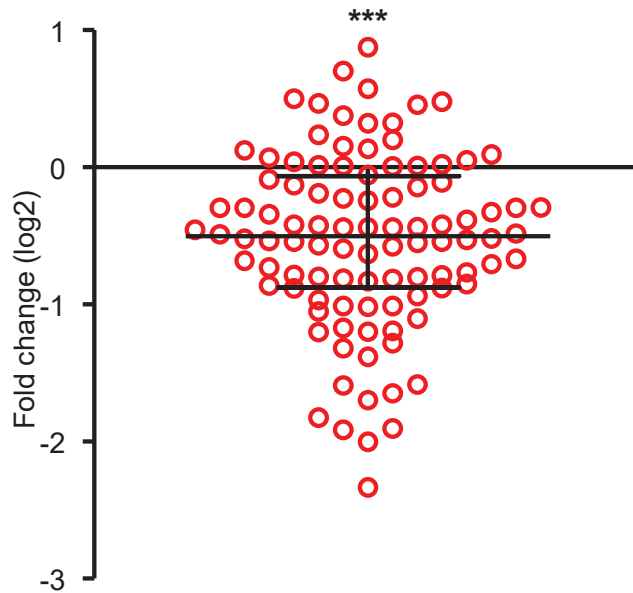


**Figure 5.1: primary hepatocellular carcinoma tissue commonly features decreased *SORBS3* mRNA expression.**

Analysis of published two-colour microarray data. Fold change ( $\log_2$ ) in *SORBS3* mRNA expression in 100 primary human hepatocellular carcinoma (HCC) tissue samples (Cyanine5) compared with adjacent non-malignant tissue samples (Cyanine3). Tumours from 76 of the 100 HCC patient samples exhibit decreased *SORBS3* mRNA expression compared with adjacent non-malignant tissue. Median fold change ( $\log_2$ ) and interquartile range are shown. \*\*\* = adjusted  $p < 0.001$  by one sample t-test with false discovery rate controlled by Benjamini–Hochberg procedure.

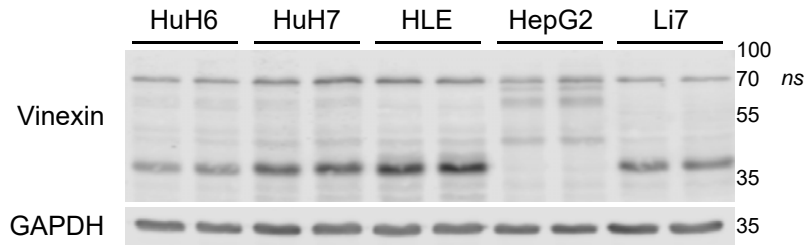
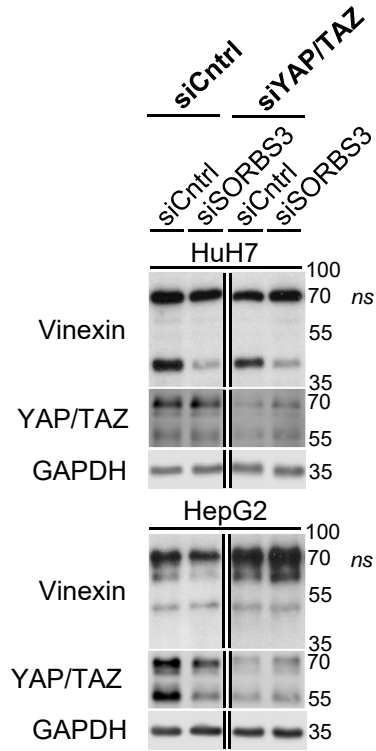
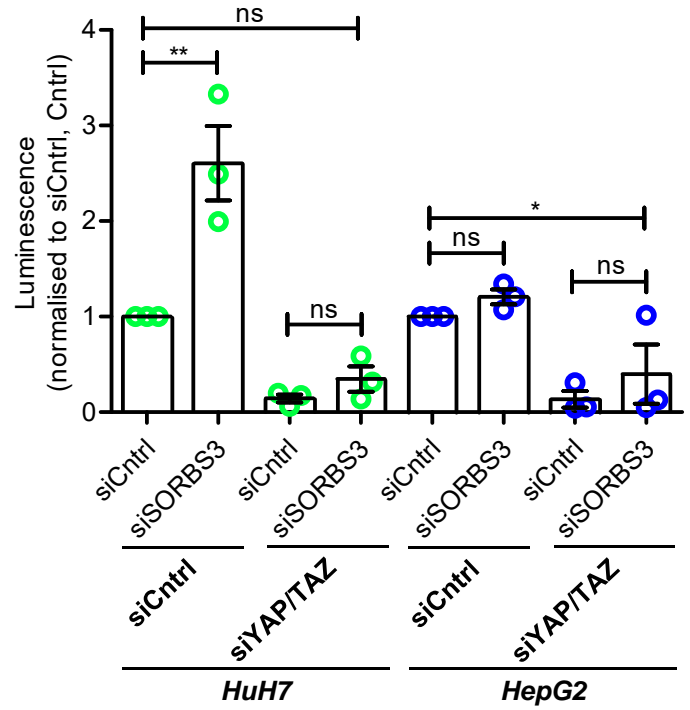
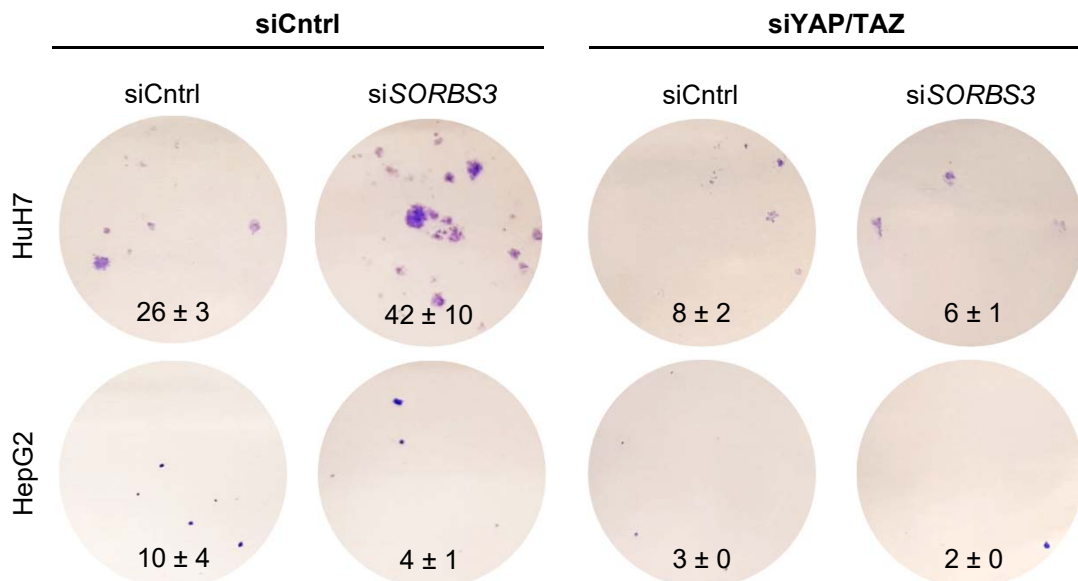
and colleagues' findings using three HCC cohorts and three breast cancer cohorts (Roessler et al., 2012), thereby supporting the notion vinexin has tumour suppressive functions.

### ***5.3 Vinexin-deficient HepG2 cells are unable to upregulate YAP/TAZ activity or downstream clonogenicity under siSORBS3 treatment***

Vinexin expression was examined in five hepatitis B virus-negative human HCC cell lines by western blotting, together with GAPDH loading control (Figure 5.2a). HuH6, HuH7, HLE and Li7 cells gave a band around 37 kDa, which corresponds to vinexin beta, together with a non-specific band around 70 kDa that is present in all cell lines tested (*ns*; including HeLa, RPE and HEK293). In contrast, HepG2 cells did not appear to express vinexin beta. These findings are in agreement with Ploeger et al., who report HepG2 cells show reduced *SORBS3* expression compared with HuH7 and HLE cells on both the mRNA and protein level (Ploeger et al., 2016). HepG2 cells did give faint bands around 60 and 45 kDa, which Ploeger et al. speculate correspond to longer vinexin isoforms such as vinexin alpha (predicted molecular weight 82 kDa).

Given these are immortalised cell lines generated from single clones, meaningful data cannot be obtained by comparing the lines directly. However, it is possible to compare the impact of interventions on vinexin-deficient and vinexin-replete cell lines. With this in mind, HepG2 (vinexin-deficient) and HuH7 (vinexin-replete) cells were treated with si*SORBS3* in the presence and absence of siRNA against *YAP* and *TAZ*. HepG2 and HuH7 cells were found to express comparable levels of *YAP* and *TAZ* by western blotting, with substantial reductions in *YAP* and *TAZ* levels under si*YAP/TAZ* treatment in both cell lines (Figure 5.2b). While treating HuH7 cells with siRNA against *SORBS3* brought about robust reductions in vinexin beta levels, there was no change in bands seen using the same antibody with HepG2 cell lysate (Figure 5.2b). This finding opposes Ploeger and colleagues' view that bands around 60 and 45 kDa correspond to longer vinexin isoforms (Ploeger et al., 2016) and implies HepG2 cells do not express any vinexin protein, which is to be expected if these cells feature the chromosome 8p deletion common in human HCC lines (Zimonjic et al., 1999).

As observed in HeLa cells (Figure 4.2a), when HuH7 cells were transfected with a *YAP/TAZ*-responsive synthetic TEAD promoter driving luciferase expression, luminescence measured by dual-luciferase reporter assay was significantly higher in si*SORBS3* treated cells compared with siCntrl treated cells (HuH7 siCntrl; siCntrl compared with siCntrl; si*SORBS3* in Figure 5.2c). Unsurprisingly given the apparent lack of vinexin expression, si*SORBS3*

**a****b****c****d**

**Figure 5.2: owing to reduced vinexin expression, unlike HuH7 hepatocellular carcinoma cells, HepG2 hepatocellular carcinoma cells cannot upregulate YAP/TAZ activity under siSORBS3 treatment.**

- a. Endogenous vinexin and GAPDH levels were examined by western blotting (images acquired using an Odyssey Imager) in HuH6, HuH7, HLE, HepG2 and Li7 hepatocellular carcinoma cells. Vinexin beta is seen around 37 kDa. *ns* = non-specific band; molecular weights shown in kDa.
- b. HuH7 and HepG2 cells were depleted of vinexin using an individual siRNA oligonucleotide against *SORBS3* (si*SORBS3*; oligo 7) in the presence or absence of pools of 4 siRNA oligonucleotides against *YAP* and *TAZ* (si*YAP/TAZ*). Endogenous vinexin, YAP/TAZ and GAPDH levels were examined by western blotting (images acquired using ECL detection reagents). Vinexin beta is seen around 37 kDa. Representative blots from 3 independent experiments are shown. *ns* = non-specific band; molecular weights shown in kDa.
- c. As part of the experiments described in b., HuH7 and HepG2 cells were transfected with synthetic TEAD promoter driving luciferase expression (pGL3b-8xGT1IC-luciferase) for 24 hours. Luminescence (firefly luciferase activity relative to Renilla luciferase activity) was measured by dual-luciferase reporter assay and normalised to control siRNA treated cells (siCntrl; Cntrl). Quantification of 3 independent experiments is shown. *ns* =  $p > 0.05$ , \* =  $p < 0.05$ , \*\* =  $p < 0.01$  by one-way ANOVA followed by Tukey's multiple comparison test. Error bars indicate SEM.
- d. HuH7 and HepG2 cells were depleted of vinexin, YAP and TAZ as in b. Cell survival and proliferation was assayed by clonogenic assay. 1,000 cells were seeded per well in 6-well plates and grown for 10 days before staining with crystal violet solution. Representative images from an experiment performed in technical triplicate are shown. Mean colonies per well  $\pm$  SD (rounded to the nearest whole number) are superimposed on images.

treatment had no effect on luminescence measured in HepG2 cells (HepG2 siCntrl; siCntrl compared with siCntrl; siSORBS3 in Figure 5.2c). Reassuringly, synthetic TEAD promoter-driven luciferase expression was substantially reduced in both HuH7 and HepG2 cells depleted of YAP and TAZ (siYAP/TAZ; Figure 5.2c).

The lack of YAP/TAZ activity upregulation in HepG2 cells following siSORBS3 treatment was observed to impact clonogenicity (Figure 5.2d). Number of colonies per well represents the number of cells from a fixed-size starting sample (1,000) that retain the ability to proliferate into colonies (Franken et al., 2006). Hence, although clonogenic assays predominantly measure cell survival, proliferative speed also comes into play; slowly proliferating cells are unable to produce colonies large enough to visualise after the 10 days allowed here.

In agreement with YAP/TAZ transcriptional activity promoting cell survival and proliferation (Zhao et al., 2008), siYAP/TAZ treatment substantially reduced both HuH7 and HepG2 colonies per well after 10 days growth (siYAP/TAZ; Figure 5.2d). Indeed siYAP/TAZ treatment was sufficient to abolish the increase in HuH7 colonies per well caused by siSORBS3 treatment (HuH7 siCntrl compared with siYAP/TAZ in Figure 5.2d), which suggests the increased clonogenicity under siSORBS3 treatment is YAP/TAZ-dependent. siSORBS3 treatment accordingly failed to increase HepG2 clonogenicity (HepG2 siCntrl; siCntrl compared with siCntrl; siSORBS3 in Figure 5.2d).

Results presented in Figure 5.2 indicate HepG2 (vinexin-deficient) cells respond to YAP/TAZ depletion as predicted by the literature, in much the same way as HuH7 (vinexin-replete) HCC cells. However, neither YAP/TAZ activity nor downstream clonogenicity is altered in HepG2 cells under siSORBS3 treatment. Taken together, these findings suggest HepG2 cells provide a useful model for exploring mechanisms by which vinexin could function as a tumour suppressor in HCC.

#### ***5.4 Vinexin alpha re-expression counters nuclear YAP/TAZ localisation in HepG2 cells***

YAP and TAZ function oncogenically in multiple human cancers, with increased YAP/TAZ transcription activity promoting tumour cell proliferation, metastatic potential and resistance to apoptosis in a multiple cancer models (see section 1.3.5.3) (Moroishi et al., 2015). Notably, YAP activation de-differentiates adult murine hepatocytes into progenitor cells that exhibit cancer stem cell-like properties, such as clonogenicity (Yimlamai et al., 2014).

In order to investigate possible functional consequences of *SORBS3* underexpression in HCC, in collaboration with PhD student Anne Jackson, I prepared polyclonal HepG2 cell lines stably expressing mEmerald-tagged vinexin alpha (mEmerald-vinexin alpha) or empty vector control (mEmerald-empty) at physiologically relevant levels. Since HepG2 cells do not appear to express any vinexin protein (Figure 5.2), we considered HepG2 cell lines stably expressing mEmerald-vinexin alpha as genetically reconstituted.

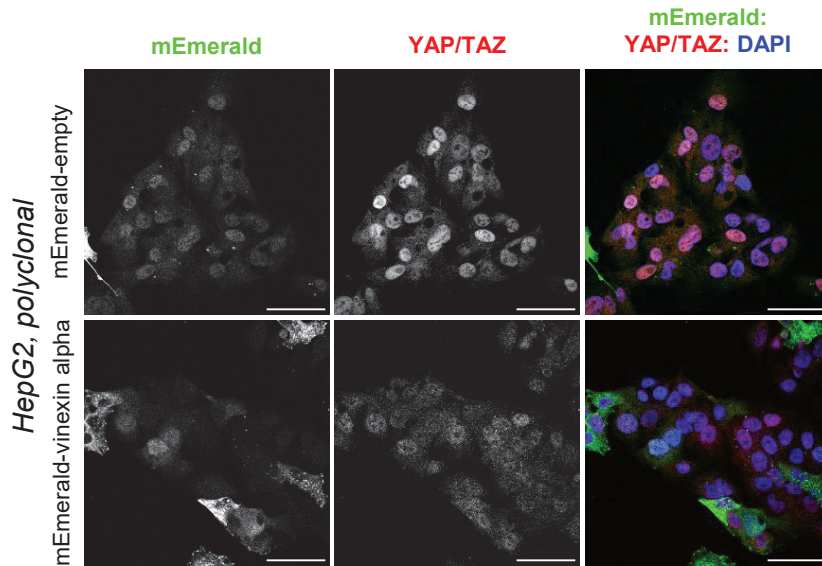
Concurrent with vinexin depletion increasing YAP/TAZ nuclear localisation in HeLa cells (Figures 4.1), around 80% of HepG2 cells stably expressing mEmerald-empty showed predominantly nuclear YAP/TAZ staining by immunofluorescence (N > C; Figure 5.3a-b). This phenotype was ameliorated by vinexin re-expression, with significantly fewer (around 65%) HepG2 cells stably expressing mEmerald-vinexin alpha showing N > C staining and significantly more (30%, compared with 17%) showing equal nuclear and cytosolic YAP/TAZ staining (N = C; Figure 5.3b). These data support the hypothesis that increased YAP/TAZ nuclear localisation and consequent hyperactivation contribute to the mechanism by which vinexin underexpression drives HCC progression.

### ***5.5 Vinexin deficiency drives autophagy in HepG2 cells***

One popular interpretation of the complicated literature linking autophagy to cancer is that, while maintenance of cellular homeostasis by autophagy can protect against malignant transformation, autophagy also drives resistance to conditions that cause cell death (as in nutrient starvation) and thereby promotes metastatic tumour progression (Galluzzi et al., 2015). For example, immunocompromised mice orthotopically implanted with autophagy-deficient HCC cells (*BECN1* or *ATG5* stable knockdown) exhibit significantly fewer pulmonary metastases than those implanted with autophagy-competent control lines (Peng et al., 2013). Follow-up experiments in this publication suggest autophagy does not impact invasion, migration or epithelial–mesenchymal transition by these cells, but that autophagy-deficient lines are more susceptible to anoikis and therefore less able to survive in the metastatic niche (Peng et al., 2013).

Autophagy was assessed in HepG2 cells stably expressing mEmerald-empty or mEmerald-vinexin alpha by measuring LC3-II (lower band of LC3 doublet) by western blotting. For these experiments, several biological replicates were performed by Anne Jackson. Concurrent with the YAP/TAZ-dependent increase in autophagy caused by vinexin depletion in HeLa cells (Figure 4.3), vinexin re-expression in HepG2 cells decreased LC3-II levels under basal

a



b

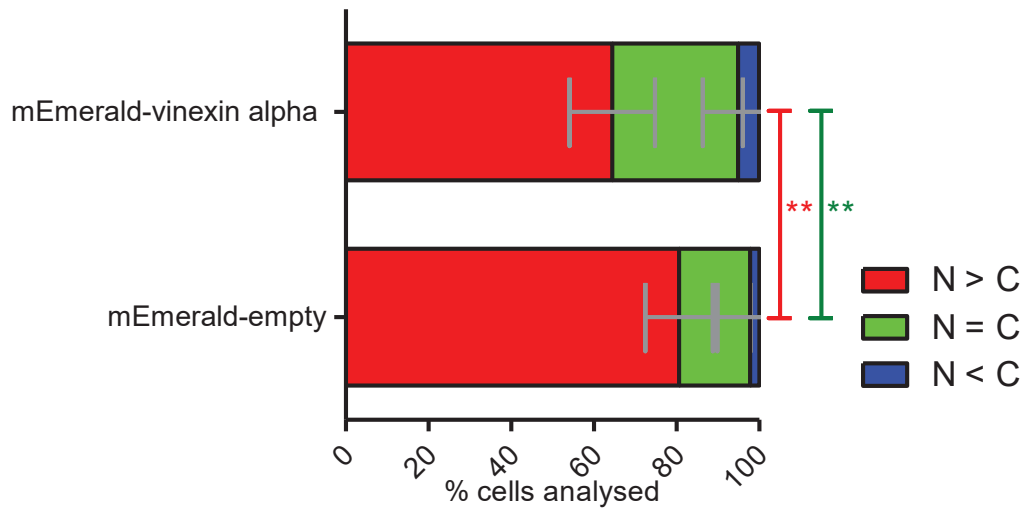


**Figure 5.3: vinexin alpha re-expression ameliorates YAP/TAZ nuclear localisation in HepG2 hepatocellular carcinoma cells.**

- a. mEmerald-vinexin alpha or empty vector control (mEmerald-empty) were stably expressed in HepG2 cells. Endogenous YAP/TAZ were examined by immunofluorescence and confocal microscopy, together with mEmerald. Representative images from 3 independent experiments are shown. Green = mEmerald; YAP/TAZ (Alexa Fluor 568); blue = DAPI. Scale bars indicate 50  $\mu$ m.
- b. Cells showing predominantly nuclear YAP/TAZ staining (N > C), equal nuclear and cytosolic YAP/TAZ staining (N = C) and predominantly cytosolic YAP/TAZ staining (N < C) were manually counted from confocal images acquired as described in a. Quantification of the representative experiment shown in a. \*\* =  $p < 0.01$  by 2-tailed Student's t-test. Red asterisks represent p value for N > C; green asterisks represent p value for N = C.  $n = 335$  (mEmerald-empty), 473 (mEmerald-vinexin alpha, siSORBS3). Error bars indicate SD.

conditions (Figure 5.4a-b). This indicates vinexin underexpression could enable HCC cells to resist tumour microenvironment stressors by upregulating autophagy. To further test this hypothesis, endogenous LC3 puncta were visualised by immunofluorescence in HepG2 cells stably expressing mEmerald-empty or mEmerald-vinexin alpha. For these experiments, coverslips were prepared for imaging by Anne Jackson before I performed the confocal microscopy. Fewer LC3 puncta were observed upon vinexin re-expression in HepG2 cells under EBSS starvation (Figure 5.4c), which was confirmed by quantification (EBSS; Figure 5.4d).

I noted an apparent discrepancy between data collected under basal conditions; vinexin re-expression decreased LC3-II levels (Figure 5.4a-b), while LC3 puncta numbers were unaltered (Basal; Figure 5.4d). However, our group has previously demonstrated these assays differentially interrogate the autophagy pathway (Korolchuk et al., 2011). Korolchuk and colleagues describe that LC3 puncta correspond to multiple autophagy structures (unclosed phagophores, autophagosomes and autolysosomes), while LC3-II protein levels represent steady-state autophagosomes only.

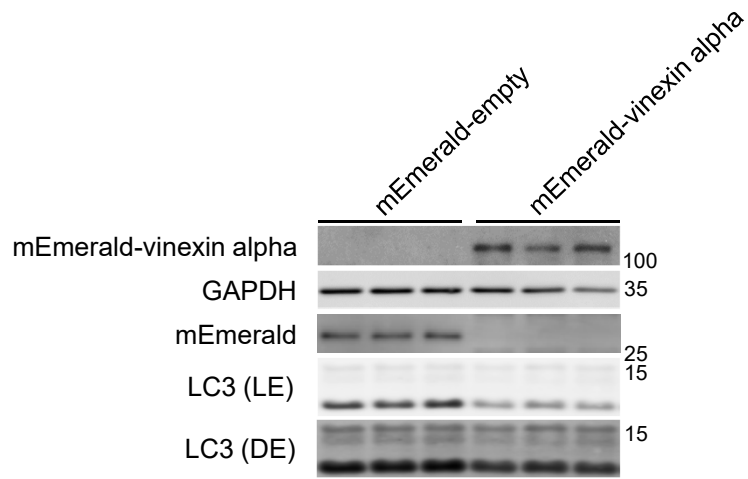
Overall, data presented in Figures 5.3 and 5.4 suggest vinexin underexpression could drive HCC progression through YAP/TAZ hyperactivation, in part because (as outlined in chapter 4) YAP/TAZ upregulation promotes autophagy.

### ***5.6 Vinexin negatively regulates clonogenicity in HepG2 cells***

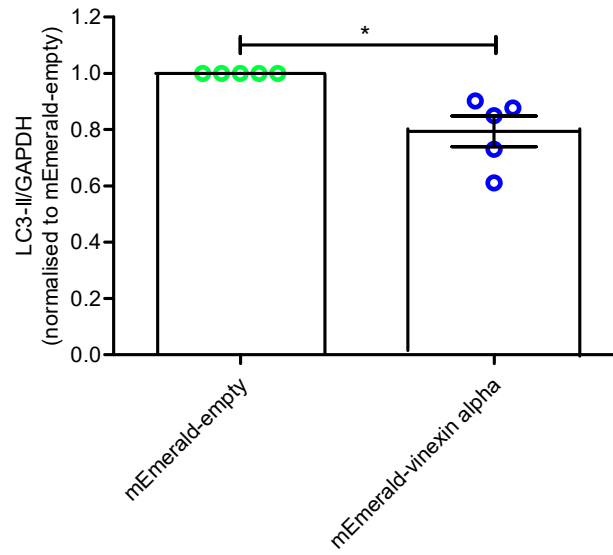
I next examined HepG2 cells stably expressing mEmerald-empty or mEmerald-vinexin alpha by clonogenic assay (introduced in section 5.3). Vinexin re-expression significantly reduced HepG2 cell clonogenic capacity. Upon quantification, HepG2 cells stably expressing mEmerald-vinexin empty formed nearly twice as many colonies per well as those stably expressing mEmerald-vinexin alpha (Figure 5.5a-b). These data indicate vinexin deficiency promotes clonogenicity, suggesting increased cell survival and proliferation contribute to the mechanism by which vinexin underexpression drives HCC progression.

As highlighted above, cancer stem cell-like progenitors derived from adult murine hepatocytes following YAP activation show enhanced clonogenic capacity (Yimlamai et al., 2014). This makes sense given YAP/TAZ/TEAD transcriptional activity promotes cell proliferation and survival (Zhao et al., 2008). With regards to the role of autophagy in clonogenicity, as with the wider role of autophagy in cancer, the published literature is complicated and context-dependent. In the seminal publication linking autophagy to cancer,

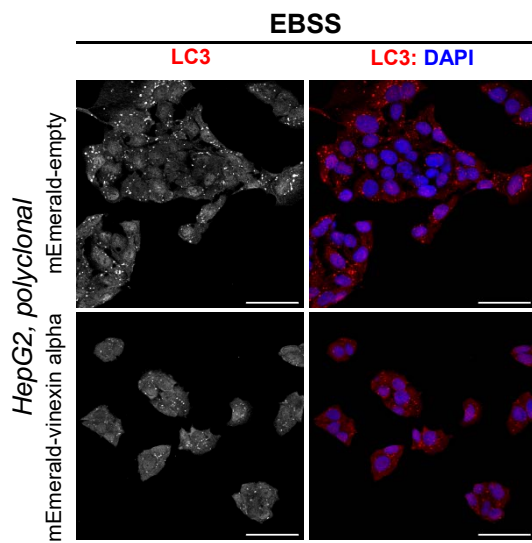
**a**



**b**



**c**



**d**

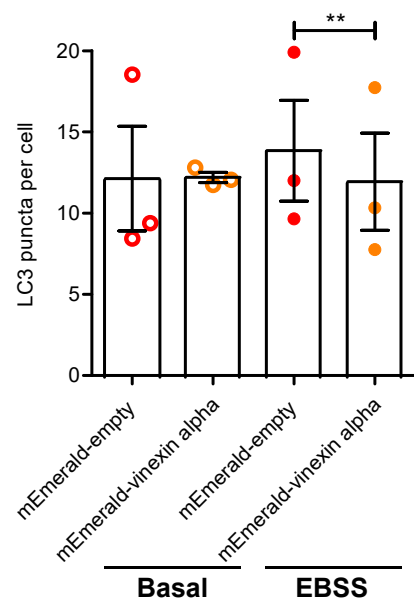


**Figure 5.4: vinexin alpha re-expression downregulates autophagy in HepG2 hepatocellular carcinoma cells.**

- a. mEmerald-vinexin alpha and mEmerald protein levels, together with endogenous GAPDH and LC3 protein levels in HepG2 cells stably expressing mEmerald-vinexin alpha or empty vector control (mEmerald-empty) were examined by western blotting. Representative blots from 5 independent experiments are shown. LE = lighter exposure; DE = darker exposure; molecular weights shown in kDa.
- b. Quantification of 5 independent experiments. LC3-II (lower band of LC3 doublet) levels are expressed relative to GAPDH loading control and normalised to LC3-II/GAPDH in cells stably expressing mEmerald-empty. \* =  $p < 0.05$  by 2-tailed one-sample t-test. Error bars indicate SEM.
- c. HepG2 cells stably expressing mEmerald-empty or mEmerald-vinexin alpha were starved in EBSS or left in complete media (basal) for 4 hours. Endogenous LC3 was examined by immunofluorescence and confocal microscopy. Representative images from the starved condition in 3 independent experiments are shown. Red = LC3 (Alexa Fluor 568); blue = DAPI. Scale bars indicate 50  $\mu\text{m}$ .
- d. LC3 puncta were counted from confocal images acquired as described in c. using ImageJ software. Quantification of 3 independent experiments is shown. \*\* =  $p < 0.01$  by 2-tailed paired t-test. Error bars indicate SEM.

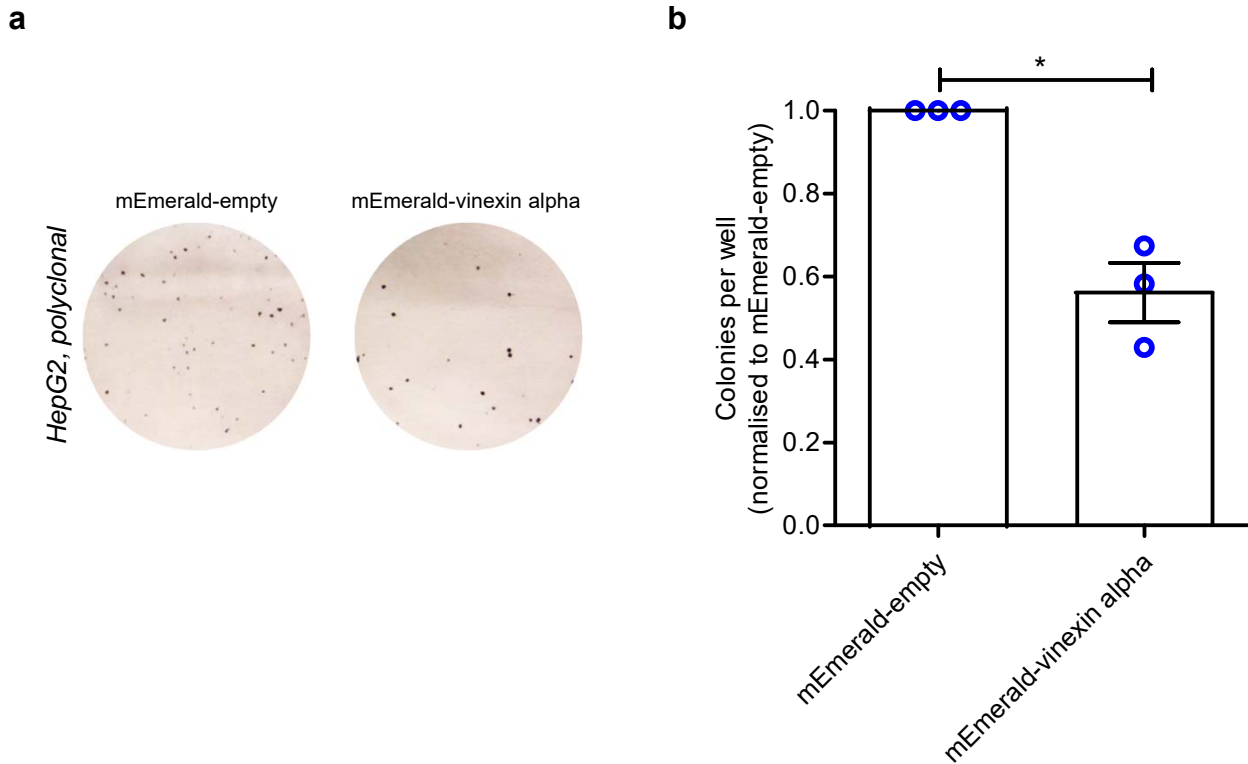


**Figure 5.5: vinexin alpha re-expression downregulates HepG2 hepatocellular carcinoma cell survival and proliferation.**

- a. Clonogenic assays were performed with HepG2 cells stably expressing mEmerald-vinexin alpha or empty vector control (mEmerald-empty). 1,000 cells were seeded per well in 6-well plates and grown for 10 days before staining with crystal violet solution. Representative images from 3 independent experiments performed in technical triplicate are shown.
- b. Cell colonies described in a. were counted manually. Quantification of 3 independent experiments. Colonies per well for mEmerald-vinexin alpha HepG2 cells are expressed relative to mEmerald-empty HepG2 cells. \* =  $p < 0.05$  by 2-tailed one-sample t-test. Error bars indicate SEM.

re-expression of the core autophagy protein Beclin-1 in MCF7 breast adenocarcinoma cells is shown to reduce proliferation by clonogenic assay (Liang et al., 1999). On the other hand, expression of the canonical autophagy adaptor p62 is required for effective colony formation following Ras-mediated oncogenic transformation (Duran et al., 2008). Accordingly, while the published literature clearly supports the notion vinexin negatively regulates clonogenicity by decreasing YAP/TAZ transcriptional activity, the likely relative contribution of decreased autophagy is unclear.

### ***5.7 Concluding remarks***

In this chapter I present findings from Dr Sterk's analysis using published microarray data from HCC samples and adjacent non-malignant tissue, which replicate Roessler and colleagues' finding that *SORBS3* is commonly underexpressed in HCC (Roessler et al., 2012). This supports the notion *SORBS3* functions as a tumour suppressor gene.

Having characterised HepG2 HCC cells as vinexin-deficient, with neither YAP/TAZ activity nor downstream clonogenicity altered under *siSORBS3* treatment, I went on to use HepG2 cells stably re-expressing vinexin to explore mechanisms by which vinexin could function as a tumour suppressor in HCC. In this way, I show that vinexin re-expression ameliorates nuclear YAP/TAZ localisation and decreases autophagy, demonstrated in chapter 4 to be downstream to YAP/TAZ activity. This reduction in autophagy is most apparent under nutrient starvation, which is relevant to the role of autophagy supporting cancer cell survival in the tumour microenvironment. I also report that vinexin re-expression decreases the clonogenic capacity of HepG2 cells. However, the relative contributions made by decreased cell proliferation and reduced apoptosis due to downregulated YAP/TAZ transcriptional activity, as opposed to decreased survival consequent to autophagy downregulation remain unclear.

Data presented in this chapter therefore support the hypothesis that vinexin functions as a tumour suppressor; opposing cancer cell proliferation and resistance to apoptosis by negatively regulating YAP/TAZ/TEAD transcriptional activity, as well as impairing cancer cell survival by decreasing autophagy. This is in addition to the mechanism recently published by Ploeger and colleagues, whereby vinexin functions cooperatively with SH2D4A to decrease tumourgenesis by inhibiting the proliferative and anti-apoptotic IL-6/STAT3 pathway (Ploeger et al., 2016).

## 6 Discussion

In this chapter I summarise the main findings presented above (see Figure 6.1), before highlighting several outstanding questions arising from the data. Finally, the intriguing possibility vinexin functions at the intersection between several cancer biology pathways is discussed (see Figure 6.2).

### 6.1 Results summary

Although Lipinski and colleagues have previously reported si*SORBS3* treatment promotes autophagy (Lipinski et al., 2010a), results presented above constitute the first in-depth characterisation of vinexin (encoded by *SORBS3*) as an autophagy regulator.

Mechanistically, I demonstrate vinexin regulates autophagy through the transcriptional coactivators YAP and TAZ. si*SORBS3* treatment alters actin cytoskeleton dynamics, increasing F-actin bundles. These structures compete with YAP/TAZ for binding to angiomotins (AMOT p130, AMOTL1 and AMOTL2) in the cytoplasm. This promotes YAP/TAZ nuclear translocation and transcriptional activity *via* TEAD transcription factors, which our lab and others have shown upregulates autophagy (Pavel et al., manuscript in preparation) (Song et al., 2015).

These findings are potentially relevant to normal brain ageing; *SORBS3* mRNA expression is increased in frontal cortex and hippocampal tissue from older human donors, while core autophagy genes (*BECN1*, *ATG5*, *ATG7* and *PIK3C3*) are concurrently transcriptionally downregulated. In addition, *SORBS3* deletion predicts worse outcomes in HCC (hepatocellular carcinoma) (Roessler et al., 2012). Data presented above confirm *SORBS3* is commonly underexpressed in HCC. Moreover, reconstituting vinexin-deficient HCC cells reduces tumourigenicity through: 1. decreasing YAP/TAZ nuclear localisation, 2. downregulating autophagy and 3. reducing clonogenicity.

Taken together, results presented in this thesis indicate vinexin is a pathophysiologically important autophagy regulator, especially with regards to HCC.

### 6.2 Outstanding questions

The findings summarised above suggest numerous follow-up experiments. These centre on two main topics: 1. Molecular mechanism linking si*SORBS3* treatment to increased autophagy, 2. *SORBS3* as a candidate tumour suppressor in HCC.

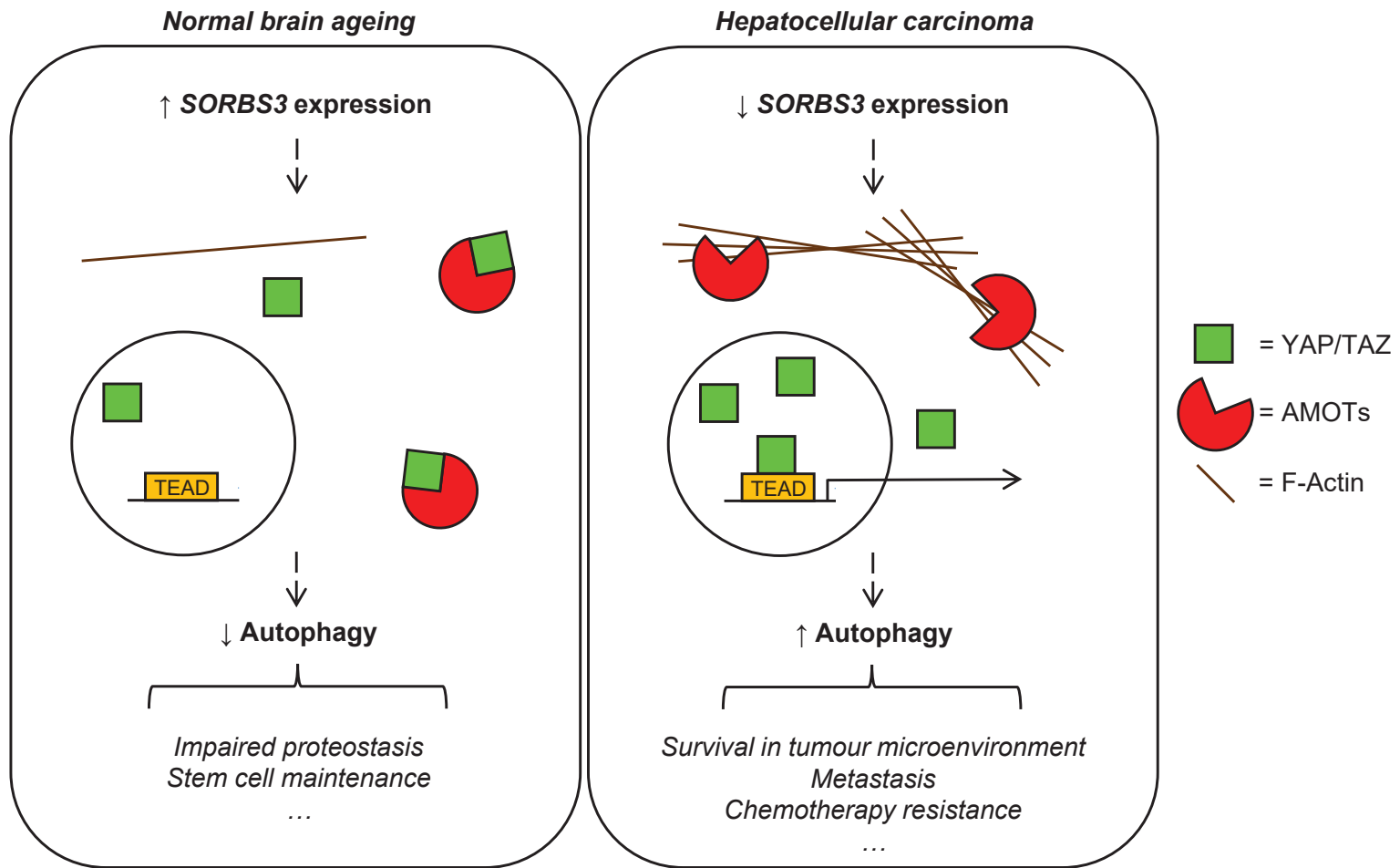


**Figure 6.1: vinexin negatively regulates autophagy through YAP/TAZ, with implications for normal brain ageing and hepatocellular carcinoma.**

Schematic diagram summarising the main findings presented in this thesis. Increased *SORBS3* expression, as observed in normal brain ageing (left panel), decreases F-actin bundles. This enables angiomotins (AMOTs) to retain YAP/TAZ in the cytosol, which downregulates autophagy. Possible deleterious functional consequences (discussed in section 1.1.7.2iii) include impaired proteostasis and stem cell maintenance in older brains. *SORBS3* underexpression, as common in hepatocellular carcinoma (right panel), decreases F-actin bundles. These structures compete with YAP/TAZ for AMOT binding, meaning YAP/TAZ is released to enter the nucleus. This upregulates YAP/TAZ transcriptional activity, which upregulates autophagy. Possible functional consequences for tumour progression (discussed in section 1.1.8.1ii) include increase cancer cell survival in the tumour microenvironment, metastasis and chemotherapy resistance.

**i. Does vinexin regulate autophagy through YAP/TAZ/TEAD transcriptional activity?**

si*SORBS3* treatment upregulates autophagy downstream to YAP/TAZ. This is assumed to involve YAP/TAZ functioning through TEAD transcription factors as this accounts for most YAP/TAZ transcriptional activity (Zanconato et al., 2015). However, I cannot exclude non-TEAD transcriptional or non-transcriptional mechanisms. This could be investigated using mutant YAP/TAZ lacking transcriptional activity, as in YAP- $\Delta$ TA (transcriptional activation domain deleted) (Zhang et al., 2012b). If vinexin does regulate autophagy through YAP/TAZ transcriptional activity, increased autophagy upon vinexin depletion in siYAP/TAZ double knockdown cells reconstituted with exogenous YAP should be ameliorated by YAP- $\Delta$ TA (used in place of wild type YAP). Other potentially useful tools include YAP-S94A (serine 94 mutated to alanine; cannot bind TEAD transcription factors) and dominant negative TEAD1 (TEAD1- $\Delta$ C; C-terminal truncated) that inhibits transcription mediated by all four TEAD transcription factors (Zhao et al., 2008).

**ii. How does si*SORBS3* treatment increase F-actin bundles?**

Vinexin beta depletion increases labile F-actin structures. This is proposed to upregulate YAP/TAZ transcriptional activity, as F-actin displaces YAP/TAZ from cytosolic sequestration by AMOTs (Mana-Capelli et al., 2014). Although vinexin has previously been implicated in actin cytoskeleton dynamics (see section 1.2.2.1), how si*SORBS3* treatment increases F-actin bundles remains to be explored.

One approach would be to investigate whether known actin regulators in the vinexin interactome are involved. These include the RHO GTPase effector rhotekin (Nagata et al., 2009) that functions in actin cytoskeleton reorganisation (Reid et al., 1996), together with the WASP family proteins N-WASP and WAVE2 (Mitsushima et al., 2006a) that promote actin polymerisation (Leng et al., 2005; Rohatgi et al., 1999). Alternatively, known F-actin modulators could be screened to identify those required for increased F-actin bundles under si*SORBS3* treatment.

**iii. Is decreased clonogenicity in ‘vinexin reconstituted’ HepG2 cells autophagy-dependent?**

Compared to HepG2 (HCC cell line) cells stably expressing mEmerald-empty, HepG2 cells reconstituted with mEmerald-vinexin alpha show reduced clonogenic capacity. This

correlates with impaired autophagy (especially under nutrient starvation) and decreased YAP/TAZ nuclear localisation.

Although proliferation makes some contribution, clonogenic assays predominantly measure cell survival (Franken et al., 2006). Autophagy facilitates cell survival under nutrient deprivation and hypoxia in the tumour microenvironment (Galluzzi et al., 2015), while YAP/TAZ transcriptional activity promotes resistance to apoptosis in cancer cells (Moroishi et al., 2015). Hence, decreased clonogenicity in reconstituted HepG2 cells might conceivably stem from either impaired autophagy or decreased YAP/TAZ nuclear localisation (or both in combination).

Provisional experiments to address this uncertainty are currently being performed by Dr Maurizio Renna. siRNA against *ATG7* and *ATG10* will be used to counter autophagosome biogenesis in the aforementioned HepG2 stable cell lines. If HepG2 cells reconstituted with mEmerald-vinexin alpha exhibit reduced clonogenicity due to impaired autophagy alone, si*ATG7/10* treated mEmerald-empty HepG2 should exhibit similar clonogenicity to mEmerald-vinexin alpha HepG2 treated with control siRNA (siCntrl). In addition, si*ATG7/10* treatment should cause no further reduction in mEmerald-vinexin alpha HepG2 clonogenicity (compared with siCntrl treated mEmerald-vinexin alpha HepG2).

More generally, how relevant the various tumour suppressive functions associated with vinexin (see Figure 6.2) are to *SORBS3* as a risk modifier gene in HCC remains to be investigated (see section 6.3 below). These functions include downregulating autophagy downstream to YAP/TAZ inhibition, together with decreasing oncogenic IL-6/STAT3 signalling (Ploeger et al., 2016) and promoting effective mitosis without improper segregation of genetic materials (Chang and Huang, 2017).

#### **iv. Does vinexin suppress cancer cell migration and invasion?**

si*SORBS3* treatment generates a ‘motile phenotype’; focal adhesions are destabilised (dynamic focal complexes favoured) and labile F-actin structures increased. Moreover, Roessler and colleagues report *SORBS3* deletion only predicts reduced survival in breast cancer cohorts featuring metastatic (node-positive) patients (Roessler et al., 2012). These findings suggest vinexin could oppose cancer progression by suppressing tumour cell dissemination. Roessler and colleagues have previously demonstrated vinexin-deficient HCC cell lines (HuH1 and Hep3B) show reduced transwell migration upon transfection with vinexin alpha (Roessler et al., 2012). However, this hypothesis could be further tested using

orthotopic xenograft models, which involve implanting HCC cells into the livers of immunocompromised mice (Yang et al., 2013). Although this would enable metastasis to be examined, data generated using orthotopic models could prove difficult to interpret since vinexin-deficient cells are hypothesised to generate a greater primary liver tumour burden (compared to vinexin-replete controls). Indeed Roessler and colleagues' have previously reported Hep3B cells expressing exogenous vinexin alpha produce significantly fewer and smaller tumours upon subcutaneous implantation into immunocompromised mice (Roessler et al., 2012).

### **6.3 Vinexin integrates multiple tumourigenic processes**

As summarised in Figure 6.2, vinexin is hypothesised to perform multifaceted roles in tumour suppression. YAP/TAZ transcriptional activity and autophagy are both well-known to influence tumour progression (Galluzzi et al., 2015; Moroishi et al., 2015). As a tumour suppressor, *SORBS3* represents a novel interface between these and other cancer biology pathways.

#### **i. YAP/TAZ transcriptional activity**

YAP and TAZ perform oncogenic roles in numerous human cancers, including HCC (Moroishi et al., 2015; Plouffe et al., 2015). These roles partially represent an aberrant progression from YAP/TAZ transcriptional activity in normal physiology, which is typically pro-proliferative and anti-apoptotic (Piccolo et al., 2014). For example, TAZ drives proliferation and anchorage-independent growth in human non-small cell lung cancer cell lines (Zhou et al., 2011). YAP/TAZ transcriptional activity is also associated with resistance to various chemotherapy agents such as doxorubicin, paclitaxel and cisplatin (Cordenonsi et al., 2011; Yang et al., 2017). In addition, YAP and TAZ function in tumour cell dissemination; depleting either decreases lung cancer cell metastases after injection into immunocompromised mice tail veins (Lau et al., 2014). These publications indicate vinexin could counter tumour progression through constraining YAP/TAZ transcriptional activity, even before considering vinexin negatively regulates autophagy.

#### **ii. Autophagy**

Autophagic contributions to genomic stability and proteostasis oppose malignant transformation (Karantza-Wadsworth et al., 2007; Mathew et al., 2009; Mathew et al., 2007). However, tumour cells also exhibit context-dependent 'autophagy addiction' (Guo et al.,

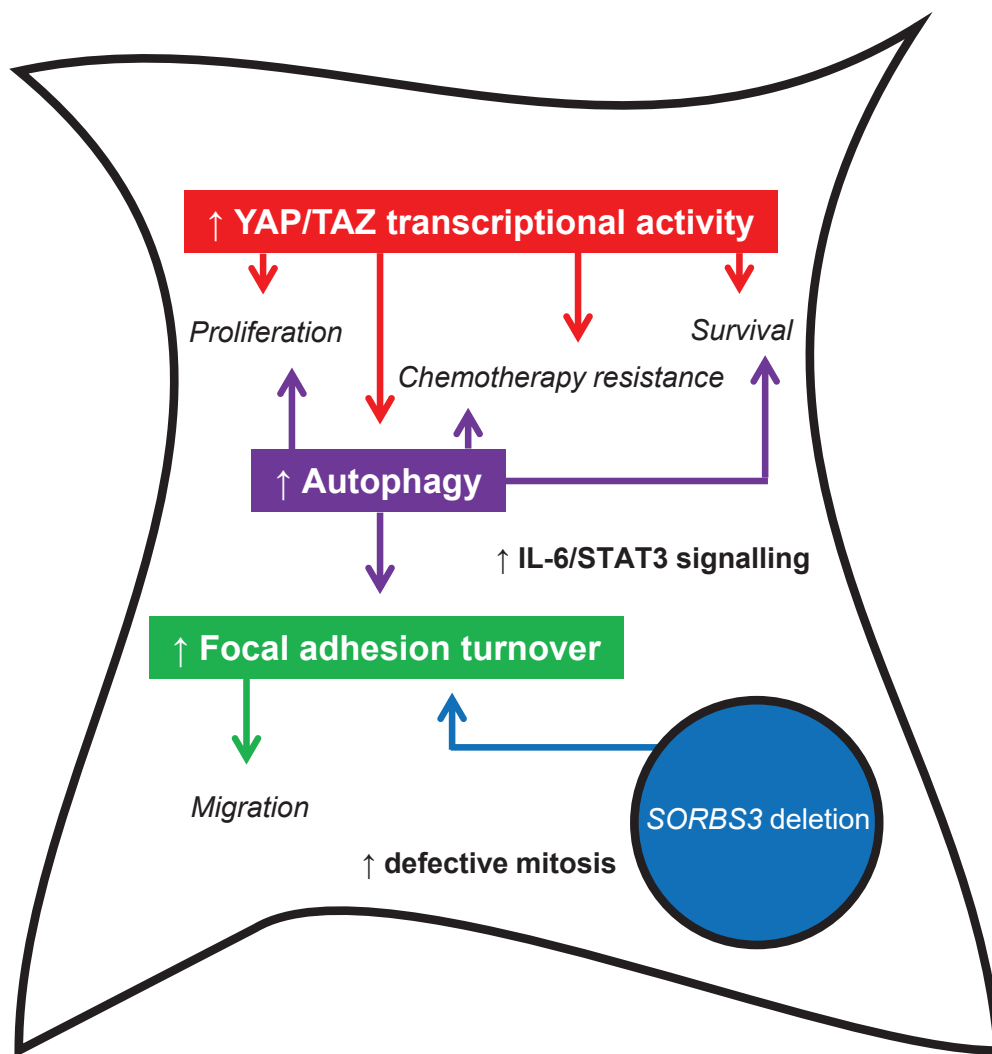


**Figure 6.2: vinexin performs multiple roles in tumour suppression.**

Schematic diagram summarising the main mechanisms by which *SORBS3* deletion is hypothesised to increase tumourigenicity. Vinexin underexpression increases YAP/TAZ transcriptional activity (red box and arrows), which upregulates autophagy (purple box and arrows). Vinexin underexpression is also associated (directly and indirectly) with increased focal adhesion turnover (green box and arrows). This promotes tumour progression through upregulating oncogenic processes, including: proliferation, survival under endogenous and exogenous stressors (such as nutrient starvation and chemotherapy) and migration (facilitating metastasis). Others have reported vinexin depletion enhances pro-proliferative, anti-apoptotic IL-6/STAT3 signalling, together with improper segregation of genetic materials *via* defective mitosis.

2011). Inhibiting autophagy (either pharmacologically or genetically) therefore decreases proliferation and survival in numerous cancer cell lines (Guo et al., 2011; Wei et al., 2011). Additionally, several research groups have demonstrated tumour cells utilise autophagy to resist chemotherapy-induced apoptosis (Galluzzi et al., 2015). Adjunct autophagy inhibition (combined with canonical chemotherapy agents) consequently has therapeutic potential in certain cancers (Amaravadi et al., 2007). Autophagy is also thought to facilitate metastasis, especially tumour cell escape from the primary site (Mowers et al., 2017). For example, Sharifi and colleagues report Atg5/Atg7-deficient 4T1 mammary carcinoma cells only generate metastases in immunocompromised mice when injected directly into the circulation (despite forming similarly sized primary tumours to autophagy-competent controls upon orthotopic implantation) (Sharifi et al., 2016). Irrespective of the molecular mechanism (decreased YAP/TAZ transcriptional activity), this literature suggests vinexin could reduce tumourigenicity by inhibiting autophagy.

### **iii. Focal adhesion turnover**

In order to metastasise, tumour cells are required to migrate. This involves focal adhesion assembly providing traction at the leading edge, which occurs in dynamic equilibrium with focal adhesion disassembly to facilitate leading edge protrusion and tail retraction (Ridley et al., 2003).

Vinexin was first identified *via* yeast two-hybrid screening using the canonical focal adhesion protein vinculin as bait (Kioka et al., 1999). Data presented above indicate vinexin stabilises focal adhesions in HeLa cells. This concurs with Kioka and colleagues' observation that vinexin alpha overexpression increases vinculin immunostaining at focal adhesions in NIH 3T3 cells (Kioka et al., 1999). There is also growing consensus that autophagy promotes focal adhesion turnover, with several alternative mechanisms proposed. For instance, Kenific et al. suggest NBR1-mediated selective autophagy contributes to focal adhesion disassembly, while Sharifi et al. report paxillin (another canonical focal adhesion protein) is targeted for autophagic degradation *via* an LC3-interacting region (Kenific et al., 2016; Sharifi et al., 2016). Rapid focal adhesion turnover typically enhances cancer cell motility, which increases metastatic propensity (Bijian et al., 2013; Xu et al., 2009b; Xu et al., 2010). Vinexin could therefore counter tumour progression *via* stabilising focal adhesions, both directly and through negatively regulating autophagy-mediated disassembly.

On the other hand, Nardone and colleagues have recently reported YAP induces focal adhesion assembly by upregulating focal adhesion-related gene expression (Nardone et al., 2017). Although the functional consequences with regards to cancer cell motility are currently unexplored, given migration requires both focal adhesion assembly and disassembly (Ridley et al., 2003), Nardone and colleagues' findings do not necessarily contradict the hypothesis *SORBS3* expression influences tumourigenicity *via* focal adhesion turnover.

#### **iv. Other tumourigenic processes**

In addition to the mechanisms discussed above, vinexin has been suggested to counter tumour progression by inhibiting IL-6/STAT3 signalling (Ploeger et al., 2016), as well as promoting effective mitosis (Chang and Huang, 2017).

Vinexin alpha is reported to indirectly downregulate pro-proliferative, anti-apoptotic IL-6/STAT3 signalling *via* oestrogen receptor alpha interactions (Ploeger et al., 2016). This concurs with previous studies ascribing oncogenic functions to the transcription factor STAT3 in HCC and other cancers (Yu et al., 2009; Zhang et al., 2012a). More recently, vinexin was shown to function in late stage mitosis. HeLa cells treated with si*SORBS3* exhibit increased abscission time due to cytoplasmic bridge resolution failure (Chang and Huang, 2017). This is seemingly incompatible with vinexin suppressing tumour cell proliferation. However, Chang and Huang argue defective mitosis is oncogenic due to improper segregation of genetic materials causing polyploidy (Fujiwara et al., 2005).

#### **6.4 Concluding remarks**

The results presented in this thesis indicate vinexin regulates autophagy through the transcriptional coactivators YAP and TAZ. These findings provide a plausible explanation for *SORBS3* deletion predicting worse outcomes in HCC (Roessler et al., 2012). The tumour suppressive roles performed by vinexin likely extend far beyond downregulating autophagy downstream to YAP/TAZ inhibition. *SORBS3* is therefore a multifaceted tumour suppressor, which inhibits several tumour progression pathways. Consequently, further investigations into *SORBS3* could have clinical implications regarding cancer treatment and tumour classification.

## 7 References

- Abercrombie, M., and Dunn, G.A. (1975). Adhesions of fibroblasts to substratum during contact inhibition observed by interference reflection microscopy. *Exp Cell Res* 92, 57-62.
- Akamatsu, M., Aota, S., Suwa, A., Ueda, K., Amachi, T., Yamada, K.M., Akiyama, S.K., and Kioka, N. (1999). Vinexin forms a signaling complex with Sos and modulates epidermal growth factor-induced c-Jun N-terminal kinase/stress-activated protein kinase activities. *J Biol Chem* 274, 35933-35937.
- Akira, S., and Takeda, K. (2004). Toll-like receptor signalling. *Nat Rev Immunol* 4, 499-511.
- Alers, S., Löffler, A.S., Paasch, F., Dieterle, A.M., Keppeler, H., Lauber, K., Campbell, D.G., Fehrenbacher, B., Schaller, M., Wesselborg, S., *et al.* (2011). Atg13 and FIP200 act independently of Ulk1 and Ulk2 in autophagy induction. *Autophagy* 7, 1423-1433.
- Ali, S., Vollaard, A.M., Widjaja, S., Surjadi, C., van de Vosse, E., and van Dissel, J.T. (2006). PARK2/PACRG polymorphisms and susceptibility to typhoid and paratyphoid fever. *Clin Exp Immunol* 144, 425-431.
- Alvers, A.L., Fishwick, L.K., Wood, M.S., Hu, D., Chung, H.S., Dunn, W.A., Jr., and Aris, J.P. (2009). Autophagy and amino acid homeostasis are required for chronological longevity in *Saccharomyces cerevisiae*. *Aging Cell* 8, 353-369.
- Amaravadi, R.K., Yu, D., Lum, J.J., Bui, T., Christophorou, M.A., Evan, G.I., Thomas-Tikhonenko, A., and Thompson, C.B. (2007). Autophagy inhibition enhances therapy-induced apoptosis in a Myc-induced model of lymphoma. *J Clin Invest* 117, 326-336.
- Antonescu, C.R., Le Loarer, F., Mosquera, J.M., Sboner, A., Zhang, L., Chen, C.L., Chen, H.W., Pathan, N., Krausz, T., Dickson, B.C., *et al.* (2013). Novel YAP1-TFE3 fusion defines a distinct subset of epithelioid hemangioendothelioma. *Genes Chromosomes Cancer* 52, 775-784.
- Aoki, H., Takada, Y., Kondo, S., Sawaya, R., Aggarwal, B.B., and Kondo, Y. (2007). Evidence that curcumin suppresses the growth of malignant gliomas in vitro and in vivo through induction of autophagy: role of Akt and extracellular signal-regulated kinase signaling pathways. *Mol Pharmacol* 72, 29-39.
- Aragona, M., Panciera, T., Manfrin, A., Giulitti, S., Michielin, F., Elvassore, N., Dupont, S., and Piccolo, S. (2013). A mechanical checkpoint controls multicellular growth through YAP/TAZ regulation by actin-processing factors. *Cell* 154, 1047-1059.
- Axe, E.L., Walker, S.A., Manifava, M., Chandra, P., Roderick, H.L., Habermann, A., Griffiths, G., and Ktistakis, N.T. (2008). Autophagosome formation from membrane compartments enriched in phosphatidylinositol 3-phosphate and dynamically connected to the endoplasmic reticulum. *J Cell Biol* 182, 685-701.
- Azzolin, L., Panciera, T., Soligo, S., Enzo, E., Bicciato, S., Dupont, S., Bresolin, S., Frasson, C., Basso, G., Guzzardo, V., *et al.* (2014). YAP/TAZ incorporation in the beta-catenin destruction complex orchestrates the Wnt response. *Cell* 158, 157-170.
- Backer, J.M. (2016). The intricate regulation and complex functions of the Class III phosphoinositide 3-kinase Vps34. *Biochem J* 473, 2251-2271.
- Bai, H., Zhang, N., Xu, Y., Chen, Q., Khan, M., Potter, J.J., Nayar, S.K., Cornish, T., Alpini, G., Bronk, S., *et al.* (2012). Yes-associated protein regulates the hepatic response after bile duct ligation. *Hepatology* 56, 1097-1107.
- Bandyopadhyay, U., Kaushik, S., Varticovski, L., and Cuervo, A.M. (2008). The chaperone-mediated autophagy receptor organizes in dynamic protein complexes at the lysosomal membrane. *Mol Cell Biol* 28, 5747-5763.

Basu, S., Totty, N.F., Irwin, M.S., Sudol, M., and Downward, J. (2003). Akt phosphorylates the Yes-associated protein, YAP, to induce interaction with 14-3-3 and attenuation of p73-mediated apoptosis. *Mol Cell* *11*, 11-23.

Beltrami, A.P., Urbanek, K., Kajstura, J., Yan, S.M., Finato, N., Bussani, R., Nadal-Ginard, B., Silvestri, F., Leri, A., Beltrami, C.A., *et al.* (2001). Evidence that human cardiac myocytes divide after myocardial infarction. *N Engl J Med* *344*, 1750-1757.

Bento, C.F., Ashkenazi, A., Jimenez-Sanchez, M., and Rubinsztein, D.C. (2016a). The Parkinson's disease-associated genes ATP13A2 and SYT11 regulate autophagy via a common pathway. *Nat Commun* *7*, 11803.

Bento, C.F., Renna, M., Ghislat, G., Puri, C., Ashkenazi, A., Vicinanza, M., Menzies, F.M., and Rubinsztein, D.C. (2016b). Mammalian Autophagy: How Does It Work? *Annu Rev Biochem* *85*, 685-713.

Berger, Z., Ravikumar, B., Menzies, F.M., Oroz, L.G., Underwood, B.R., Pangalos, M.N., Schmitt, I., Wullner, U., Evert, B.O., O'Kane, C.J., *et al.* (2006). Rapamycin alleviates toxicity of different aggregate-prone proteins. *Hum Mol Genet* *15*, 433-442.

Bijian, K., Loughheed, C., Su, J., Xu, B., Yu, H., Wu, J.H., Riccio, K., and Alaoui-Jamali, M.A. (2013). Targeting focal adhesion turnover in invasive breast cancer cells by the purine derivative reversine. *Br J Cancer* *109*, 2810-2818.

Bjedov, I., Toivonen, J.M., Kerr, F., Slack, C., Jacobson, J., Foley, A., and Partridge, L. (2010). Mechanisms of life span extension by rapamycin in the fruit fly *Drosophila melanogaster*. *Cell Metab* *11*, 35-46.

Bjorkoy, G., Lamark, T., Brech, A., Outzen, H., Perander, M., Overvatn, A., Stenmark, H., and Johansen, T. (2005). p62/SQSTM1 forms protein aggregates degraded by autophagy and has a protective effect on huntingtin-induced cell death. *J Cell Biol* *171*, 603-614.

Blommaert, E.F., Luiken, J.J., Blommaert, P.J., van Woerkom, G.M., and Meijer, A.J. (1995). Phosphorylation of ribosomal protein S6 is inhibitory for autophagy in isolated rat hepatocytes. *J Biol Chem* *270*, 2320-2326.

Bork, P., and Sudol, M. (1994). The WW domain: a signalling site in dystrophin? *Trends Biochem Sci* *19*, 531-533.

Bostaille, N., Gauquier, A., Stainier, D.Y., Raible, D.W., and Vanhollebeke, B. (2017). Defective *adgr2* (*gpr124*) splicing and function in zebrafish *ouchless* mutants. In *Development* (England: (c) 2017. Published by The Company of Biologists Ltd.), pp. 8-11.

Bouley, S.J., Maginnis, M.S., Derdowski, A., Gee, G.V., O'Hara, B.A., Nelson, C.D., Bara, A.M., Atwood, W.J., and Dugan, A.S. (2014). Host cell autophagy promotes BK virus infection. *Virology* *456-457*, 87-95.

Braak, H., Braak, E., and Bohl, J. (1993). Staging of Alzheimer-related cortical destruction. *Eur Neurol* *33*, 403-408.

Brown, E.J., Beal, P.A., Keith, C.T., Chen, J., Shin, T.B., and Schreiber, S.L. (1995). Control of p70 s6 kinase by kinase activity of FRAP in vivo. *Nature* *377*, 441-446.

Budi, E.H., Duan, D., and Derynck, R. (2017). Transforming Growth Factor-beta Receptors and Smads: Regulatory Complexity and Functional Versatility. *Trends Cell Biol*.

Bulgakova, N.A., and Knust, E. (2009). The Crumbs complex: from epithelial-cell polarity to retinal degeneration. *J Cell Sci* *122*, 2587-2596.

Burglin, T.R. (1991). The TEA domain: a novel, highly conserved DNA-binding motif. In *Cell* (United States), pp. 11-12.

Cadwell, K., Liu, J.Y., Brown, S.L., Miyoshi, H., Loh, J., Lennerz, J.K., Kishi, C., Kc, W., Carrero, J.A., Hunt, S., *et al.* (2008). A key role for autophagy and the autophagy gene *Atg16l1* in mouse and human intestinal Paneth cells. *Nature* *456*, 259-263.

Cai, J., Zhang, N., Zheng, Y., de Wilde, R.F., Maitra, A., and Pan, D. (2010). The Hippo signaling pathway restricts the oncogenic potential of an intestinal regeneration program. *Genes Dev* 24, 2383-2388.

Camargo, F.D., Gokhale, S., Johnnidis, J.B., Fu, D., Bell, G.W., Jaenisch, R., and Brummelkamp, T.R. (2007). YAP1 increases organ size and expands undifferentiated progenitor cells. *Curr Biol* 17, 2054-2060.

Campbell, H.K., Maiers, J.L., and DeMali, K.A. (2017). Interplay between tight junctions & adherens junctions. *Exp Cell Res*.

Cao, X., Pfaff, S.L., and Gage, F.H. (2008). YAP regulates neural progenitor cell number via the TEA domain transcription factor. *Genes Dev* 22, 3320-3334.

Carames, B., Taniguchi, N., Otsuki, S., Blanco, F.J., and Lotz, M. (2010). Autophagy is a protective mechanism in normal cartilage, and its aging-related loss is linked with cell death and osteoarthritis. *Arthritis Rheum* 62, 791-801.

Cardenas, C., Miller, R.A., Smith, I., Bui, T., Molgo, J., Muller, M., Vais, H., Cheung, K.H., Yang, J., Parker, I., *et al.* (2010). Essential regulation of cell bioenergetics by constitutive InsP3 receptor Ca<sup>2+</sup> transfer to mitochondria. *Cell* 142, 270-283.

Cardoso, C.M., Groth-Pedersen, L., Hoyer-Hansen, M., Kirkegaard, T., Corcelle, E., Andersen, J.S., Jaattela, M., and Nylandsted, J. (2009). Depletion of kinesin 5B affects lysosomal distribution and stability and induces peri-nuclear accumulation of autophagosomes in cancer cells. *PLoS One* 4, e4424.

Carpenter, A.E., Jones, T.R., Lamprecht, M.R., Clarke, C., Kang, I.H., Friman, O., Guertin, D.A., Chang, J.H., Lindquist, R.A., Moffat, J., *et al.* (2006). CellProfiler: image analysis software for identifying and quantifying cell phenotypes. *Genome Biol* 7, R100.

Chan, E.H., Nousiainen, M., Chalamalasetty, R.B., Schafer, A., Nigg, E.A., and Sillje, H.H. (2005). The Ste20-like kinase Mst2 activates the human large tumor suppressor kinase Lats1. *Oncogene* 24, 2076-2086.

Chan, E.Y., Longatti, A., McKnight, N.C., and Tooze, S.A. (2009a). Kinase-inactivated ULK proteins inhibit autophagy via their conserved C-terminal domains using an Atg13-independent mechanism. *Mol Cell Biol* 29, 157-171.

Chan, S.W., Lim, C.J., Chong, Y.F., Pobbati, A.V., Huang, C., and Hong, W. (2011). Hippo pathway-independent restriction of TAZ and YAP by angiomin. *J Biol Chem* 286, 7018-7026.

Chan, S.W., Lim, C.J., Guo, K., Ng, C.P., Lee, I., Hunziker, W., Zeng, Q., and Hong, W. (2008). A role for TAZ in migration, invasion, and tumorigenesis of breast cancer cells. *Cancer Res* 68, 2592-2598.

Chan, S.W., Lim, C.J., Loo, L.S., Chong, Y.F., Huang, C., and Hong, W. (2009b). TEADs mediate nuclear retention of TAZ to promote oncogenic transformation. *J Biol Chem* 284, 14347-14358.

Chang, Y.W., and Huang, Y.S. (2017). Midbody localization of Vinexin recruits Rhotekin to facilitate cytokinetic abscission. *Cell Cycle*, 0.

Chen, D., Fan, W., Lu, Y., Ding, X., Chen, S., and Zhong, Q. (2012). A mammalian autophagosome maturation mechanism mediated by TECPR1 and the Atg12-Atg5 conjugate. *Mol Cell* 45, 629-641.

Chen, G.C., Lee, J.Y., Tang, H.W., Debnath, J., Thomas, S.M., and Settleman, J. (2008). Genetic interactions between *Drosophila melanogaster* Atg1 and paxillin reveal a role for paxillin in autophagosome formation. *Autophagy* 4, 37-45.

Chen, H., Cohen, D.M., Choudhury, D.M., Kioka, N., and Craig, S.W. (2005). Spatial distribution and functional significance of activated vinculin in living cells. *J Cell Biol* 169, 459-470.

Chen, K., Gao, L., Liu, Y., Zhang, Y., Jiang, D.S., Wei, X., Zhu, X.H., Zhang, R., Chen, Y., Yang, Q., *et al.* (2013). Vinexin-beta protects against cardiac hypertrophy by blocking the Akt-dependent signalling pathway. *Basic Res Cardiol* 108, 338.

Chen, L., Chan, S.W., Zhang, X., Walsh, M., Lim, C.J., Hong, W., and Song, H. (2010). Structural basis of YAP recognition by TEAD4 in the hippo pathway. *Genes Dev* 24, 290-300.

Chen, M., Hong, M.J., Sun, H., Wang, L., Shi, X., Gilbert, B.E., Corry, D.B., Kheradmand, F., and Wang, J. (2014a). Essential role for autophagy in the maintenance of immunological memory against influenza infection. *Nat Med* 20, 503-510.

Chen, Q., Zhang, N., Gray, R.S., Li, H., Ewald, A.J., Zahnow, C.A., and Pan, D. (2014b). A temporal requirement for Hippo signaling in mammary gland differentiation, growth, and tumorigenesis. *Genes Dev* 28, 432-437.

Chiang, H.L., Terlecky, S.R., Plant, C.P., and Dice, J.F. (1989). A role for a 70-kilodalton heat shock protein in lysosomal degradation of intracellular proteins. *Science* 246, 382-385.

Choi, A.M., Ryter, S.W., and Levine, B. (2013). Autophagy in human health and disease. *N Engl J Med* 368, 651-662.

Chu, C.Y., Chang, C.C., Prakash, E., and Kuo, M.L. (2008). Connective tissue growth factor (CTGF) and cancer progression. *J Biomed Sci* 15, 675-685.

Ciani, B., Layfield, R., Cavey, J.R., Sheppard, P.W., and Searle, M.S. (2003). Structure of the ubiquitin-associated domain of p62 (SQSTM1) and implications for mutations that cause Paget's disease of bone. *J Biol Chem* 278, 37409-37412.

Clevers, H. (2006). Wnt/beta-catenin signaling in development and disease. *Cell* 127, 469-480.

Cordenonsi, M., Zanconato, F., Azzolin, L., Forcato, M., Rosato, A., Frasson, C., Inui, M., Montagner, M., Parenti, A.R., Poletti, A., *et al.* (2011). The Hippo transducer TAZ confers cancer stem cell-related traits on breast cancer cells. *Cell* 147, 759-772.

Costes, S.V., Daelemans, D., Cho, E.H., Dobbin, Z., Pavlakis, G., and Lockett, S. (2004). Automatic and quantitative measurement of protein-protein colocalization in live cells. *Biophys J* 86, 3993-4003.

Coue, M., Brenner, S.L., Spector, I., and Korn, E.D. (1987). Inhibition of actin polymerization by latrunculin A. *FEBS Lett* 213, 316-318.

Criollo, A., Maiuri, M.C., Tasdemir, E., Vitale, I., Fiebig, A.A., Andrews, D., Molgo, J., Diaz, J., Lavandro, S., Harper, F., *et al.* (2007). Regulation of autophagy by the inositol trisphosphate receptor. *Cell Death Differ* 14, 1029-1039.

Cuervo, A.M., and Dice, J.F. (1996). A receptor for the selective uptake and degradation of proteins by lysosomes. *Science* 273, 501-503.

Cui, C.B., Cooper, L.F., Yang, X., Karsenty, G., and Aukhil, I. (2003). Transcriptional coactivation of bone-specific transcription factor Cbfa1 by TAZ. *Mol Cell Biol* 23, 1004-1013.

Das, A., Fischer, R.S., Pan, D., and Waterman, C.M. (2016). YAP Nuclear Localization in the Absence of Cell-Cell Contact Is Mediated by a Filamentous Actin-dependent, Myosin II- and Phospho-YAP-independent Pathway during Extracellular Matrix Mechanosensing. *J Biol Chem* 291, 6096-6110.

De Duve, C., and Wattiaux, R. (1966). Functions of lysosomes. *Annu Rev Physiol* 28, 435-492.

de Melker, A.A., van der Horst, G., and Borst, J. (2004). c-Cbl directs EGF receptors into an endocytic pathway that involves the ubiquitin-interacting motif of Eps15. *J Cell Sci* 117, 5001-5012.

DeBosch, B.J., Heitmeier, M.R., Mayer, A.L., Higgins, C.B., Crowley, J.R., Kraft, T.E., Chi, M., Newberry, E.P., Chen, Z., Finck, B.N., *et al.* (2016). Trehalose inhibits solute carrier 2A (SLC2A) proteins to induce autophagy and prevent hepatic steatosis. *Sci Signal* 9, ra21.

Del Re, D.P., Yang, Y., Nakano, N., Cho, J., Zhai, P., Yamamoto, T., Zhang, N., Yabuta, N., Nojima, H., Pan, D., *et al.* (2013). Yes-associated protein isoform 1 (Yap1) promotes cardiomyocyte survival and growth to protect against myocardial ischemic injury. *J Biol Chem* 288, 3977-3988.

Deretic, V., Kimura, T., Timmins, G., Moseley, P., Chauhan, S., and Mandell, M. (2015). Immunologic manifestations of autophagy. *J Clin Invest* 125, 75-84.

Di Palma, T., D'Andrea, B., Liguori, G.L., Liguoro, A., de Cristofaro, T., Del Prete, D., Pappalardo, A., Mascia, A., and Zannini, M. (2009). TAZ is a coactivator for Pax8 and TTF-1, two transcription factors involved in thyroid differentiation. *Exp Cell Res* 315, 162-175.

Di Stefano, P., Cabodi, S., Boeri Erba, E., Margaria, V., Bergatto, E., Giuffrida, M.G., Silengo, L., Tarone, G., Turco, E., and Defilippi, P. (2004). P130Cas-associated protein (p140Cap) as a new tyrosine-phosphorylated protein involved in cell spreading. *Mol Biol Cell* 15, 787-800.

Diao, J., Liu, R., Rong, Y., Zhao, M., Zhang, J., Lai, Y., Zhou, Q., Wilz, L.M., Li, J., Vivona, S., *et al.* (2015). ATG14 promotes membrane tethering and fusion of autophagosomes to endolysosomes. *Nature* 520, 563-566.

Dice, J.F., Chiang, H.L., Spencer, E.P., and Backer, J.M. (1986). Regulation of catabolism of microinjected ribonuclease A. Identification of residues 7-11 as the essential pentapeptide. *J Biol Chem* 261, 6853-6859.

Donati, A., Cavallini, G., Paradiso, C., Vittorini, S., Pollera, M., Gori, Z., and Bergamini, E. (2001). Age-related changes in the regulation of autophagic proteolysis in rat isolated hepatocytes. *J Gerontol A Biol Sci Med Sci* 56, B288-293.

Dong, J., Feldmann, G., Huang, J., Wu, S., Zhang, N., Comerford, S.A., Gayyed, M.F., Anders, R.A., Maitra, A., and Pan, D. (2007). Elucidation of a universal size-control mechanism in *Drosophila* and mammals. *Cell* 130, 1120-1133.

Dooley, H.C., Razi, M., Polson, H.E., Girardin, S.E., Wilson, M.I., and Tooze, S.A. (2014). WIPI2 links LC3 conjugation with PI3P, autophagosome formation, and pathogen clearance by recruiting Atg12-5-16L1. *Mol Cell* 55, 238-252.

Dupont, S., Morsut, L., Aragona, M., Enzo, E., Giulitti, S., Cordenonsi, M., Zanconato, F., Le Digabel, J., Forcato, M., Bicciato, S., *et al.* (2011). Role of YAP/TAZ in mechanotransduction. *Nature* 474, 179-183.

Duran, A., Linares, J.F., Galvez, A.S., Wikenheiser, K., Flores, J.M., Diaz-Meco, M.T., and Moscat, J. (2008). The signaling adaptor p62 is an important NF-kappaB mediator in tumorigenesis. *Cancer Cell* 13, 343-354.

Dusaban, S.S., and Brown, J.H. (2015). PLCepsilon mediated sustained signaling pathways. *Adv Biol Regul* 57, 17-23.

Egan, D.F., Chun, M.G., Vamos, M., Zou, H., Rong, J., Miller, C.J., Lou, H.J., Raveendra-Panickar, D., Yang, C.C., Sheffler, D.J., *et al.* (2015). Small Molecule Inhibition of the Autophagy Kinase ULK1 and Identification of ULK1 Substrates. *Mol Cell* 59, 285-297.

Egan, D.F., Shackelford, D.B., Mihaylova, M.M., Gelino, S., Kohnz, R.A., Mair, W., Vasquez, D.S., Joshi, A., Gwinn, D.M., Taylor, R., *et al.* (2011). Phosphorylation of ULK1 (hATG1) by AMP-activated protein kinase connects energy sensing to mitophagy. *Science* 331, 456-461.

Fader, C.M., Sanchez, D.G., Mestre, M.B., and Colombo, M.I. (2009). TI-VAMP/VAMP7 and VAMP3/cellubrevin: two v-SNARE proteins involved in specific steps of the autophagy/multivesicular body pathways. *Biochim Biophys Acta* 1793, 1901-1916.

Feather, S.A., Winyard, P.J., Dodd, S., and Woolf, A.S. (1997). Oral-facial-digital syndrome type 1 is another dominant polycystic kidney disease: clinical, radiological and histopathological features of a new kindred. *Nephrol Dial Transplant* *12*, 1354-1361.

Feng, X., Degese, M.S., Iglesias-Bartolome, R., Vaque, J.P., Molinolo, A.A., Rodrigues, M., Zaidi, M.R., Ksander, B.R., Merlino, G., Sodhi, A., *et al.* (2014). Hippo-independent activation of YAP by the GNAQ uveal melanoma oncogene through a trio-regulated rho GTPase signaling circuitry. *Cancer Cell* *25*, 831-845.

Ferrigno, O., Lallemand, F., Verrecchia, F., L'Hoste, S., Camonis, J., Atfi, A., and Mauviel, A. (2002). Yes-associated protein (YAP65) interacts with Smad7 and potentiates its inhibitory activity against TGF-beta/Smad signaling. *Oncogene* *21*, 4879-4884.

Flucke, U., Vogels, R.J., de Saint Aubain Somerhausen, N., Creytens, D.H., Riedl, R.G., van Gorp, J.M., Milne, A.N., Huysentruyt, C.J., Verdijk, M.A., van Asseldonk, M.M., *et al.* (2014). Epithelioid Hemangioendothelioma: clinicopathologic, immunohistochemical, and molecular genetic analysis of 39 cases. *Diagn Pathol* *9*, 131.

Forbes, S.A., Beare, D., Boutselakis, H., Bamford, S., Bindal, N., Tate, J., Cole, C.G., Ward, S., Dawson, E., Ponting, L., *et al.* (2017). COSMIC: somatic cancer genetics at high-resolution. *Nucleic Acids Res* *45*, D777-d783.

Fossdal, R., Jonasson, F., Kristjansdottir, G.T., Kong, A., Stefansson, H., Gosh, S., Gulcher, J.R., and Stefansson, K. (2004). A novel TEAD1 mutation is the causative allele in Sveinsson's chorioretinal atrophy (helicoid peripapillary chorioretinal degeneration). *Hum Mol Genet* *13*, 975-981.

Frake, R.A., Ricketts, T., Menzies, F.M., and Rubinsztein, D.C. (2015). Autophagy and neurodegeneration. *J Clin Invest* *125*, 65-74.

Franken, N.A., Rodermond, H.M., Stap, J., Haveman, J., and van Bree, C. (2006). Clonogenic assay of cells in vitro. *Nat Protoc* *1*, 2315-2319.

Fujita, N., Hayashi-Nishino, M., Fukumoto, H., Omori, H., Yamamoto, A., Noda, T., and Yoshimori, T. (2008). An Atg4B mutant hampers the lipidation of LC3 paralogues and causes defects in autophagosome closure. *Mol Biol Cell* *19*, 4651-4659.

Fujiwara, T., Bandi, M., Nitta, M., Ivanova, E.V., Bronson, R.T., and Pellman, D. (2005). Cytokinesis failure generating tetraploids promotes tumorigenesis in p53-null cells. *Nature* *437*, 1043-1047.

Fullgrave, J., Ghislat, G., Cho, D.H., and Rubinsztein, D.C. (2016). Transcriptional regulation of mammalian autophagy at a glance. *J Cell Sci* *129*, 3059-3066.

Fullgrave, J., Klionsky, D.J., and Joseph, B. (2014). The return of the nucleus: transcriptional and epigenetic control of autophagy. In *Nat Rev Mol Cell Biol (England)*, pp. 65-74.

Furuta, N., Fujita, N., Noda, T., Yoshimori, T., and Amano, A. (2010). Combinational soluble N-ethylmaleimide-sensitive factor attachment protein receptor proteins VAMP8 and Vti1b mediate fusion of antimicrobial and canonical autophagosomes with lysosomes. *Mol Biol Cell* *21*, 1001-1010.

Galluzzi, L., Pietrocola, F., Bravo-San Pedro, J.M., Amaravadi, R.K., Baehrecke, E.H., Cecconi, F., Codogno, P., Debnath, J., Gewirtz, D.A., Karantza, V., *et al.* (2015). Autophagy in malignant transformation and cancer progression. *Embo j* *34*, 856-880.

Ganley, I.G. (2013). Autophagosome maturation and lysosomal fusion. *Essays Biochem* *55*, 65-78.

Ganley, I.G., Lam du, H., Wang, J., Ding, X., Chen, S., and Jiang, X. (2009). ULK1.ATG13.FIP200 complex mediates mTOR signaling and is essential for autophagy. *J Biol Chem* *284*, 12297-12305.

Gao, C., Cao, W., Bao, L., Zuo, W., Xie, G., Cai, T., Fu, W., Zhang, J., Wu, W., Zhang, X., *et al.* (2010). Autophagy negatively regulates Wnt signalling by promoting Dishevelled degradation. *Nat Cell Biol* *12*, 781-790.

Gao, T., Zhou, D., Yang, C., Singh, T., Penzo-Mendez, A., Maddipati, R., Tzatsos, A., Bardeesy, N., Avruch, J., and Stanger, B.Z. (2013). Hippo signaling regulates differentiation and maintenance in the exocrine pancreas. *Gastroenterology* *144*, 1543-1553, 1553.e1541.

Gao, X., Zhang, Y., Arrazola, P., Hino, O., Kobayashi, T., Yeung, R.S., Ru, B., and Pan, D. (2002). Tsc tumour suppressor proteins antagonize amino-acid-TOR signalling. *Nat Cell Biol* *4*, 699-704.

Ge, L., Melville, D., Zhang, M., and Schekman, R. (2013). The ER-Golgi intermediate compartment is a key membrane source for the LC3 lipidation step of autophagosome biogenesis. *Elife* *2*, e00947.

Ge, L., Zhang, M., and Schekman, R. (2014). Phosphatidylinositol 3-kinase and COPII generate LC3 lipidation vesicles from the ER-Golgi intermediate compartment. *Elife* *3*, e04135.

Geiger, B., Spatz, J.P., and Bershadsky, A.D. (2009). Environmental sensing through focal adhesions. *Nat Rev Mol Cell Biol* *10*, 21-33.

Goode, B.L., and Eck, M.J. (2007). Mechanism and function of formins in the control of actin assembly. *Annu Rev Biochem* *76*, 593-627.

Gordon, P.B., and Seglen, P.O. (1988). Prelysosomal convergence of autophagic and endocytic pathways. *Biochem Biophys Res Commun* *151*, 40-47.

Grossman, R.L., Heath, A.P., Ferretti, V., Varmus, H.E., Lowy, D.R., Kibbe, W.A., and Staudt, L.M. (2016). Toward a Shared Vision for Cancer Genomic Data. *N Engl J Med* *375*, 1109-1112.

GTEX Consortium (2013). The Genotype-Tissue Expression (GTEx) project. *Nat Genet* *45*, 580-585.

Guan, H., Cheng, W.L., Guo, J., Chao, M.L., Zhang, Y., Gong, J., Zhu, X.Y., She, Z.G., Huang, Z., and Li, H. (2017). Vinexin beta Ablation Inhibits Atherosclerosis in Apolipoprotein E-Deficient Mice by Inactivating the Akt-Nuclear Factor kappaB Inflammatory Axis. *J Am Heart Assoc* *6*.

Guo, J.Y., Chen, H.Y., Mathew, R., Fan, J., Strohecker, A.M., Karsli-Uzunbas, G., Kamphorst, J.J., Chen, G., Lemons, J.M., Karantza, V., *et al.* (2011). Activated Ras requires autophagy to maintain oxidative metabolism and tumorigenesis. *Genes Dev* *25*, 460-470.

Gutierrez, M.G., Master, S.S., Singh, S.B., Taylor, G.A., Colombo, M.I., and Deretic, V. (2004a). Autophagy is a defense mechanism inhibiting BCG and Mycobacterium tuberculosis survival in infected macrophages. *Cell* *119*, 753-766.

Gutierrez, M.G., Munafò, D.B., Beron, W., and Colombo, M.I. (2004b). Rab7 is required for the normal progression of the autophagic pathway in mammalian cells. *J Cell Sci* *117*, 2687-2697.

Gwinn, D.M., Shackelford, D.B., Egan, D.F., Mihaylova, M.M., Mery, A., Vasquez, D.S., Turk, B.E., and Shaw, R.J. (2008). AMPK phosphorylation of raptor mediates a metabolic checkpoint. *Mol Cell* *30*, 214-226.

Haack, T.B., Hogarth, P., Kruer, M.C., Gregory, A., Wieland, T., Schwarzmayr, T., Graf, E., Sanford, L., Meyer, E., Kara, E., *et al.* (2012). Exome sequencing reveals de novo WDR45 mutations causing a phenotypically distinct, X-linked dominant form of NBIA. *Am J Hum Genet* *91*, 1144-1149.

Hailey, D.W., Rambold, A.S., Satpute-Krishnan, P., Mitra, K., Sougrat, R., Kim, P.K., and Lippincott-Schwartz, J. (2010). Mitochondria supply membranes for autophagosome biogenesis during starvation. *Cell* *141*, 656-667.

Hamasaki, M., Furuta, N., Matsuda, A., Nezu, A., Yamamoto, A., Fujita, N., Oomori, H., Noda, T., Haraguchi, T., Hiraoka, Y., *et al.* (2013). Autophagosomes form at ER-mitochondria contact sites. *Nature* *495*, 389-393.

Hampe, J., Franke, A., Rosenstiel, P., Till, A., Teuber, M., Huse, K., Albrecht, M., Mayr, G., De La Vega, F.M., Briggs, J., *et al.* (2007). A genome-wide association scan of nonsynonymous SNPs identifies a susceptibility variant for Crohn disease in ATG16L1. *Nat Genet* *39*, 207-211.

Happe, H., van der Wal, A.M., Leonhard, W.N., Kunnen, S.J., Breuning, M.H., de Heer, E., and Peters, D.J. (2011). Altered Hippo signalling in polycystic kidney disease. *J Pathol* *224*, 133-142.

Hardie, D.G., Ross, F.A., and Hawley, S.A. (2012). AMPK: a nutrient and energy sensor that maintains energy homeostasis. *Nat Rev Mol Cell Biol* *13*, 251-262.

Harding, T.M., Morano, K.A., Scott, S.V., and Klionsky, D.J. (1995). Isolation and characterization of yeast mutants in the cytoplasm to vacuole protein targeting pathway. *J Cell Biol* *131*, 591-602.

Harrison, D.E., Strong, R., Sharp, Z.D., Nelson, J.F., Astle, C.M., Flurkey, K., Nadon, N.L., Wilkinson, J.E., Frenkel, K., Carter, C.S., *et al.* (2009). Rapamycin fed late in life extends lifespan in genetically heterogeneous mice. *Nature* *460*, 392-395.

Hars, E.S., Qi, H., Ryazanov, A.G., Jin, S., Cai, L., Hu, C., and Liu, L.F. (2007). Autophagy regulates ageing in *C. elegans*. *Autophagy* *3*, 93-95.

Hau, J.C., Erdmann, D., Mesrouze, Y., Furet, P., Fontana, P., Zimmermann, C., Schmelzle, T., Hofmann, F., and Chene, P. (2013). The TEAD4-YAP/TAZ protein-protein interaction: expected similarities and unexpected differences. *Chembiochem* *14*, 1218-1225.

Hayashi-Nishino, M., Fujita, N., Noda, T., Yamaguchi, A., Yoshimori, T., and Yamamoto, A. (2009). A subdomain of the endoplasmic reticulum forms a cradle for autophagosome formation. *Nat Cell Biol* *11*, 1433-1437.

Heallen, T., Morikawa, Y., Leach, J., Tao, G., Willerson, J.T., Johnson, R.L., and Martin, J.F. (2013). Hippo signaling impedes adult heart regeneration. *Development* *140*, 4683-4690.

Heallen, T., Zhang, M., Wang, J., Bonilla-Claudio, M., Klysik, E., Johnson, R.L., and Martin, J.F. (2011). Hippo pathway inhibits Wnt signaling to restrain cardiomyocyte proliferation and heart size. *Science* *332*, 458-461.

Hebron, M.L., Lonskaya, I., and Moussa, C.E. (2013). Nilotinib reverses loss of dopamine neurons and improves motor behavior via autophagic degradation of alpha-synuclein in Parkinson's disease models. *Hum Mol Genet* *22*, 3315-3328.

Hemelaar, J., Lelyveld, V.S., Kessler, B.M., and Ploegh, H.L. (2003). A single protease, Apg4B, is specific for the autophagy-related ubiquitin-like proteins GATE-16, MAP1-LC3, GABARAP, and Apg8L. *J Biol Chem* *278*, 51841-51850.

Hirst, J., Bright, N.A., Rous, B., and Robinson, M.S. (1999). Characterization of a fourth adaptor-related protein complex. *Mol Biol Cell* *10*, 2787-2802.

Hong, J.H., Hwang, E.S., McManus, M.T., Amsterdam, A., Tian, Y., Kalmukova, R., Mueller, E., Benjamin, T., Spiegelman, B.M., Sharp, P.A., *et al.* (2005). TAZ, a transcriptional modulator of mesenchymal stem cell differentiation. *Science* *309*, 1074-1078.

Hosokawa, N., Hara, T., Kaizuka, T., Kishi, C., Takamura, A., Miura, Y., Iemura, S., Natsume, T., Takehana, K., Yamada, N., *et al.* (2009a). Nutrient-dependent mTORC1 association with the ULK1-Atg13-FIP200 complex required for autophagy. *Mol Biol Cell* *20*, 1981-1991.

Hosokawa, N., Sasaki, T., Iemura, S., Natsume, T., Hara, T., and Mizushima, N. (2009b). Atg101, a novel mammalian autophagy protein interacting with Atg13. *Autophagy* *5*, 973-979.

Hossain, Z., Ali, S.M., Ko, H.L., Xu, J., Ng, C.P., Guo, K., Qi, Z., Ponniah, S., Hong, W., and Hunziker, W. (2007). Glomerulocystic kidney disease in mice with a targeted inactivation of *Wwtr1*. *Proc Natl Acad Sci U S A* *104*, 1631-1636.

Howell, M., Borchers, C., and Milgram, S.L. (2004). Heterogeneous nuclear ribonuclear protein U associates with YAP and regulates its co-activation of Bax transcription. *J Biol Chem* 279, 26300-26306.

Hu, J.K., Du, W., Shelton, S.J., Oldham, M.C., DiPersio, C.M., and Klein, O.D. (2017). An FAK-YAP-mTOR Signaling Axis Regulates Stem Cell-Based Tissue Renewal in Mice. *Cell Stem Cell* 21, 91-106.e106.

Huang, W., Lv, X., Liu, C., Zha, Z., Zhang, H., Jiang, Y., Xiong, Y., Lei, Q.Y., and Guan, K.L. (2012). The N-terminal phosphodegron targets TAZ/WWTR1 protein for SCFbeta-TrCP-dependent degradation in response to phosphatidylinositol 3-kinase inhibition. *J Biol Chem* 287, 26245-26253.

Huotari, J., and Helenius, A. (2011). Endosome maturation. *Embo j* 30, 3481-3500.

Hurley, J.H., and Young, L.N. (2017). Mechanisms of Autophagy Initiation. *Annu Rev Biochem* 86, 225-244.

Ichimura, Y., Kirisako, T., Takao, T., Satomi, Y., Shimonishi, Y., Ishihara, N., Mizushima, N., Tanida, I., Kominami, E., Ohsumi, M., *et al.* (2000). A ubiquitin-like system mediates protein lipidation. *Nature* 408, 488-492.

Imaizumi, K. (2011). Diet and atherosclerosis in apolipoprotein E-deficient mice. *Biosci Biotechnol Biochem* 75, 1023-1035.

Inoki, K., Zhu, T., and Guan, K.L. (2003). TSC2 mediates cellular energy response to control cell growth and survival. *Cell* 115, 577-590.

Itakura, E., Kishi, C., Inoue, K., and Mizushima, N. (2008). Beclin 1 forms two distinct phosphatidylinositol 3-kinase complexes with mammalian Atg14 and UVRAG. *Mol Biol Cell* 19, 5360-5372.

Itakura, E., Kishi-Itakura, C., and Mizushima, N. (2012). The hairpin-type tail-anchored SNARE syntaxin 17 targets to autophagosomes for fusion with endosomes/lysosomes. *Cell* 151, 1256-1269.

Ito, H., Atsuzawa, K., Sudo, K., Di Stefano, P., Iwamoto, I., Morishita, R., Takei, S., Semba, R., Defilippi, P., Asano, T., *et al.* (2008). Characterization of a multidomain adaptor protein, p140Cap, as part of a pre-synaptic complex. *J Neurochem* 107, 61-72.

Ito, H., Usuda, N., Atsuzawa, K., Iwamoto, I., Sudo, K., Katoh-Semba, R., Mizutani, K., Morishita, R., Deguchi, T., Nozawa, Y., *et al.* (2007). Phosphorylation by extracellular signal-regulated kinase of a multidomain adaptor protein, vinexin, at synapses. *J Neurochem* 100, 545-554.

Jager, S., Bucci, C., Tanida, I., Ueno, T., Kominami, E., Saftig, P., and Eskelinen, E.L. (2004). Role for Rab7 in maturation of late autophagic vacuoles. *J Cell Sci* 117, 4837-4848.

Jahreiss, L., Menzies, F.M., and Rubinsztein, D.C. (2008). The itinerary of autophagosomes: from peripheral formation to kiss-and-run fusion with lysosomes. *Traffic* 9, 574-587.

Jia, K., and Levine, B. (2007). Autophagy is required for dietary restriction-mediated life span extension in *C. elegans*. *Autophagy* 3, 597-599.

Jou, Y.S., Lee, C.S., Chang, Y.H., Hsiao, C.F., Chen, C.F., Chao, C.C., Wu, L.S., Yeh, S.H., Chen, D.S., and Chen, P.J. (2004). Clustering of minimal deleted regions reveals distinct genetic pathways of human hepatocellular carcinoma. *Cancer Res* 64, 3030-3036.

Jung, C.H., Jun, C.B., Ro, S.H., Kim, Y.M., Otto, N.M., Cao, J., Kundu, M., and Kim, D.H. (2009). ULK-Atg13-FIP200 complexes mediate mTOR signaling to the autophagy machinery. *Mol Biol Cell* 20, 1992-2003.

Jutten, B., and Rouschop, K.M. (2014). EGFR signaling and autophagy dependence for growth, survival, and therapy resistance. *Cell Cycle* 13, 42-51.

Kabeya, Y., Mizushima, N., Ueno, T., Yamamoto, A., Kirisako, T., Noda, T., Kominami, E., Ohsumi, Y., and Yoshimori, T. (2000). LC3, a mammalian homologue of yeast Apg8p, is localized in autophagosome membranes after processing. *Embo j* 19, 5720-5728.

Kallio, M.A., Tuimala, J.T., Hupponen, T., Klemela, P., Gentile, M., Scheinin, I., Koski, M., Kaki, J., and Korpelainen, E.I. (2011). Chipster: user-friendly analysis software for microarray and other high-throughput data. *BMC Genomics* *12*, 507.

Kanai, F., Marignani, P.A., Sarbassova, D., Yagi, R., Hall, R.A., Donowitz, M., Hisaminato, A., Fujiwara, T., Ito, Y., Cantley, L.C., *et al.* (2000). TAZ: a novel transcriptional co-activator regulated by interactions with 14-3-3 and PDZ domain proteins. *Embo j* *19*, 6778-6791.

Karantza-Wadsworth, V., Patel, S., Kravchuk, O., Chen, G., Mathew, R., Jin, S., and White, E. (2007). Autophagy mitigates metabolic stress and genome damage in mammary tumorigenesis. *Genes Dev* *21*, 1621-1635.

Kaushik, S., and Cuervo, A.M. (2012). Chaperone-mediated autophagy: a unique way to enter the lysosome world. *Trends Cell Biol* *22*, 407-417.

Kenific, C.M., Stehbens, S.J., Goldsmith, J., Leidal, A.M., Faure, N., Ye, J., Wittmann, T., and Debnath, J. (2016). NBR1 enables autophagy-dependent focal adhesion turnover. *J Cell Biol* *212*, 577-590.

Kim, E., Goraksha-Hicks, P., Li, L., Neufeld, T.P., and Guan, K.L. (2008). Regulation of TORC1 by Rag GTPases in nutrient response. *Nat Cell Biol* *10*, 935-945.

Kim, J., Kundu, M., Viollet, B., and Guan, K.L. (2011a). AMPK and mTOR regulate autophagy through direct phosphorylation of Ulk1. *Nat Cell Biol* *13*, 132-141.

Kim, M., Kim, T., Johnson, R.L., and Lim, D.S. (2015). Transcriptional co-repressor function of the hippo pathway transducers YAP and TAZ. *Cell Rep* *11*, 270-282.

Kim, M., Sandford, E., Gatica, D., Qiu, Y., Liu, X., Zheng, Y., Schulman, B.A., Xu, J., Semple, I., Ro, S.H., *et al.* (2016). Mutation in ATG5 reduces autophagy and leads to ataxia with developmental delay. *Elife* *5*.

Kim, N.G., Koh, E., Chen, X., and Gumbiner, B.M. (2011b). E-cadherin mediates contact inhibition of proliferation through Hippo signaling-pathway components. *Proc Natl Acad Sci U S A* *108*, 11930-11935.

Kimura, A., Baumann, C.A., Chiang, S.H., and Saltiel, A.R. (2001). The sorbin homology domain: a motif for the targeting of proteins to lipid rafts. *Proc Natl Acad Sci U S A* *98*, 9098-9103.

Kimura, S., Noda, T., and Yoshimori, T. (2007). Dissection of the autophagosome maturation process by a novel reporter protein, tandem fluorescent-tagged LC3. *Autophagy* *3*, 452-460.

Kioka, N., Ito, T., Yamashita, H., Uekawa, N., Umemoto, T., Motoyoshi, S., Imai, H., Takahashi, K., Watanabe, H., Yamada, M., *et al.* (2010). Crucial role of vinexin for keratinocyte migration in vitro and epidermal wound healing in vivo. *Exp Cell Res* *316*, 1728-1738.

Kioka, N., Sakata, S., Kawauchi, T., Amachi, T., Akiyama, S.K., Okazaki, K., Yaen, C., Yamada, K.M., and Aota, S. (1999). Vinexin: a novel vinculin-binding protein with multiple SH3 domains enhances actin cytoskeletal organization. *J Cell Biol* *144*, 59-69.

Kioka, N., Ueda, K., and Amachi, T. (2002). Vinexin, CAP/ponsin, ArgBP2: a novel adaptor protein family regulating cytoskeletal organization and signal transduction. *Cell Struct Funct* *27*, 1-7.

Kitada, T., Asakawa, S., Hattori, N., Matsumine, H., Yamamura, Y., Minoshima, S., Yokochi, M., Mizuno, Y., and Shimizu, N. (1998). Mutations in the parkin gene cause autosomal recessive juvenile parkinsonism. *Nature* *392*, 605-608.

Kitagawa, M. (2007). A Sveinsson's chorioretinal atrophy-associated missense mutation in mouse Tead1 affects its interaction with the co-factors YAP and TAZ. *Biochem Biophys Res Commun* *361*, 1022-1026.

Klionsky, D.J., Abdalla, F.C., Abeliovich, H., Abraham, R.T., Acevedo-Arozena, A., Adeli, K., Agholme, L., Agnello, M., Agostinis, P., Aguirre-Ghiso, J.A., *et al.* (2012). Guidelines for the use and interpretation of assays for monitoring autophagy. *Autophagy* 8, 445-544.

Klionsky, D.J., Cregg, J.M., Dunn, W.A., Jr., Emr, S.D., Sakai, Y., Sandoval, I.V., Sibirny, A., Subramani, S., Thumm, M., Veenhuis, M., *et al.* (2003). A unified nomenclature for yeast autophagy-related genes. In *Dev Cell (United States)*, pp. 539-545.

Knorr, R.L., Lipowsky, R., and Dimova, R. (2015). Autophagosome closure requires membrane scission. *Autophagy* 11, 2134-2137.

Kochl, R., Hu, X.W., Chan, E.Y., and Tooze, S.A. (2006). Microtubules facilitate autophagosome formation and fusion of autophagosomes with endosomes. *Traffic* 7, 129-145.

Komatsu, M., Waguri, S., Chiba, T., Murata, S., Iwata, J., Tanida, I., Ueno, T., Koike, M., Uchiyama, Y., Kominami, E., *et al.* (2006). Loss of autophagy in the central nervous system causes neurodegeneration in mice. *Nature* 441, 880-884.

Komatsu, M., Waguri, S., Ueno, T., Iwata, J., Murata, S., Tanida, I., Ezaki, J., Mizushima, N., Ohsumi, Y., Uchiyama, Y., *et al.* (2005). Impairment of starvation-induced and constitutive autophagy in Atg7-deficient mice. *J Cell Biol* 169, 425-434.

Korolchuk, V.I., Saiki, S., Lichtenberg, M., Siddiqi, F.H., Roberts, E.A., Imarisio, S., Jahreiss, L., Sarkar, S., Futter, M., Menzies, F.M., *et al.* (2011). Lysosomal positioning coordinates cellular nutrient responses. *Nat Cell Biol* 13, 453-460.

Kovacs, M., Toth, J., Hetenyi, C., Malnasi-Csizmadia, A., and Sellers, J.R. (2004). Mechanism of blebbistatin inhibition of myosin II. *J Biol Chem* 279, 35557-35563.

Kuma, A., Hatano, M., Matsui, M., Yamamoto, A., Nakaya, H., Yoshimori, T., Ohsumi, Y., Tokuhi, T., and Mizushima, N. (2004). The role of autophagy during the early neonatal starvation period. *Nature* 432, 1032-1036.

Kunz, J.B., Schwarz, H., and Mayer, A. (2004). Determination of four sequential stages during microautophagy in vitro. *J Biol Chem* 279, 9987-9996.

Lau, A.N., Curtis, S.J., Fillmore, C.M., Rowbotham, S.P., Mohseni, M., Wagner, D.E., Beede, A.M., Montoro, D.T., Sinkevicius, K.W., Walton, Z.E., *et al.* (2014). Tumor-propagating cells and Yap/Taz activity contribute to lung tumor progression and metastasis. *Embo j* 33, 468-481.

Lazarou, M., Sliter, D.A., Kane, L.A., Sarraf, S.A., Wang, C., Burman, J.L., Sideris, D.P., Fogel, A.I., and Youle, R.J. (2015). The ubiquitin kinase PINK1 recruits autophagy receptors to induce mitophagy. *Nature* 524, 309-314.

Lee, H.K., Lund, J.M., Ramanathan, B., Mizushima, N., and Iwasaki, A. (2007). Autophagy-dependent viral recognition by plasmacytoid dendritic cells. *Science* 315, 1398-1401.

Lee, H.K., Mattei, L.M., Steinberg, B.E., Alberts, P., Lee, Y.H., Chervonsky, A., Mizushima, N., Grinstein, S., and Iwasaki, A. (2010a). In vivo requirement for Atg5 in antigen presentation by dendritic cells. *Immunity* 32, 227-239.

Lee, J.M., Wagner, M., Xiao, R., Kim, K.H., Feng, D., Lazar, M.A., and Moore, D.D. (2014). Nutrient-sensing nuclear receptors coordinate autophagy. *Nature* 516, 112-115.

Lee, K.P., Lee, J.H., Kim, T.S., Kim, T.H., Park, H.D., Byun, J.S., Kim, M.C., Jeong, W.I., Calvisi, D.F., Kim, J.M., *et al.* (2010b). The Hippo-Salvador pathway restrains hepatic oval cell proliferation, liver size, and liver tumorigenesis. *Proc Natl Acad Sci U S A* 107, 8248-8253.

Lei, Q.Y., Zhang, H., Zhao, B., Zha, Z.Y., Bai, F., Pei, X.H., Zhao, S., Xiong, Y., and Guan, K.L. (2008). TAZ promotes cell proliferation and epithelial-mesenchymal transition and is inhibited by the hippo pathway. *Mol Cell Biol* 28, 2426-2436.

Leng, Y., Zhang, J., Badour, K., Arpaia, E., Freeman, S., Cheung, P., Siu, M., and Siminovitch, K. (2005). Abelson-interactor-1 promotes WAVE2 membrane translocation and

Abelson-mediated tyrosine phosphorylation required for WAVE2 activation. *Proc Natl Acad Sci U S A* *102*, 1098-1103.

Levy, D., Adamovich, Y., Reuven, N., and Shaul, Y. (2008). Yap1 phosphorylation by c-Abl is a critical step in selective activation of proapoptotic genes in response to DNA damage. *Mol Cell* *29*, 350-361.

Li, M., Guo, S., Zhang, P., Gong, J., Zheng, A., Zhang, Y., and Li, H. (2015). Vinexin-beta deficiency protects against cerebral ischaemia/reperfusion injury by inhibiting neuronal apoptosis. *J Neurochem* *134*, 211-221.

Li, W.W., Li, J., and Bao, J.K. (2012). Microautophagy: lesser-known self-eating. *Cell Mol Life Sci* *69*, 1125-1136.

Li, Z., Zhao, B., Wang, P., Chen, F., Dong, Z., Yang, H., Guan, K.L., and Xu, Y. (2010). Structural insights into the YAP and TEAD complex. *Genes Dev* *24*, 235-240.

Lian, I., Kim, J., Okazawa, H., Zhao, J., Zhao, B., Yu, J., Chinnaiyan, A., Israel, M.A., Goldstein, L.S., Abujarour, R., *et al.* (2010). The role of YAP transcription coactivator in regulating stem cell self-renewal and differentiation. *Genes Dev* *24*, 1106-1118.

Liang, C., Lee, J.S., Inn, K.S., Gack, M.U., Li, Q., Roberts, E.A., Vergne, I., Deretic, V., Feng, P., Akazawa, C., *et al.* (2008a). Beclin1-binding UVRAG targets the class C Vps complex to coordinate autophagosome maturation and endocytic trafficking. *Nat Cell Biol* *10*, 776-787.

Liang, N., Zhang, C., Dill, P., Panasyuk, G., Pion, D., Koka, V., Gallazzini, M., Olson, E.N., Lam, H., Henske, E.P., *et al.* (2014). Regulation of YAP by mTOR and autophagy reveals a therapeutic target of tuberous sclerosis complex. *J Exp Med* *211*, 2249-2263.

Liang, W.S., Reiman, E.M., Valla, J., Dunckley, T., Beach, T.G., Grover, A., Niedzielko, T.L., Schneider, L.E., Mastroeni, D., Caselli, R., *et al.* (2008b). Alzheimer's disease is associated with reduced expression of energy metabolism genes in posterior cingulate neurons. *Proc Natl Acad Sci U S A* *105*, 4441-4446.

Liang, X.H., Jackson, S., Seaman, M., Brown, K., Kempkes, B., Hibshoosh, H., and Levine, B. (1999). Induction of autophagy and inhibition of tumorigenesis by beclin 1. *Nature* *402*, 672-676.

Liao, J.K. (2002). Isoprenoids as mediators of the biological effects of statins. *J Clin Invest* *110*, 285-288.

Lin, F., Ghislat, G., Luo, S., Renna, M., Siddiqi, F., and Rubinsztein, D.C. (2015). XIAP and cIAP1 amplifications induce Beclin 1-dependent autophagy through NFkappaB activation. *Hum Mol Genet* *24*, 2899-2913.

Lin, F., Hiesberger, T., Cordes, K., Sinclair, A.M., Goldstein, L.S., Somlo, S., and Igarashi, P. (2003). Kidney-specific inactivation of the KIF3A subunit of kinesin-II inhibits renal ciliogenesis and produces polycystic kidney disease. *Proc Natl Acad Sci U S A* *100*, 5286-5291.

Lin, M.G., and Hurley, J.H. (2016). Structure and function of the ULK1 complex in autophagy. *Curr Opin Cell Biol* *39*, 61-68.

Lingwood, D., and Simons, K. (2010). Lipid rafts as a membrane-organizing principle. *Science* *327*, 46-50.

Lipinski, M.M., Hoffman, G., Ng, A., Zhou, W., Py, B.F., Hsu, E., Liu, X., Eisenberg, J., Liu, J., Blenis, J., *et al.* (2010a). A genome-wide siRNA screen reveals multiple mTORC1 independent signaling pathways regulating autophagy under normal nutritional conditions. In *Dev Cell* (United States: 2010 Elsevier Inc), pp. 1041-1052.

Lipinski, M.M., Zheng, B., Lu, T., Yan, Z., Py, B.F., Ng, A., Xavier, R.J., Li, C., Yankner, B.A., Scherzer, C.R., *et al.* (2010b). Genome-wide analysis reveals mechanisms modulating autophagy in normal brain aging and in Alzheimer's disease. *Proc Natl Acad Sci U S A* *107*, 14164-14169.

Liu, C.Y., Zha, Z.Y., Zhou, X., Zhang, H., Huang, W., Zhao, D., Li, T., Chan, S.W., Lim, C.J., Hong, W., *et al.* (2010). The hippo tumor pathway promotes TAZ degradation by phosphorylating a phosphodegron and recruiting the SCF $\beta$ -TrCP E3 ligase. *J Biol Chem* 285, 37159-37169.

Liu, X., Wan, N., Zhang, X.J., Zhao, Y., Zhang, Y., Hu, G., Wan, F., Zhang, R., Zhu, X., Xia, H., *et al.* (2015). Vinexin-beta exacerbates cardiac dysfunction post-myocardial infarction via mediating apoptotic and inflammatory responses. *Clin Sci (Lond)* 128, 923-936.

Loerch, P.M., Lu, T., Dakin, K.A., Vann, J.M., Isaacs, A., Geula, C., Wang, J., Pan, Y., Gabuzda, D.H., Li, C., *et al.* (2008). Evolution of the aging brain transcriptome and synaptic regulation. *PLoS One* 3, e3329.

Lonskaya, I., Hebron, M.L., Algarzae, N.K., Desforges, N., and Moussa, C.E. (2012). Decreased parkin solubility is associated with impairment of autophagy in the nigrostriatum of sporadic Parkinson's disease. *Neuroscience* 232c, 90.

Lu, L., Li, Y., Kim, S.M., Bossuyt, W., Liu, P., Qiu, Q., Wang, Y., Halder, G., Finegold, M.J., Lee, J.S., *et al.* (2010). Hippo signaling is a potent in vivo growth and tumor suppressor pathway in the mammalian liver. *Proc Natl Acad Sci U S A* 107, 1437-1442.

Lv, M., Shen, Y., Yang, J., Li, S., Wang, B., Chen, Z., Li, P., and Liu, P. (2017). Angiotensin Family Members: Oncogenes or Tumor Suppressors? *Int J Biol Sci* 13, 772-781.

Maejima, Y., Kyoji, S., Zhai, P., Liu, T., Li, H., Ivessa, A., Sciarretta, S., Del Re, D.P., Zablocki, D.K., Hsu, C.P., *et al.* (2013). Mst1 inhibits autophagy by promoting the interaction between Beclin1 and Bcl-2. *Nat Med* 19, 1478-1488.

Mahoney, W.M., Jr., Hong, J.H., Yaffe, M.B., and Farrance, I.K. (2005). The transcriptional co-activator TAZ interacts differentially with transcriptional enhancer factor-1 (TEF-1) family members. *Biochem J* 388, 217-225.

Maiuri, M.C., Le Toumelin, G., Criollo, A., Rain, J.C., Gautier, F., Juin, P., Tasdemir, E., Pierron, G., Troulinaki, K., Tavernarakis, N., *et al.* (2007). Functional and physical interaction between Bcl-X(L) and a BH3-like domain in Beclin-1. *Embo j* 26, 2527-2539.

Makita, R., Uchijima, Y., Nishiyama, K., Amano, T., Chen, Q., Takeuchi, T., Mitani, A., Nagase, T., Yatomi, Y., Aburatani, H., *et al.* (2008). Multiple renal cysts, urinary concentration defects, and pulmonary emphysematous changes in mice lacking TAZ. *Am J Physiol Renal Physiol* 294, F542-553.

Malmquist, S.J., Abramsson, A., McGraw, H.F., Linbo, T.H., and Raible, D.W. (2013). Modulation of dorsal root ganglion development by ErbB signaling and the scaffold protein Sorbs3. In *Development (England)*, pp. 3986-3996.

Mana-Capelli, S., Paramasivam, M., Dutta, S., and McCollum, D. (2014). Angiotensins link F-actin architecture to Hippo pathway signaling. *Mol Biol Cell* 25, 1676-1685.

Manderfield, L.J., Engleka, K.A., Aghajanian, H., Gupta, M., Yang, S., Li, L., Baggs, J.E., Hogenesch, J.B., Olson, E.N., and Epstein, J.A. (2014). Pax3 and hippo signaling coordinate melanocyte gene expression in neural crest. *Cell Rep* 9, 1885-1895.

Manzanillo, P.S., Ayres, J.S., Watson, R.O., Collins, A.C., Souza, G., Rae, C.S., Schneider, D.S., Nakamura, K., Shiloh, M.U., and Cox, J.S. (2013). The ubiquitin ligase parkin mediates resistance to intracellular pathogens. *Nature* 501, 512-516.

Matecic, M., Smith, D.L., Pan, X., Maqani, N., Bekiranov, S., Boeke, J.D., and Smith, J.S. (2010). A microarray-based genetic screen for yeast chronological aging factors. *PLoS Genet* 6, e1000921.

Mathew, R., Karp, C.M., Beaudoin, B., Vuong, N., Chen, G., Chen, H.Y., Bray, K., Reddy, A., Bhanot, G., Gelinas, C., *et al.* (2009). Autophagy suppresses tumorigenesis through elimination of p62. *Cell* 137, 1062-1075.

Mathew, R., Kongara, S., Beaudoin, B., Karp, C.M., Bray, K., Degenhardt, K., Chen, G., Jin, S., and White, E. (2007). Autophagy suppresses tumor progression by limiting chromosomal instability. *Genes Dev* *21*, 1367-1381.

Matsuda, N., Sato, S., Shiba, K., Okatsu, K., Saisho, K., Gautier, C.A., Sou, Y.S., Saiki, S., Kawajiri, S., Sato, F., *et al.* (2010). PINK1 stabilized by mitochondrial depolarization recruits Parkin to damaged mitochondria and activates latent Parkin for mitophagy. *J Cell Biol* *189*, 211-221.

Matsunaga, K., Saitoh, T., Tabata, K., Omori, H., Satoh, T., Kurotori, N., Maejima, I., Shirahama-Noda, K., Ichimura, T., Isobe, T., *et al.* (2009). Two Beclin 1-binding proteins, Atg14L and Rubicon, reciprocally regulate autophagy at different stages. *Nat Cell Biol* *11*, 385-396.

Matsuyama, M., Mizusaki, H., Shimono, A., Mukai, T., Okumura, K., Abe, K., Shimada, K., and Morohashi, K. (2005). A novel isoform of Vinexin, Vinexin gamma, regulates Sox9 gene expression through activation of MAPK cascade in mouse fetal gonad. *Genes Cells* *10*, 421-434.

McEwan, D.G., Popovic, D., Gubas, A., Terawaki, S., Suzuki, H., Stadel, D., Coxon, F.P., Miranda de Stegmann, D., Bhogaraju, S., Maddi, K., *et al.* (2015). PLEKHM1 regulates autophagosome-lysosome fusion through HOPS complex and LC3/GABARAP proteins. *Mol Cell* *57*, 39-54.

Mele, M., Ferreira, P.G., Reverter, F., DeLuca, D.S., Monlong, J., Sammeth, M., Young, T.R., Goldmann, J.M., Pervouchine, D.D., Sullivan, T.J., *et al.* (2015). Human genomics. The human transcriptome across tissues and individuals. *Science* *348*, 660-665.

Melendez, A., Tallozy, Z., Seaman, M., Eskelinen, E.L., Hall, D.H., and Levine, B. (2003). Autophagy genes are essential for dauer development and life-span extension in *C. elegans*. *Science* *301*, 1387-1391.

Mercer, C.A., Kaliappan, A., and Dennis, P.B. (2009). A novel, human Atg13 binding protein, Atg101, interacts with ULK1 and is essential for macroautophagy. *Autophagy* *5*, 649-662.

Mira, M.T., Alcasis, A., Nguyen, V.T., Moraes, M.O., Di Flumeri, C., Vu, H.T., Mai, C.P., Nguyen, T.H., Nguyen, N.B., Pham, X.K., *et al.* (2004). Susceptibility to leprosy is associated with PARK2 and PACRG. *Nature* *427*, 636-640.

Mitani, A., Nagase, T., Fukuchi, K., Aburatani, H., Makita, R., and Kurihara, H. (2009). Transcriptional coactivator with PDZ-binding motif is essential for normal alveolarization in mice. *Am J Respir Crit Care Med* *180*, 326-338.

Mitchener, J.S., Shelburne, J.D., Bradford, W.D., and Hawkins, H.K. (1976). Cellular autophagocytosis induced by deprivation of serum and amino acids in HeLa cells. *Am J Pathol* *83*, 485-492.

Mitchison, T.J., and Cramer, L.P. (1996). Actin-based cell motility and cell locomotion. *Cell* *84*, 371-379.

Mitsushima, M., Sezaki, T., Akahane, R., Ueda, K., Suetsugu, S., Takenawa, T., and Kioka, N. (2006a). Protein kinase A-dependent increase in WAVE2 expression induced by the focal adhesion protein vinexin. *Genes Cells* *11*, 281-292.

Mitsushima, M., Suwa, A., Amachi, T., Ueda, K., and Kioka, N. (2004). Extracellular signal-regulated kinase activated by epidermal growth factor and cell adhesion interacts with and phosphorylates vinexin. In *J Biol Chem (United States)*, pp. 34570-34577.

Mitsushima, M., Takahashi, H., Shishido, T., Ueda, K., and Kioka, N. (2006b). Abl kinase interacts with and phosphorylates vinexin. *FEBS Lett* *580*, 4288-4295.

Mitsushima, M., Ueda, K., and Kioka, N. (2006c). Vinexin beta regulates the phosphorylation of epidermal growth factor receptor on the cell surface. *Genes Cells* *11*, 971-982.

Mitsushima, M., Ueda, K., and Kioka, N. (2007). Involvement of phosphatases in the anchorage-dependent regulation of ERK2 activation. *Exp Cell Res* 313, 1830-1838.

Mizushima, N., Kuma, A., Kobayashi, Y., Yamamoto, A., Matsubae, M., Takao, T., Natsume, T., Ohsumi, Y., and Yoshimori, T. (2003). Mouse Apg16L, a novel WD-repeat protein, targets to the autophagic isolation membrane with the Apg12-Apg5 conjugate. *J Cell Sci* 116, 1679-1688.

Mizushima, N., Noda, T., Yoshimori, T., Tanaka, Y., Ishii, T., George, M.D., Klionsky, D.J., Ohsumi, M., and Ohsumi, Y. (1998). A protein conjugation system essential for autophagy. *Nature* 395, 395-398.

Mizushima, N., Yamamoto, A., Hatano, M., Kobayashi, Y., Kabeya, Y., Suzuki, K., Tokuhi, T., Ohsumi, Y., and Yoshimori, T. (2001). Dissection of autophagosome formation using Apg5-deficient mouse embryonic stem cells. *J Cell Biol* 152, 657-668.

Mizutani, K., Ito, H., Iwamoto, I., Morishita, R., Deguchi, T., Nozawa, Y., Asano, T., and Nagata, K.I. (2007a). Essential roles of ERK-mediated phosphorylation of vinexin in cell spreading, migration and anchorage-independent growth. *Oncogene* 26, 7122-7131.

Mizutani, K., Nagata, K., Ito, H., Ehara, H., Nozawa, Y., and Deguchi, T. (2007b). Possible roles of vinexinbeta in growth and paclitaxel sensitivity in human prostate cancer PC-3 cells. *Cancer Biol Ther* 6, 1800-1804.

Mohler, P.J., Kreda, S.M., Boucher, R.C., Sudol, M., Stutts, M.J., and Milgram, S.L. (1999). Yes-associated protein 65 localizes p62(c-Yes) to the apical compartment of airway epithelia by association with EBP50. *J Cell Biol* 147, 879-890.

Moreau, K., Ghislat, G., Hochfeld, W., Renna, M., Zavodszky, E., Runwal, G., Puri, C., Lee, S., Siddiqi, F., Menzies, F.M., *et al.* (2015). Transcriptional regulation of Annexin A2 promotes starvation-induced autophagy. *Nat Commun* 6, 8045.

Moreau, K., Ravikumar, B., Renna, M., Puri, C., and Rubinsztein, D.C. (2011). Autophagosome precursor maturation requires homotypic fusion. *Cell* 146, 303-317.

Morin-Kensicki, E.M., Boone, B.N., Howell, M., Stonebraker, J.R., Teed, J., Alb, J.G., Magnuson, T.R., O'Neal, W., and Milgram, S.L. (2006). Defects in yolk sac vasculogenesis, chorioallantoic fusion, and embryonic axis elongation in mice with targeted disruption of Yap65. *Mol Cell Biol* 26, 77-87.

Moroishi, T., Hansen, C.G., and Guan, K.L. (2015). The emerging roles of YAP and TAZ in cancer. *Nat Rev Cancer* 15, 73-79.

Mortimore, G.E., and Schworer, C.M. (1977). Induction of autophagy by amino-acid deprivation in perfused rat liver. *Nature* 270, 174-176.

Mowers, E.E., Sharifi, M.N., and Macleod, K.F. (2017). Autophagy in cancer metastasis. *Oncogene* 36, 1619-1630.

Muller, O., Sattler, T., Flotenmeyer, M., Schwarz, H., Plattner, H., and Mayer, A. (2000). Autophagic tubes: vacuolar invaginations involved in lateral membrane sorting and inverse vesicle budding. *J Cell Biol* 151, 519-528.

Murakami, M., Nakagawa, M., Olson, E.N., and Nakagawa, O. (2005). A WW domain protein TAZ is a critical coactivator for TBX5, a transcription factor implicated in Holt-Oram syndrome. *Proc Natl Acad Sci U S A* 102, 18034-18039.

Murakami, M., Tominaga, J., Makita, R., Uchijima, Y., Kurihara, Y., Nakagawa, O., Asano, T., and Kurihara, H. (2006). Transcriptional activity of Pax3 is co-activated by TAZ. *Biochem Biophys Res Commun* 339, 533-539.

Nagai, H., Pineau, P., Tiollais, P., Buendia, M.A., and Dejean, A. (1997). Comprehensive allelotyping of human hepatocellular carcinoma. *Oncogene* 14, 2927-2933.

Nagasato, A.I., Yamashita, H., Matsuo, M., Ueda, K., and Kioka, N. (2017). The distribution of vinculin to lipid rafts plays an important role in sensing stiffness of extracellular matrix. *Biosci Biotechnol Biochem* 81, 1136-1147.

Nagata, K., Ito, H., Iwamoto, I., Morishita, R., and Asano, T. (2009). Interaction of a multi-domain adaptor protein, vinexin, with a Rho-effector, Rhotekin. *Med Mol Morphol* *42*, 9-15.

Nakagawa, I., Amano, A., Mizushima, N., Yamamoto, A., Yamaguchi, H., Kamimoto, T., Nara, A., Funao, J., Nakata, M., Tsuda, K., *et al.* (2004). Autophagy defends cells against invading group A *Streptococcus*. *Science* *306*, 1037-1040.

Nardone, G., Oliver-De La Cruz, J., Vrbsky, J., Martini, C., Pribyl, J., Skladal, P., Pesl, M., Caluori, G., Pagliari, S., Martino, F., *et al.* (2017). YAP regulates cell mechanics by controlling focal adhesion assembly. *Nat Commun* *8*, 15321.

Narendra, D., Tanaka, A., Suen, D.F., and Youle, R.J. (2008). Parkin is recruited selectively to impaired mitochondria and promotes their autophagy. *J Cell Biol* *183*, 795-803.

Nedjic, J., Aichinger, M., Emmerich, J., Mizushima, N., and Klein, L. (2008). Autophagy in thymic epithelium shapes the T-cell repertoire and is essential for tolerance. *Nature* *455*, 396-400.

Nilsson, P., Loganathan, K., Sekiguchi, M., Matsuba, Y., Hui, K., Tsubuki, S., Tanaka, M., Iwata, N., Saito, T., and Saido, T.C. (2013). Abeta secretion and plaque formation depend on autophagy. *Cell Rep* *5*, 61-69.

Nishioka, N., Inoue, K., Adachi, K., Kiyonari, H., Ota, M., Ralston, A., Yabuta, N., Hirahara, S., Stephenson, R.O., Ogonuki, N., *et al.* (2009). The Hippo signaling pathway components Lats and Yap pattern Tead4 activity to distinguish mouse trophectoderm from inner cell mass. *Dev Cell* *16*, 398-410.

Oberstein, A., Jeffrey, P.D., and Shi, Y. (2007). Crystal structure of the Bcl-XL-Beclin 1 peptide complex: Beclin 1 is a novel BH3-only protein. *J Biol Chem* *282*, 13123-13132.

Oka, T., Mazack, V., and Sudol, M. (2008). Mst2 and Lats kinases regulate apoptotic function of Yes kinase-associated protein (YAP). *J Biol Chem* *283*, 27534-27546.

Oka, T., and Sudol, M. (2009). Nuclear localization and pro-apoptotic signaling of YAP2 require intact PDZ-binding motif. *Genes Cells* *14*, 607-615.

Ono, Y., and Sorimachi, H. (2012). Calpains: an elaborate proteolytic system. *Biochim Biophys Acta* *1824*, 224-236.

Ota, M., and Sasaki, H. (2008). Mammalian Tead proteins regulate cell proliferation and contact inhibition as transcriptional mediators of Hippo signaling. *Development* *135*, 4059-4069.

Paludan, C., Schmid, D., Landthaler, M., Vockerodt, M., Kube, D., Tuschl, T., and Munz, C. (2005). Endogenous MHC class II processing of a viral nuclear antigen after autophagy. *Science* *307*, 593-596.

Pankiv, S., Alemu, E.A., Brech, A., Bruun, J.A., Lamark, T., Overvatn, A., Bjorkoy, G., and Johansen, T. (2010). FYCO1 is a Rab7 effector that binds to LC3 and PI3P to mediate microtubule plus end-directed vesicle transport. *J Cell Biol* *188*, 253-269.

Pankiv, S., Clausen, T.H., Lamark, T., Brech, A., Bruun, J.A., Outzen, H., Overvatn, A., Bjorkoy, G., and Johansen, T. (2007). p62/SQSTM1 binds directly to Atg8/LC3 to facilitate degradation of ubiquitinated protein aggregates by autophagy. *J Biol Chem* *282*, 24131-24145.

Paramasivam, M., Sarkeshik, A., Yates, J.R., 3rd, Fernandes, M.J., and McCollum, D. (2011). Angiomotin family proteins are novel activators of the LATS2 kinase tumor suppressor. *Mol Biol Cell* *22*, 3725-3733.

Park, K.S., Whitsett, J.A., Di Palma, T., Hong, J.H., Yaffe, M.B., and Zannini, M. (2004). TAZ interacts with TTF-1 and regulates expression of surfactant protein-C. *J Biol Chem* *279*, 17384-17390.

Patel, N.R., Salim, A.A., Sayeed, H., Sarabia, S.F., Hollingsworth, F., Warren, M., Jakacky, J., Tanas, M., Oliveira, A.M., Rubin, B.P., *et al.* (2015). Molecular characterization of

epithelioid haemangioendotheliomas identifies novel WWTR1-CAMTA1 fusion variants. *Histopathology* 67, 699-708.

Pattingre, S., Tassa, A., Qu, X., Garuti, R., Liang, X.H., Mizushima, N., Packer, M., Schneider, M.D., and Levine, B. (2005). Bcl-2 antiapoptotic proteins inhibit Beclin 1-dependent autophagy. *Cell* 122, 927-939.

Pavel, M., Imarisio, S., Menzies, F.M., Jimenez-Sanchez, M., Siddiqi, F.H., Wu, X., Renna, M., O'Kane, C.J., Crowther, D.C., and Rubinsztein, D.C. (2016). CCT complex restricts neuropathogenic protein aggregation via autophagy. *Nat Commun* 7, 13821.

Paz, M., Lopez-Casas, P.P., and Mazo, J. (2007). Changes in vinexin expression patterns in the mouse testis induced by developmental exposure to 17beta-estradiol. *Biol Reprod* 77, 605-613.

Pena-Llopis, S., Vega-Rubin-de-Celis, S., Schwartz, J.C., Wolff, N.C., Tran, T.A., Zou, L., Xie, X.J., Corey, D.R., and Brugarolas, J. (2011). Regulation of TFEB and V-ATPases by mTORC1. *Embo j* 30, 3242-3258.

Peng, Y.F., Shi, Y.H., Ding, Z.B., Ke, A.W., Gu, C.Y., Hui, B., Zhou, J., Qiu, S.J., Dai, Z., and Fan, J. (2013). Autophagy inhibition suppresses pulmonary metastasis of HCC in mice via impairing anoikis resistance and colonization of HCC cells. *Autophagy* 9, 2056-2068.

Pengo, N., Scolari, M., Oliva, L., Milan, E., Mainoldi, F., Raimondi, A., Fagioli, C., Merlini, A., Mariani, E., Pasqualetto, E., *et al.* (2013). Plasma cells require autophagy for sustainable immunoglobulin production. *Nat Immunol* 14, 298-305.

Piccolo, S., Dupont, S., and Cordenonsi, M. (2014). The biology of YAP/TAZ: hippo signaling and beyond. *Physiol Rev* 94, 1287-1312.

Pickford, F., Masliah, E., Britschgi, M., Lucin, K., Narasimhan, R., Jaeger, P.A., Small, S., Spencer, B., Rockenstein, E., Levine, B., *et al.* (2008). The autophagy-related protein beclin 1 shows reduced expression in early Alzheimer disease and regulates amyloid beta accumulation in mice. *J Clin Invest* 118, 2190-2199.

Ploeger, C., Waldburger, N., Fraas, A., Goepfert, B., Pusch, S., Breuhahn, K., Wang, X.W., Schirmacher, P., and Roessler, S. (2016). Chromosome 8p tumor suppressor genes SH2D4A and SORBS3 cooperate to inhibit interleukin-6 signaling in hepatocellular carcinoma. *Hepatology* 64, 828-842.

Plouffe, S.W., Hong, A.W., and Guan, K.L. (2015). Disease implications of the Hippo/YAP pathway. *Trends Mol Med* 21, 212-222.

Praskova, M., Xia, F., and Avruch, J. (2008). MOBKL1A/MOBKL1B phosphorylation by MST1 and MST2 inhibits cell proliferation. *Curr Biol* 18, 311-321.

Puri, C., Renna, M., Bento, C.F., Moreau, K., and Rubinsztein, D.C. (2013). Diverse autophagosome membrane sources coalesce in recycling endosomes. *Cell* 154, 1285-1299.

Pyo, J.O., Yoo, S.M., Ahn, H.H., Nah, J., Hong, S.H., Kam, T.I., Jung, S., and Jung, Y.K. (2013). Overexpression of Atg5 in mice activates autophagy and extends lifespan. *Nat Commun* 4, 2300.

Qu, X., Zou, Z., Sun, Q., Luby-Phelps, K., Cheng, P., Hogan, R.N., Gilpin, C., and Levine, B. (2007). Autophagy gene-dependent clearance of apoptotic cells during embryonic development. *Cell* 128, 931-946.

Ragni, C.V., Diguet, N., Le Garrec, J.F., Novotova, M., Resende, T.P., Pop, S., Charon, N., Guillemot, L., Kitasato, L., Badouel, C., *et al.* (2017). Amotl1 mediates sequestration of the Hippo effector Yap1 downstream of Fat4 to restrict heart growth. *Nat Commun* 8, 14582.

Ran, F.A., Hsu, P.D., Lin, C.Y., Gootenberg, J.S., Konermann, S., Trevino, A.E., Scott, D.A., Inoue, A., Matoba, S., Zhang, Y., *et al.* (2013a). Double nicking by RNA-guided CRISPR Cas9 for enhanced genome editing specificity. *Cell* 154, 1380-1389.

Ran, F.A., Hsu, P.D., Wright, J., Agarwala, V., Scott, D.A., and Zhang, F. (2013b). Genome engineering using the CRISPR-Cas9 system. *Nat Protoc* 8, 2281-2308.

Ravikumar, B., Acevedo-Arozena, A., Imarisio, S., Berger, Z., Vacher, C., O'Kane, C.J., Brown, S.D., and Rubinsztein, D.C. (2005). Dynein mutations impair autophagic clearance of aggregate-prone proteins. *Nat Genet* *37*, 771-776.

Ravikumar, B., Berger, Z., Vacher, C., O'Kane, C.J., and Rubinsztein, D.C. (2006). Rapamycin pre-treatment protects against apoptosis. *Hum Mol Genet* *15*, 1209-1216.

Ravikumar, B., Duden, R., and Rubinsztein, D.C. (2002). Aggregate-prone proteins with polyglutamine and polyalanine expansions are degraded by autophagy. *Hum Mol Genet* *11*, 1107-1117.

Ravikumar, B., Moreau, K., Jahreiss, L., Puri, C., and Rubinsztein, D.C. (2010a). Plasma membrane contributes to the formation of pre-autophagosomal structures. *Nat Cell Biol* *12*, 747-757.

Ravikumar, B., Sarkar, S., Davies, J.E., Futter, M., Garcia-Arencibia, M., Green-Thompson, Z.W., Jimenez-Sanchez, M., Korolchuk, V.I., Lichtenberg, M., Luo, S., *et al.* (2010b). Regulation of mammalian autophagy in physiology and pathophysiology. *Physiol Rev* *90*, 1383-1435.

Reginensi, A., Scott, R.P., Gregorieff, A., Bagherie-Lachidan, M., Chung, C., Lim, D.S., Pawson, T., Wrana, J., and McNeill, H. (2013). Yap- and Cdc42-dependent nephrogenesis and morphogenesis during mouse kidney development. *PLoS Genet* *9*, e1003380.

Reid, T., Furuyashiki, T., Ishizaki, T., Watanabe, G., Watanabe, N., Fujisawa, K., Morii, N., Madaule, P., and Narumiya, S. (1996). Rhotekin, a new putative target for Rho bearing homology to a serine/threonine kinase, PKN, and rhotillin in the rho-binding domain. *J Biol Chem* *271*, 13556-13560.

Ridley, A.J., Schwartz, M.A., Burridge, K., Firtel, R.A., Ginsberg, M.H., Borisy, G., Parsons, J.T., and Horwitz, A.R. (2003). Cell migration: integrating signals from front to back. *Science* *302*, 1704-1709.

Rioux, J.D., Xavier, R.J., Taylor, K.D., Silverberg, M.S., Goyette, P., Huett, A., Green, T., Kuballa, P., Barmada, M.M., Datta, L.W., *et al.* (2007). Genome-wide association study identifies new susceptibility loci for Crohn disease and implicates autophagy in disease pathogenesis. *Nat Genet* *39*, 596-604.

Ritchie, M.E., Phipson, B., Wu, D., Hu, Y., Law, C.W., Shi, W., and Smyth, G.K. (2015). limma powers differential expression analyses for RNA-sequencing and microarray studies. *Nucleic Acids Res* *43*, e47.

Ritchie, M.E., Silver, J., Oshlack, A., Holmes, M., Diyagama, D., Holloway, A., and Smyth, G.K. (2007). A comparison of background correction methods for two-colour microarrays. *Bioinformatics* *23*, 2700-2707.

Rizzo, M.A., Davidson, M.W., and Piston, D.W. (2009). Fluorescent protein tracking and detection: fluorescent protein structure and color variants. *Cold Spring Harb Protoc* *2009*, pdb.top63.

Rocchi, A., Yamamoto, S., Ting, T., Fan, Y., Sadleir, K., Wang, Y., Zhang, W., Huang, S., Levine, B., Vassar, R., *et al.* (2017). A *Becn1* mutation mediates hyperactive autophagic sequestration of amyloid oligomers and improved cognition in Alzheimer's disease. *PLoS Genet* *13*, e1006962.

Roczniak-Ferguson, A., Petit, C.S., Froehlich, F., Qian, S., Ky, J., Angarola, B., Walther, T.C., and Ferguson, S.M. (2012). The transcription factor TFEB links mTORC1 signaling to transcriptional control of lysosome homeostasis. *Sci Signal* *5*, ra42.

Roessler, S., Long, E.L., Budhu, A., Chen, Y., Zhao, X., Ji, J., Walker, R., Jia, H.L., Ye, Q.H., Qin, L.X., *et al.* (2012). Integrative genomic identification of genes on 8p associated with hepatocellular carcinoma progression and patient survival. *Gastroenterology* *142*, 957-966.e912.

Rohatgi, R., Ma, L., Miki, H., Lopez, M., Kirchhausen, T., Takenawa, T., and Kirschner, M.W. (1999). The interaction between N-WASP and the Arp2/3 complex links Cdc42-dependent signals to actin assembly. *Cell* 97, 221-231.

Rohn, T.T., Wirawan, E., Brown, R.J., Harris, J.R., Masliah, E., and Vandenabeele, P. (2011). Depletion of Beclin-1 due to proteolytic cleavage by caspases in the Alzheimer's disease brain. *Neurobiol Dis* 43, 68-78.

Rose, C., Menzies, F.M., Renna, M., Acevedo-Arozena, A., Corrochano, S., Sadiq, O., Brown, S.D., and Rubinsztein, D.C. (2010). Rilmenidine attenuates toxicity of polyglutamine expansions in a mouse model of Huntington's disease. *Hum Mol Genet* 19, 2144-2153.

Rosenbluh, J., Nijhawan, D., Cox, A.G., Li, X., Neal, J.T., Schafer, E.J., Zack, T.I., Wang, X., Tsherniak, A., Schinzel, A.C., *et al.* (2012). beta-Catenin-driven cancers require a YAP1 transcriptional complex for survival and tumorigenesis. *Cell* 151, 1457-1473.

Rosenfeldt, M.T., O'Prey, J., Morton, J.P., Nixon, C., MacKay, G., Mrowinska, A., Au, A., Rai, T.S., Zheng, L., Ridgway, R., *et al.* (2013). p53 status determines the role of autophagy in pancreatic tumour development. *Nature* 504, 296-300.

Rubinsztein, D.C. (2006). The roles of intracellular protein-degradation pathways in neurodegeneration. *Nature* 443, 780-786.

Rubinsztein, D.C., Bento, C.F., and Deretic, V. (2015). Therapeutic targeting of autophagy in neurodegenerative and infectious diseases. *J Exp Med* 212, 979-990.

Rubinsztein, D.C., Marino, G., and Kroemer, G. (2011). Autophagy and aging. *Cell* 146, 682-695.

Russell, R.C., Tian, Y., Yuan, H., Park, H.W., Chang, Y.Y., Kim, J., Kim, H., Neufeld, T.P., Dillin, A., and Guan, K.L. (2013). ULK1 induces autophagy by phosphorylating Beclin-1 and activating VPS34 lipid kinase. *Nat Cell Biol* 15, 741-750.

Saitoh, T., Fujita, N., Jang, M.H., Uematsu, S., Yang, B.G., Satoh, T., Omori, H., Noda, T., Yamamoto, N., Komatsu, M., *et al.* (2008). Loss of the autophagy protein Atg16L1 enhances endotoxin-induced IL-1beta production. *Nature* 456, 264-268.

Saito, H., Nishimura, T., Muramatsu, K., Kodera, H., Kumada, S., Sugai, K., Kasai-Yoshida, E., Sawaura, N., Nishida, H., Hoshino, A., *et al.* (2013). De novo mutations in the autophagy gene WDR45 cause static encephalopathy of childhood with neurodegeneration in adulthood. *Nat Genet* 45, 445-449, 449e441.

Sancak, Y., Bar-Peled, L., Zoncu, R., Markhard, A.L., Nada, S., and Sabatini, D.M. (2010). Regulator-Rag complex targets mTORC1 to the lysosomal surface and is necessary for its activation by amino acids. *Cell* 141, 290-303.

Sancak, Y., Peterson, T.R., Shaul, Y.D., Lindquist, R.A., Thoreen, C.C., Bar-Peled, L., and Sabatini, D.M. (2008). The Rag GTPases bind raptor and mediate amino acid signaling to mTORC1. *Science* 320, 1496-1501.

Sanchez-Mut, J.V., Aso, E., Panayotis, N., Lott, I., Dierssen, M., Rabano, A., Urduinguio, R.G., Fernandez, A.F., Astudillo, A., Martin-Subero, J.I., *et al.* (2013). DNA methylation map of mouse and human brain identifies target genes in Alzheimer's disease. *Brain* 136, 3018-3027.

Sancho, R., Cremona, C.A., and Behrens, A. (2015). Stem cell and progenitor fate in the mammalian intestine: Notch and lateral inhibition in homeostasis and disease. *EMBO Rep* 16, 571-581.

Sardiello, M., Palmieri, M., di Ronza, A., Medina, D.L., Valenza, M., Gennarino, V.A., Di Malta, C., Donaudy, F., Embrione, V., Polishchuk, R.S., *et al.* (2009). A gene network regulating lysosomal biogenesis and function. *Science* 325, 473-477.

Sarkar, S., Davies, J.E., Huang, Z., Tunnacliffe, A., and Rubinsztein, D.C. (2007). Trehalose, a novel mTOR-independent autophagy enhancer, accelerates the clearance of mutant huntingtin and alpha-synuclein. *J Biol Chem* 282, 5641-5652.

Sarkar, S., Floto, R.A., Berger, Z., Imarisio, S., Cordenier, A., Pasco, M., Cook, L.J., and Rubinsztein, D.C. (2005). Lithium induces autophagy by inhibiting inositol monophosphatase. *J Cell Biol* 170, 1101-1111.

Sarkar, S., Korolchuk, V.I., Renna, M., Imarisio, S., Fleming, A., Williams, A., Garcia-Arencibia, M., Rose, C., Luo, S., Underwood, B.R., *et al.* (2011). Complex inhibitory effects of nitric oxide on autophagy. *Mol Cell* 43, 19-32.

Sato-Kusubata, K., Yajima, Y., and Kawashima, S. (2000). Persistent activation of Gsalpha through limited proteolysis by calpain. *Biochem J* 347 Pt 3, 733-740.

Schindelin, J., Arganda-Carreras, I., Frise, E., Kaynig, V., Longair, M., Pietzsch, T., Preibisch, S., Rueden, C., Saalfeld, S., Schmid, B., *et al.* (2012). Fiji: an open-source platform for biological-image analysis. *Nat Methods* 9, 676-682.

Schlegelmilch, K., Mohseni, M., Kirak, O., Pruszek, J., Rodriguez, J.R., Zhou, D., Kreger, B.T., Vasioukhin, V., Avruch, J., Brummelkamp, T.R., *et al.* (2011). Yap1 acts downstream of alpha-catenin to control epidermal proliferation. *Cell* 144, 782-795.

Schwartz, M.A. (2010). Integrins and extracellular matrix in mechanotransduction. *Cold Spring Harb Perspect Biol* 2, a005066.

Seok, S., Fu, T., Choi, S.E., Li, Y., Zhu, R., Kumar, S., Sun, X., Yoon, G., Kang, Y., Zhong, W., *et al.* (2014). Transcriptional regulation of autophagy by an FXR-CREB axis. *Nature* 516, 108-111.

Settembre, C., Di Malta, C., Polito, V.A., Garcia Arcencibia, M., Vetrini, F., Erdin, S., Erdin, S.U., Huynh, T., Medina, D., Colella, P., *et al.* (2011). TFEB links autophagy to lysosomal biogenesis. *Science* 332, 1429-1433.

Sharifi, M.N., Mowers, E.E., Drake, L.E., Collier, C., Chen, H., Zamora, M., Mui, S., and Macleod, K.F. (2016). Autophagy Promotes Focal Adhesion Disassembly and Cell Motility of Metastatic Tumor Cells through the Direct Interaction of Paxillin with LC3. *Cell Rep* 15, 1660-1672.

Shi, S., and Stanley, P. (2006). Evolutionary origins of Notch signaling in early development. *Cell Cycle* 5, 274-278.

Shibata, M., Lu, T., Furuya, T., Degterev, A., Mizushima, N., Yoshimori, T., MacDonald, M., Yankner, B., and Yuan, J. (2006). Regulation of intracellular accumulation of mutant Huntingtin by Beclin 1. *J Biol Chem* 281, 14474-14485.

Silvis, M.R., Kreger, B.T., Lien, W.H., Klezovitch, O., Rudakova, G.M., Camargo, F.D., Lantz, D.M., Seykora, J.T., and Vasioukhin, V. (2011). alpha-catenin is a tumor suppressor that controls cell accumulation by regulating the localization and activity of the transcriptional coactivator Yap1. *Sci Signal* 4, ra33.

Simonsen, A., Cumming, R.C., Brech, A., Isakson, P., Schubert, D.R., and Finley, K.D. (2008). Promoting basal levels of autophagy in the nervous system enhances longevity and oxidant resistance in adult *Drosophila*. *Autophagy* 4, 176-184.

Smyth, G.K., and Speed, T. (2003). Normalization of cDNA microarray data. *Methods* 31, 265-273.

Song, Q., Mao, B., Cheng, J., Gao, Y., Jiang, K., Chen, J., Yuan, Z., and Meng, S. (2015). YAP enhances autophagic flux to promote breast cancer cell survival in response to nutrient deprivation. *PLoS One* 10, e0120790.

Sorrentino, G., Ruggeri, N., Specchia, V., Cordenonsi, M., Mano, M., Dupont, S., Manfrin, A., Ingallina, E., Sommaggio, R., Piazza, S., *et al.* (2014). Metabolic control of YAP and TAZ by the mevalonate pathway. *Nat Cell Biol* 16, 357-366.

Stamos, J.L., and Weis, W.I. (2013). The beta-catenin destruction complex. *Cold Spring Harb Perspect Biol* 5, a007898.

Steele, J.W., Ju, S., Lachenmayer, M.L., Liken, J., Stock, A., Kim, S.H., Delgado, L.M., Alfaro, I.E., Bernales, S., Verdile, G., *et al.* (2013). Latrepirdine stimulates autophagy and

reduces accumulation of alpha-synuclein in cells and in mouse brain. *Mol Psychiatry* 18, 882-888.

Strano, S., Monti, O., Pediconi, N., Baccharini, A., Fontemaggi, G., Lapi, E., Mantovani, F., Damalas, A., Citro, G., Sacchi, A., *et al.* (2005). The transcriptional coactivator Yes-associated protein drives p73 gene-target specificity in response to DNA Damage. *Mol Cell* 18, 447-459.

Strano, S., Munarriz, E., Rossi, M., Castagnoli, L., Shaul, Y., Sacchi, A., Oren, M., Sudol, M., Cesareni, G., and Blandino, G. (2001). Physical interaction with Yes-associated protein enhances p73 transcriptional activity. *J Biol Chem* 276, 15164-15173.

Sudol, M. (1994). Yes-associated protein (YAP65) is a proline-rich phosphoprotein that binds to the SH3 domain of the Yes proto-oncogene product. *Oncogene* 9, 2145-2152.

Sudol, M. (2013). YAP1 oncogene and its eight isoforms. In *Oncogene* (England), p. 3922.

Sudol, M., Bork, P., Einbond, A., Kastury, K., Druck, T., Negrini, M., Huebner, K., and Lehman, D. (1995). Characterization of the mammalian YAP (Yes-associated protein) gene and its role in defining a novel protein module, the WW domain. *J Biol Chem* 270, 14733-14741.

Suwa, A., Mitsushima, M., Ito, T., Akamatsu, M., Ueda, K., Amachi, T., and Kioka, N. (2002). Vinexin beta regulates the anchorage dependence of ERK2 activation stimulated by epidermal growth factor. In *J Biol Chem* (United States), pp. 13053-13058.

Tabata, K., Matsunaga, K., Sakane, A., Sasaki, T., Noda, T., and Yoshimori, T. (2010). Rubicon and PLEKHM1 negatively regulate the endocytic/autophagic pathway via a novel Rab7-binding domain. *Mol Biol Cell* 21, 4162-4172.

Takahashi, H., Mitsushima, M., Okada, N., Ito, T., Aizawa, S., Akahane, R., Umemoto, T., Ueda, K., and Kioka, N. (2005). Role of interaction with vinculin in recruitment of vinexins to focal adhesions. *Biochem Biophys Res Commun* 336, 239-246.

Tan, D., Cai, Y., Wang, J., Zhang, J., Menon, S., Chou, H.T., Ferro-Novick, S., Reinisch, K.M., and Walz, T. (2013). The EM structure of the TRAPP3 complex leads to the identification of a requirement for COPII vesicles on the macroautophagy pathway. *Proc Natl Acad Sci U S A* 110, 19432-19437.

Tan, X., Thapa, N., Sun, Y., and Anderson, R.A. (2015). A kinase-independent role for EGF receptor in autophagy initiation. *Cell* 160, 145-160.

Tanida, I., Tanida-Miyake, E., Komatsu, M., Ueno, T., and Kominami, E. (2002). Human Apg3p/Aut1p homologue is an authentic E2 enzyme for multiple substrates, GATE-16, GABARAP, and MAP-LC3, and facilitates the conjugation of hApg12p to hApg5p. *J Biol Chem* 277, 13739-13744.

Tanida, I., Tanida-Miyake, E., Ueno, T., and Kominami, E. (2001). The human homolog of *Saccharomyces cerevisiae* Apg7p is a Protein-activating enzyme for multiple substrates including human Apg12p, GATE-16, GABARAP, and MAP-LC3. *J Biol Chem* 276, 1701-1706.

Taylor, R.C., and Dillin, A. (2011). Aging as an event of proteostasis collapse. *Cold Spring Harb Perspect Biol* 3.

Terman, A. (1995). The effect of age on formation and elimination of autophagic vacuoles in mouse hepatocytes. *Gerontology* 41 Suppl 2, 319-326.

The Cancer Genome Atlas Research Network (2017). Comprehensive and Integrative Genomic Characterization of Hepatocellular Carcinoma. *Cell* 169, 1327-1341.e1323.

Thompson, O., Moore, C.J., Hussain, S.A., Kleino, I., Peckham, M., Hohenester, E., Ayscough, K.R., Saksela, K., and Winder, S.J. (2010). Modulation of cell spreading and cell-substrate adhesion dynamics by dystroglycan. *J Cell Sci* 123, 118-127.

Thorvaldsdottir, H., Robinson, J.T., and Mesirov, J.P. (2013). Integrative Genomics Viewer (IGV): high-performance genomics data visualization and exploration. *Brief Bioinform* *14*, 178-192.

Thumm, M., Egner, R., Koch, B., Schlumpberger, M., Straub, M., Veenhuis, M., and Wolf, D.H. (1994). Isolation of autophagocytosis mutants of *Saccharomyces cerevisiae*. *FEBS Lett* *349*, 275-280.

Thurnherr, T., Mah, W.C., Lei, Z., Jin, Y., Rozen, S.G., and Lee, C.G. (2016). Differentially Expressed miRNAs in Hepatocellular Carcinoma Target Genes in the Genetic Information Processing and Metabolism Pathways. *Sci Rep* *6*, 20065.

Thurston, T.L., Ryzhakov, G., Bloor, S., von Muhlinen, N., and Randow, F. (2009). The TBK1 adaptor and autophagy receptor NDP52 restricts the proliferation of ubiquitin-coated bacteria. *Nat Immunol* *10*, 1215-1221.

Thurston, T.L., Wandel, M.P., von Muhlinen, N., Foeglein, A., and Randow, F. (2012). Galectin 8 targets damaged vesicles for autophagy to defend cells against bacterial invasion. *Nature* *482*, 414-418.

Tian, Y., Kolb, R., Hong, J.H., Carroll, J., Li, D., You, J., Bronson, R., Yaffe, M.B., Zhou, J., and Benjamin, T. (2007). TAZ promotes PC2 degradation through a SCFbeta-Trcp E3 ligase complex. *Mol Cell Biol* *27*, 6383-6395.

Toh, P.P., Luo, S., Menzies, F.M., Rasko, T., Wanker, E.E., and Rubinsztein, D.C. (2013). Myc inhibition impairs autophagosome formation. *Hum Mol Genet* *22*, 5237-5248.

Townson, S.M., Dobrzycka, K.M., Lee, A.V., Air, M., Deng, W., Kang, K., Jiang, S., Kioka, N., Michaelis, K., and Oesterreich, S. (2003). SAFB2, a new scaffold attachment factor homolog and estrogen receptor corepressor. *J Biol Chem* *278*, 20059-20068.

Tsukada, M., and Ohsumi, Y. (1993). Isolation and characterization of autophagy-defective mutants of *Saccharomyces cerevisiae*. *FEBS Lett* *333*, 169-174.

Tsukamoto, S., Kuma, A., Murakami, M., Kishi, C., Yamamoto, A., and Mizushima, N. (2008). Autophagy is essential for preimplantation development of mouse embryos. *Science* *321*, 117-120.

Tujague, M., Thomsen, J.S., Mizuki, K., Sadek, C.M., and Gustafsson, J.A. (2004). The focal adhesion protein vinexin alpha regulates the phosphorylation and activity of estrogen receptor alpha. *J Biol Chem* *279*, 9255-9263.

Tuloup-Minguez, V., Hamai, A., Greffard, A., Nicolas, V., Codogno, P., and Botti, J. (2013). Autophagy modulates cell migration and beta1 integrin membrane recycling. *Cell Cycle* *12*, 3317-3328.

Tumbarello, D.A., Waxse, B.J., Arden, S.D., Bright, N.A., Kendrick-Jones, J., and Buss, F. (2012). Autophagy receptors link myosin VI to autophagosomes to mediate Tom1-dependent autophagosome maturation and fusion with the lysosome. *Nat Cell Biol* *14*, 1024-1035.

Umamoto, T., Inomoto, T., Ueda, K., Hamaguchi, M., and Kioka, N. (2009a). v-Src-mediated transformation suppresses the expression of focal adhesion protein vinexin. *Cancer Lett* *279*, 22-29.

Umamoto, T., Tanaka, K., Ueda, K., and Kioka, N. (2009b). Tyrosine phosphorylation of vinexin in v-Src-transformed cells attenuates the affinity for vinculin. *Biochem Biophys Res Commun* *387*, 191-195.

Valente, E.M., Abou-Sleiman, P.M., Caputo, V., Muqit, M.M., Harvey, K., Gispert, S., Ali, Z., Del Turco, D., Bentivoglio, A.R., Healy, D.G., *et al.* (2004). Hereditary early-onset Parkinson's disease caused by mutations in PINK1. *Science* *304*, 1158-1160.

Valente, E.M., Bentivoglio, A.R., Dixon, P.H., Ferraris, A., Ialongo, T., Frontali, M., Albanese, A., and Wood, N.W. (2001). Localization of a novel locus for autosomal recessive early-onset parkinsonism, PARK6, on human chromosome 1p35-p36. *Am J Hum Genet* *68*, 895-900.

van Amerongen, R., and Nusse, R. (2009). Towards an integrated view of Wnt signaling in development. *Development* *136*, 3205-3214.

Varelas, X. (2014). The Hippo pathway effectors TAZ and YAP in development, homeostasis and disease. *Development* *141*, 1614-1626.

Varelas, X., Sakuma, R., Samavarchi-Tehrani, P., Peerani, R., Rao, B.M., Dembowy, J., Yaffe, M.B., Zandstra, P.W., and Wrana, J.L. (2008). TAZ controls Smad nucleocytoplasmic shuttling and regulates human embryonic stem-cell self-renewal. *Nat Cell Biol* *10*, 837-848.

Vassilev, A., Kaneko, K.J., Shu, H., Zhao, Y., and DePamphilis, M.L. (2001). TEAD/TEF transcription factors utilize the activation domain of YAP65, a Src/Yes-associated protein localized in the cytoplasm. *Genes Dev* *15*, 1229-1241.

Velikkakath, A.K., Nishimura, T., Oita, E., Ishihara, N., and Mizushima, N. (2012). Mammalian Atg2 proteins are essential for autophagosome formation and important for regulation of size and distribution of lipid droplets. *Mol Biol Cell* *23*, 896-909.

Vicencio, J.M., Ortiz, C., Criollo, A., Jones, A.W., Kepp, O., Galluzzi, L., Joza, N., Vitale, I., Morselli, E., Tailler, M., *et al.* (2009). The inositol 1,4,5-trisphosphate receptor regulates autophagy through its interaction with Beclin 1. *Cell Death Differ* *16*, 1006-1017.

Vicinanza, M., Korolchuk, V.I., Ashkenazi, A., Puri, C., Menzies, F.M., Clarke, J.H., and Rubinsztein, D.C. (2015). PI(5)P regulates autophagosome biogenesis. *Mol Cell* *57*, 219-234.

Vilarino-Guell, C., Wider, C., Ross, O.A., Dachsel, J.C., Kachergus, J.M., Lincoln, S.J., Soto-Ortolaza, A.I., Cobb, S.A., Wilhoite, G.J., Bacon, J.A., *et al.* (2011). VPS35 mutations in Parkinson disease. *Am J Hum Genet* *89*, 162-167.

Vilchez, D., Saez, I., and Dillin, A. (2014). The role of protein clearance mechanisms in organismal ageing and age-related diseases. *Nat Commun* *5*, 5659.

von Gise, A., Lin, Z., Schlegelmilch, K., Honor, L.B., Pan, G.M., Buck, J.N., Ma, Q., Ishiwata, T., Zhou, B., Camargo, F.D., *et al.* (2012). YAP1, the nuclear target of Hippo signaling, stimulates heart growth through cardiomyocyte proliferation but not hypertrophy. *Proceedings of the National Academy of Sciences* *109*, 2394-2399.

Wachtel, M., and Schafer, B.W. (2015). Unpeaceful roles of mutant PAX proteins in cancer. *Semin Cell Dev Biol* *44*, 126-134.

Wada, K., Itoga, K., Okano, T., Yonemura, S., and Sasaki, H. (2011). Hippo pathway regulation by cell morphology and stress fibers. *Development* *138*, 3907-3914.

Wakabayashi, M., Ito, T., Mitsushima, M., Aizawa, S., Ueda, K., Amachi, T., and Kioka, N. (2003). Interaction of Iq-dlg/KIAA0583, a membrane-associated guanylate kinase family protein, with vinexin and beta-catenin at sites of cell-cell contact. *J Biol Chem* *278*, 21709-21714.

Wang, H., Sun, H.Q., Zhu, X., Zhang, L., Albanesi, J., Levine, B., and Yin, H. (2015). GABARAPs regulate PI4P-dependent autophagosome:lysosome fusion. *Proc Natl Acad Sci U S A* *112*, 7015-7020.

Wang, P., Liu, Z., Chen, H., Ye, N., Cheng, X., and Zhou, J. (2017). Exchange proteins directly activated by cAMP (EPACs): Emerging therapeutic targets. *Bioorg Med Chem Lett* *27*, 1633-1639.

Wang, P., Mao, B., Luo, W., Wei, B., Jiang, W., Liu, D., Song, L., Ji, G., Yang, Z., Lai, Y.Q., *et al.* (2014a). The alteration of Hippo/YAP signaling in the development of hypertrophic cardiomyopathy. *Basic Res Cardiol* *109*, 435.

Wang, W., Huang, J., and Chen, J. (2011). Angiomotin-like proteins associate with and negatively regulate YAP1. *J Biol Chem* *286*, 4364-4370.

Wang, X., Su, L., and Ou, Q. (2012). Yes-associated protein promotes tumour development in luminal epithelial derived breast cancer. *Eur J Cancer* *48*, 1227-1234.

Wang, Y., Dong, Q., Zhang, Q., Li, Z., Wang, E., and Qiu, X. (2010). Overexpression of yes-associated protein contributes to progression and poor prognosis of non-small-cell lung cancer. *Cancer Sci* *101*, 1279-1285.

Wang, Z., Wu, Y., Wang, H., Zhang, Y., Mei, L., Fang, X., Zhang, X., Zhang, F., Chen, H., Liu, Y., *et al.* (2014b). Interplay of mevalonate and Hippo pathways regulates RHAMM transcription via YAP to modulate breast cancer cell motility. *Proc Natl Acad Sci U S A* *111*, E89-98.

Warr, M.R., Binnewies, M., Flach, J., Reynaud, D., Garg, T., Malhotra, R., Debnath, J., and Passegue, E. (2013). FOXO3A directs a protective autophagy program in haematopoietic stem cells. *Nature* *494*, 323-327.

Wartosch, L., Gunesdogan, U., Graham, S.C., and Luzio, J.P. (2015). Recruitment of VPS33A to HOPS by VPS16 Is Required for Lysosome Fusion with Endosomes and Autophagosomes. *Traffic* *16*, 727-742.

Watts, R.G., and Howard, T.H. (1992). Evidence for a gelsolin-rich, labile F-actin pool in human polymorphonuclear leukocytes. *Cell Motil Cytoskeleton* *21*, 25-37.

Webb, C., Upadhyay, A., Giuntini, F., Eggleston, I., Furutani-Seiki, M., Ishima, R., and Bagby, S. (2011). Structural features and ligand binding properties of tandem WW domains from YAP and TAZ, nuclear effectors of the Hippo pathway. *Biochemistry* *50*, 3300-3309.

Webb, J.L., Ravikumar, B., Atkins, J., Skepper, J.N., and Rubinsztein, D.C. (2003). Alpha-Synuclein is degraded by both autophagy and the proteasome. *J Biol Chem* *278*, 25009-25013.

Webster, C.P., Smith, E.F., Bauer, C.S., Moller, A., Hautbergue, G.M., Ferraiuolo, L., Myszczyńska, M.A., Higginbottom, A., Walsh, M.J., Whitworth, A.J., *et al.* (2016). The C9orf72 protein interacts with Rab1a and the ULK1 complex to regulate initiation of autophagy. *Embo j* *35*, 1656-1676.

Wei, H., Wei, S., Gan, B., Peng, X., Zou, W., and Guan, J.L. (2011). Suppression of autophagy by FIP200 deletion inhibits mammary tumorigenesis. *Genes Dev* *25*, 1510-1527.

Wei, Y., Pattingre, S., Sinha, S., Bassik, M., and Levine, B. (2008). JNK1-mediated phosphorylation of Bcl-2 regulates starvation-induced autophagy. *Mol Cell* *30*, 678-688.

Wild, P., Farhan, H., McEwan, D.G., Wagner, S., Rogov, V.V., Brady, N.R., Richter, B., Korac, J., Waidmann, O., Choudhary, C., *et al.* (2011). Phosphorylation of the autophagy receptor optineurin restricts Salmonella growth. *Science* *333*, 228-233.

Williams, A., Sarkar, S., Cuddon, P., Ttofi, E.K., Saiki, S., Siddiqi, F.H., Jahreiss, L., Fleming, A., Pask, D., Goldsmith, P., *et al.* (2008). Novel targets for Huntington's disease in an mTOR-independent autophagy pathway. *Nat Chem Biol* *4*, 295-305.

Williams, R.S., Cheng, L., Mudge, A.W., and Harwood, A.J. (2002). A common mechanism of action for three mood-stabilizing drugs. *Nature* *417*, 292-295.

Winslow, A.R., Chen, C.W., Corrochano, S., Acevedo-Arozena, A., Gordon, D.E., Peden, A.A., Lichtenberg, M., Menzies, F.M., Ravikumar, B., Imarisio, S., *et al.* (2010). alpha-Synuclein impairs macroautophagy: implications for Parkinson's disease. *J Cell Biol* *190*, 1023-1037.

Wong, C.H., Iskandar, K.B., Yadav, S.K., Hirpara, J.L., Loh, T., and Pervaiz, S. (2010). Simultaneous induction of non-canonical autophagy and apoptosis in cancer cells by ROS-dependent ERK and JNK activation. *PLoS One* *5*, e9996.

Wong, P.M., Feng, Y., Wang, J., Shi, R., and Jiang, X. (2015). Regulation of autophagy by coordinated action of mTORC1 and protein phosphatase 2A. *Nat Commun* *6*, 8048.

Wood, C.K., Turner, C.E., Jackson, P., and Critchley, D.R. (1994). Characterisation of the paxillin-binding site and the C-terminal focal adhesion targeting sequence in vinculin. *J Cell Sci* *107 (Pt 2)*, 709-717.

Wu, X., Fleming, A., Ricketts, T., Pavel, M., Virgin, H., Menzies, F.M., and Rubinsztein, D.C. (2016). Autophagy regulates Notch degradation and modulates stem cell development and neurogenesis. *Nat Commun* 7, 10533.

Wu, X., Won, H., and Rubinsztein, D.C. (2013). Autophagy and mammalian development. *Biochem Soc Trans* 41, 1489-1494.

Wu, Y.T., Tan, H.L., Huang, Q., Kim, Y.S., Pan, N., Ong, W.Y., Liu, Z.G., Ong, C.N., and Shen, H.M. (2008). Autophagy plays a protective role during zVAD-induced necrotic cell death. *Autophagy* 4, 457-466.

Wulf, E., Deboen, A., Bautz, F.A., Faulstich, H., and Wieland, T. (1979). Fluorescent phallotoxin, a tool for the visualization of cellular actin. *Proc Natl Acad Sci U S A* 76, 4498-4502.

Wurzer, B., Zaffagnini, G., Fracchiolla, D., Turco, E., Abert, C., Romanov, J., and Martens, S. (2015). Oligomerization of p62 allows for selection of ubiquitinated cargo and isolation membrane during selective autophagy. *Elife* 4, e08941.

Xin, M., Kim, Y., Sutherland, L.B., Murakami, M., Qi, X., McAnally, J., Porrello, E.R., Mahmoud, A.I., Tan, W., Shelton, J.M., *et al.* (2013). Hippo pathway effector Yap promotes cardiac regeneration. *Proc Natl Acad Sci U S A* 110, 13839-13844.

Xu, M.Z., Yao, T.J., Lee, N.P., Ng, I.O., Chan, Y.T., Zender, L., Lowe, S.W., Poon, R.T., and Luk, J.M. (2009a). Yes-associated protein is an independent prognostic marker in hepatocellular carcinoma. *Cancer* 115, 4576-4585.

Xu, X., Araki, K., Li, S., Han, J.H., Ye, L., Tan, W.G., Konieczny, B.T., Bruinsma, M.W., Martinez, J., Pearce, E.L., *et al.* (2014). Autophagy is essential for effector CD8(+) T cell survival and memory formation. *Nat Immunol* 15, 1152-1161.

Xu, Y., Benlimame, N., Su, J., He, Q., and Alaoui-Jamali, M.A. (2009b). Regulation of focal adhesion turnover by ErbB signalling in invasive breast cancer cells. *Br J Cancer* 100, 633-643.

Xu, Y., Bismar, T.A., Su, J., Xu, B., Kristiansen, G., Varga, Z., Teng, L., Ingber, D.E., Mammoto, A., Kumar, R., *et al.* (2010). Filamin A regulates focal adhesion disassembly and suppresses breast cancer cell migration and invasion. *J Exp Med* 207, 2421-2437.

Xue, W., Kitzing, T., Roessler, S., Zuber, J., Krasnitz, A., Schultz, N., Revill, K., Weissmueller, S., Rappaport, A.R., Simon, J., *et al.* (2012). A cluster of cooperating tumor-suppressor gene candidates in chromosomal deletions. *Proc Natl Acad Sci U S A* 109, 8212-8217.

Yagi, R., Chen, L.F., Shigesada, K., Murakami, Y., and Ito, Y. (1999). A WW domain-containing yes-associated protein (YAP) is a novel transcriptional co-activator. *Embo j* 18, 2551-2562.

Yamamoto, A., Tagawa, Y., Yoshimori, T., Moriyama, Y., Masaki, R., and Tashiro, Y. (1998). Bafilomycin A1 prevents maturation of autophagic vacuoles by inhibiting fusion between autophagosomes and lysosomes in rat hepatoma cell line, H-4-II-E cells. *Cell Struct Funct* 23, 33-42.

Yamashita, H., Ichikawa, T., Matsuyama, D., Kimura, Y., Ueda, K., Craig, S.W., Harada, I., and Kioka, N. (2014). The role of the interaction of the vinculin proline-rich linker region with vinexin alpha in sensing the stiffness of the extracellular matrix. *J Cell Sci* 127, 1875-1886.

Yang, C., Tan, J., Zhu, J., Wang, S., and Wei, G. (2017). YAP promotes tumorigenesis and cisplatin resistance in neuroblastoma. *Oncotarget* 8, 37154-37163.

Yang, H., Cho, M.E., Li, T.W., Peng, H., Ko, K.S., Mato, J.M., and Lu, S.C. (2013). MicroRNAs regulate methionine adenosyltransferase 1A expression in hepatocellular carcinoma. *J Clin Invest* 123, 285-298.

Yeatman, T.J. (2004). A renaissance for SRC. *Nat Rev Cancer* 4, 470-480.

Yi, C., Shen, Z., Stemmer-Rachamimov, A., Dawany, N., Troutman, S., Showe, L.C., Liu, Q., Shimono, A., Sudol, M., Holmgren, L., *et al.* (2013). The p130 isoform of angiomin is required for Yap-mediated hepatic epithelial cell proliferation and tumorigenesis. *Sci Signal* 6, ra77.

Yimlamai, D., Christodoulou, C., Galli, G.G., Yanger, K., Pepe-Mooney, B., Gurung, B., Shrestha, K., Cahan, P., Stanger, B.Z., and Camargo, F.D. (2014). Hippo pathway activity influences liver cell fate. *Cell* 157, 1324-1338.

Yu, F.X., Zhao, B., Panupinthu, N., Jewell, J.L., Lian, I., Wang, L.H., Zhao, J., Yuan, H., Tumaneng, K., Li, H., *et al.* (2012). Regulation of the Hippo-YAP pathway by G-protein-coupled receptor signaling. *Cell* 150, 780-791.

Yu, H., Pardoll, D., and Jove, R. (2009). STATs in cancer inflammation and immunity: a leading role for STAT3. *Nat Rev Cancer* 9, 798-809.

Yu, W.H., Cuervo, A.M., Kumar, A., Peterhoff, C.M., Schmidt, S.D., Lee, J.H., Mohan, P.S., Mercken, M., Farmery, M.R., Tjernberg, L.O., *et al.* (2005). Macroautophagy--a novel Beta-amyloid peptide-generating pathway activated in Alzheimer's disease. *J Cell Biol* 171, 87-98.

Yuan, M., Tomlinson, V., Lara, R., Holliday, D., Chelala, C., Harada, T., Gangeswaran, R., Manson-Bishop, C., Smith, P., Danovi, S.A., *et al.* (2008). Yes-associated protein (YAP) functions as a tumor suppressor in breast. *Cell Death Differ* 15, 1752-1759.

Yue, Z., Jin, S., Yang, C., Levine, A.J., and Heintz, N. (2003). Beclin 1, an autophagy gene essential for early embryonic development, is a haploinsufficient tumor suppressor. *Proc Natl Acad Sci U S A* 100, 15077-15082.

Zaffagnini, G., and Martens, S. (2016). Mechanisms of Selective Autophagy. *J Mol Biol* 428, 1714-1724.

Zanconato, F., Forcato, M., Battilana, G., Azzolin, L., Quaranta, E., Bodega, B., Rosato, A., Bicciato, S., Cordenonsi, M., and Piccolo, S. (2015). Genome-wide association between YAP/TAZ/TEAD and AP-1 at enhancers drives oncogenic growth. *Nat Cell Biol* 17, 1218-1227.

Zavodszky, E., Seaman, M.N., Moreau, K., Jimenez-Sanchez, M., Breusegem, S.Y., Harbour, M.E., and Rubinsztein, D.C. (2014). Mutation in VPS35 associated with Parkinson's disease impairs WASH complex association and inhibits autophagy. *Nat Commun* 5, 3828.

Zender, L., Spector, M.S., Xue, W., Flemming, P., Cordon-Cardo, C., Silke, J., Fan, S.T., Luk, J.M., Wigler, M., Hannon, G.J., *et al.* (2006). Identification and validation of oncogenes in liver cancer using an integrative oncogenomic approach. *Cell* 125, 1253-1267.

Zhang, C.H., Xu, G.L., Jia, W.D., Li, J.S., Ma, J.L., Ren, W.H., Ge, Y.S., Yu, J.H., Liu, W.B., and Wang, W. (2012a). Activation of STAT3 signal pathway correlates with twist and E-cadherin expression in hepatocellular carcinoma and their clinical significance. *J Surg Res* 174, 120-129.

Zhang, H., Liu, C.Y., Zha, Z.Y., Zhao, B., Yao, J., Zhao, S., Xiong, Y., Lei, Q.Y., and Guan, K.L. (2009). TEAD transcription factors mediate the function of TAZ in cell growth and epithelial-mesenchymal transition. *J Biol Chem* 284, 13355-13362.

Zhang, H., Pasolli, H.A., and Fuchs, E. (2011). Yes-associated protein (YAP) transcriptional coactivator functions in balancing growth and differentiation in skin. *Proc Natl Acad Sci U S A* 108, 2270-2275.

Zhang, J., Li, X., Yao, B., Shen, W., Sun, H., Xu, C., Wu, J., and Shi, Y. (2007). Solution structure of the first SH3 domain of human vinexin and its interaction with vinculin peptides. *Biochemical and Biophysical Research Communications* 357, 931-937.

Zhang, X., Grusche, F.A., and Harvey, K.F. (2012b). Control of tissue growth and cell transformation by the Salvador/Warts/Hippo pathway. *PLoS One* 7, e31994.

Zhao, B., Li, L., Lu, Q., Wang, L.H., Liu, C.Y., Lei, Q., and Guan, K.L. (2011a). Angiomin is a novel Hippo pathway component that inhibits YAP oncoprotein. *Genes Dev* 25, 51-63.

Zhao, B., Li, L., Tumaneng, K., Wang, C.Y., and Guan, K.L. (2010). A coordinated phosphorylation by Lats and CK1 regulates YAP stability through SCF(beta-TRCP). *Genes Dev* *24*, 72-85.

Zhao, B., Li, L., Wang, L., Wang, C.Y., Yu, J., and Guan, K.L. (2012). Cell detachment activates the Hippo pathway via cytoskeleton reorganization to induce anoikis. *Genes Dev* *26*, 54-68.

Zhao, B., Tumaneng, K., and Guan, K.L. (2011b). The Hippo pathway in organ size control, tissue regeneration and stem cell self-renewal. *Nat Cell Biol* *13*, 877-883.

Zhao, B., Wei, X., Li, W., Udan, R.S., Yang, Q., Kim, J., Xie, J., Ikenoue, T., Yu, J., Li, L., *et al.* (2007). Inactivation of YAP oncoprotein by the Hippo pathway is involved in cell contact inhibition and tissue growth control. *Genes Dev* *21*, 2747-2761.

Zhao, B., Ye, X., Yu, J., Li, L., Li, W., Li, S., Lin, J.D., Wang, C.Y., Chinnaiyan, A.M., Lai, Z.C., *et al.* (2008). TEAD mediates YAP-dependent gene induction and growth control. *Genes Dev* *22*, 1962-1971.

Zhao, Y., and Yang, X. (2015). The Hippo pathway in chemotherapeutic drug resistance. *Int J Cancer* *137*, 2767-2773.

Zheng, Y.T., Shahnazari, S., Brech, A., Lamark, T., Johansen, T., and Brumell, J.H. (2009). The adaptor protein p62/SQSTM1 targets invading bacteria to the autophagy pathway. *J Immunol* *183*, 5909-5916.

Zhong, Y., Wang, Q.J., Li, X., Yan, Y., Backer, J.M., Chait, B.T., Heintz, N., and Yue, Z. (2009). Distinct regulation of autophagic activity by Atg14L and Rubicon associated with Beclin 1-phosphatidylinositol-3-kinase complex. In *Nat Cell Biol (England)*, pp. 468-476.

Zhou, D., Conrad, C., Xia, F., Park, J.S., Payer, B., Yin, Y., Lauwers, G.Y., Thasler, W., Lee, J.T., Avruch, J., *et al.* (2009). Mst1 and Mst2 maintain hepatocyte quiescence and suppress hepatocellular carcinoma development through inactivation of the Yap1 oncogene. *Cancer Cell* *16*, 425-438.

Zhou, Y., Huang, T., Cheng, A.S., Yu, J., Kang, W., and To, K.F. (2016). The TEAD Family and Its Oncogenic Role in Promoting Tumorigenesis. *Int J Mol Sci* *17*.

Zhou, Z., Hao, Y., Liu, N., Raptis, L., Tsao, M.S., and Yang, X. (2011). TAZ is a novel oncogene in non-small cell lung cancer. *Oncogene* *30*, 2181-2186.

Zimonjic, D.B., Keck, C.L., Thorgeirsson, S.S., and Popescu, N.C. (1999). Novel recurrent genetic imbalances in human hepatocellular carcinoma cell lines identified by comparative genomic hybridization. *Hepatology* *29*, 1208-1214.

Zimprich, A., Benet-Pages, A., Struhal, W., Graf, E., Eck, S.H., Offman, M.N., Haubenberger, D., Spielberger, S., Schulte, E.C., Lichtner, P., *et al.* (2011). A mutation in VPS35, encoding a subunit of the retromer complex, causes late-onset Parkinson disease. *Am J Hum Genet* *89*, 168-175.

Zoncu, R., Bar-Peled, L., Efeyan, A., Wang, S., Sancak, Y., and Sabatini, D.M. (2011a). mTORC1 senses lysosomal amino acids through an inside-out mechanism that requires the vacuolar H(+)-ATPase. *Science* *334*, 678-683.

Zoncu, R., Efeyan, A., and Sabatini, D.M. (2011b). mTOR: from growth signal integration to cancer, diabetes and ageing. *Nat Rev Mol Cell Biol* *12*, 21-35.

## 8 Appendix

### 8.1 Abbreviations

A431	Human squamous carcinoma cells
A549	Human lung carcinoma cells
Abeta	Amyloid beta
ABL	ABL proto-oncogene 1, non-receptor tyrosine kinase
AC	Adenylyl cyclase
AD	Alzheimer's disease
ADP	Adenosine diphosphate
AKT	AKT serine/threonine kinase 1
AKT1S1	AKT substrate 1 (also known as PRAS40)
AMOT/L1/L2	Angiomtin/-like 1/-like 2
AMP	Adenosine monophosphate
ANOVA	Analysis of variance
AP-1	Activator protein 1
ApoE	Apolipoprotein E
APP	Amyloid precursor protein
ARGBP2	ARG-binding protein 2 (also known as SORBS2)
ARP2/3	Actin-related proteins 2/3
ATG	Autophagy-related
ATP	Adenosine triphosphate
AXIN1	Axis inhibition protein 1
BAF	Bafilomycin A1
BAX	BCL2-associated X protein
BCL2	B-cell lymphoma 2 protein
BCL2L1/L2	BCL2-like 1/-like 2
BDL	Bile duct ligation
BECN1	Beclin 1
BH3	BCL2 homologous 3 domain
BIRC2/5	Baculoviral IAP repeat containing 2/3 protein
BKPyV	Human BK polyomavirus
BSA	Bovine serum albumin

CAMK4	Calcium/calmodulin-dependent protein kinase 4
cAMP	Cyclic adenosine monophosphate
CAMTA1	Calmodulin binding transcription activator 1
CAP	CBL-associated protein (also known as SORBS1)
CAPZ	Capping protein (actin filament) muscle Z-Line
CBL	CBL proto-oncogene, E3 ubiquitin protein ligase
CCDC25	Coiled-coil domain containing 25 protein
CCNA2	Cyclin A2
CD4	Cluster of differentiation 4 protein
CD63	Cluster of differentiation 4 protein (also known as lysosome-associated membrane glycoprotein 3)
CDC2/6/42	Cell division cycle protein 2/6/42
ChIP	Chromatin immunoprecipitation
cIAP1	Cellular inhibitor of apoptosis protein 1 (also known as BIRC2)
CNS	Central nervous system
COPII	Coat protein complex II
CREB	cAMP response element binding transcription factor
CRISPR	Clustered regularly interspaced short palindromic repeats
CRTC2	CREB regulated transcription coactivator 2
CSNK1D/E	Casein kinase I isoform delta/epsilon
CTGF	Connective tissue growth factor
DAG	Diacylglycerol
DAPI	4',6-diamidino-2-phenylindole
DC	Dendritic cell
DDIT4	DNA damage inducible transcript 4 protein
DIAPH3	Diaphanous related formin 3
DLC1	Deleted in liver cancer 1 protein
DLG5	Discs, large homolog 5 protein
DMEM	Dulbecco's modified Eagle's medium
DMSO	Dimethyl sulfoxide
DNA	Deoxyribonucleic acid
DSS	4,4-dimethyl-4-silapentane-1-sulfonic acid
DTT	Dithiothreitol

Dvl1-3	Dishevelled proteins 1-3
EBNA1	Epstein–Barr virus nuclear antigen 1
EBSS	Earle's balanced salt solution
EBV	Epstein–Barr virus
ECL	Electrochemiluminescent
ECM	Extracellular matrix
EDA2R	Ectodysplasin A2 receptor
EDTA	Ethylenediaminetetraacetic acid
EGF	Epidermal growth factor
EGFR	Epidermal growth factor receptor
EGTA	Ethylene glycol-bis(2-aminoethylether)-N,N,N',N'-tetraacetic acid
ELP3	Elongator acetyltransferase complex subunit 3
EMT	Epithelial-mesenchymal transition
EPAC	Exchange factor directly activated by cAMP 1
ER	Endoplasmic reticulum
ERGIC	ER-Golgi intermediate compartment
ERK1/2	Extracellular signal-regulated kinase 1/2
FACS	Fluorescence-activated cell sorting
FAT4	FAT atypical cadherin 4
FGF	Fibroblast growth factor
FIP200	Focal adhesion kinase family kinase-interacting protein of 200 kDa
FOXO3A	Forkhead box O3A
FXR	Farnesoid X receptor
FYCO1	FYVE and coiled-coil domain containing 1 protein
GABARAP/L1/L2	Gamma-aminobutyric acid receptor-associated protein/-like 1/-like2
GAPDH	Glyceraldehyde 3-phosphate dehydrogenase
GDP	Guanosine diphosphate
GFP	Green fluorescent protein
GGPP	Geranylgeranyl diphosphate
GIN51	GIN5 complex subunit 1

GNAQ	G protein subunit alpha Q
GPCR	G protein-coupled receptor
GTE <sub>x</sub>	Genotype-tissue expression project
GTP	Guanosine triphosphate
H1299	Human non-small cell lung carcinoma cells
H4	Human neuroglioma cells
HA	Hemagglutinin
HaCaT	Human keratinocyte cells
HCC	Hepatocellular carcinoma
HCM	Hypertrophic cardiomyopathy
HCT-116	Human colon carcinoma cells
HD	Huntington's disease
HEK 293	Human embryonic kidney cells
HeLa	Human cervical cancer cells
HEPES	4-(2-Hydroxyethyl)piperazine-1-ethanesulfonic acid
HepG2	Human hepatocellular carcinoma cells
HLE	Human hepatocellular carcinoma cells
HNRNPU	Heterogeneous nuclear ribonucleoprotein U
HOPS	Homotypic fusion and vacuole protein sorting
HRP	Horseradish peroxidase
HSCs	Hematopoietic stem cells
Htt	Huntingtin
HuH1	Human hepatocellular carcinoma cells
HuH6	Human hepatocellular carcinoma cells
HuH7	Human hepatocellular carcinoma cells
I1R	Imidazoline-1 receptor
iBMK	Immortalized baby mouse kidney epithelial cells
ICD10	International Classification of Diseases, tenth revision
IgG	Immunoglobulin G
IKK2	Inhibitor of nuclear factor kappa-B kinase 2
IL-1 $\beta$ /-6/-18	Interleukin-1 $\beta$ /-6/-18
iMMECs	Immortalized mouse mammary epithelial cells
IP3	Inositol trisphosphate

IP3R	Inositol trisphosphate receptor
JNK1	c-Jun N-terminal kinase 1
KIF3A/5B	Kinesin family member 3A/5B
KRAS	Kirsten Ras oncogene
LAMP2A	Lysosome-associated membrane protein 2
LATS1/2	Large tumour suppressor 1/2
LC3	Microtubule-associated proteins 1A/1B light chain 3B
LCMV	Lymphocytic choriomeningitis
Li7	Human hepatocellular carcinoma cells
LIR	LC3-interacting region
LNCaP	Androgen-sensitive human prostate adenocarcinoma cells
LRP6	Low density lipoprotein receptor-related protein 6
MAPK	Mitogen-activated protein kinase
MCF10A	Human breast epithelial cells
MCF7	Human breast cancer cells
MCL1	Myeloid cell leukemia 1 protein
MEF	Mouse embryonic fibroblasts
MHC I/II	Major histocompatibility complex I/II
MI	Myocardial infarction
MKP3	Mitogen-activated protein kinase phosphatase 3
MMTV	Mouse mammary tumour virus
MOB1/2	Mps one binder kinase 1/2
MSC	Mesenchymal stem cells
MST1/2	Mammalian sterile twenty-like kinase 1/2
mTOR	Mechanistic target of rapamycin
mTORC1	Mechanistic target of rapamycin complex 1/2
MYBL1	MYB proto-oncogene like 1
MYC	Myelocytomatosis oncogene
MYH7	Myosin heavy chain 7
NBIA	Neurodegeneration with Brain Iron Accumulation disorder
NBR1	Neighbour of BRCA1 gene 1 protein
NCBI	National Centre for Biotechnology Information
NCK1/2	Non-catalytic region of tyrosine kinase adaptor protein 1/2

NDP52	Nuclear dot protein 52
NIH3T3	Mouse embryonic fibroblast cells
NKX2-1	Neurokinin 2 homeobox 1 transcription factor (also known as TTF-1)
NO	Nitric oxide
NSCLC	Non-small cell lung carcinoma
NuRD	Nucleosome remodelling deacetylase
N-WASP	Neural Wiskott-Aldrich syndrome protein
OFD1	Oral-facial-digital syndrome 1 protein
PAX3/8	Paired box transcription factor 3/8
PBS	Phosphate-buffered saline
PC-3	Human prostate cancer cells
PCAF	p300/CBP-associated factor histone acetyltransferase
PCR	Polymerase chain reaction
PD	Parkinson's disease
PDAC	Pancreatic ductal adenocarcinoma
PE	Phosphatidylethanolamine
PFA	Paraformaldehyde
PI(3)P	Phosphatidylinositol 3-phosphate
PI(4)P	Phosphatidylinositol 4-phosphate
PI(5)P	Phosphatidylinositol 5-phosphate
PI3KC3	Phosphatidylinositol 3-kinase catalytic subunit type 3
PI4K2A	Phosphatidylinositol 4-kinase type 2 alpha
PINK	PTEN-induced putative kinase 1
PIP2	Phosphatidylinositol 4,5-bisphosphate
PIPES	1,4-Piperazinediethanesulfonic acid, Piperazine-1,4-bis(2-ethanesulfonic acid), Piperazine-N,N'-bis(2-ethanesulfonic acid)
PKD	Polycystic kidney disease
PKD2	Polycystin 2
PLC	Phospholipase C
PLEKHM1	Pleckstrin homology domain-containing family M member 1
PP2A	Protein phosphatase 2
PPARalpha/gamma	Peroxisome proliferator-activated receptor alpha/gamma

PROSC	Proline synthetase cotranscribed homolog protein
PTEN	Phosphatase and tensin homolog
PVDF	Polyvinylidene fluoride
PXN	Paxillin
PyMT	Polyomavirus middle T antigen
RAB1A/7/7A	RAS-associated protein 1A/7/7A
RAC	RAS-related C3 botulinum toxin substrate
RAS	Rat sarcoma protein
RNA	Ribonucleic acid
ROCK	RHO-associated protein kinase
ROS	Reactive oxygen species
RPE	Human retinal pigment epithelial cells
Rpkm	Reads per kilobase of transcript per million
RPMI-1640	Roswell Park Memorial Institute medium-1640
RUNX	Runt-related transcription factor
S6	Ribosomal protein S6
SAFB2	Scaffold attachment factor B2
SCF(BTRC)	Skp1-Cul1-F-box protein (beta-transducin repeat containing E3 ubiquitin protein ligase)
SD	Standard deviation
SDS	Sodium dodecyl sulphate
SEM	Standard error of the mean
SENDA	Static encephalopathy of childhood with neurodegeneration in adulthood
SFTPC	Surfactant protein C
SH2D4A	SH2 Domain Containing 4A protein
SH3	SRC homology 3 domain
SHH	Sonic hedgehog protein
SHIP2	SH2 domain-containing inositol 5'-phosphatase 2
siRNA	Short interfering RNA
SLCA2/GLUT	Solute carrier family 1 member 2/Glutamate/aspartate transporter 2
SMAD2/3/4	Sma- and Mad-related protein 2/3/4

SNAP29	Synaptosome associated protein 29
SNARE	Soluble N-ethylmaleimide-sensitive factor attachment protein receptors
SOCS7	Suppressor of cytokine signalling 7
SORBS1/2/3	Sorbin and SH3 domain containing 1/2/3
SOS1/2	Son of sevenless homolog 1/2
SRCIN1	SRC kinase signalling inhibitor 1
STAT3	Signal transducer and activator of transcription 3
STR	Short tandem repeat
T24	Human bladder carcinoma cells
T6BP	Tumour necrosis factor receptor-associated factor 6-binding protein
TAZ	Transcriptional co-activator with PDZ-binding motif (also known as WWTR1)
TBK1	Tumour necrosis factor receptor-associated factor family member-associated NF-Kappa-B activator binding kinase 1
TBX5	T-box transcription factor 5
TEAD1/2/3/4	TEA domain family member 1/2/3/4
TECPR1	Tectonin beta-propeller repeat containing 1 protein
TEC	Thymic epithelial cells
TFE3	Transcription factor E3
TFEB	Transcription factor EB
TLR7	Toll-like receptor 7
TNFSF10	Tumour necrosis factor superfamily member 10
TNNT2	Troponin T2, cardiac type
TP53/73	Tumour protein p53/73
TSC1/2	Tuberous sclerosis protein 1/2
TTF-1	Thyroid transcription factor-1
TUBA1A	Tubulin alpha 1a
ULK1	Unc-51-like autophagy activating kinase 1
UVRAG	UV radiation resistance-associated gene
VAMP3/7	Vesicle-associated membrane protein 3/7

VPS11/15/16/18/33A/3 4/39/41	Vacuolar protein sorting-associated protein 11/15/16/18/33A/34/39/41
VSV	Vesicular stomatitis virus
VTI1B	Vesicle transport through interaction with t-SNAREs homolog 1B
WASH	WASP and Scar homologue
WAVE1/2	WASP-family verprolin homologous protein 1/2
WIP1/2/4	WD repeat domain phosphoinositide-interacting protein 1/2/4
WWTR1	WW domain-containing transcription regulator protein 1
XIAP	X-linked inhibitor of apoptosis protein
YAP	YES-associated protein 1
YES1	Tyrosine-protein kinase YES